Synthesis of amine-epoxy based polymers and their potential application in the remediation of selected organic dyes from synthetic effluents

Submitted in fulfilment of the requirements of the Degree of Master of Applied Science in Chemistry: in the Faculty of Applied Sciences at Durban University of Technology

Sharista Raghunath

2016

Promoter: Professor R.M. Gengan

DECLARATION

I, Sharista Raghunath hereby declare that this dissertation entitled "**Synthesis of amine-epoxy based polymers and their potential application in the remediation of selected organic dyes from synthetic effluents''**, submitted to the Durban University of Technology, in fulfillment of the requirements for the award of the Degree of Master of Applied Sciences, Organic Chemistry, in the Faculty of Applied Sciences, is the result of my own work and that all sources used or quoted have been indicated and acknowledged by means of complete references.

Signed: Sharista Raghunath ……

Date: ……..

Signed: Professor R. M. Gengan (Promoter) ……

Date: ……

Department of Chemistry
Durban University of Technology

DEDICATION

This dissertation is dedicated to my late grandparents, my parents, Suresh and Veronica, who are my pillars of strength, my beloved family and to the merciful God Almighty.

ACKNOWLEDGEMENT

I thank God for the strength and wisdom granted upon me to undertake and complete this research.

I would like to express my heartiest gratitude to:
My supervisor, **Professor R. M. Gengan** for his time, continual guidance and support throughout my study and for proof reading and editing the thesis. You have exposed me to the wonderful world of polymer research and have opened up a world of opportunities for me.

Dr. A. Krishnan for his expert advice, continual guidance and patience during my study, for equipping me with the knowledge and methodologies used in research, and for encouraging me on this journey.

Dr. D. Pienaar for his expert advice, assistance and guidance with the editing the thesis.

A special thanks to my research team members, **Mr. M. Thangaraj, Mr. S. Mahalingam, Mr. V. Kumar and Mr. A. Murugesan** for their assistance and guidance.

I would like to give special thanks to **Mr. J. Chetty, Ms. I. Monga**, and the team of laboratory technicians who assisted me during my study.

I would like to thank the **ADA and BERTIE LEVENSTEIN BURSARY SCHEME** for providing me with the funding for my research.

I would like to acknowledge the Department of Chemistry (Faculty of Applied Sciences) for granting me the opportunity to conduct valuable research and for providing assistance as requested.

ABSTRACT

The presence of dyes in effluent poses various environmental as well as health hazards for many organisms. Although various remediation strategies have been implemented to reduce their effect, dyes still manage to infiltrate into the environment and hence new strategies are required to address some of the problems. This study investigated the innovation of two cationic water-soluble polymers viz., Proline-Epichlorohydrin-Ethylenediamine Polymer (PEP) and Thiazolidine-Epichlorohydrin-Ethylenediamine Polymer (TEP) that were used to remediate selected synthetic dyes from synthetic effluent by adsorption and dye reduction. Both polymers were synthesized using monomers of a secondary amine, epichlorohydrin and ethylenediamine and were subsequently characterized and modified and their remediation potential studied.

In the first study, PEP was synthesized and characterized by ^{1}H-NMR Spectroscopy, FT-IR Spectroscopy, dynamic light scattering, and thermogravimetric analysis (TGA). Thereafter PEP was modified with bentonite clay, by simple mixing of the reactants, to form a Proline-Epichlorohydrin-Ethylenediamine Polymer-bentonite composite (PRO-BEN); it was characterized by FT-IR Spectroscopy, scanning electron microscopy (SEM)/ energy dispersive X-ray spectroscopy (EDX), dynamic light scattering (DLS), transmission electron microscopy (TEM) and X-ray photoelectron spectroscopy (XPS). Adsorption studies were then undertaken with a synthetic effluent containing three textile dyes, viz., Reactive Blue 222 (RB 222), Reactive Red 195 (RR 195) and Reactive Yellow (RY 145). Various conditions were investigated including pH of the solution, temperature, sodium chloride concentration, initial dye concentration and the dosage of adsorbent used. The experimental data for all dyes followed a Langmuir isotherm. The adsorption process was found to be pseudo-second order. According to the thermodynamic parameters, the adsorption of the dyes was classified as physisorption and the reaction was spontaneous and exothermic. The data were also compared using studies with alumina as an adsorbent. Results showed that PRO-BEN exhibited better absorptivity and desorption than alumina making its use a better recyclable remediation strategy for the removal of organic dyes in wastewater treatment plants.

In the second study, TEP was synthesized and then characterized by FT-IR Spectroscopy, ^{1}H-NMR Spectroscopy, TGA and DLS. Thereafter, TEP was used to prepare TEP capped gold nanoparticles (TEP-AuNPs). Herein, two methods were investigated: the Turkevich method and an adaptation of the Turkevich method using bagasse extract. The TEP-AuNPs was

characterized by FT-IR Spectroscopy, SEM, EDX, DLS and TEM. Thereafter the reduction of each of Allura Red, Congo Red and Methylene Blue was investigated with the TEP-AuNPs for its catalytic activity toward dye reduction. This study showed that the batch of AuNPs prepared by the Turkevich method had higher rates of dye reduction compared with AuNPs prepared using bagasse extract. Also the quantity of TEP used as capping agent greatly influenced the size, shape and surface charge of the nanoparticles as well as their catalytic performance: the Vroman effect explained this behavior of the TEP-AuNPs.

It was finally concluded that whilst PRO-BEN, in the first study, showed excellent dye remediation properties, the second study on TEP-AuNPs showed good catalytic activity for the reduction of selected dyes, however, it was more effective at lower polymer concentration. Finally, both materials displayed good potential for the clean-up of selected synthetic dyes from synthetic effluents.

LIST OF PUBLICATIONS AND CONFERENCE PROCEEDINGS

Some aspects of this dissertation can be found as a research article and a conference proceeding:

International Conference:

Concentration effect and kinetic evaluation of the thiazolidine polymer capped AuNPs, International Conference on Composites, Biocomposites and Nanocomposites (**ICCBN)**, Durban, South Africa, 23 – 28 October **2015.**

Publication:

Sorption isotherms, kinetic and optimization process of novel proline based polymer nanocomposite for the removal of selected textile dyes from industrial wastewater. Sharista Raghunath, Anand Krishnan, Robert Moonsamy Gengan, Mithil Kumar Nayunigari and Arjun Maity. *Journal of Photochemistry & Photobiology, B: Biology*, DOI: 10.1013/j.jphotobiol.2016.10.012

LIST OF TABLES

LIST OF FIGURES

LIST OF APPENDICES

ABBREVIATIONS

Å	- Angstrom
DNA	- deoxyribose nucleic acid
RNA	- ribose nucleic acid
IUPAC	- International Union of Pure and Applied Chemistry
MΩ	- MegaOhm
˚C	- Centigrade
MHz	- Megahertz
min	- Minute
µl	- Microlitre
µM	- Micromolar
M	- Molar
mmol	- Millimolar
s	- Seconds
g	- Grams
mg	- Milligrams
ρ	- Density
cm	- Centimetre
DSC	- Differential scanning calorimeter
$\frac{dn}{dc}$	- Refractive Index increment
kcps	- kilocounts per seconds
kDa	- kiloDaltons
AU	- Absorbance units
mS	- Mili siemens
mV	- Millivolts
eV	- Electron volts
d.nm	- Distribution in nanometres
viz.	- Namely
ml	- Milliliter
nm	- Nanometer
LOD	- Limit of detection
LOQ	- Limit of quantification

E	- Extinction co-efficient
SEM	- Scanning Electron Microscope
FT-IR	- Fourier Transform Infrared Spectroscopy
^{1}H-NMR	- Proton Nuclear Magnetic Resonance Spectroscopy
DSC	- Differential Scanning Calorimetry
TGA	- Thermo-Gravimetric Analysis
SEM	- Scanning Electron Microscope
TEM	- Transmission Electron Microscopy
Temp.	- Temperature
EDX	- Energy Dispersive X-Ray Spectroscopy
UV-Vis	- Ultraviolet/Visible Spectroscopy
SA	- South Arica
AuNP	- Gold nanoparticle
AuNPs	- Gold nanoparticles
TEP	- Thiazolidine-Epichlorohydrin-Ethylenediamine Polymer
PEP	- Proline-Epichlorohydrin-Ethylenediamine Polymer
PRO-BEN	- Proline polymer-bentonite composite
RB 222	- Reactive blue 222
RR 195	- Reactive red 195
RY 145	- Reactive yellow 145
aq	- Aqueous
mols	- Moles
conc.	- Concentrated
LOD	- Limit of detection
LOQ	- Limit of quantification
DF	- Dilution factor
0ppm TEP-Na- AuNPs	- Gold nanoparticles of 0 ppm TEP capping with sodium citrate
1ppm TEP-Na- AuNPs	- Gold nanoparticles of 1 ppm TEP capping with sodium citrate
5ppm TEP-Na- AuNPs	- Gold nanoparticles of 5 ppm TEP capping with sodium citrate
10ppm TEP-Na- AuNPs	- Gold nanoparticles of 10 ppm TEP capping with sodium citrate
30ppm TEP-Na- AuNPs	- Gold nanoparticles of 30 ppm TEP capping with sodium citrate
50ppm TEP-Na- AuNPs	- Gold nanoparticles of 50 ppm TEP capping with sodium citrate
0ppm TEP-AuNPs	- Gold nanoparticles of 0 ppm TEP capping with bagasse extract
1ppm TEP-AuNPs	- Gold nanoparticles of 1 ppm TEP capping with bagasse extract

5ppm TEP-AuNPs	- Gold nanoparticles of 5 ppm TEP capping with bagasse extract
10ppm TEP-AuNPs	- Gold nanoparticles of 10ppm TEP capping with bagasse extract
30ppm TEP-AuNPs	- Gold nanoparticles of 30ppm TEP capping with bagasse extract
50ppm TEP-AuNPs	- Gold nanoparticles of 50ppm TEP capping with bagasse extract
MB	- Methylene Blue
AR	- Allura Red
CR	- Congo Red
CEC	- Cationic exchange capacity
ATR	- Attenuated total reflectance
BEN	- Bentonite
DLS	- Dynamic light scattering
SLS	- Static light scattering
ppm	- $mg.L^{-1}$
rpm	- Revolutions per minute

Table of Contents

Chapter One: Introduction

1.1. General Introduction

Dyes have long been used in many industries such as paper and pulp, textile, plastic, leather, cosmetics and food industries. These coloured compounds are not only aesthetically displeasing when discharged into the environment but also inhibit sunlight penetration into water and affects the aquatic ecosystem since they are toxic to some microorganisms (Koprivanac and Kusic 2012: 3) and may cause direct destruction or inhibition of their enzymatic pathways, as well as pose other hazards and environmental problems. Dyes are usually stable and difficult to biodegrade because of their complex aromatic molecular structures. Most dyes are carcinogenic, cause nausea, asthma, skin rashes, and seizures (Dale 2008). For this reason, the removal of dyes from water is under continual improvement.

Recently, the use of polymers to remove dyes from water has gained favour because of their easy synthesis and low cost of manufacturing. Several studies reported the adsorption of dyes using polymers (Koprivanac and Kusic 2009: 3) (Szyguła *et al.* 2009: 2981) (Hu and Hsieh 2016: 858) as the method of choice, however other remediation methods include flocculation (Guibal and Roussy 2007: 35), aggregation (Wei *et al.* 2015: 354) and biological treatments (Ogugbue *et al.* 2012: 1145) (Zhang *et al.* (2014: 5860)

Also recently, studies involving the removal of dyes from water by metallic nanoparticles has been investigated whilst the reduction of common dyes (Azad *et al.* 2011: 3953) (Wunder *et al.* 2010: 8817) has been reported.

1.2. Purpose of the Study

The purpose of this study was to synthesize two novel water-soluble amine-epoxy polymers and to use each of them in the removal of selected organic dyes from synthetic textile dye effluent in the following two ways;

(i) adsorb dyes on a polymer-clay composite

(ii) reduce dyes by means of polymer-capped nanoparticles

1.3. Objectives of the Research

The objectives of the adsorption study were to:

1.3.1. Synthesize a novel polymer by using proline, epichlorohydrin and ethylenediamine and characterize this polymer by analytical techniques.

1.3.2. Prepare the polymer-bentonite composite using the Proline-Epichlorohydrin-Ethylenediamine Polymer and bentonite clay and characterize it using several analytical techniques.

1.3.3. Study the removal of three reactive dyes from a synthetic textile effluent by adsorption.

The objectives of the reduction study were to:

1.3.4. Synthesize a novel polymer by using thiazolidine, epichlorohydrin and ethylenediamine and characterise this polymer by spectroscopic techniques.

1.3.5. Synthesize a polymer-gold nanoparticle composite using bagasse extract as a reductant to gold and characterize this material by spectroscopic techniques.

1.3.6. Study the reduction of three dyes by dye reduction.

1.4. Structure of the Thesis

This thesis is divided into four chapters.

Chapter One summarizes the intention of the study, the reasons for removing dues from effluent, the importance of polymers to remediate wastewater, brief discussion of important reports on adsorption and reduction of dyes. This chapter also sheds light on the purpose of the study and the objectives.

Chapter Two provides a detailed literature survey encompassing the various types of polymers and their use in environmental applications. Polymers that are chemically synthesized as well as polymers that are derived naturally will be briefly discussed. The previous technologies used in water treatment for dyestuff will be outlined. Special emphasis will be placed on the general theory of dye adsorption: background information, laws and equations of adsorption isotherms and kinetic laws will be thoroughly discussed. Also the involvement of water soluble polymers will be highlighted. A literature search on dye adsorption will be highlighted.

The basic theory of nanoparticles will be also be discussed. Special emphasis will also be placed on gold nanoparticles (AuNPs): their properties and methods of synthesis will be discussed. Previous mechanisms involving the use of AuNPs will be outlined.

Chapter Three presents, in the case of adsorption study, the general introduction, the experimental including synthesis and characterization of Proline-Epichlorohydrin-Ethylenediamine Polymer (PEP) and Proline-Epichlorohydrin-Ethylenediamine Polymer-bentonite composite (PRO-BEN) and the adsorption of the dyes. Thereafter the results from the adsorption studies will be discussed. Also, a comparison of results obtained from studies based on alumina and PRO-BEN will be discussed.

Chapter Four discusses, in the case of the reduction study, the general introduction, the experimental including synthesis and characterization of Thiazolidine-Epichlorohydrin-Ethylenediamine Polymer (TEP) and TEP-capped gold nanoparticles (AuNPs) using bagasse and sodium citrate, separately, as a reductant. The results from the decolourization process of dye-laden water will be discussed.

1.5. References

Azad, U., Ganesan, V.and Pal, M. 2011. Catalytic reduction of organic dyes at gold nanoparticles impregnated silica materials: influence of functional groups and surfactants. *Journal of Nanoparticle Research,* 13 (9): 3951-3959.

Dale, E. 2008. *Synthetic Dyes: A look at Environmental & Human Risks* (online). Available: https://greencotton.wordpress.com/2008/06/18/synthetic-dyes-a-look-at-the-good-the-bad-and-the-ugly/ [Accessed 16 August 2015].

Guibal, E.and Roussy, J. 2007. Coagulation and flocculation of dye-containing solutions using a biopolymer (Chitosan). *Reactive and Functional Polymers,* 67 (1): 33-42.

Hu, S.and Hsieh, Y.-L. 2016. Silver nanoparticle synthesis using lignin as reducing and capping agents: A kinetic and mechanistic study. *International Journal of Biological Macromolecules,* 82: 856-862.

Koprivanac, N.and Kusic, H. 2009. Hazardous Organic Pollutants in Coloured Wastewaters. 1st ed. New York, US: Nova Science Publishers, Inc.

Ogugbue, C. J., Sawidis, T.and Oranusi, N. A. 2012. Bioremoval of chemically different synthetic dyes by Aeromonas hydrophila in simulated wastewater containing dyeing auxiliaries. *Annals of Microbiology,* 62 (3): 1141-1153.

Wei, Y., Dong, X., Ding, A.and Xie, D. 2015. Characterization and coagulation–flocculation behavior of an inorganic polymer coagulant – poly-ferric-zinc-sulfate. *Journal of the Taiwan Institute of Chemical Engineers*.

Wunder, S., Polzer, F., Lu, Y., Mei, Y.and Ballauff, M. 2010. Kinetic Analysis of Catalytic Reduction of 4-Nitrophenol by Metallic Nanoparticles Immobilized in Spherical Polyelectrolyte Brushes. *The Journal of Physical Chemistry C,* 114 (19): 8814-8820.

Zhang, T., Song, Y.-J., Zhang, X.-Y.and Wu, J.-Y. 2014. Synthesis of Silver Nanostructures by Multistep Methods. *Sensors,* 14 (4): 5860.

Chapter Two: Literature Survey

2.1. General Introduction

Polymers are substances containing a large number of structural units joined by the same type of linkage. They have large molecular masses and can be non-ionic, negatively or positively charged. Their existence can be traced back to the beginning of life where they have been present in humans, animals and plants as molecules such as DNA, RNA and proteins (Young and Lovell 2011: 3). However, polymers were only acknowledged in the 19th century.

The use of polymers in wastewater treatment began in the 1960's where the main methods used were coagulation and flocculation (John *et al.* 2012: 576). These methods were a major breakthrough in wastewater treatment and stimulated more studies which led to the development of better cationic, anionic and neutral polymers. During this time, the polymers that were most popular were dimethylamine polymer (epi-DMA) and polydiallyldimethylammonium chloride (poly-DADMAC) (Fig. 2.1) (John *et al.* 2012: 577): these were ionic polymers. Later developments included the preparation of water-soluble polymers for the treatment of wastewater where adsorption became the preferred methodology. However, the cost for the treatment of wastewater was high due to large volumes of effluent being produced and discharged from industries. This drawback fostered intensive studies for the synthesis of new polymers with the aim of increasing polymers yields at low cost and thereby maximizing profits. Today, synthetic as well as natural polymers are used for various wastewater treatment processes but the desire to create a better polymer is ongoing.

(a) (b)

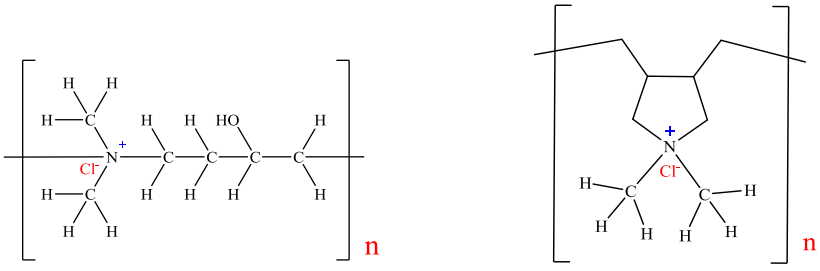

Figure 2.1. The back-bone structure of a (a) dimethylamine polymer and (b) polydiallyldimethylammonium chloride polymer

2.2. The History of Polymers

The term "polymer" was first introduced by Jöns Jakob Berzelius in 1833. He investigated two compounds viz. ethene and butene both of which have empirical formula of CH_2, and he viewed their composition as equal. He wrote: "To describe this equality of composition coupled with a difference of properties I suggest that such substances be called polymeric" (Morris 2005: 7 – 13). In 1861, Thomas Graham noticed that organic substances such as cellulose and starch, when mixed in certain solutions, displayed anomalous properties. He found that they could neither pass through filter paper nor be purified into their crystalline form and called them colloids. He thought that colloids were made up of a large number of molecules bonded by "association" (Elliott 2005: 5 – 11). These forces kept atoms in the molecules together but were strong enough to prevent the colloids from displaying crystalloid properties. Later, the micelle theory arose: it was assumed that large molecules were aggregates of smaller molecules held together by weak intermolecular forces. In 1858, Carl von Nägeli proposed that a micelle was an aggregate of thousands of molecules orientated in a crystalline array. He argued that in a micellar complex, small molecules were bonded by strong "primary valences" and the entire aggregate was bonded by significant weaker "secondary valences".

In 1866, Pierre-Eugène-Marcellin Berthelot described the word "polymer" correctly after his observation that on heating styrene up to 200 ℃ for a few hours, a polymer was formed Fontanille (2002). This was the production of the first synthetic polymer. Thereafter there was a vigorous study on polymers which led to many products having different physical and chemical properties. In 1870, John Wesley Hyatt found that when cellulose nitrate was reacted with camphor, in the presence of heat and pressure, a substance was produced which could be hardened permanently. In 1887, Count Hilaire de Chardonnet discovered that by spinning cellulose nitrate, artificial textile fibres could be made, however this product was flammable due to the presence of nitrogen from the nitrate. Further studies by French scientists resulted in solving this problem by treating the fibres with acid sulfide however the first synthetic fibre was industrialized only in 1890. In 1909, Leo Baekeland synthesized the first plastic by synthesizing a new polymer from phenol and formaldehyde and thereafter mixing in fillers.

2.3. Classification and Types of Polymers

A polymer is a substance consisting of molecules of either the same type or more than one type which are bonded to one another by covalent bonding (Young and Lovell 2011: 3). Many monomer units bonded together to form long high molecular weight chains are known as polymers. That single molecule that is used to form the polymer is known as a monomer whilst

the process in its formation is known as polymerization. These monomeric units covalently bond to each other to form dimers, trimers etc. until eventually a polymer (Cheremisinoff 1989: 758).

Polymers are classified as linear, branched, cyclic and networked (Fig. 2.2) (Young and Lovell 2011: 3). Linear polymers are straight chains with two distinct ends. Cyclic polymers have no distinct chain ends. Branched polymers have chains that protrude from junction points on the main chain. Network polymers or cross-linked polymers are made up of polymeric chains joined at junction points as a three dimensional structure.

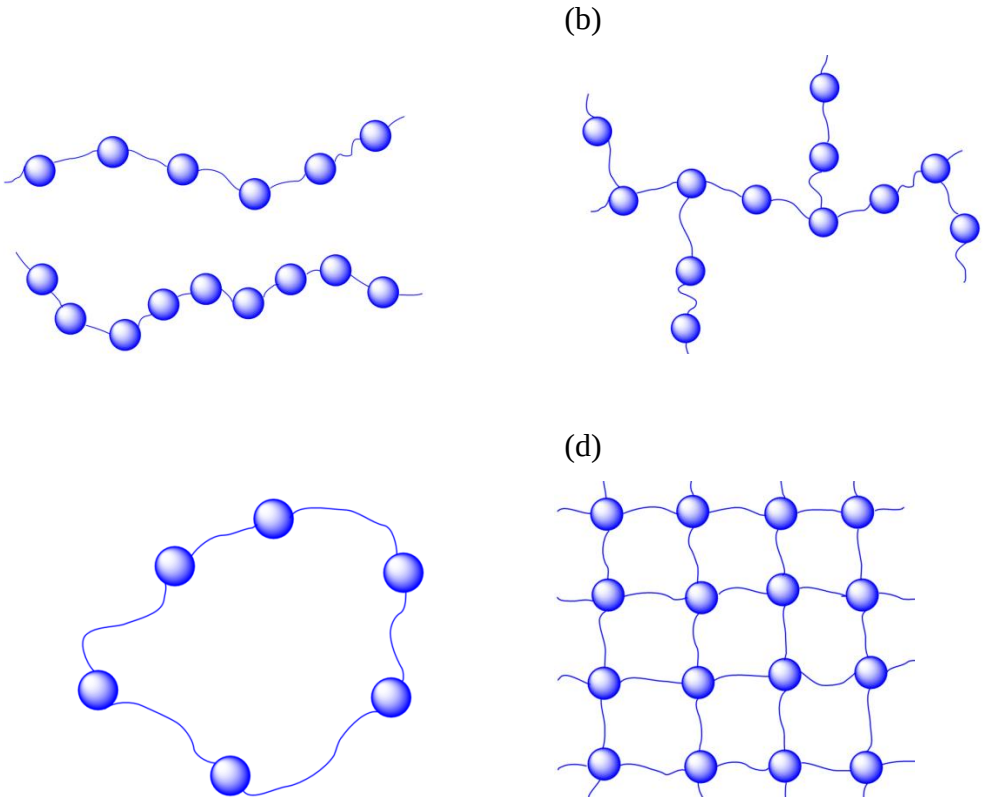

Figure 2.2. Schematic illustration of (a) linear, (b) branched, (c) cyclic and (d) network polymers

There are many types of polymers such as elastomers, fibres, rubber, cellulose and starch and plastics such as thermoplastics and thermosets (Guerra and Eduardo 2013: 20). Thermoplastics are polymers that can be re-molded after re-heating. They therefore are limited by the number of times heating can be carried out and are recyclable to certain extent. The thermoset polymer usually require liquid reactants which are heated to form a solid cross-linked polymeric network. When thermoset polymers are heated, the covalent bonds between monomers break and hence the polymer may break down. These polymers cannot be recycled. Elastomers and

rubber are much more flexible and can be used as modifiers in thermosetting plastics, tyres and adhesives (Guerra and Eduardo 2013: 25). Fibres are used for their strength and rigidity whilst paints and coatings are used for their ability to form films. A flow diagram on polymer classification is presented in Fig. 2.3.

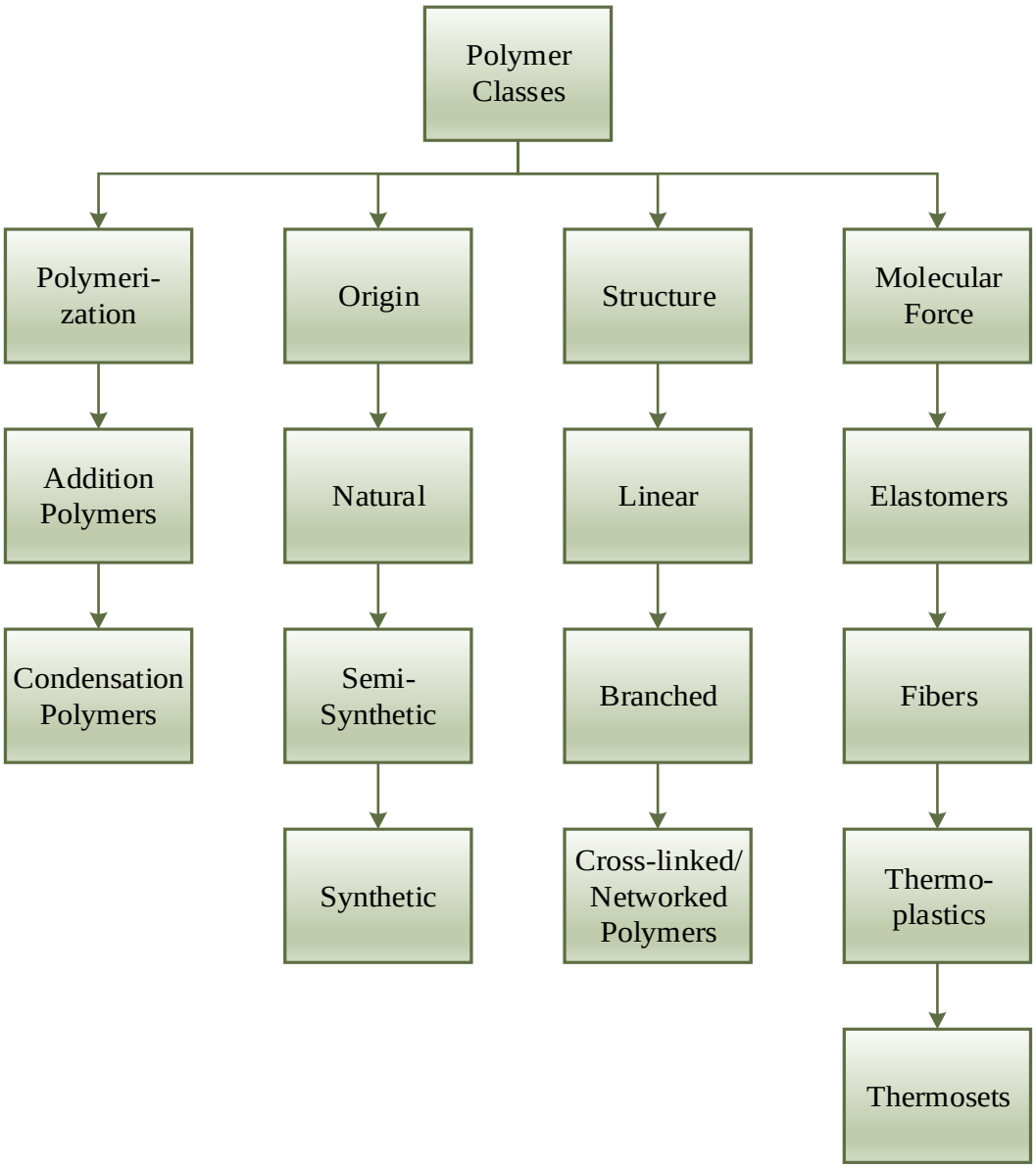

Figure 2.3. Hierarchical classes of polymers

2.4. Homopolymers and Copolymers

Homopolymers contain monomers of the same kind (Fig. 2.4) whereas a copolymer contains more than one type of monomer. Copolymers are divided into sub-groups i.e. statistical, random and alternating. Statistical copolymers have their repeating units arranged in Markovian statistical laws (Young and Lovell 2011: 6). Random copolymers is another form

of a statistical copolymer which have their repeating units arranged randomly in the polymeric chain. Alternating copolymers contain monomers which are arranged in an alternate fashion.

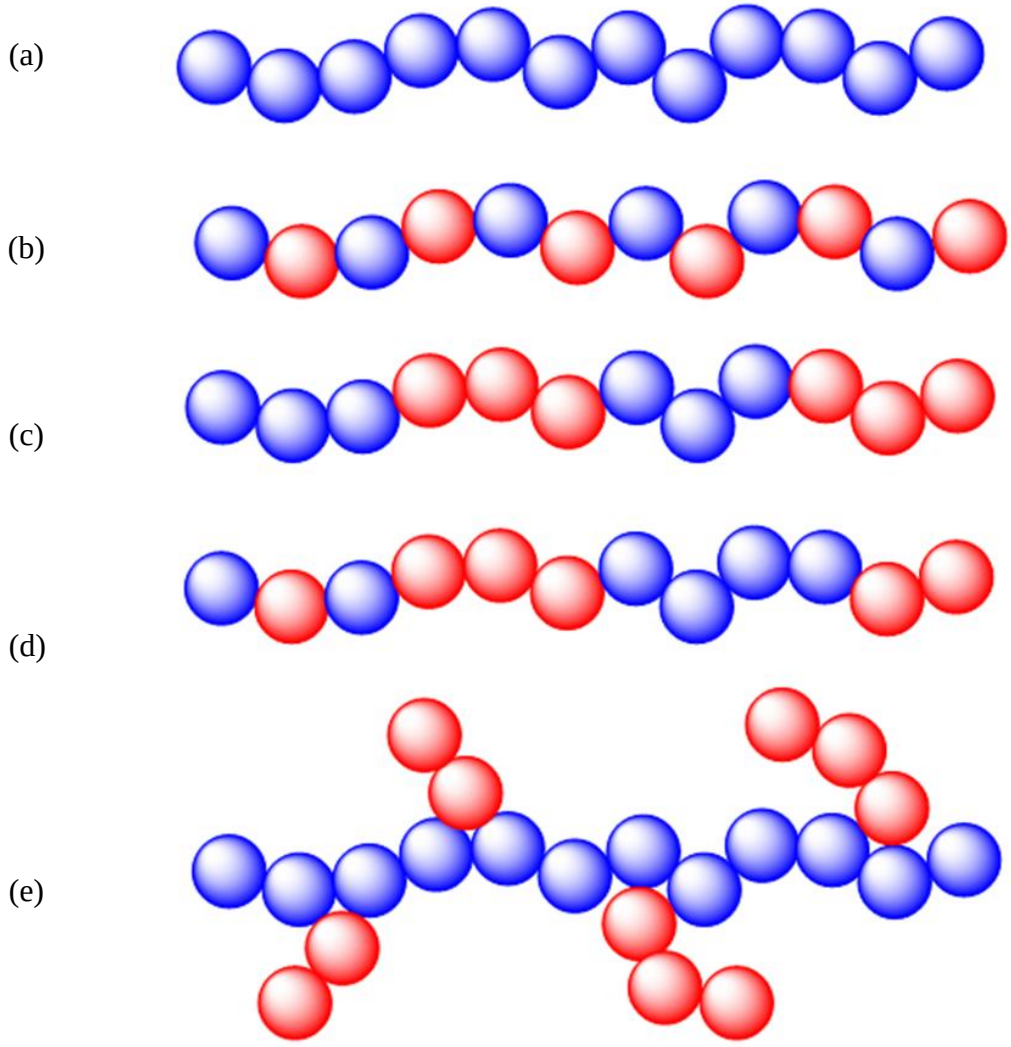

Figure 2.4. Schematic representation of (a) homopolymer, and copolymer (b) alternating, (c) block, (d) random and (e) graft copolymer

2.5. Ionic Polymers

Ionic polymers contain both an ionic and a covalent bond (Wilson and Prosser 2012: 1). They are divided into anionic, cationic and ampholytic groups which carry negative, positive and both negative and positive charge moieties, respectively, with various counter ions.

Ionic polymers tend to be more water-soluble than other groups and of these, the cationic polymers are widely used in remediation studies. The common cationic moieties includes ammonium, phosphonium and sulfonium ions.

2.6. Types of Polymerizations

There are two types of reaction viz., step-growth and chain-growth polymerization, (Matyjaszewski 1996: 3) also referred to as condensation and addition polymerization, respectively. In step-growth polymerization, monomers react with each other and loses a small molecule such as water and carbon dioxide. In this reaction, the monomer is used up much faster in the early stages of the reaction and more vigorous conditions are needed to form large molecular weight polymers. Also there is no need for species to initiate or terminate the reaction. Chain-growth polymerization requires an unsaturated monomer which reacts at this site and adds on one at a time. The mechanism for this type of polymerization occurs in the following four stages:

- The chain initiation stage: a chemical species is required to start the polymerization process.
- The chain propagation step: the monomer reacts with the active site of the polymer chain.
- Chain transfer: this step ends the polymer chain and the reaction site is transferred to a new polymer chain.

Chain termination step: this occurs by polymer chain combination or disproportionation leading to the end of the polymerization process.

Free-radical and ionic polymerizations follow the same four steps as mentioned above.

2.7. Water-Soluble Polymers

Water-soluble polymers are more widely used because of the following properties (Williams 2008: 140):

- Increases the viscosity of a solution as it is diluted
- Creates gels and causes particle aggregation in solutions
- Allows for the controlled release and attachment of active species
- Stabilizes colloidal dispersions by adsorption thereby preventing aggregation

These properties make them valuable for industries such as water purification, sugar refining, pulp and paper manufacturing, and pharmaceutical industries.

The NIIR Project Consultancy Services Board of Consultants & Engineers (NPCS India) reported that there are three main types of synthetic water soluble polymers that are used in

industries. These are polyvinyl pyrrolidone, polyvinyl acetate and polyethylene oxide (Fig. 2.5). These are thermoplastics, available in a wide range of molecular weights and commonly applied as thickeners and stabilizers.

(a) (b) (c)

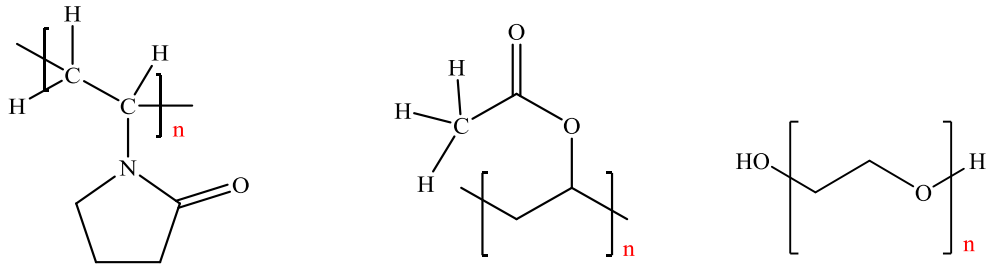

Figure 2.5. Structure of (a) polyvinyl pyrrolidone, (b) polyvinyl acetate and (c) polyethylene oxide

During the past 30 years, polymers containing quaternary ammonium groups have gained wide popularity in water treatment due to their high cationicity and effectiveness at all pH values (Cho *et al.* 2002: 131 – 137). These polymers are used also as flocculants but only a few are commercially popular These include polydimethylaminoethyl (meth)acrylate methyl chloride (polyDMAEM-MCQ) and polydiallyldimethylammonium chloride (polyDADMAC) (Salamone 1998: 491).

2.8. Applications of Polymers in Wastewater Remediation

Flocculation and coagulation are important techniques for water treatment hence studies for new cationic polymers are being continuously undertake.

2.9. The Use of Flocculation for Wastewater Remediation

Flocculation is used in many industrial processes such as water purification and wastewater treatment. This process is usually induced by positively charged synthetic polymers. The versatility of cationic polymers for the remediation of wastewater was reported by Fontanille (2002) whereby two polymers, viz., poly(allylamine hydrochloride) and poly(acrylic acid) were alternately fabricated on a polysulfone membrane. Recently a new water-soluble polymer containing a carboxyl-amide moiety was used for turbid suspensions containing bentonite (Asanov and Matniyazova 2012: 200 – 204). (Chesters *et al.* 2009: 144 – 151) reported on a cationic polymers using membrane technology but this was not viable because of "membrane fouling". The use of a quaternary ammonium copolymer for calcium carbonate flocculation in

water treatment for the paper industry was also reported (Cho *et al.* 2002: 131 – 137). Sahu and Chaudhari (2013: 241 – 257) reported on the use of a natural cationic polymer for the calcium carbonate flocculation in water treatment for the paper industry. Recently, Fast and Gude (2015: 153 – 160) conducted a study with chitosan to remove algae from effluent whereas Vandamme *et al.* (2010: 525 – 530) found a cationic starch which contained a quaternary ammonium group which was more effective because of its wide pH range. The removal of microalgae by guar gum containing a quaternary ammonium group was also reported by Banerjee *et al.* (2013: 675 – 681). A cationic-modified amylopectin and glycogen using N-(3-chloro-2-hydroxypropyl) trimethylammonium chloride were used as flocculation agent in a coal and water suspension. It was reported that the cationic-modified glycogen was the best flocculant (Pal *et al.* 2008: 590 – 596). The removal of dissolved organic nitrogen from effluent by polyDADMAC by coagulation, was reported by Lee and Westerhoff (2006: 3769). The treatment of laundry waste water by polyDADMAC was reported by Kim *et al.* (2014: 167 – 174).

2.9.1. The Use of Adsorption for Wastewater Remediation

Adsorption is a popular technique: It is inexpensive, the targeted contaminant can be removed by choosing the correct adsorbate and it is recyclable. Cationic polymers are often used to coat or intercalate other primary adsorbents for the removal of a chosen type of contaminant in the matrix. The adsorption of humic acid in wastewater was carried out using a cationic monodisperse polymer which was coated with iron oxide particles Kim and Walker (2001: 123 – 131). Amuda *et al.* (2007: 174 – 181) incorporated chitosan onto coconut shell remains as a biosorbent for the removal of heavy metals (Amuda *et al.* 2007: 174 – 181). Cho *et al.* (2011: 298 – 305) reported that by coating a cationic polymer on activated carbon, nitrate and chromium (VI) could be adsorbed. It was reported by Goel *et al.* (2015: 444 – 451) that cellulose was cationically modified, by radiation grafting, for the removal of anionic dyes from wastewater. The use of epi-DMA cationic polymer and clay materials to remove disperse dyes (Yue *et al.* 2007: 279 – 290), acid dyes (Li *et al.* 2010: 489 – 497), non-ionic and anionic dyes (Li *et al.* 2010: 1601 – 1611) and reactive dyes (Li *et al.* 2009: 1170 – 1178) from wastewater showed great potential for water remediation.

2.10. The Dyeing Industry and Pollution

The textile industry is one of the major contributors to water pollution based on an estimation that effluent from textile industry amounts to 20 % of the world's water pollution. It was

reported that approximately 0.7 – 0.8 million tons of synthetic dyes are produced annually and about 10,000 dyes were consumed by textile companies (Ahmed *et al.* 2015: 317 – 324). It was also estimated that 10 % – 15 % of dyes are lost during the dying process and is discharged into the environment (Ahmed *et al.* 2015: 317 – 324).

2.11. Types of Dyes

In earlier times, natural dyes were extracted from plant sources such as roots, leaves, bark, wood and fungi and lichens (Adrosko 2012: 13 – 14). The extraction was time consuming, yields were low therefore they were expensive. Later, synthetic dyes originated because of the high demand by industries for its application in different types of materials such as plastics, clothes and food products. There are different types of dyes which includes azoic, direct reactive, disperse and basic dyes.

2.11.1. Direct Dyes

These dyes can be either anionic or cationic. They are mostly used to colour cotton, linen and rayon. These are not very bright and gradually lose colour after fibres are washed. Also, they are cheaper, do not need to be applied in alkaline condition and are much simpler to apply. Many of these dyes contain aromatic rings with sulfonate groups which makes them soluble in water. The chromophores include azo groups, oxazine and phthalocyanine (Erkurt 2010: 157 – 167), (Thakor *et al.* 2011: 4029 – 4036), (Aspland 1997: 410) (Fig. 2.6).

(a)

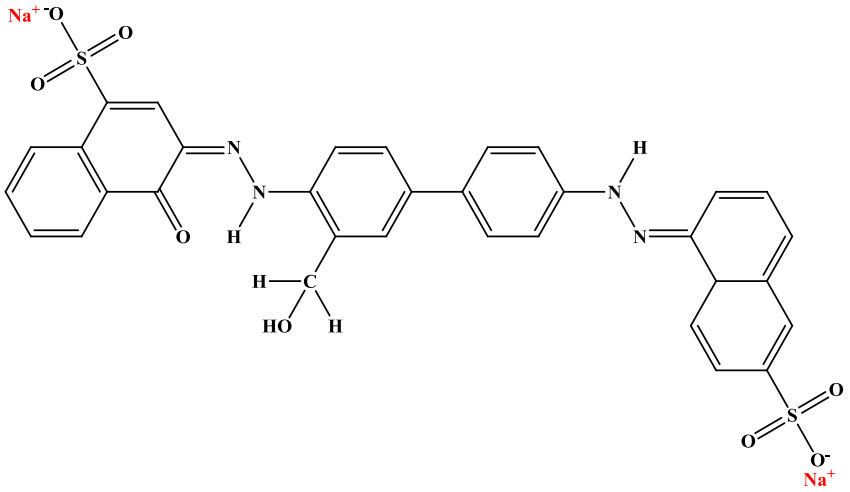

(b)

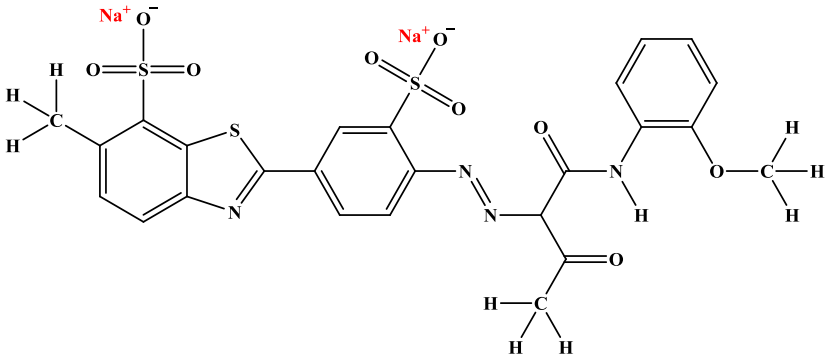

(c)

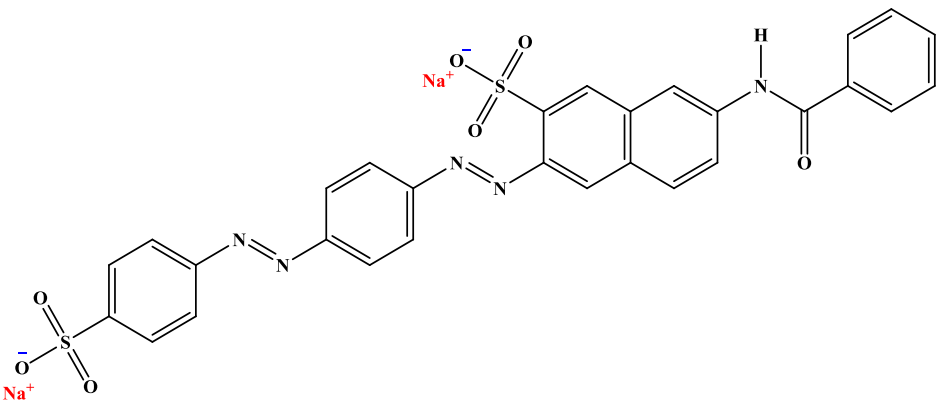

Figure 2.6. The structure of direct dyes (a) Direct Yellow 27, (b) Direct Blue 98 and (c) Direct Red

2.11.2. Azoic Dyes

These dyes contain many aromatic rings and are characterized by the double bond between two consecutive nitrogen atoms (Fig. 2.7). These dyes exist in three colours; red, brown and yellow. They are made mainly from aromatic amines (Panda 2013: 63). They exhibit intense

colour in apparel dyeing, are more stable in a range of pH values and do not degrade upon oxidation. They do not pose a serious threat to humans unless consumed at 250 mg/kg – 2,000 mg/kg body weight, however, their presence significantly affects water bodies.

2.11.3. Reactive Dyes

Reactive dyes such as RB 222, RR 195 and RY 145 are used to dye cotton. They contain azo moieties thereby promoting their colour fastness and vivid colour. In addition, they range in various shades and can be easily applied. They are easily removed from textiles by bleaching agents, however the azo moieties can hinder this process. They form covalent bonds with the textiles via the carbon atoms in the dye to the heteroatoms present in the textile surface (Choudhury 2006: 514).

(a)

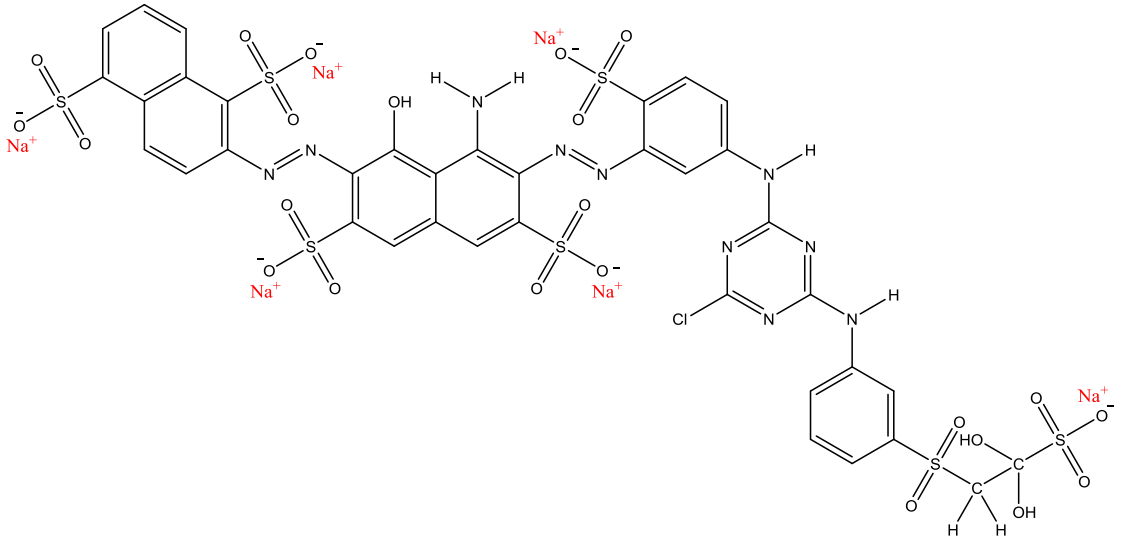

(b)

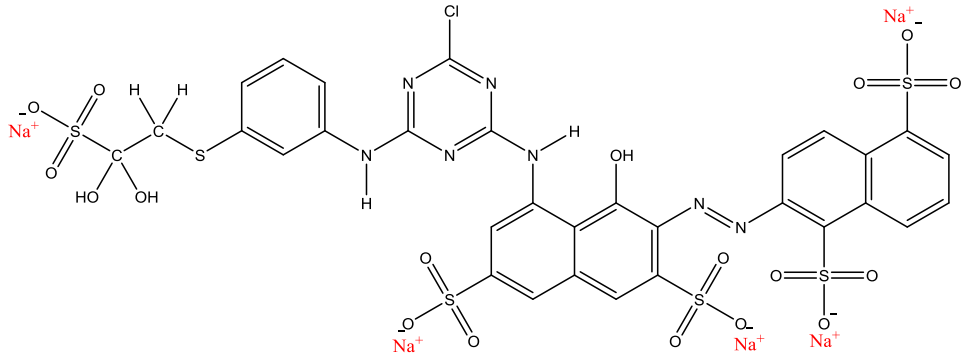

(c)

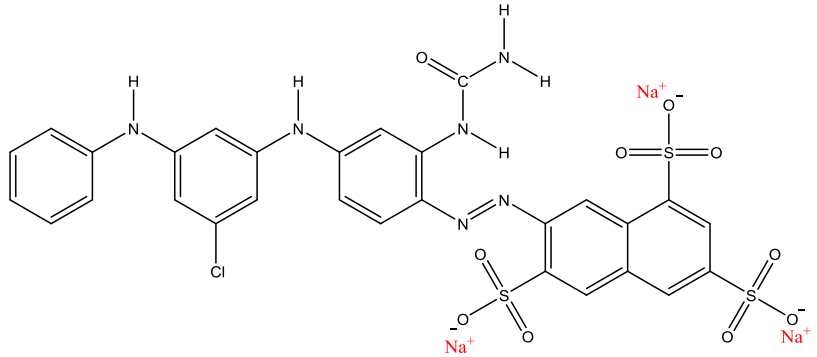

Figure 2.7. Molecular structures of (a) RB 222, (b) RR 195 and (c) RY 145

2.12. Removal of dyes from Water

The increased awareness of the adverse effects of dyes present in water bodies prompted scientists to find new ways to remove them from water bodies. This includes biological,

chemical and physical methods, electrocoagulation, photocatalytic degradation, adsorption and the use of nanocomposites (Karthik *et al.* 2014: 301-307).

2.13. Adsorption Isotherms

Adsorption is the most favoured technique for water remediation. In 1918 Langmuir characterized adsorption as an isotherm known as the Langmuir adsorption (Langmuir 1918: 1361 – 1403) which resulted in the characterization of many other isotherms.

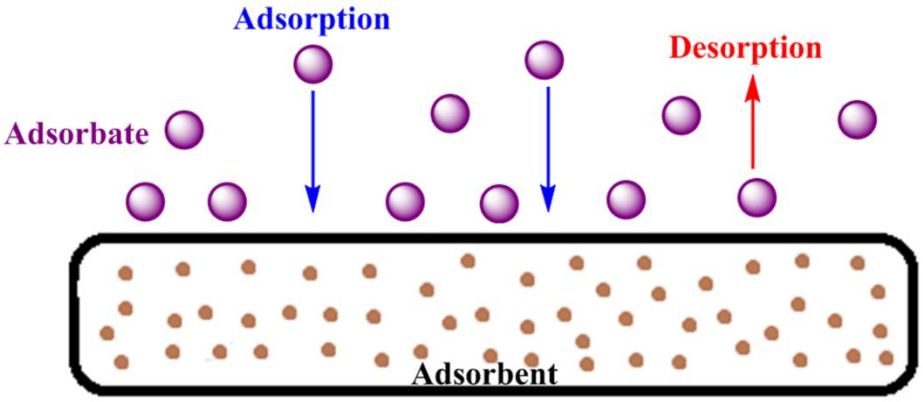

Figure 2.8. A schematic of the adsorption process

Adsorption involves a phase transfer of substance onto a substrate from a liquid or gas phase (Fig. 2.8). The adsorbate can interact with the adsorbent physically or chemically, known as physisorption, or chemisorption, respectively. In physisorption, the interaction is by Van de Waals forces, dipole-dipole interactions, dispersion forces and induction forces. These forces are generally weak forces and the enthalpy of adsorption is smaller than 50 kJ/mol. Chemisorption involves chemical reactions on the surface of the adsorbent. The enthalpy of adsorption is greater than 50 kJ/mol. Factors that affect adsorption include the nature, the surface area and the degree of activation of the adsorbent. Adsorption conditions such as temperature, pH and salt concentration of adsorption medium, pressure and quantity of adsorbent must be optimized for best adsorption.

An adsorption isotherm is a graph describing the amount of adsorbate adsorbed onto the surface of an adsorbent at a pressure and constant temperature. A basic equation expressing the process of adsorption is:

$$A_{adsorbate} + B_{adsorbent} \leftrightarrow AB_{adsorption} \tag{2.1}$$

where the forward process is adsorption and the reverse process is desorption. The isotherms that are commonly used are the Langmuir isotherm (Saraydin *et al.* 1998: 227 – 236), the Freundlich isotherm (Freundlich and Hatfield 1926), Temkin isotherm (Temkin and Pyzhev 1940: 327 – 356) and the Frumkin isotherm (Frumkin 1919: 792 – 802).

Type I Langmuir isotherm determines the monolayer coverage of the adsorbate to the adsorbent (Saraydin *et al.* 1998: 227 – 236). This isotherm is based on three assumptions (Atkins and de Paula 2014: 2):

- No further adsorption takes place beyond monolayer coverage
- All adsorption sites on the adsorbent are equal
- There are no interactions between adsorbed molecules in neighbouring sites

Over the years this isotherm has been modified to yield four types of Langmuir isotherms in accordance to the Giles classification system (Giles *et al.* 1960: 3973 – 3993). This system divides the isotherm into four classes, depending on the initial slope, the shape of the curves and the changes in the slope. This adsorption process is described as:

$$A + adsorbent\ active\ site\ \leftrightarrow A_{adsorption} \tag{2.2}$$

The derivation is attained by taking the assumptions into account, if θ = fractional surface coverage sites, then $(1 - \theta)$ is the sites on adsorbent available for adsorption. Thus:

$$Rate\ of\ adsorption = kad\ [A](1 - \theta) \tag{2.3}$$

$$Rate\ of\ desorption = \ k_d\ \theta \tag{2.4}$$

where $[A]$ is the concentration of the adsorbent,
k_{ad} is the rate constant dependent on temperature and independent on θ nor [A],
k_d is the desorption rate constant.

At equilibrium, the rate of adsorption equals the rate of desorption and the equation is solved in terms of θ:

$$\theta = \frac{k_{ad}[A]}{1 + k_{ad}[A]}$$

(2.5)

Type I linear equation is commonly used:

$$\frac{C_e}{q_e} = \frac{C_e}{q_m} + \frac{1}{K_L q_m}$$

(2.6)

C_e/ mg/L is the concentration of dye at equilibrium,

q_m / mg/g is the quantity of dye adsorbed at complete monolayer coverage,

q_e / mg/g is the quantity of dye adsorbed at equilibrium,

K_L/ L/mg represents the Langmuirian constant.

A linear plot of $\frac{C_e}{qe}$ as a function of C_e yields the gradient of $\frac{1}{qm}$ and a y-intercept of $1/K_L q_m$. From this, the total adsorption at monolayer coverage can be obtained. To indicate the favourability of adsorption of the Langmuir isotherm, the separation factor is calculated:

$$RL = \frac{1}{(1 + b\ Co)}$$

(2.7)

RL is the unitless separation factor. For favourable adsorption, it must lie $0 < RL < 1$

b is the Langmuir constant

Co is the initial concentration of analyte

RL must lie between zero and one to be regarded as favorable adsorption.

The Freundlich isotherm describes the heterogeneity of an adsorbent. This isotherm is only applicable in media with low concentrations of $[A]$, the concentration of the dyes (Freundlich and Hatfield (1926):

$$\ln(q_e) = lnK_F + \frac{1}{n \ln(C_e)}$$

(2.8)

K_F denotes the adsorption capacity,

$\frac{1}{n}$ represents the adsorption intensity.

A linear plot of $ln\ (qe)$ as a function of $ln\ (Ce)$ yields the gradient of $\frac{1}{n}$ and a y-intercept of $ln\ (K_F)$ and from the linear plot, the extent of heterogeneity can be attained. Should $1 < n < 10$, the sorption process is favourable (Dada *et al.* 2012: 38 – 45).

The Temkin isotherm involves the adsorbent-adsorbate interactions. It indicates that the heat of adsorption decreases linearly as the dyes adsorbed onto the adsorbent surface (equation 2.8) (Temkin and Pyzhev 1940: 327 – 356):

$$q_e = \frac{RT}{b_T}\ lnA_T + \frac{RT}{b_T}\ lnC_e \tag{2.9}$$

A_T/ L/g is the Temkin isotherm equilibrium binding constant,

b_T is the Temkin isotherm constant,

R = 8.314 J/mol.K is the universal gas constant,

T = 298 K is the standard temperature,

$(\frac{RT}{b_T})$ / J/mol is the heat of adsorption constant.

A linear plot of q_e as a function of lnC_e yields the gradient of $\frac{RT}{b_T}$ and a y-intercept of lnA_T. From the plot, A_T value indicates whether the process is physisorption or chemisorption (Dada *et al.* 2012: 38 – 45).

The Frumkin isotherm (Frumkin 1919: 792 – 802) is used to describe the interaction between adsorbed dye molecules onto a homogenous surface of an adsorbent. After taking the log on either sides of equation 2.8,

$$\left(\frac{Q_e}{1} - Q_e\right) e2aQ_e\ =\ KC_e \tag{2.10}$$

$$\log\left(\frac{Q_e}{1} - Q_e\right).\frac{1}{C_e} = \log K +\ 2aQ_e \tag{2.11}$$

A linear plot of $log\ \left(\frac{Q_e}{1} - Q_e\right).\frac{1}{C_e}$ as a function of Q_e from equation 2.10 gives the values of a and K from the slope and intercept respectively. If a it is a positive value, it indicates an

attraction between the dye molecules in the monolayer. A negative value indicated a repulsive interaction.

2.14. Adsorption Kinetics

Adsorption kinetics is a common tool used to determine the order and kinetic fitting of adsorption data in terms of the adsorption diffusion and adsorption reaction models. Both give valuable information on the kinetic processes. The adsorption diffusion model gives information about diffusion of the adsorbate across the film coating the adsorbent particulates (film diffusion), the diffusion of adsorbate molecules within the liquid entrapped within the pores and the pore walls of the adsorbent (intra-particle diffusion) and the adsorption and desorption of adsorbate molecules and the adsorption sites on the adsorbent (mass action). The adsorption reaction models derived from the calculations of chemical kinetics focuses on adsorption diffusion model (Qiu *et al.* 2009: 716 – 724).

The adsorption kinetic mechanisms commonly used are the Langergren's pseudo-first order (Lagergren 1898: 1 – 39), Ho's and McKay's pseudo-second order (McKay 1982: 759 – 772) and the Elovich equation on intraparticle diffusion (Weber and Morris 1962: 231 – 266) from the adsorption diffusion model is also commonly used.

Langergren's pseudo-first order rate equation describes the liquid-solid phase of adsorption based on the adsorption capacity:

$$\log(q_e - q_t) = \log(q_t) - \frac{K_{L1}t}{2.303} \tag{2.12}$$

A plot of $\log(q_e - q_t)$ as a function of t/ min yields a linear graph which k_{L1} can be obtained from the gradient and q_e from the y-intercept (Lagergren 1898: 1 – 39).

The pseudo-second order rate equation rate is based on the capacity of adsorption from concentration of the analyte and is given as (McKay 1982: 759 – 772):

$$\frac{t}{q_t} = \frac{1}{K_{H2}q_e} + \frac{t}{q_e} \tag{2.13.}$$

The intra-particle diffusion mole is usually tested because adsorbate uptake changes proportionately with $t^{0.5}$ and not contact time itself. For an adsorption process where the intra-particle diffusion is the rate-limiting step, a linear plot of q_t as a function of $t^{0.5}$ is obtained:

$$q_t = K_{IPD} t^{0.5} + C \tag{2.14}$$

where K_{IPD} is the intraparticle diffusion rate constant and q_t/ mg/g is the adsorption capacities at time t/ min. From the plot, the K_{IPD} and the intraparticle diffusion constant C can be obtained from the gradient and y-intercept, respectively. According to the model, if the linear curve passes via the origin, this implies that the intraparticle diffusion is the only rate-determining step. Should it not pass the origin, this implies that the rate-limiting step may involve both film and intraparticle diffusion.

2.15. Water Application of Adsorption

The removal of inorganic and organic pollutants from wastewater has been extensively studied using biological, physicochemical and adsorption processes. Activated carbon is commonly used for the removal of hazardous pollutants from aqueous solutions, because it has a large surface area and a high adsorption capacity. However, it is non-selective and requires expensive regeneration processes (Cheng *et al.* 2008: 538 – 546). As an alternative, materials which are available in abundance in nature, recyclable, cheaper and presenting interesting adsorption properties are clay materials (Özcan and Özcan 2004: 39 – 46).

For the past 100 years, adsorption processes have been applied to drinking water for the removal of metals, anionic species and organic pollutants such as phenols, chlorinated hydrocarbons, pesticides and pharmaceutical species (Worch 2012: 1 – 3).

Many adsorbents including activated carbon, activated sludge, polymeric adsorbent, oxidic adsorbents, zeolite and montmorillonite are used for adsorption. Also natural adsorbents, agricultural adsorbents and agricultural wastes and industrial adsorbents are being used because they are inexpensive and readily available. Some examples are presented in Table 2.1.

Table 2.1. Examples of natural, agricultural and industrial adsorbents (Worch 2012: 1 – 3)

Natural adsorbents	Agricultural adsorbents	Industrial adsorbents
Wood	Corncob waste	Bagasse
Coal	Shells	Red mud
Peat	Straw	Palm oil ash
Clays	Fruit peels	Shale oil ash

2.15.1. Activated Alumina

Activated alumina has been used as an absorbent from the 20th century. Due to its high strength, ease of regeneration and large surface area, it is used as a remediation agent in the removal of arsenic and fluoride. It is also used as a remediation tool in industrial and municipal effluents. Activated alumina is advantageous since it can be secured in a bed or it can remove pollutants as filterable grains. It is also a cheaper alternative. This efficiency of adsorption for this material can be pH dependent (Lehr 2004: 1288).

Saha *et al.* (2008: 26 – 32) coated the surface of alumina with trimesic acid to remove Fe (III) and Fe (II) from water. Kluczka *et al.* (2007: 105 – 113) reported the use of activated alumina

for the removal of boron. Even today, these adsorbents are still used and modified to optimize adsorption efficiency. It was reported by Dou *et al.* (2015: 2755 – 2762) that the removal of arsenic from water by alumina could be used for the possible application into rivers. Succinic acid was also removed using alumina adsorbent (İnci *et al.* 2011: 4449 – 4453).

2.15.2. Clay Materials as an Adsorbent

Clay and modified clays are widely used as adsorbents for the removal of ions and organic pollutants from aqueous solutions, due to their low cost, large specific surface areas, mechanical and chemical stabilities, layered structures and high cation-exchange capacities (Wang *et al.* 2012: 519 – 528). Sodium bentonite (SBT) is a 2:1 clay mineral predominantly composed of montmorillonite clay. The surface of bentonite is hydrophilic because inorganic cations, such as Na^{+} and $Ca^{2+,}$ are strongly hydrated in the presence of water. As a result, the adsorption efficiency of natural bentonite for organic molecules is very low. However, the adsorption properties of bentonite can be improved by modifying the clay surface with an organic molecules (Saha *et al.* 2008: 26 – 32) (Gitipour *et al.* 1997: 191 – 198). This is favoured by van der Waals interactions between the organic cations and the reduced solvent shielding of ions in the inter-lamellar environment (Shen 2001: 989 – 995) where the nature of the exchanged mineral surfaces readily changes from hydrophilic to hydrophobic. The bentonite adsorption efficiency depends on a phenomenon called cationic exchange capacity (CEC) which allows for the ionic exchange of pollutant species with their natural cations present in the clay structure. The uptake of pollutant species itself involves many mechanisms such as direct bonding to clay surface, complexation and ion exchange. Although most clays have a negative surface charge, they are still able to adsorb metal ions due to their high porosity size and surface area resulting inorganic pollutants being poorly adsorbed. To increase adsorption, surface modifications are usually made by the addition of salts, acids, bases, surfactants, chelating agents, polymers and other organic and inorganic substances. The four main clay material groups are illite, kaolinite, vermiculite and smectite group (Fig. 2.9). Sodium bentonite (SBT) belongs to the smectite group and carries a negative surface charge. It has three-layer of minerals consisting of two tetrahedral layers sandwiched around a central octahedral layer (Fig. 2.10). The oxide anions at the apices of the tetrahedral subunits face inward where they surround cations such as aluminium, iron, and magnesium which forms the octahedral subunits of the octahedral layer. The bonding that occurs within these layers link them and results in a sheet like structure. The overall negative charge is due to the sum of all the oxide anions (O^{2-})

which is greater than the total positive charge contributed by the sum of all the cations such as Si^{4+}, Al^{3+}, Fe^{2+}, Fe^{3+}, Mg^{2+}.

SBT sheets are approximately 1 nm thick and a few microns in diameter. It has the ability to swell in water, however due to its high absorption capacity it can be dehydrated numerous times without losing its swelling properties. This property makes it a good adsorbent.

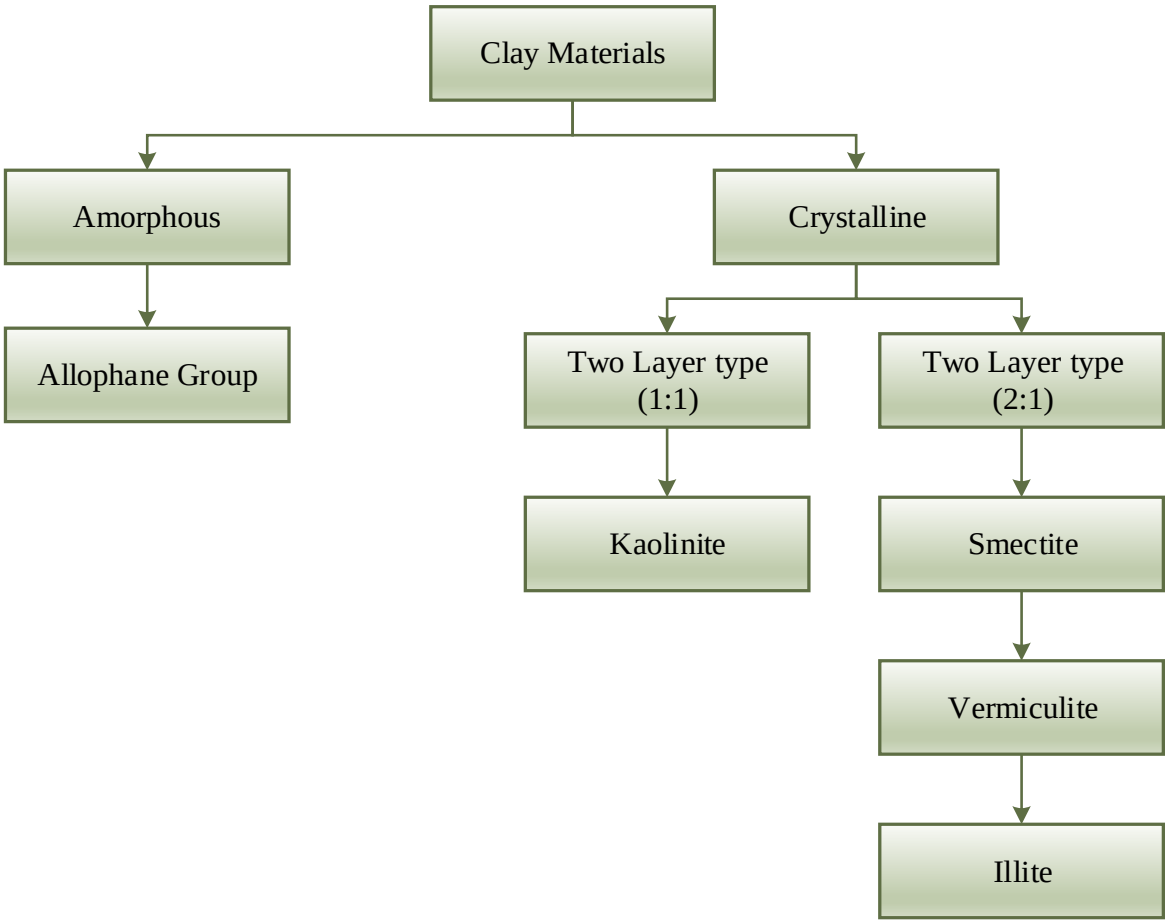

Figure 2.9. Classification of clay materials

A significant number of studies report the use of clays as adsorbents for dyes. A study by Rahman *et al.* (2015: 375-382) compared sepiolite, kaolin and synthetic talc for the removal of Reactive Yellow 138:1, an anionic reactive dye. It was discovered that synthetic talc proved to be a better adsorbent followed by kaolin and sepiolite. Another study confirmed the increase in monolayer coverage capacities with temperature (Tekbaş et al. (2009: 205-211). Sternik et al. (2011: 607-615) found that sodium bentonite adsorbed Basic Red 1 dye better than sodium clinoptilolite due to the larger surface area of the particles compared with sodium clinoptilolite. The comparison of the adsorption dye capacities of the clays are tabulated below (Table 2.2).

Table 2.2. Comparison of the adsorption capacities of various clays

Type of clay	Dye adsorbed	Reported adsorption capacity/ $mg.g^{-1}$	Citation
Illite	Methyl Violet 2B	180.7	Kooh *et al.* (2016: 783)
Vermiculite	Astrazon Red	51.00	Stawiński *et al.* (2017: 107-115)
Smectite	Indanthrene Blue RS	13.92	Chaari *et al.* (2009: 1623-1628)
Kaolinite	Reactive Yellow 138:1	3.73	Rahman *et al.* (2015: 375-382)

2.15.3. Literature Survey of Bentonite

Numerous investigations of bentonite and modified bentonite have been undertaken and are also continuing because of the excellent physio-chemical properties of bentonite to remove organic and inorganic pollutants from the environment. The removal of malachite green, a cationic dye , from an aqueous solutions was reported (Tahir and Rauf 2006: 1842 – 1848). They observed that adsorption decreased when the temperature of the dye solution was increased. Other analytes that were adsorbed by bentonite included Methylene Blue (Hong *et al.* 2009: 630 – 633) (Leodopoulos *et al.* 2015: 74 – 107) (Bulut and Karaer 2015: 1635 – 1644). It was found that the adsorption process was also endothermic and at higher temperatures, adsorption process became more effective. Bentonite was also used to remove a pharmaceutical ingredient, amoxicillin, from water (Putra *et al.* 2009: 2419 – 2430). It was found that although bentonite adsorbed less amoxicillin, it could still be used as alternative especially since activated carbon is expensive.

A thermodynamic study was conducted for the adsorption of nickel (II) from an aqueous solutions (Tahir and Rauf 2003: 2003 – 2009). They reported that it followed the Langmuir, Freundlich and Dubinin–Radushkevich isotherms and adsorption was endothermic: the adsorption process is normally exothermic and therefore this study proved otherwise. Tahir and Naseem (2007: 312 – 321) reported the uptake of chromium (III) from a tannery effluent: adsorption followed the Langmuir isotherm and the reaction was endothermic and spontaneous. It was reported that zinc adsorbs onto bentonite at pH 8.00 concluding that physisorption, a spontaneous and endothermic adsorption occurred (Bellir *et al.* 2013: 5035 – 5048). It was also reported that the removal of silver using a fixed-bed bentonite column, was more effective than

static adsorption (Cantuaria *et al.* 2015: 91 – 104). Salman *et al.* (2007: 51 – 56) found that the exposure of hydrochloric acid onto the bentonite surface hindered the adsorption of humic acid because it decreased the aluminium oxide and ferrous oxide content in the bentonite. Amari *et al.* (2010: 457 – 461) observed that toluene was adsorbed better on H_2SO_4-activated bentonite than on raw bentonite. Magnoli *et al.* (2014: 2063 – 2070) observed that tryptophan adsorbed better onto sodium bentonite than aflatoxin. Tahir and Rauf (2004: 285 – 292) found that common cations such as zinc, manganese, lead, cadmium, nickel, cobalt and chromium hindered the adsorption of iron.

For adsorbates that do not adsorb easily on bentonite, surface modifications are usually carried out. The use of surfactants, polymers and organic compounds to produce organo-composites were studied. Herein the surface of the bentonite clay was altered so as to be more affinitive to the selected target analyte. Alginate bentonite composite was used to remove phenol from aqueous solutions. Better adsorption occurred than a powdered F400 carbon and bentonite composite (Hank *et al.* 2014: 2256 – 2263). A study in 2008 reported a polyacrylamide intercalated bentonite to remove humic acid in aqueous solutions (Anirudhan *et al.* 2008: 147 – 156). This composite was also used to remove lead, radium, actinium and thallium (Şimşek *et al.* 2003: 315 – 321). Another study reported the use of polypyrrole as an intercalating agent to bentonite for the removal of zinc and cadmium from aqueous solutions. The adsorption followed a Langmuir plot as the metals were highly affinitive to the surface of the modified bentonite (Ben Bouabdallah and Djelali 2015: 321 – 330). Natural polymers such as chitosan were also used to intercalate into bentonite for the removal of methylene blue (Bulut and Karaer 2015: 61 – 67). Chitosan modified adsorbents were also used in the removal of amido black 10B which adsorbed at lower pH values (Liu *et al.* 2015: 1129 – 1135). Other modifying agents used to customize and enhance the adsorption of selected analytes by bentonite are presented in Table 2.3.

Table 2.3. Modifying agents used in bentonite for adsorption

Modifying agent	Analytes removed	Medium	Citation
Polyurethane	Moisture	-	Pinto *et al.* (2007: 885 – 892)
humic acid-immobilized-amine-modified polyacrylamide	Copper, Zinc, Cobalt	Aqueous solution	Anirudhan and Suchithra (2010: 146 – 156)
cetylpyridinium	Reactive Red 120	Aqueous solution	Tabak *et al.* (2010: 1199 – 1207)
N-2-hydroxypropyl trimethyl ammonium chloride chitosan	Cadmium	Aqueous solution	Huang *et al.* (2011: 297 – 304)
Hexadecyltrimethyl-ammonium bromide	Thorium	Aqueous solution	Wang *et al.* (2012: 519 – 528)
Carbon nanotube	Cesium	Aqueous solution	Yang *et al.* (2014: 46 – 52)
4-vinylpyridine	Toluene	Aqueous solution	Mansri and Ramdani (2015: 1765 – 1776)

Other possible methods for removal of dyes include the use of nanocomposites, in particular, those containing nanoparticles. This is favoured due to their ability to reduce the organic dye into a new product which might show less toxicity than the initial dye used.

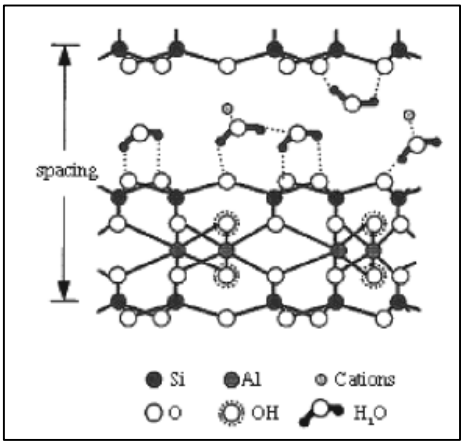

Figure 2.10. The (2:1) layer of bentonite with its constituents, Siebers (2009: 1)

2.16. General Introduction to Gold Nanoparticles

Recently the use of gold nanoparticles (AuNPs) has captured the attention of researchers because they can be easily synthesized and their size and shape (Table 2.4) can be controlled by using proper reagents and conditions. In general, nanoparticles can either be monodispersed, nanoparticles of the same average size, or polydispersed, nanoparticles of various sizes. The nanoparticles are useful in chemical, biological and physical systems because of its small size of less than 100 nm. Properties such as increased catalytic activity, better heat and electrical conductivity, improved photoemissions and surface modifications are reported (Thakor 2011: 4029 – 4036). Many shapes of AuNPs are reported such as nanorods, nanowires, nanospheres, nanostars, nanocubes, nanoboxes and nanoprisms (Zhang *et al.* 2015: 1 – 12) (Langille *et al.* 2012: 14542 – 14554). AuNPs of sizes less than 100 nm usually exist in aqueous medium whilst those of less than 3 nm exhibit outstanding catalytic activity (Abdelhalim *et al.* 2012: 1 – 5).

Table 2.4. Previous studies showing of various shapes of AuNPs

Shape of gold nanoparticles	Application	Citation
Triangles	Vapour sensing	Ankamwar *et al.* (2005: 19 – 26)
Spheres	Antioxidant capacity	Vilela *et al.* (2012: 341 – 349)
Rods	Sensing applications	Vigderman *et al.* (2012: 4811 – 4841)
Cubes	4-Nitroaniline Reduction	Chiu *et al.* (2012: 23757 – 23763)
Octahedra	4-Nitroaniline Reduction	Chiu *et al.* (2012: 23757 – 23763)
Stars	Biomedical application	Chirico *et al.* (2015: 80)

2.16.1. The Surface Plasmon Resonance Phenomenon

All metal nanoparticles have surface plasmon resonance which is a consequence of the oscillation of mobile electrons at the surface of the metal film. When the wave vector of the incident light matches the wavelength of the surface plasmons, the electrons will "resonate", hence the term surface plasmon resonance. The 'coupling' of the incident light to the surface plasmons results in a loss of energy and therefore a reduction in the intensity of the reflected light will arise (Fig. 2.11) The AuNPs usually exhibit an absorption peak in the UV profile between 500 nm to 600 nm. Two characteristic trends are witnessed in the UV profile of AuNPs: the red coloured solutions containing AuNPs exhibit narrow, tall peaks which leans towards a blue shift whilst the blue/purple AuNPs exhibit broad, stomped peaks which leans towards a red shift.

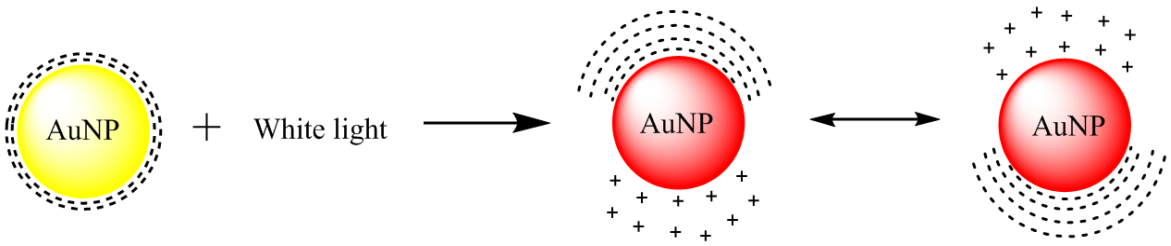

Figure 2.11. Illustration of surface plasmon resonance of a gold nanoparticle

2.16.2. Some Properties of Gold Nanoparticles

AuNPs have high surface energies which promote their coagulation and aggregation in order to reach stability. When gold nanoparticles aggregate, a red shift (blue/purple appearance) is observed by their UV profile. Furthermore the red/crimson colour of the solution mixture indicates that the size of AuNPs are smaller compared to blue/purple coloured solutions. In order to prevent excessive aggregation of nanoparticles, a stabilizing, capping, agent is usually added.

2.16.3. Synthesis of Gold Nanoparticles

There are many methods for the syntheses of AuNPs which produce different shapes (Fig. 2.12) which are used for different applications as summarized in Table 2.4. The well-known methods are the Turkevich, Brust and Perrault methods, whilst green synthesis and sonolysis are also reported. Other methods include photo-reduction, electrochemistry, sonochemistry and galvanic replacement (Li 2015: 1756 – 1789). There are two skeletal approaches to the synthesis of AuNPs: the "top-down" approach and the "bottom-up" approach (Fig. 2.13).

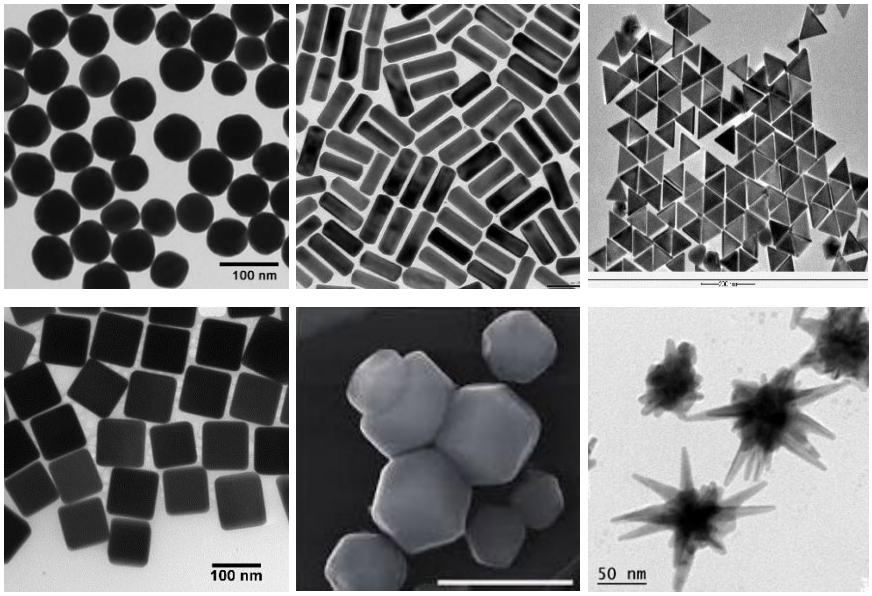

Figure 2.12. Gold (a) nanospheres, (b) nanorods, (c) nanotriangles, (d) nanocubes, (e) nanopolyhedra and (f) nanostars (Khlebtsov and Dykman 2011: 1647 – 1671)

The "top-down" approach (Fig. 14) describes the synthesis plan such that bulk gold is broken down into nanoscale particles. This method is achieved by specialized techniques such as

electron-beam lithography, focused ion beam lithography and on-wire lithography. In the "bottom-up" approach, the dissolved gold salt in the medium is grown into AuNPs.

Turkevich *et al.* (1951: 55 – 75) discovered a simple method for producing monodisperse AuNPs by the addition of sodium citrate to a boiling gold solution (Fig. 2.13). They reported that the nanoparticles formed instantly, first forming nanorods (purple coloured solution) then gold nanospheres (crimson coloured solution). The citrate played two key roles: one was to reduce the gold (III) solution to AuNPs and second, to cap the AuNPs to prevent aggregation.

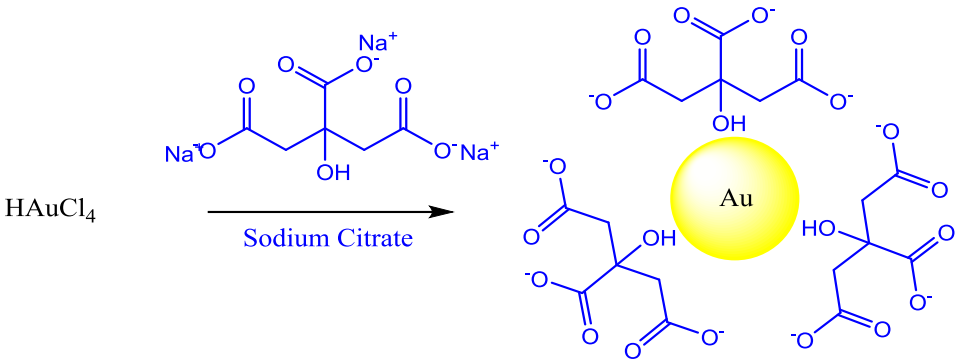

Figure 2.13. A schematic diagram for the synthesis of gold nanoparticle by the Turkevich method

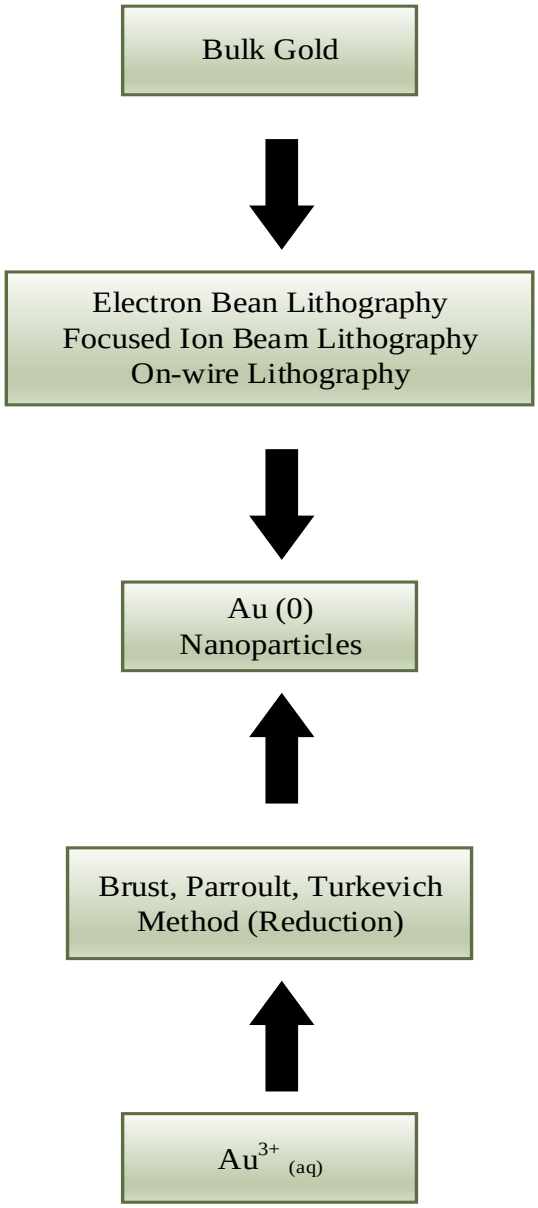

Figure 2.14. Illustration of the top-down approach and the bottom-up approach

The Brust-Schiffrin method was discovered in the 1990's (Hussain *et al.* 2003: 4831 – 4835) (Brust *et al.* 1995: 1655 – 1656). Here, the synthesis of AuNPs was with a thiolated molecules in a non-immiscible organic liquid such as toluene. The reagents consisted of a solution of tetraoctylammonium bromide (TOAB) in toluene and sodium borohydride (Brust *et al.* 1995: 795 – 797) where the latter was the reducing agent and TOAB was the capping agent. The TOAB, due to its surfactant properties, assisted in transporting the dissolved gold and the sodium citrate into toluene. The AuNPs were capped with the hydrophobic thiolated compound which allowed for its isolation and dispersion in other organic solvents (Schmid and Corain

2003: 3081 – 3098). This method is widely used to synthesize monolayer protected clusters due to its ease of synthesis. The general reaction for the synthesis of AuNPs by the Brust-Schiffrin method is presented in Fig. 2.15 (Brust *et al.* 1995: 1655 – 1656)

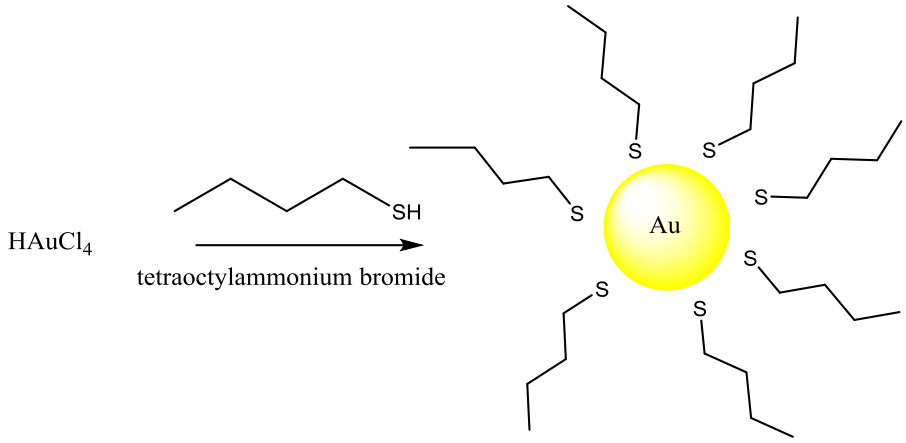

Figure 2.15. A schematic diagram for the synthesis of gold nanoparticle by the Brust-Schiffrin method

Another more favoured method for the synthesis of gold nanoparticles, classified as a green method, is by using plant extracts which contain organic compounds which can reduce the gold solution. The advantages of using green methodology is that the use of toxic chemicals and solvents are eliminated, unreacted chemicals can be easily disposed, there is low energy consumption for the reaction and the materials are renewable. In most cases there is no need for a stabilizing agent since plant extracts have an abundance of natural compounds which might prevent aggregation of nanoparticles. Some possible reducing agents include carotenoids, isoprenes, reducing sugars, flavonoids and polyphenols. Also biological organisms such as algae and bacteria can reduce gold (III) solutions to AuNPs. Some examples of "green" synthetic methods for the formation of colloidal gold is summarized in Table 2.5.

Table 2.5. Green synthetic methods for the formation of gold nanoparticles

Plant Extract	Application	Citation
Grape seeds, skin and stalk	Experimental design	Krishnaswamy *et al.* (2014: 210 – 220)
Argemone mexicana L. Leaf	-	Varun *et al.* (2015: 42 – 44)
Stevia rebaudian aleaf	Stability	Sadeghi *et al.* (2015: 101 – 106)
Honey	-	Philip (2009: 650 – 653)
Cinnamomum zeylanicum leaf	-	Smitha *et al.* (2009: 735 – 739)
Abroma augusta Linn bark	Catalytic reduction	Das *et al.* (2014: 867 – 873)
Lantana camara Linn	Catalytic activity	Dash *et al.* (2014: 343 – 350)
Gelatin	Biological effects on Osteoblast cells	Suarasan *et al.* (2015: 1222 – 131)
Moringa oleifera petals	Anti-cancer and catalytic activity	Anand *et al.* (2015: 1105 – 1111)
Casein hydrolytic peptides	Anti-cancer assessment (DU145 cell line)	Ghodake *et al.* (2016: 185 – 189)
Zizyphus mauritiana	Antibacterial activity	Sadeghi (2015: 265 – 273)
Blue green alga	Antibacterial efficacy	Uma Suganya *et al.* (2015: 351 – 356)
Streptomyces clavuligerus	Inducing mitotic arrest (G2/M phase)	Ganesh *et al.* (2015: 18738 – 18750)
Green tea	Anti-tumor activities and hepatoprotection	Mukherjee *et al.* (2015: 1283 – 1297)

Stabilizing agents play an important role in determining the shape and size of AuNPs. Stabilizers such as dendrimers (Giorgetti *et al.* 2009: 3731 – 3753), surfactants (Giorgetti *et al.* (2009: 3731 – 3753), ligands (Nath *et al.* 2010: 333 – 352), ionic liquids (Dong *et al.* 2014: 465 – 471) and polymers are used. These capping agents provide stability of the AuNPs by preventing Ostwald ripening by creating steric and electrostatic hindrance. Usually, molecules that are present in the AuNPs medium will bind to the surface of the AuNPs by electrostatic attraction or by covalent bonding. When this occurs, a double layer of charge occurs within the region of AuNPs surface thus hindering the aggregation of the AuNPs and thereby preventing particle size growth. Usually an organic compound is added into the reaction medium as illustrated by the Turkevich method where citrate acts as a capping agent by weakly associating itself to the surface of AuNPs

Polymers, especially water soluble polymers, can also be used to stabilize AuNPs. Here the long polymer chain and suitable functional groups present in the polymer provide adequate steric and/or electrostatic hindrance between individual AuNPs. They usually form core-shell nanostructures with AuNPs: the polymer is the shell and AuNPs is the core (Fig. 2.16).

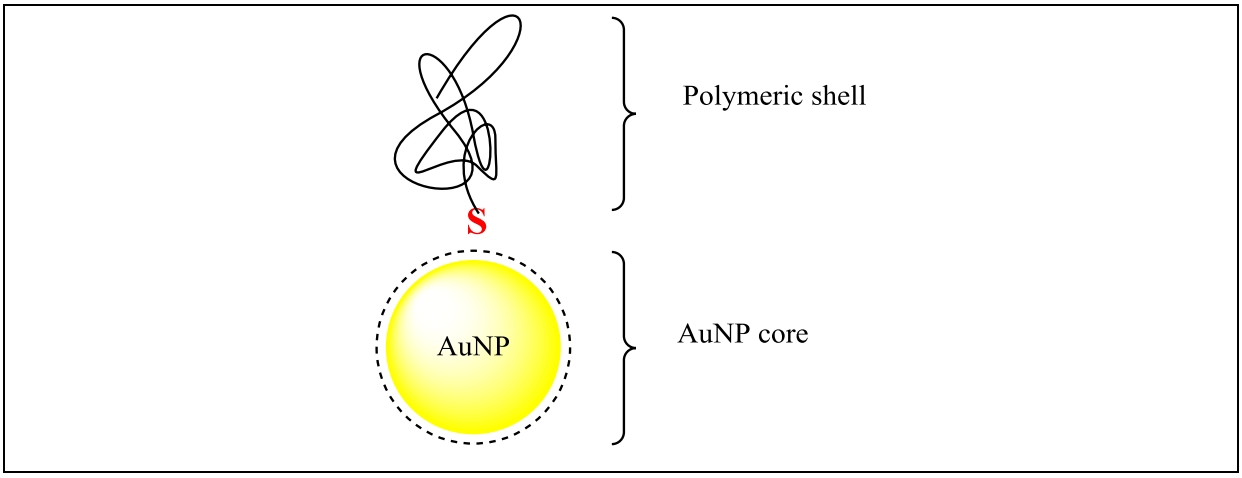

Figure 2.16. Depiction of the core-shell structured AuNPs

Many studies have been undertaken with different types of polymers in synthesizing AuNPs. Yang *et al.* (2012: 939 – 946) reported on a conjugated water-soluble polyfluorene compound which capped the AuNPs and imparted a fluorescent colour whilst Chili and Revaprasadu (2008: 3896 – 3899) used polyvinylpyrrolidone as the capping agent. Other water-soluble polymers include 3-*n*-propyl-4-picolinium silsesquioxane chloride (Silva *et al.* 2014: 70 – 77),

polythiophene (Guan *et al.* 2008: 319 – 324) (Panda and Chattopadhyay 2007: 962 – 967), poly (4-vinyl phenol) (Maji *et al.* 2014: 51745 – 51753) and chitosan (Tsai *et al.* 2013: 86 – 91).

Organo-sulphur compounds such as the thiols, disulphides and thioethers were also used as capping agents. Thiols were found to be better stabilizers better than disulfides and thioethers however polymeric thioethers are better than thioethers. Andrews *et al.* (2010: 59) reported that by carefully selecting the capping agent, the shelf life of AuNPs can be improved whilst either retaining or improving its applicability in various applications. Sulphur based capping agents include polymeric thiolated monoethyl ethers (Shimmin *et al.* 2004: 5613 –5620) dihydrolipoic acid (Roux *et al.* 2005: 2526 – 2536), cysteine (Aryal *et al.* (2006: 160 – 163), 5-amino-2-mercapto-1,3,4-thiadiazole (Kannan and John 2011: 7029 – 7037), polythiophenes (Kannan and John 2011: 7029 – 7037) and phenothiazine (Gupta *et al.* 2014: 793 – 798).

2.17. Analytical techniques for characterizing gold nanoparticles

The main technique that is used to confirm the presence of AuNPs is UV/Visible spectroscopy. The spectrum exhibits a characteristic absorbance in the range 500 nm – 600 nm due to the surface plasmon resonance. Dynamic light scattering studies are carried out to determine the surface charge, stability and the average size of the AuNPs. Usually they bear a negatively-charged surface, unless the AuNPs are capped with positively-charged compounds. Transmission electron microscopy gives the morphology of the AuNPs which is the shape and size distribution of AuNPs. Energy-dispersive X-ray Spectroscopy gives the elemental composition of the capped-AuNPs. X-ray Photoelectron Spectroscopy provides the type of bonds between elements present in the AuNPs and their binding energies. FT-IR Spectroscopy can be done with attenuated total reflectance to determine the functional groups of organic compounds present.

2.18. References

Abdelhalim, M. a. K., Mady., M. M.and Ghannam., M. M. 2012. Physical properties of different gold nanoparticles: Ultraviolet-visible and fluorescence measurements. *Nanomedicine & Nanotechnology*, 3 (3): 1 – 5.

Adrosko, R. J. 2012. Natural Dyes and Home Dyeing. 1st ed. New York: Dover Publications.

Ahmed, F., Alim, A., Alam, F., Islam, T.and Talukder, A. 2015. Bio-Geo-Chemical Characterization of Bangladeshi Textile Effluents. *Advances in Microbiology*, 5 (5): 317 – 324.

Amari, A., Chlendi, M., Gannouni, A.and Bellagi, A. 2010. Optimised activation of bentonite for toluene adsorption. *Applied Clay Science*, 47 (3–4): 457 – 461.

Amuda, O. S., Giwa, A. A.and Bello, I. A. 2007. Removal of heavy metal from industrial wastewater using modified activated coconut shell carbon. *Biochemical Engineering Journal*, 36 (2): 174 – 181.

Anand, K., Gengan, R. M., Phulukdaree, A.and Chuturgoon, A. 2015. Agroforestry waste Moringa oleifera petals mediated green synthesis of gold nanoparticles and their anti-cancer and catalytic activity. *Journal of Industrial and Engineering Chemistry*, 21: 1105 – 1111.

Andrews, D., Scholes, G.and Wiederrecht, G. eds. 2010. *Comprehensive Nanoscience and Technology*, London: Academic Press.

Anirudhan, T. S.and Suchithra, P. S. 2010. Heavy metals uptake from aqueous solutions and industrial wastewaters by humic acid-immobilized polymer/bentonite composite: Kinetics and equilibrium modeling. *Chemical Engineering Journal*, 156 (1): 146 – 156.

Anirudhan, T. S., Suchithra, P. S.and Rijith, S. 2008. Amine-modified polyacrylamide-bentonite composite for the adsorption of humic acid in aqueous solutions. *Colloids and Surfaces A: Physicochemical and Engineering Aspects*, 326 (3): 147 – 156.

Ankamwar, B., Chaudhary, M.and Sastry, M. 2005. Gold nanotriangles biologically synthesized using tamarind leaf extract and potential application in vapor sensing. *Synthesis and Reactivity in Inorganic, Metal-Organic, and Nano-Metal Chemistry*, 35 (1): 19 – 26.

Aryal, S., Remant, B. K. C., Dharmaraj, N., Bhattarai, N., Kim, C. H.and Kim, H. Y. 2006. Spectroscopic identification of SAu interaction in cysteine capped gold nanoparticles. *Spectrochimica Acta Part A: Molecular and Biomolecular Spectroscopy*, 63 (1): 160 – 163.

Asanov, A. A.and Matniyazova, G. K. 2012. Flocculation purification of turbid waters by means of carboxyl – amide water – soluble polymers. *Journal of Water Chemistry and Technology,* 34 (4): 200 – 204.

Aspland, J. R. 1997. Textile Dyeing and Colouration. 1st ed. North Carolina: American Association of Textile Chemists and Colourists.

Atkins, P.and De Paula, J. 2014. Atkins' Physical Chemistry. OUP Oxford.

Banerjee, C., Ghosh, S., Sen, G., Mishra, S., Shukla, P.and Bandopadhyay, R. 2013. Study of algal biomass harvesting using cationic guar gum from the natural plant source as flocculant. *Carbohydrate Polymers,* 92 (1): 675 – 681.

Bellir, K., Lehocine, M. B.and Meniai, A. H. 2013. Zinc removal from aqueous solutions by adsorption onto bentonite. *Desalination and Water Treatment,* 51 (25 – 27): 5035 – 5048.
Ben Bouabdallah, A.and Djelali, N. E. 2015. Adsorption of zinc and cadmium from aqueous solutions using bentonite/polypyrrole composite. *Revue Roumaine De Chimie,* 60 (4): 321 – 330.

Brust, M., Bethell, D., Schiffrin, D. J.and Kiely, C. J. 1995. Novel gold-dithiol nano-networks with non-metallic electronic properties. *Advanced Materials,* 7 (9): 795 – 797.

Brust, M., Fink, J., Bethell, D., Schiffrin, D. J.and Kiely, C. 1995. Synthesis and reactions of functionalised gold nanoparticles. *Journal of the Chemical Society, Chemical Communications,* (16): 1655 – 1656.

Bulut, Y.and Karaer, H. 2015. Adsorption of methylene blue from aqueous solution by crosslinked chitosan/bentonite composite. *Journal of Dispersion Science and Technology,* 36 (1): 61 – 67.

Bulut, Y.and Karaer, H. 2015. Removal of Methylene Blue from Aqueous Solution by Crosslinked Chitosan-g-Poly(Acrylic Acid)/Bentonite Composite. *Chemical Engineering Communications,* 202 (12): 1635 – 1644.

Cantuaria, M. L., Nascimento, E. S., Neto, A. F. A., Dos Santos, O. a. A.and Vieira, M. G. A. 2015. Removal and recovery of silver by dynamic adsorption on bentonite clay using a fixed-bed column system. *Adsorption Science & Technology,* 33 (2): 91 – 104.

Chaari, I., Feki, M., Medhioub, M., Bouzid, J., Fakhfakh, E.and Jamoussi, F. 2009. Adsorption of a textile dye "Indanthrene Blue RS (C.I. Vat Blue 4)" from aqueous solutions onto smectite-rich clayey rock. *Journal of Hazardous Materials,* 172 (2 – 3): 1623 – 1628

Cheng, W., Wang, S. G., Lu, L., Gong, W. X., Liu, X. W., Gao, B. Y.and Zhang, H. Y. 2008. Removal of malachite green (MG) from aqueous solutions by native and heat-treated anaerobic granular sludge. *Biochemical Engineering Journal,* 39 (3): 538-546.

Cheremisinoff, N. P. (ed.) 1989. *Handbook of polymer science and technology: Performance properties of elastics and elastomers,* New York: Marcel Dekker, Inc.

Chesters, S. P., Darton, E. G., Gallego, S.and Vigo, F. D. 2009. The safe use of cationic flocculants with reverse osmosis membranes. *Desalination and Water Treatment,* 6 (1 – 3): 144 – 151.

Chili, M. M.and Revaprasadu, N. 2008. Synthesis of anisotropic gold nanoparticles in a water-soluble polymer. *Materials Letters,* 62 (23): 3896 – 3899.

Chirico, G., Borzenkov, M.and Pallavicini, P. 2015. Physical Properties of Gold Nanostars. *Gold Nanostars: Synthesis, Properties and Biomedical Application*. 1st ed. Switzerland: Springer International Publishing.

Chiu, C. Y., Chung, P. J., Lao, K. U., Liao, C. W.and Huang, M. H. 2012. Facet-Dependent Catalytic Activity of Gold Nanocubes, Octahedra, and Rhombic Dodecahedra toward 4-Nitroaniline Reduction. *The Journal of Physical Chemistry C*, 116 (44): 23757 – 23763.

Cho, D.-W., Chon, C.-M., Kim, Y., Jeon, B.-H., Schwartz, F. W., Lee, E.-S.and Song, H. 2011. Adsorption of nitrate and Cr(VI) by cationic polymer-modified granular activated carbon. *Chemical Engineering Journal*, 175: 298 – 305.

Cho, M. S., Song, B. K.and Yoon, K. J. 2002. Flocculation Characteristics of Copolymer of Acrylamide with Quaternary Ammonium Cationic Monomer (Running) Flocculation by Cationic polyacrylamide. *Journal of Industrial and Engineering Chemistry*, 8 (2): 131 – 137.

Choudhury, A. K. R. 2006. Textile Preparation and Dyeing. 1st ed. New Hampshire: Science Publishers.

Dada, A. O., Olalekan, A. P., Olatunya, A. M.and Dada, O. 2012. Langmuir, Freundlich, Temkin and Dubinin-Radushkevich Isotherms Studies of Equilibrium Sorption of Zn^{2+} Unto Phosphoric Acid Modified Rice Husk. *IOSR Journal of Applied Chemistry* 3(1): 38 – 45.

Das, S., Bag, B. G.and Basu, R. 2014. Abroma augusta Linn bark extract-mediated green synthesis of gold nanoparticles and its application in catalytic reduction. *Applied nanoscience*, 5 (7): 867 – 873.

Dash, S. S., Bag, B. G.and Hota, P. 2014. Lantana camara Linn leaf extract mediated green synthesis of gold nanoparticles and study of its catalytic activity. *Applied nanoscience*, 5 (3): 343 – 350.

Dong, M., Nan, Z., Liu, P., Zhang, Y., Xue, Z., Lu, X.and Liu, X. 2014. Two-phase synthesis of hydrophobic ionic liquid-capped gold nanoparticles and their application for sensing cholesterol. *Electrochimica Acta*, 132: 465 – 471.

Dou, J., Qin, W., Ding, A., Xie, E., Zheng, L.and Ding, W. 2015. Engineering application of activated alumina adsorption dams for emergency treatment of arsenic-contaminated rivers. *Environmental Technology*, 36 (21): 2755 – 2762.

Elliott, E. 2005. Polymers and People: An Informal History. Chemical Heritage Foundation.

Erkurt, H. A. (ed.) 2010. *Biodegradation of Azo Dyes*, Heidelberg: Springer-Verlag Berlin Heidelberg.

Fast, S. A.and Gude, V. G. 2015. Ultrasound-chitosan enhanced flocculation of low algal turbid waters. *Journal of Industrial and Engineering Chemistry,* 24: 153 – 160.

Fontanille, Y. G., Dunod. 2002. *A History of Polymers* (online). Paris. Available: http://www.polymerexpert.fr/en/presentation/histoire – des – polymeres/ [Accessed 10 June 2014].

Freundlich, H.and Hatfield, H. 1926. Colloid [and] capillary chemistry. London: Methuen.

Frumkin, A. N. 1919. By influencing the adsorption of neutral molecules by an electric field. *Zeitschrift für Physik A Hadrons and Nuclei* 35 (10): 792 – 802.

Ganesh, K. C., Poornachandra, Y.and Chandrasekhar, C. 2015. Green synthesis of bacterial mediated anti-proliferative gold nanoparticles: inducing mitotic arrest (G2/M phase) and apoptosis (intrinsic pathway). *Nanoscale,* 7 (44): 18738 – 18750.

Ghodake, G., Kim, D. Y., Jo, J. H., Jang, J.and Lee, D. S. 2016. One-step green synthesis of gold nanoparticles using casein hydrolytic peptides and their anti-cancer assessment using the DU145 cell line. *Journal of Industrial and Engineering Chemistry,* 33: 185 – 189.

Giles, C. H., Macewan, T. H., Nakhwa, S. N.and Smith, D. 1960. Studies in adsorption. Part XI. A system of classification of solution adsorption isotherms, and its use in diagnosis of adsorption mechanisms and in measurement of specific surface areas of solids. *Journal of the Chemical Society* 3:3973 – 3993.

Giorgetti, E., Giusti, A., Giammanco, F., Marsili, P.and Laza, S. 2009. Dendrimer-Capped Nanoparticles Prepared by Picosecond Laser Ablation in Liquid Environment. *Molecules,* 14 (9): 3731 – 3753.

Gitipour, S., Bowers, M.and Bodocsi, A. 1997. The Use of Modified Bentonite for Removal of Aromatic Organics from Contaminated Soil. *Journal of Colloid and Interface Science,* 196 (2): 191 – 198.

Goel, N. K., Kumar, V., Misra, N.and Varshney, L. 2015. Cellulose based cationic adsorbent fabricated via radiation grafting process for treatment of dyes waste water. *Carbohydrate Polymers,* 132: 444 – 451.

Guan, H., Zhou, P., Zhou, X.and He, Z. 2008. Sensitive and selective detection of aspartic acid and glutamic acid based on polythiophene-gold nanoparticles composite. *Talanta,* 77 (1): 319 – 324.

Guerra, E. S.and Eduardo, V. L. 2013. Handbook of Polymer Synthesis, Characterization, and Processing. 1st ed. New Jersey: John Wiley & Sons.

Gupta, S., Singh, A. K., Jain, R. K., Chandra, R.and Prakash, R. 2014. Phenothiazine -Capped Gold Nanoparticles: Photochemically Assisted Synthesis and Application in Electrosensing of Phosphate Ions. *Chemelectrochem,* 1 (4): 793 – 798.

Hank, D., Azi, Z., Ait Hocine, S., Chaalal, O.and Hellal, A. 2014. Optimization of phenol adsorption onto bentonite by factorial design methodology. *Journal of Industrial and Engineering Chemistry,* 20 (4): 2256 – 2263.

Hong, S., Wen, C., He, J., Gan, F.and Ho, Y. S. 2009. Adsorption thermodynamics of Methylene Blue onto bentonite. *Journal of Hazardous Materials,* 167 (1 – 3): 630 – 3.

Huang, R., Wang, B., Yang, B., Zheng, D.and Zhang, Z. 2011. Equilibrium, kinetic and thermodynamic studies of adsorption of Cd(II) from aqueous solution onto HACC–bentonite. *Desalination,* 280 (1–3): 297 – 304.

Hussain, I., Brust, M., Papworth, A. J.and Cooper, A. I. 2003. Preparation of Acrylate-Stabilized Gold and Silver Hydrosols and Gold−Polymer Composite Films. *Langmuir,* 19 (11): 4831 – 4835.

İnci, İ., Bayazit, Ş. S.and Aşçi, Y. S. 2011. Separation of Succinic Acid from Aqueous Solution by Alumina Adsorption. *Journal of Chemical & Engineering Data,* 56 (12): 4449 – 4453.

John, C., Crittenden, R., Rhodes Trussell, David W. Hand, J., K.and Howe, G. 2012. Water Treatment: Principles and Design. 3rd ed. New Jersey: John Wiley & Sons.

Kannan, P.and John, S. A. 2011. Fabrication of conducting polymer-gold nanoparticles film on electrodes using monolayer protected gold nanoparticles and its electrocatalytic application. *Electrochimica Acta,* 56 (20): 7029 – 7037.

Karthik, V., Saravanan, K., P.Bharathi, V.Dharanyaand C.Meiara 2014. An overview of treatments for the removal of textile dyes. *Journal of Chemical and Pharmaceutical Sciences,* 7 (4): 301 – 307.

Khlebtsov, N.and Dykman, L. 2011. Biodistribution and toxicity of engineered gold nanoparticles: a review of in vitro and in vivo studies. *Chemical Society Reviews,* 40 (3): 1647 – 1671.

Kim, E. K.and Walker, H. W. 2001. Effect of cationic polymer additives on the adsorption of humic acid onto iron oxide particles. *Colloids and Surfaces A: Physicochemical and Engineering Aspects,* 194 (1–3): 123 – 131.

Kim, H.-C., Shang, X., Huang, J.-H.and Dempsey, B. A. 2014. Treating laundry waste water: Cationic polymers for removal of contaminants and decreased fouling in microfiltration. *Journal of Membrane Science,* 456: 167 – 174.

Kluczka, J., Trojanowska, J., Zolotajkin, M., Ciba, J., Turek, M.and Dydo, P. 2007. Boron Removal from Wastewater Using Adsorbents. *Environmental Technology,* 28 (1): 105 – 113.

Kooh, M. R. R., Dahri, M. K., Lim, L. B. L., Lim, L. H.and Malik, O. A. 2016. Batch adsorption studies of the removal of methyl violet 2B by soya bean waste: isotherm, kinetics and artificial neural network modelling. *Environmental Earth Sciences,* 75 (9): 783

Krishnaswamy, K., Vali, H.and Orsat, V. 2014. Value-adding to grape waste: Green synthesis of gold nanoparticles. *Journal of Food Engineering*, 142: 210 – 220.

Lagergren, S. 1898. Zur theorie der sogenannten adsorption gelˆster stoffe. Kungliga

Svenska Vetenskapsakademiens. *Handlingar*, 24 (4): 1 – 39.

Langille, M. R., Personick, M. L., Zhang, J.and Mirkin, C. A. 2012. Defining rules for the shape evolution of gold nanoparticles. *Journal of the American Chemical Society*, 134 (35): 14542 – 14554.

Langmuir, I. 1918. The adsorption of gases on plane surfaces of glass, mica and platinum. *Journal of the American Chemical Society*, 40 (9): 1361 – 1403.

Lehr, J. H. (ed.) 2004. *Wiley's Remediation Technologies Handbook: Major Contaminant: Chemicals and Chemical Groups*, New Jersey: John Wiley & Sons.

Leodopoulos, C., Doulia, D.and Gimouhopoulos, K. 2015. Adsorption of Cationic Dyes onto Bentonite. *Separation & Purification Reviews*, 44 (1): 74 – 107.

Li, Q. 2015. Anisotropic Nanomaterials: Preparation, Properties, and Applications. *Angewandte Chemie*, 53 (7): 1756 – 1789.

Li, Q., Yue, Q.-Y., Sun, H.-J., Su, Y.and Gao, B.-Y. 2010. A comparative study on the properties, mechanisms and process designs for the adsorption of non-ionic or anionic dyes onto cationic-polymer/bentonite. *Journal of Environmental Management*, 91 (7): 1601 – 1611.

Li, Q., Yue, Q. Y., Su, Y., Gao, B. Y.and Li, J. 2009. Two-step kinetic study on the adsorption and desorption of reactive dyes at cationic polymer/bentonite. *Journal of Hazardous Materials*, 165 (1–3): 1170 – 1178.

Li, Q., Yue, Q. Y., Su, Y., Gao, B. Y.and Sun, H. J. 2010. Equilibrium, thermodynamics and process design to minimize adsorbent amount for the adsorption of acid dyes onto cationic polymer-loaded bentonite. *Chemical Engineering Journal*, 158 (3): 489 – 497.

Liu, Q., Yang, B., Zhang, L.and Huang, R. 2015. Adsorption of an anionic azo dye by cross-linked chitosan/bentonite composite. *International Journal of Biological Macromolecules,* 72: 1129 – 1135.

Magnoli, A. P., Copia, P., Monge, M. P., Magnoli, C. E., Dalcero, A. M.and Chiacchiera, S. M. 2014. Negligible effects of tryptophan on the aflatoxin adsorption of sodium bentonite. *Food Additives & Contaminants: Part A,* 31 (12): 2063 – 2070.

Maji, T., Banerjee, S., Biswas, M.and Mandal, T. K. 2014. In situ synthesis of ultra-small platinum nanoparticles using a water soluble polyphenolic polymer with high catalytic activity. *RSC Advances,* 4 (93): 51745 – 51753.

Mansri, A.and Ramdani, N. 2015. In situ polymerization of 4-vinylpyridine/bentonite composites and their application for toluene removal. *Research on Chemical Intermediates,* 41 (3): 1765 – 1776.

Matyjaszewski, K. (ed.) 1996. *Cationic Polymerizations: Mechanisms, Synthesis & Applications,* New York: Marcel Dekker, Inc.

Mckay, G. 1982. Adsorption of dyestuffs from aqueous solutions with activated carbon I: Equilibrium and batch contact-time studies. *Journal of Chemical Technology and Biotechnology,* 32 (7 – 12): 759 – 772.

Morris, P. J. 2005. Polymer Pioneers: A Popular History of the Science and Technology of Large Molecules. Chemical Heritage Foundation.

Mukherjee, S., Ghosh, S., Das, D. K., Chakraborty, P., Choudhury, S., Gupta, P., Adhikary, A., Dey, S.and Chattopadhyay, S. 2015. Gold-conjugated green tea nanoparticles for enhanced anti-tumor activities and hepatoprotection-synthesis, characterization and in vitro evaluation. *The Journal of Nutritional Biochemistry,* 26 (11): 1283 – 1297.

Nath, S., Jana, S., Pradhan, M.and Pal, T. 2010. Ligand-stabilized metal nanoparticles in organic solvent. *Journal of Colloid and Interface Science,* 341 (2): 333 – 352.

Özcan, A. S.and Özcan, A. 2004. Adsorption of acid dyes from aqueous solutions onto acid-activated bentonite. *Journal of Colloid and Interface Science,* 276 (1): 39 – 46.

Pal, S., Sen, G., Karmakar, N. C., Mal, D.and Singh, R. P. 2008. High performance flocculating agents based on cationic polysaccharides in relation to coal fine suspension. *Carbohydrate Polymers,* 74 (3): 590 – 596.

Panda, B. R.and Chattopadhyay, A. 2007. A water-soluble polythiophene-Au nanoparticle composite for pH sensing. *Journal of Colloid and Interface Science,* 316 (2): 962 – 967.

Panda, H. 2013. A Concise Guide on Textile Dyes, Pigments and Dye Intermediates with Textile Printing Technology. 1st ed. Delhi: NIIR Project Consultancy Services.

Philip, D. 2009. Honey mediated green synthesis of gold nanoparticles. *Spectrochimica Acta Part A: Molecular and Biomolecular Spectroscopy,* 73 (4): 650 – 653.

Pinto, M. R. O., Silva, S. M. D. L., De Carvalho, L. H.and D'almeida, J. R. M. 2007. Water Sorption of a Polyurethane/Bentonite Composite: Effects of Bentonite Content and Drying Conditions. *International Journal of Polymeric Materials and Polymeric Biomaterials,* 56 (9): 885 – 892.

Putra, E. K., Pranowo, R., Sunarso, J., Indraswati, N.and Ismadji, S. 2009. Performance of activated carbon and bentonite for adsorption of amoxicillin from wastewater: Mechanisms, isotherms and kinetics. *Water Research,* 43 (9): 2419 – 2430.

Qiu, H., Lv, L., Pan, B. C., Zhang, Q. J., Zhang, W. M.and Zhang, Q. X. 2009. Critical review in adsorption kinetic models. *Journal of Zhejiang University Science A,* 10 (5): 716 – 724.

Rahman, A., Kishimoto, N.and Urabe, T. 2015. Adsorption characteristics of clay adsorbents – sepiolite, kaolin and synthetic talc – for removal of Reactive Yellow 138:1. *Water and Environment Journal,* 29 (3): 375 – 382.

Roux, S., Garcia, B., Bridot, J. L., Salome, M., Marquette, C., Lemelle, L., Gillet, P., Blum, L., Perriat, P.and Tillement, O. 2005. Synthesis, characterization of dihydrolipoic acid capped gold nanoparticles, and functionalization by the electroluminescent luminol. *LANGMUIR,* 21 (6): 2526 – 2536.

Sadeghi, B. 2015. Zizyphus mauritiana extract-mediated green and rapid synthesis of gold nanoparticles and its antibacterial activity. *Journal of Nanostructure in Chemistry,* 5 (3): 265 – 273.

Sadeghi, B., Mohammadzadeh, M.and Babakhani, B. 2015. Green synthesis of gold nanoparticles using Stevia rebaudiana leaf extracts: Characterization and their stability. *Journal of Photochemistry and Photobiology B: Biology,* 148: 101 – 106.

Saha, B., Chakraborty, S.and Das, G. 2008. A comparative metal ion adsorption study by trimesic acid coated alumina: a potent adsorbent. *Journal of colloid and interface science,* 323 (1): 26 – 32.

Sahu, O. P.and Chaudhari, P. K. 2013. Review on Chemical treatment of Industrial Waste Water *Journal of Applied Sciences and Environmental Management,* 17 (2): 241 – 257.

Salamone, J. C. (ed.) 1998. *Concise Polymeric Materials Encyclopedia,* Florida: Taylor & Francis.

Salman, M., El – Eswed, B.and Khalili, F. 2007. Adsorption of humic acid on bentonite. *Applied Clay Science,* 38 (1–2): 51 – 56.

Saraydin, D., Karadag, E.and Aydin, F. 1998. Removal of water soluble cationic dyes with trisyl silicas. *Turkish Journal of Chemistry,* 22 (3): 227 – 236.

Schmid, G.and Corain, B. 2003. Nanoparticulated Gold: Syntheses, Structures, Electronics, and Reactivities. *European Journal of Inorganic Chemistry,* (17): 3081 – 3098.

Shen, Y.-H. 2001. Preparations of organobentonite using nonionic surfactants. *Chemosphere,* 44 (5): 989 – 995.

Shimmin, R. G., Schoch, A. B.and Braun, P. V. 2004. Polymer Size and Concentration Effects on the Size of Gold Nanoparticles Capped by Polymeric Thiols. *Langmuir,* 20 (13): 5613 – 5620.

Siebers, N. 2009. Bentonite Functionalised With 2-(3-(2-aminoethylthio)propylthio)ethanamine (Aepe) for the Removal of Hg(II) from Wastewaters. 1st ed. Hamburg: Diplomica – Verlag.

Silva, P. S., Gasparini, B. C., Magosso, H. A.and Spinelli, A. 2014. Gold nanoparticles hosted in a water-soluble silsesquioxane polymer applied as a catalytic material onto an electrochemical sensor for detection of nitrophenol isomers. *Journal of Hazardous Materials,* 273: 70 – 77.

Şimşek, S., Ulusoy, U.and Ceyhan, Ö. 2003. Adsorption of UO_2^{2+}, Tl^{+}, Pb^{2+}, Ra^{2+} and Ac^{3+} onto polyacrylamide-bentonite composite. *Journal of Radioanalytical & Nuclear Chemistry,* 256 (2): 315 – 321.

Smitha, S. L., Philip, D.and Gopchandran, K. G. 2009. Green synthesis of gold nanoparticles using Cinnamomum zeylanicum leaf broth. *Spectrochimica Acta Part A: Molecular and Biomolecular Spectroscopy,* 74 (3): 735 – 739.

Stawiński, W., Węgrzyn, A., Dańko, T., Freitas, O., Figueiredo, S.and Chmielarz, L. 2017. Acid-base treated vermiculite as high performance adsorbent: Insights into the mechanism of cationic dyes adsorption, regeneration, recyclability and stability studies. *Chemosphere,* 173: 107 – 115.

Sternik, D., Majdan, M., Deryło-Marczewska, A., Żukociński, G., Gładysz-Płaska, A., Gun'ko, V.and Mikhalovsky, S. 2011. Influence of Basic Red 1 dye adsorption on thermal stability of Na-clinoptilolite and Na-bentonite. *Journal of Thermal Analysis & Calorimetry,* 103 (2): 607 – 615.

Suarasan, S., Suarasan, S., Focsan, M., Soritau, O.and Maniu, D. 2015. One-pot, green synthesis of gold nanoparticles by gelatin and investigation of their biological effects on Osteoblast cells. *Colloids and surfaces, B, Biointerfaces,* 132: 122 – 131.

Tabak, A., Baltas, N., Afsin, B., Emirik, M., Caglar, B.and Eren, E. 2010. Adsorption of Reactive Red 120 from aqueous solutions by cetylpyridinium-bentonite. *Journal Of Chemical Technology And Biotechnology,* 85 (9): 1199 – 1207.

Tahir, S. S.and Naseem, R. 2007. Removal of Cr(III) from tannery wastewater by adsorption onto bentonite clay. *Separation and Purification Technology,* 53 (3): 312 – 321.

Tahir, S. S.and Rauf, N. 2003. Thermodynamic studies of Ni(II) adsorption onto bentonite from aqueous solution. *The Journal of Chemical Thermodynamics,* 35 (12): 2003 – 2009.

Tahir, S. S.and Rauf, N. 2004. Removal of Fe(II) from the wastewater of a galvanized pipe manufacturing industry by adsorption onto bentonite clay. *Journal of Environmental Management,* 73 (4): 285 – 292.

Tahir, S. S.and Rauf, N. 2006. Removal of a cationic dye from aqueous solutions by adsorption onto bentonite clay. *Chemosphere,* 63 (11): 1842 – 1848.

Tekbaş, M., Bektaş, N.and Yatmaz, H. C. 2009. Adsorption studies of aqueous basic dye solutions using sepiolite. *Desalination,* 249 (1): 205 – 211.

Temkin, M. I.and Pyzhev, V. 1940. Kinetics of ammonia synthesis on promoted iron catalyst. *Acta Phys. Chim, USSR,* (12): 327 – 356.

Thakor, A. S., Jokerst, J., Zavaleta, C., Massoud, T. F.and Gambhir, S. S. 2011. Gold Nanoparticles: A Revival in Precious Metal Administration to Patients. *American Chemical Society Nano Letters,* 11 (10): 4029 – 4036.

Tsai, T. H., Yu, C. C., Liu, Y. C.and Yang, K. H. 2013. Effectively catalytic decomposition of acetaldehydes in spirits by using chitosan-capped gold nanoparticles. *Journal Of Applied Polymer Science,* 130 (1): 86 – 91.

Turkevich, J., Stevenson, P. C.and Hillier, J. 1951. A study of the nucleation and growth processes in the synthesis of colloidal gold. *Discussions of the Faraday Society,* 11 (0): 55 – 75.

Uma Suganya, K. S., Uma Suganya, K. S., Govindaraju, K., Ganesh Kumar, V.and Stalin Dhas, T. 2015. Blue green alga mediated synthesis of gold nanoparticles and its antibacterial efficacy against Gram positive organisms. *Materials science & engineering. C,* 47: 351 – 356.

Vandamme, D., Foubert, I., Meesschaert, B.and Muylaert, K. 2010. Flocculation of microalgae using cationic starch. *Journal of Applied Phycology,* 22 (4): 525 – 530.

Varun, S., Sellappa, S., Khan, M. R.and Vijayakumar, S. 2015. Green Synthesis of Gold Nanoparticles Using Argemone mexicana L. Leaf Extract and its Characterization. *International Journal of Pharmaceutical Sciences Review and Research,* 32 (2): 42 – 44.

Vigderman, L., Khanal, B. P.and Zubarev, E. R. 2012. Functional Gold Nanorods: Synthesis, Self-Assembly, and Sensing Applications. *Advanced Materials,* 24 (36): 4811 – 4841.

Vilela, D., González, M.and Escarpa, A. 2012. Gold-nanosphere formation using food sample endogenous polyphenols for in-vitro assessment of antioxidant capacity. *Analytical and Bioanalytical Chemistry*, 404 (2): 341 – 349.

Wang, Y.-Q., Zhang, Z.-B., Li, Q.and Liu, Y.-H. 2012. Adsorption of thorium from aqueous solution by HDTMA-pillared bentonite. *Journal of Radioanalytical & Nuclear Chemistry,* 293 (2): 519 – 528.

Weber, W. J.and Morris, C. J. Advances in water pollution research: removal of biologically resistant pollutant from waste water by adsorption. *In:* SOUTHGATE, B. A., ed. Proceeding of 1st International Conference on Water Pollution Research, September 1962 London,. Oxford, UK: Pergamon Press, 231 – 266.

Williams, P. A. 2008. Handbook of Industrial Water Soluble Polymers. Chichester, GBR: Wiley.

Wilson, A. D.and Prosser, H. J. eds. 2012. *Developments in Ionic Polymers-2*, New York: Elsevier Applied Science Publishers LTD.

Worch, E. 2012. Adsorption Technology in Water Treatment: Fundamentals, Processes, and Modeling. 1st ed. Boston: Walter de Gruyter GmbH & Co.

Yang, P. J., Chu, H. C., Lee, Y. H., Kobayashi, T., Chen, T. C.and Lin, H. C. 2012. Quenching effects of gold nanoparticles in nanocomposites formed in water-soluble conjugated polymer nanoreactors. *Polymer,* 53 (4): 939 – 946.

Yang, S., Han, C., Wang, X.and Nagatsu, M. 2014. Characteristics of cesium ion sorption from aqueous solution on bentonite and carbon nanotube-based composites. *Journal of Hazardous Materials,* 274: 46 – 52.

Young, R. J.and Lovell, P. A. 2011. Introduction to Polymers. 3rd ed. Florida: Taylor & Francis Group.

Yue, Q. Y., Li, Q., Gao, B. Y.and Wang, Y. 2007. Kinetics of adsorption of disperse dyes by polyepicholorohydrin-dimethylamine cationic polymer/bentonite. *Separation and Purification Technology,* 54 (3): 279 – 290.

Zhang, L., Liu, Q., Hu, P.and Huang, R. 2015. Adsorptive removal of methyl orange using enhanced cross-linked chitosan/bentonite composite. *Desalination and Water Treatment,* 57 (36): 1 – 12.

Chapter Three: The Synthesis and Characterisation of Proline-Epichlorohydrin-Ethylenediamine Polymer and its Bentonite Composite and its Adsorption Studies for the Remediation of Textile Dyes

3.1. General Introduction

Today, we all use synthetic dyes for many applications such as colouring food, leather, textiles, paper, drugs, cosmetics, for printing inks, varnishes, paints, oils and soaps (Singh 2002: 88) (Mittal *et al.* 2007: 243 – 248). Consequently, these dyes make their way into dams, lakes and the sea as industrial and domestic effluent. Some of the dyes can be a health risk for both humans and aquatic life because of their toxicity and carcinogenicity (Mittal *et al.* 2007: 243 – 248). Anionic reactive textile dyes, such as Reactive Red (RR), Reactive Yellow (RY) and Reactive Blue (RB) are bi-functional dyes which are in demand due to their bright colours and excellent colour fastness (Doble and Kumar 2005: 54). However, approximately 10 % of the dyes are lost during the colouring process whilst about 2 % are discharged as effluent. As a result, the estimated concentration of dyes in wastewater is around 10 mg/L to 200 mg/L (Dada *et al.* 2012: 38 – 45) and is visible in wastewater.

There are many ways of removing organic compounds, including dyes, from effluent. This include oxidation (Keen *et al.* 2012: 6222 – 6227), using sludge (Gulnaz *et al.* 2004: 183 – 188), through coagulation (Szyguła *et al.* 2009: 2979 – 2986), ion-exchange membranes and adsorption (Huang *et al.* 2011: 102 – 109) (Li *et al.* 2010: 1601 – 1611) (Shen *et al.* (2009: 99 – 107.) (Yue *et al.* 2007: 279 – 290). Adsorption is the preferred method since the cost of adsorbents is low, it is easily available, can be re-used and gives better results than alternate methods (Kulshrestha *et al.* 2004: 4097 – 4105). In the remediation of dyes from wastewater, adsorbents such as silica (Huang *et al.* 2011: 102 – 109), cellulose (Annadurai *et al.* 2002: 263 – 274), activated carbon (Choy *et al.* 1999: 57 – 71) and hen feathers (Mittal *et al.* 2007: 243 – 248)were used. Some of the adsorbents were expensive, not easily available and required tedious preparation before the adsorption process. Sodium bentonite (SBN) is one of the adsorbents of choice because it is cheap, easily available and has good adsorption capacity. When SBN is in contact with water, a hydrophilic surface is produced because of the hydrated Na^{+} and Ca^{2+} ions. Hence SBN becomes ineffective for the adsorption of anionic organic pollutants such as anionic reactive textile dyes and therefore surface modifications become necessary.

In this study a new polymer, containing a quaternary ammonium ion, was synthesized, characterised and subsequently reacted with SBN to produce a new composite. The composite was fully characterised and adsorption studies for the removal of three anionic reactive textile dyes (Fig. 3.1) from a synthetic industrial effluent were investigated.

3.2. Experimental

3.2.1. Materials

Bentonite, L-proline, epichlorohydrin, ethylenediamine, sodium hydroxide, hydrochloric acid and sulphuric acid were purchased from Sigma-Aldrich. Alumina (58 Å pore size) was used without prior treatment. The dyes, viz., RB 222, RR 195 and RY 145 (Fig. 3.1) were purchased from Colchem Chemicals and Dyes (SA). Double deionized water (18.00 MΩ) was used to make all aqueous solutions. Glassware was thoroughly washed with doubled deionized water. For pH studies, the dye solution was adjusted with either 1.000 M HCl or 0.1000 M NaOH. Whatman filter paper no. 1 was used for all filtrations. All measurements were done in triplicate and the standard deviations were calculated.

(a)

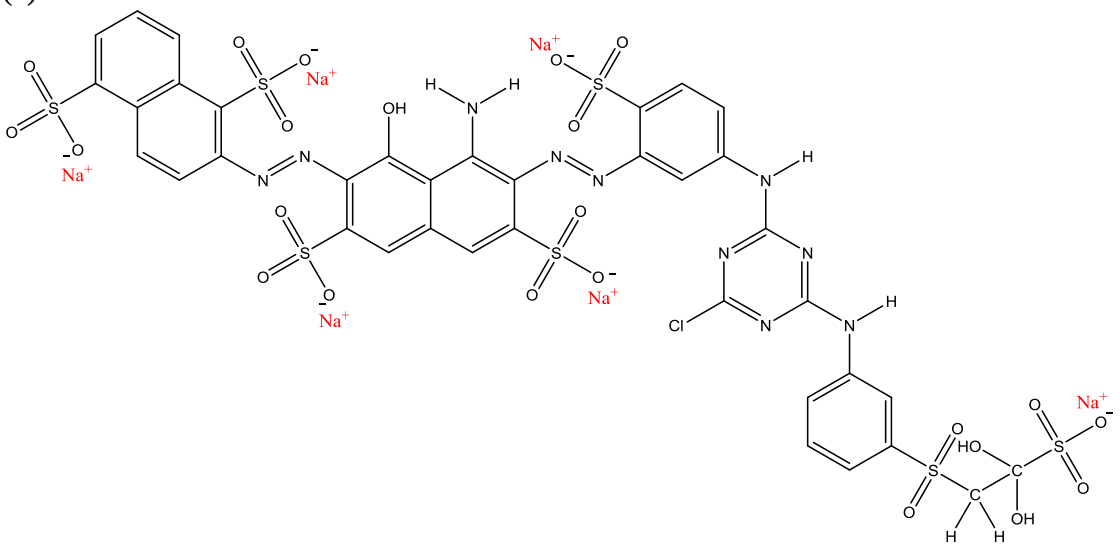

(b)

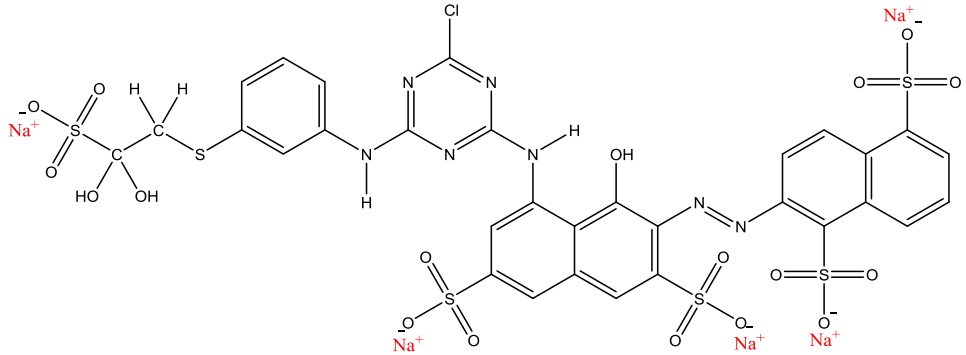

(c)

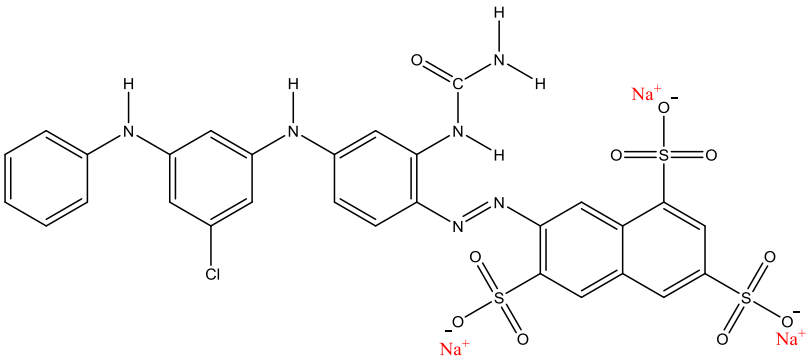

Figure 3.1. Chemical structures of (a) Reactive Blue 222, (b) Reactive Red 195 and (c) Reactive Yellow 145

3.2.2. Instrumentation

A Varian 800 FT-IR spectrophotometer Scimitar Series with attenuated total reflectance (ATR) was used. All samples were analysed from 4000 cm^{-1} to 400 cm^{-1} with a resolution of 2 cm^{-1}. A Mettler-Toledo TGA 2 (SF) with aluminium pans was used and heating conducted at a scan rate of 10 ˚C/min from 25 ˚C to 650 ˚C under nitrogen flow of 50 ml/min. A Malvern Zetasizer

Nano-ZS (Malvern Instruments Ltd, UK), a quartz U-tube cuvette and the Zetasizer software 7.04 were used: the angle measurement was set at 172.2 ˚C with a laser wavelength of 633.0 nm. A disposable folded capillary cell (Fig. 3.2) was used for zeta potential measurements.

(a) (b) (c)

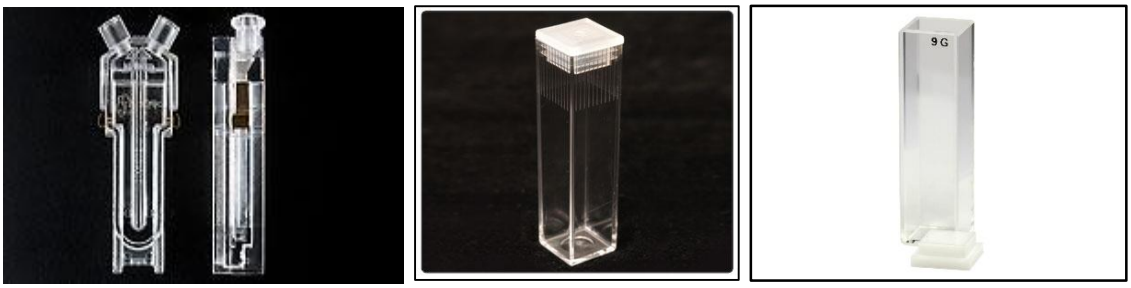

Figure 3.2. (a) The disposable folded capillary cell for zeta potential measurements and (b) the disposable polystyrene cell for particle size measurements and (c) glass cuvette used for static light scattering studies

A Bruker (400 MHz) spectrophotometer was used for ^{1}H-NMR Spectroscopy. A ZEISS EVO HD 15 Environmental Scanning Electron Microscope with an acceleration voltage of 20.00 kV was used study to the topography (structure and orientation) and the element mapping of the composite. TEM images were captured using the JEOL 1010 TEM using a Mega view III camera and iTEM software. A UV-1700 PharmaSpec Spectrophotometer, with glass cuvette of path length of 1 cm was used to measure absorbance. Spectra were scanned at 0.5000 nm/s from 200 nm to 800 nm.

3.2.3. Synthesis of Proline-Epichlorohydrin-Ethylenediamine Polymer (PEP)

An accurate mass of 22.50 g (0.2400 mols) of epichlorohydrin was added to 40.24 g of double distilled water containing 3.55 g (0.03000 mols) of L-proline. Thereafter 15.51 g (0.2600 mols) of ethylenediamine was added dropwise, with stirring, into the mixture, the temperature was increased to 70 ℃ and the mixture was allowed to react for one hour. Thereafter an additional 7.510 g (0.08100 mols) of epichlorohydrin was added and the mixture was allowed to react for a further 24 hours. Concentrated sulphuric acid (0.10 mL) was added to stop the reaction and the polymer was purified by repeated washings with acetone (Panzer and Rabinowitz 1971: 4).

3.2.4. Synthesis of Proline-Epichlorohydrin-Ethylenediamine Polymer-Bentonite Composite (PRO-BEN)

A 3 % PEP solution (Yue *et al.* 2007: 268 – 275) was prepared by dissolving 3.000 g of PEP in 100 mL of distilled water. Although Yue *et al*. (2007) reported a 4 % solution to be the optimum polymer concentration, we found that a 3 % PEP solution displayed the same efficiency in adsorption. Bentonite was activated by heating it in an oven at 100 ˚C for 24 hours. An accurate mass of 12.00 g of this activated bentonite was transferred in a 500 mL beaker, 100 mL of double deionized water was added and the slurry was allowed to stir on a hotplate for 30 minutes at 70 ˚C. Thereafter all the 3 % PEP solution was added and the mixture was stirred for 24 hours. The slurry was vacuum filtered and the residue was collected and placed in an oven at 100 ˚C for 24 hours. The composite was ground using a mortar and pestle, the filtrate was discarded (Shen *et al.* 2009: 99 – 107) whilst the solid composite was used as an adsorbent.

3.2.5. Preparation of Textile Dye Standards for Adsorption Studies

A 100.0 mg/L stock solution of mixed dye was prepared by weighing 0.05000 g of each dye i.e., RB 222, RY 145 and RR 195 into a 500 mL volumetric flask. The mixture was dissolved in double deionized water and the solution was made accurately to 500 mL. Thereafter aliquots of 10 mL, 20 mL, 30 mL, 40 mL and 50 mL were quantitatively transferred into five separate 100 mL volumetric flasks and each of the solution was made up to 100 mL with double deionized water (Fig. 3.3). The absorbance of each solution was obtained by UV-Vis Spectroscopy and a calibration graph was constructed to determine molar absorptivity constants/ $mol^{-1}.L.cm^{-1}$. The LOD and LOQ values for the dyes were also calculated.

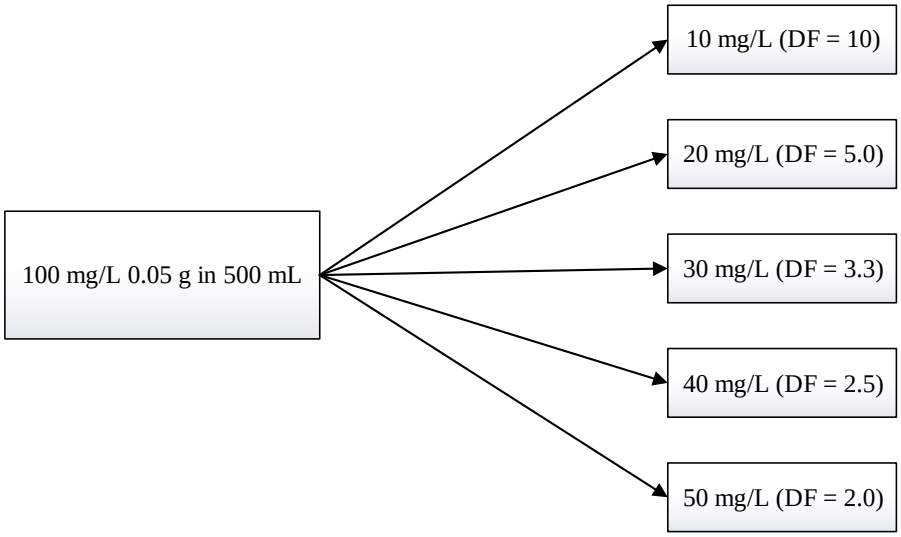

Figure 3.3. A summary showing the concentration of mixed textile dyes

3.2.6. Determination of the Factors Affecting Adsorption

In this study, the 40.00 mg/L mixed dye solution was adjusted to pH 5.21 and the mass of PRO-BEN selected was 0.1500 g unless stated otherwise.

3.2.6.1. The Effect of Quantity PRO-BEN on Dye Adsorption

Into four Erlenmeyer flasks was added 0.05000 g, 0.1000 g, 0.1500 g and 0.2000 g of PRO-BEN, separately. Thereafter an accurate aliquot of 100 mL of the 40.00 mg/L mixed dye solution was added into each flask and simultaneously the stopwatch and mechanical shaker was started. This was conducted at ambient temperature at 120 rpm for three hours. After every 10 minutes, an aliquot of 5 mL of a sample was removed, centrifuged for 10 minutes and filtered. The filtrate was collected and the absorbance was determined by UV-Vis Spectroscopy.

3.2.6.2. The Effect of Initial Dye Concentration on Adsorption

Into eight Erlenmeyer flasks, 0.1500 g of PRO-BEN and alumina, presented in Table 3.1, was added. Thereafter 100 mL of various concentration of mixed dye standard, presented in Table 3.1, was added into each flask and simultaneously the mechanical shaker and stopwatch was started. This was conducted at ambient temperature for 3 hours at 120 rpm. After every 10 minutes, 5 mL of sample was removed, centrifuged for 10 minutes and filtered. The filtrate was collected and the absorbance was determined by UV-Vis Spectroscopy

Table 3.1. The quantity of PRO-BEN used for various concentrations of dye solutions

Dye Concentration (mg/L)	Type of Adsorbent	Mass of Adsorbent (g)
20.00	PRO-BEN	0.1510
20.00	Alumina	0.1510
30.00	PRO-BEN	0.1505
30.00	Alumina	0.1510
40.00	PRO-BEN	0.1502
40.00	Alumina	0.1522
50.00	PRO-BEN	0.1522
50.00	Alumina	0.1544

3.2.6.3. The Effect of Sodium Chloride Concentration on Adsorption

Into six thoroughly cleaned Erlenmeyer flasks, 0.1500 g of PRO-BEN was added and 100 mL of the 40.00 mg/L dye solution, containing sodium chloride (Table 3.2) were poured into the flasks and the stopwatch was started. After every 10 minutes, 5 mL of sample was removed, centrifuged for 10 minutes and filtered. The filtrate was quantified by UV-Vis Spectroscopy.

Table 3.2. Quantity of sodium chloride used in the 100 mL dye solutions

Mass of NaCl used/ g	Concentration of NaCl in dye mixture ($mg.L^{-1}$)	Type of Adsorbent
0.2904	2904	PRO-BEN
0.2904	2904	Alumina
0.5808	5808	PRO-BEN
0.5808	5808	Alumina
1.170	11700	PRO-BEN
1.170	11700	Alumina

3.2.6.4. The Effect of pH of the Dye Solution on Adsorption

An aliquot of 40.00 mL of a 100 mg/L mixed dye solution was quantitatively transferred separately into each of eight 100 mL beakers. A pH electrode was inserted into each solution to record the initial pH reading. The pH was then adjusted with either 0.1000 M HCl or 0.1000 M NaOH solution. The pH of the dye solutions that were studied were 2.00, 5.21, 7.00 and 11.00. Once the desired pH had been reached, the dye solution was quantitatively transferred into the remaining 100 mL volumetric flask and the solution was made up to 100 mL. These eight solutions were then transferred into Erlenmeyer flasks containing the respective adsorbents and simultaneously the mechanical shaker and stopwatch was started. This was conducted at ambient temperature for 3 hours at 120 rpm. After every 10 minutes, 5 mL of sample was removed, centrifuged for 10 minutes and filtered. The filtrate was quantified by UV-Vis Spectroscopy

An additional experiment was set-up to determine the trend in dye adsorption with various pH values. 100 mL of dye solution (adjusted to pH values of 1.00 – 11.00) were adsorbed onto an accurate quantity of 0.1500 g of PRO-BEN. The UV-Visible results were recorded to determine the optimum pH that can be used for the adsorption process.

3.2.6.5. The Effect of Temperature of the Dye Solution on Adsorption

The desired temperature (Table 3.3) was pre-set in the oven shaker and equilibrated. Then 100 mL of a 40.00 mg/L mixed dye solution was transferred, separately, into eight Erlenmeyer flasks containing PRO-BEN or alumina and simultaneously the mechanical shaker and stopwatch was started. This was conducted at ambient temperature for 3 hours at 120 rpm. After every 10 minutes, 5 mL of sample was removed, centrifuged for 10 minutes and filtered. The filtrate was collected and the absorbance was determined by UV-Vis Spectroscopy.

Table 3.3. The temperature used for adsorption studies

Temperature of dye solution/ ˚C	Type of adsorbent	Mass of adsorbent used/ g
25.00	PRO-BEN	0.1502
25.00	Alumina	0.1522
35.00	PRO-BEN	0.1515
35.00	Alumina	0.1528
45.00	PRO-BEN	0.1510
45.00	Alumina	0.1520

3.2.7. The Adsorption of Textile Dyes from an Industrial Effluent

An aliquot of 500 mL of an effluent sample was collected, filtered and the pH was adjusted to 4.01 and thereafter 100 mL of the solution was transferred into each of 2 Erlenmeyer flasks containing the PRO-BEN and alumina, separately. The mechanical shaker and stopwatch was started simultaneously. This was conducted at ambient temperature for 3 hours at 120 rpm. After every 10 minutes, 5 mL of sample was removed, centrifuged for 10 minutes and filtered. The filtrate was collected and the absorbance was determined by UV-Vis Spectroscopy.

3.2.8. Desorption Studies

A quantity of 1.500 g of PRO-BEN and alumina was added separately to 100 mL of 1000 mg/L mixed dye solution. The mechanical shaker was started and after six hours, the solution was filtered and the residue was collected and dried in an oven at 100 ˚C for 24 hours. Thereafter the PRO-BEN and alumina sample was crushed with a mortar and pestle to a fine powder and used for adsorption studies. It must be mentioned that in a preliminary study, sodium hydroxide was found to desorb the dyes better than other basic solutions.

3.2.8.1. Desorption By Variation Of Sodium Hydroxide Concentration

The quantity of the desorbent (0.1500 g) was weighed into separate Erlenmeyer flasks. Then 100 mL of the respective concentrations of sodium hydroxide solution was transferred into the flasks, the stopwatch and mechanical shaker was started: the temperatures studied is presented in Table 3.4. After every 10 minutes, 5 mL of sample was removed, centrifuged for 10 minutes and filtered. The filtrate was collected and the absorbance was determined by UV-Vis Spectroscopy triplicate analyses was conducted.

Table 3.4. The quantity of desorbent used at various sodium hydroxide

Concentration of sodium hydroxide (M)	Type of adsorbent	Mass of desorbent used (g)		
		25 ˚C	35 ˚C	45 ˚C
0.0001000	PRO-BEN	0.1521	0.1509	0.1512
0.0001000	Alumina	0.1521	0.1521	0.1521
0.0005000	PRO-BEN	0.1513	0.1507	0.1513
0.0005000	Alumina	0.1513	0.1513	0.1513
0.001000	PRO-BEN	0.1500	0.1511	0.1509
0.001000	Alumina	0.1500	0.1500	0.1500
0.005000	PRO-BEN	0.1515	0.1509	0.1505
0.005000	Alumina	0.1515	0.1515	0.1515
0.01000	PRO-BEN	0.1508	0.1509	0.1523
0.01000	Alumina	0.1508	0.1508	0.1508
0.1000	PRO-BEN	0.1508	0.1509	0.1523
0.1000	Alumina	0.1508	0.1508	0.1508
1.000	PRO-BEN	0.1508	0.1509	0.152
1.000	Alumina	0.1508	0.1508	0.1508

3.3. Results and Discussion

The first objective was to synthesise a water-soluble polymer by using L-proline, epichlorohydrin and ethylenediamine as monomers (Fig. 3.4). When the two monomers viz. epichlorohydrin and L-proline were added, two layers were observed however after the addition of ethylenediamine, the solution homogenized and the colour changed from colourless to yellow. After 24 hours of reaction, a thick brownish viscous liquid was produced.

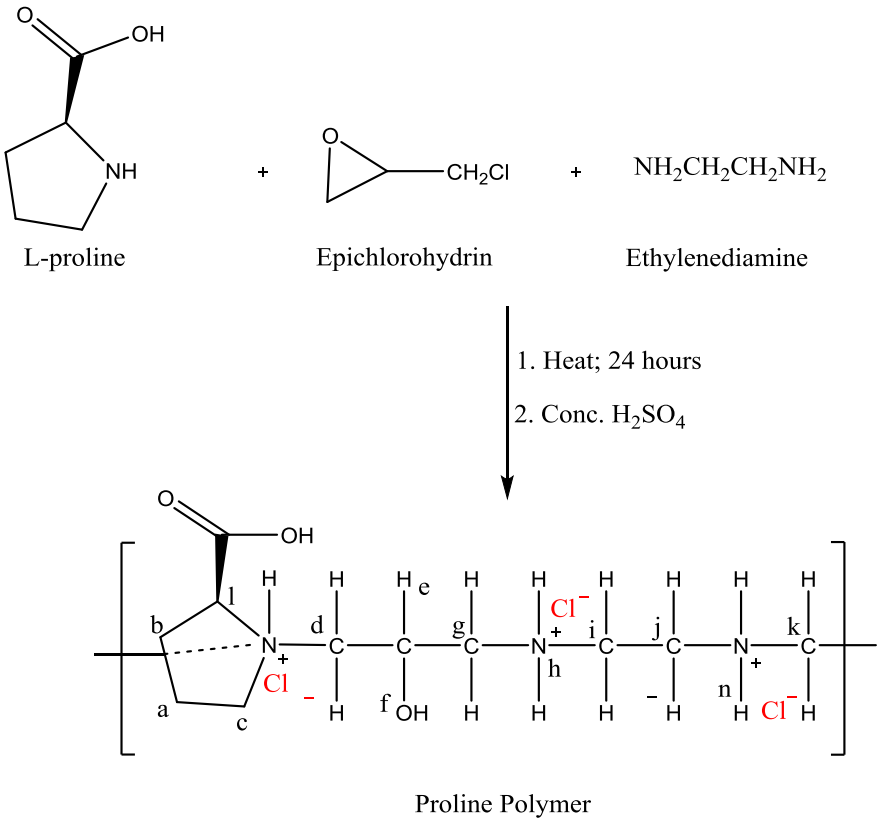

Figure 3.4. A reaction scheme for the synthesis of Proline-Epichlorohydrin-Ethylenediamine Polymer

3.3.1. Characterization of Proline-Epichlorohydrin-Ethylenediamine Polymer

3.3.1.1. Infra-Red Spectroscopy of Proline-Epichlorohydrin-Ethylenediamine Polymer

The following absorption bands (Fig. 3.5) were observed for the polymer: O-H stretch at around 3339 cm^{-1}, C-H stretch at 3013 cm^{-1} and 2930 cm^{-1}, C=O (acid) stretch at 1736 cm^{-1}, C-H bend at 1459 cm^{-1} and C-N stretch at 1216 cm^{-1}.

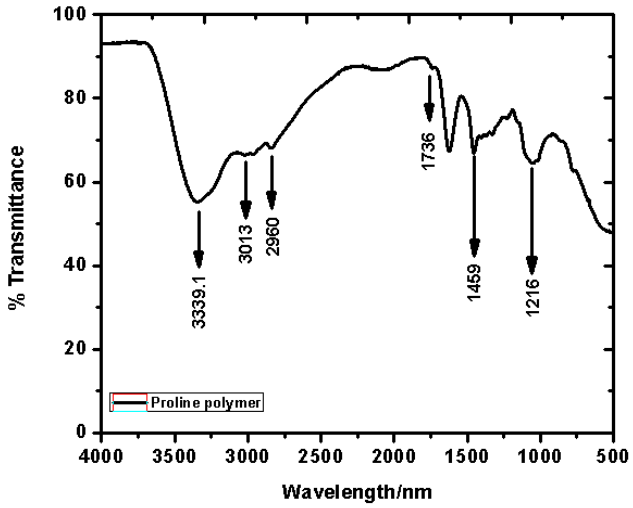

Figure 3.5. FT-IR spectrum of Proline-Epichlorohydrin-Ethylenediamine polymer

3.3.1.2. ^{1}H-NMR Spectroscopy of Proline-Epichlorohydrin-Ethylenediamine polymer

The ^{1}H-NMR and expanded spectra of PEP are presented in Appendix 1, whilst the chemical shifts and spin multiplicities are presented in Table 3.5.

Since the polymer PEP was synthesized from three aliphatic monomers, several equivalent and non-equivalent protons were observed; hence it was difficult to assign the chemical shifts unambiguously. However when analysing the back-bone of the polymer, the research report by Li *et al.* (2010: 1601-1611) was used. The OH and NH protons appeared at δ 4.310 and 4.500, respectively. The COOH proton did not appear in the spectrum due to its exchange with D_2O (Pavia *et al.* 2014: 784) which was the only solvent in which the polymer was soluble. There were several CH_2 protons which appeared at δ 1.930 to δ 3.590 depending on the shielding and de-shielding effect.

Table 3.5. The chemical shifts for Proline-Epichlorohydrin-Ethylenediamine polymer

Label	Chemical shifts (ppm) and multiplicity
a	1.930 (m)
b	2.080 (m)
c	2.290 (m)
d	2.420 (m)
g, j	2.730(t)
j, g	3.410 (t)
n	3.050 (t)
i, k	3.590 (m)
h	4.310 (t)
f	4.500 (d)

3.3.1.3. Thermal analysis of Proline-Epichlorohydrin-Ethylenediamine Polymer

The DSC/TGA profiles for PEP are shown in Fig. 3.6. The initial mass of the polymer was recorded as 3.727 mg and a ramping rate of 10 ˚C/min was used. The TGA profile showed a mass loss of 100 % at 258.8 ˚C which could be the loss of some hydrocarbon portions. The DSC thermogram shows an endothermic peak at 257.1 ˚C that corresponds to the decomposition temperature.

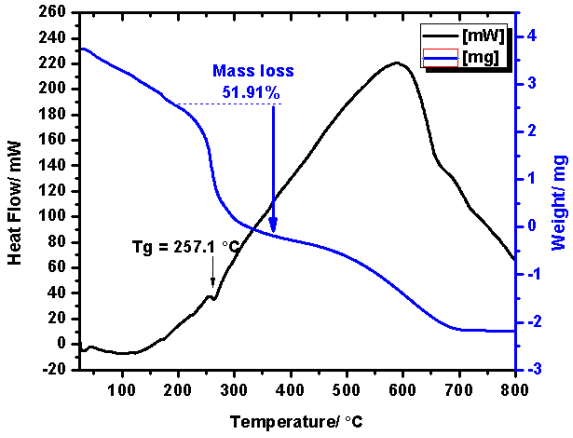

Figure 3.6. DSC/TGA thermogram of Proline-Epichlorohydrin-Ethylenediamine Polymer

3.3.1.4. Molecular weight of Proline-Epichlorohydrin-Ethylenediamine Polymer

Static light scattering (SLS) was used to determine the molecular weight of PEP. Each of the four samples (Table 3.6) was filtered, analysed and the molecular weight was determined based on the Debye plot calculation where 15 repeated measurements at 25 ˚C and at 172.2˚ for each sample. The required $\frac{dn}{dc}$ value was calculated from the gradient of the calibration graph of refractive index of the polymer solution as a function of concentration (Fig. 3.7). The refractive indices of the solutions were recorded at 25 ˚C in triplicate. The counts per second (obtained from the instrument) for the highest standard did not exceed 400 kcps. The angle used was 90˚ to minimize the influence of possible dust particles on the results.

Table 3.6. Data for the Debye plot for Proline-Epichlorohydrin-Ethylenediamine Polymer

Concentration/ g.mL^{-1}	**Refractive Index**
0.000	1.33290 ± 1.000×10^{-5}
0.3020	1.33303 ± 1.000×10^{-5}
0.4420	1.33306 ± 1.000×10^{-5}
0.6340	1.33307 ± 2.000×10^{-5}
0.8060	1.33310 ± 1.000×10^{-5}
1.020	1.33313 ± 1.000×10^{-5}
3.036	1.33344 ± 2.000×10^{-5}
5.060	1.33375 ± 1.000×10^{-5}
7.038	1.33406 ± 1.000×10^{-5}
10.11	1.33453 ± 3.000×10^{-5}

The graph of refractive index versus concentration showed good correlation as indicated by a high regression value of 0.9968. The $\frac{dn}{dc}$ value for the PEP was 0.1488 mL.g^{-1} ± 6.764×10^{-7} mL.g^{-1}.

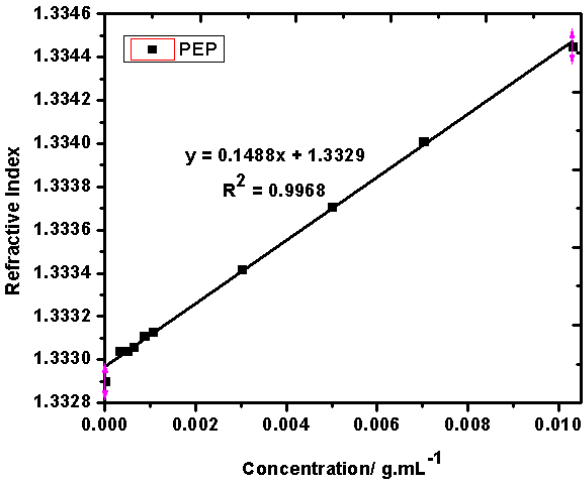

Figure 3.7. Calibration graph of refractive index versus concentration of Proline-Epichlorohydrin-Ethylenediamine Polymer solutions

The slope and intercept from Fig. 3.7 were used to determine the Debye plot equations where k and R_θ are constants which are calculated from equations 3.1 – 3.3:

$$\frac{kC}{R_\theta} = \frac{1}{M_w} + 2A_2C \qquad (3.1)$$

$$k = \frac{2\pi^2}{\lambda_0{}^4 N_A}\left(\frac{dn}{dc}\, n_0\right) \qquad (3.2)$$

$$R_\theta = R_S\left(\frac{I_A\, n_0{}^2}{I_S n_S{}^2}\right) \qquad (3.3)$$

C / g.mL^{-1} is the concentration of the polymer solution,

A_2/ mL.mol.g^{-2} is the second viral co-efficient describing the strength of interaction between the polymer molecules and the solvent.

M_w is the absolute molecular weight in Daltons,

k/ mol.cm^2.g^{-1} is the optical constant,

λ_0 / nm is the wavelength of the SLS method,

N_A/ mol^{-1} is the Avogadro's number,

n_0 is the refractive index of distilled water,

n_S is the refractive index of toluene standard,

R_S is the Rayleigh ratio of toluene,

I_A / kcps is the intensity of the analyte,

I_S / kcps is the intensity of the toluene standard

R_θ/ cm^{-1} is the Rayleigh ratio between the scattered and incident light intensity.

Table 3.7. The Debye plot for absolute molecular weight of Proline-Epichlorohydrin-Ethylenediamine Polymer

Concentration/ g.mL^{-1}	**I_{Sample} / cps ×10^5**	**I_A/ cps ×10^5**	**R_θ/ ×10^{-5} cm^{-1}**	**Kc/ R_θ ×10^{-5}**
0.0003020	0.6690	0.7710	0.9007	5.385
0.0004420	0.8820	1.286	1.502	5.131
0.0006340	1.060	1.788	2.089	4.874
0.0008060	1.249	2.326	2.717	4.763
$\frac{dn}{dc}$ = 0.1488 mL.g^{-1}± 6.764×10^{-7} mL.g^{-1}				
k = 1.606 x10^{-7} mol.cm^2.g^{-1}				
I_S = 172200 cps				
I_0 = 3.250 × 10^4 cps				
n_S = 1.497 cps				
n_0 = 1.33300				
M_W = 174.1 kDa ± 2.929 kDa				
A_2 = -1.271 x 10^{-3} mL.mol.g^{-2} ± 5.752 x 10^{-8} mL.mol.g^{-2}				

The absolute molecular weight was calculated as 174.1 kDa (Table 3.7) whilst the second viral co-efficient was -1.271 x 10^{-3} mL.mol.g^{-2} ± 5.752 x 10^{-8} mL.mol.g^{-2} (Fig. 3.8). The negative value was attained, implying that the interaction between the polymer and solvent are not very strong, indicating that it may aggregate.

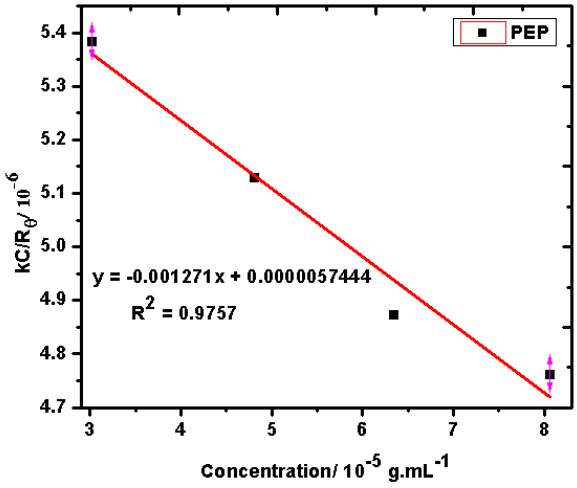

Figure 3.8. The Debye plot for Proline-Epichlorohydrin-Ethylenediamine Polymer

A summary of data obtained for the Proline-Epichlorohydrin-Ethylenediamine polymer is presented in Table 3.8.

Table 3.8. Summary of data obtained for the Proline-Epichlorohydrin-Ethylenediamine polymer

Characteristics	**Proline-Epichlorohydrin-Ethylenediamine Polymer**
Appearance	Thick yellow
Zeta Potential/ mV	+6.940 ± 1.135
Decomposition temperature/ ˚C	258.8 ± 1.500
Density/ g/mL	$1.013 \pm 1.000\times10^{-3}$
Refractive Index	$1.344 \pm 2.000\times10^{-3}$
Conductivity/ mS/cm	$0.05430 \pm 2.301\times10^{-3}$
Solubility	Ethylene glycol, Water

3.3.2. The synthesis and characterisation of Proline-Epichlorohydrin-Ethylenediamine Polymer-Bentonite composite

The next objective was to synthesize a composite containing PEP and bentonite. Briefly a 3 % PEP solution was mixed with a slurry of bentonite. The mixture was filtered after 24 hours of reaction and the solid was purified and then used for adsorption studies.

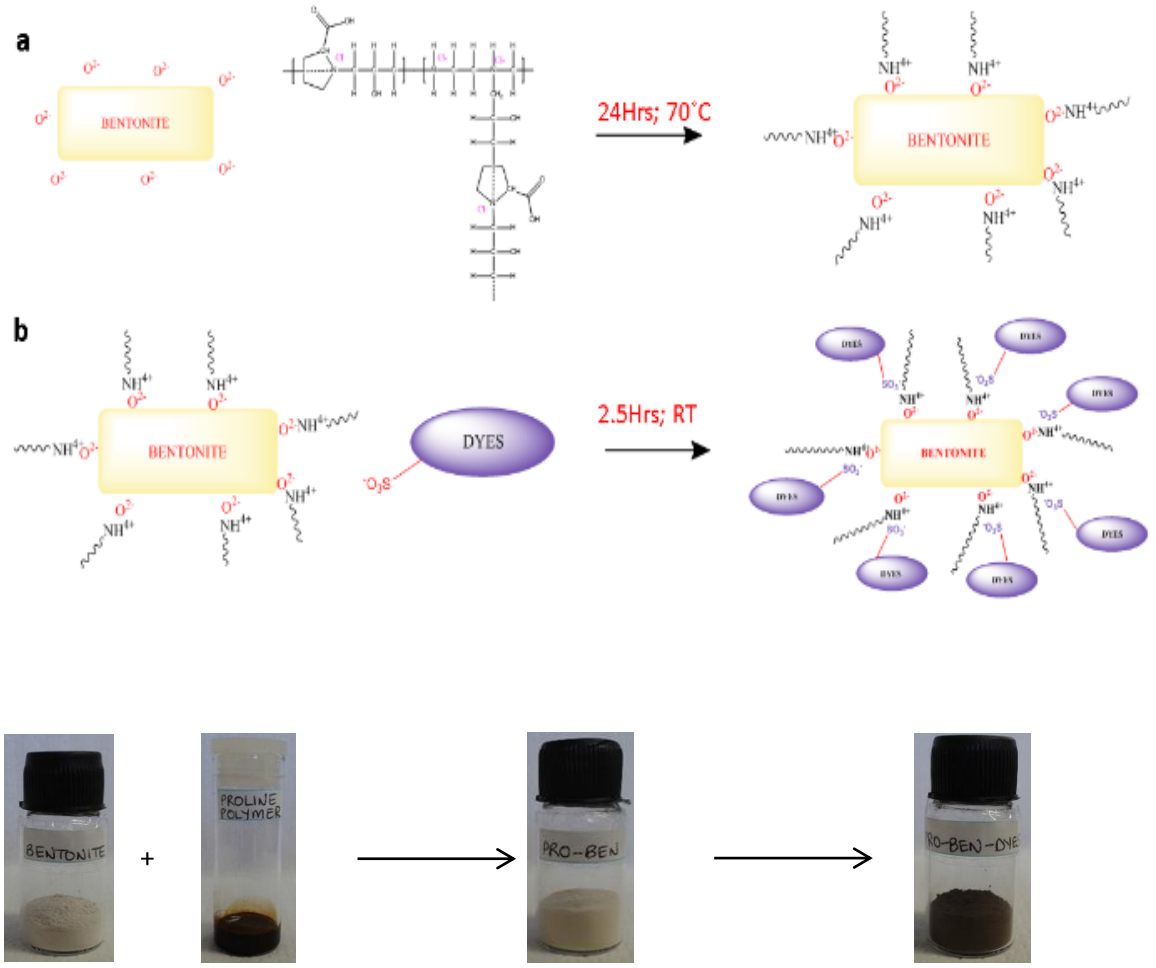

Figure 3.9. Scheme of (a) bentonite modification and (b) anionic dye adsorption

3.3.2.1. The FT-IR spectra of bentonite and the polymer-bentonite composite

The FT-IR spectra of bentonite and the polymer-bentonite composite is presented in Fig. 3.10.

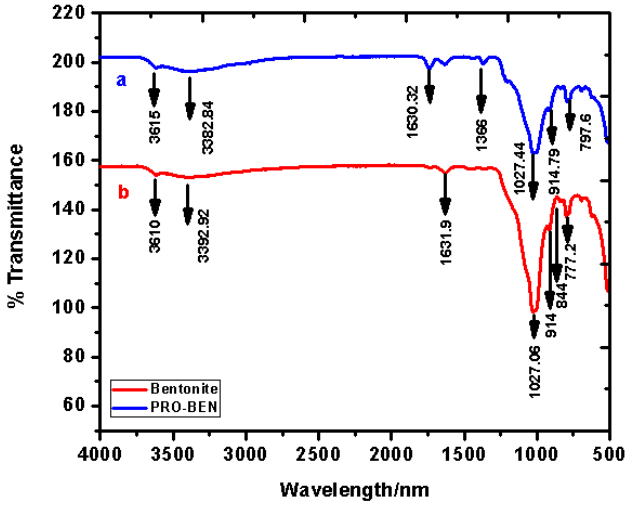

Figure 3.10. The FT-IR spectra of (a) PRO-BEN composite and (b) pure bentonite

PRO-BEN and bentonite exhibited absorption peaks at approximately 3382 to 3615 cm^{-1} and 3392 to 3610 cm^{-1} , respectively, corresponding to the O-H stretch of water molecules as atmospheric moisture. Chaudhary and Datta (2013: 193 – 201) and Navratilova *et al.* (2007: 59 – 65) reported that the absorption at approximately 1630 cm^{-1} could be due to either the O-H or C=O groups. The rest of the vibrations in both spectra corresponded to the characteristic bentonite responses as described in literature: Si-O stretch at 777.0 cm^{-1}, 797.0 cm^{-1} and 1027 cm^{-1}; Al-Al-OH deformation at 914.0 $cm^{-1}$and Al-Mg-OH vibration at 844.0 cm^{-1}, however, , there were additional weak vibrational bands at around 1366 cm^{-1} (Fig. 3.10 (a)). The latter could be due to the C-H bend from PEP thereby indicating it was successful bonded into the bentonite structure: similar results were also reported in literature (Li *et al.* 2009: 1170 – 1178) (Navratilova *et al.* 2007: 59 – 65).

3.3.2.2. The SEM/EDX profiles of Proline-Epichlorohydrin-Ethylenediamine Polymer and proline-epichlorohydrin-ethylenediamine polymer bentonite composite

The morphologies of PEP and PRO-BEN were studied using SEM/EDX (Fig. 3.11). PEP showed a sheet-like uneven surface whilst PRO-BEN appeared as particles in the range of 0.5 µm – 2 µm. The EDX spectrum (Fig. 3.11 (c)) showed that PRO-BEN contained 32.70 % silicon and 36.72 % of oxygen whilst 2.590 % of aluminium and 0.5300 % of magnesium were

also detected. These four elements are found in the tetrahedral and octahedral layers of bentonite. The oxide ions are found on the ends of the layers which initially impart a negative charge to the bentonite.

(a) (b)

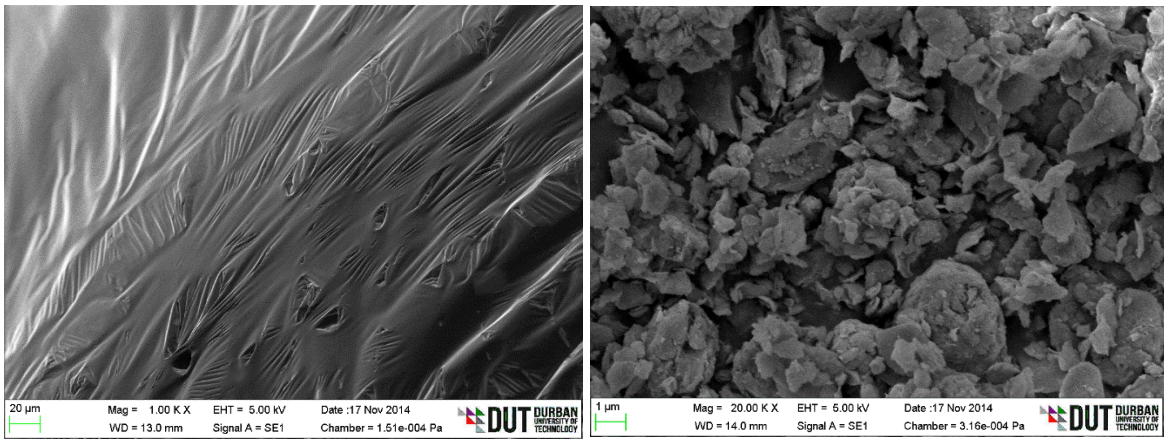

(c)

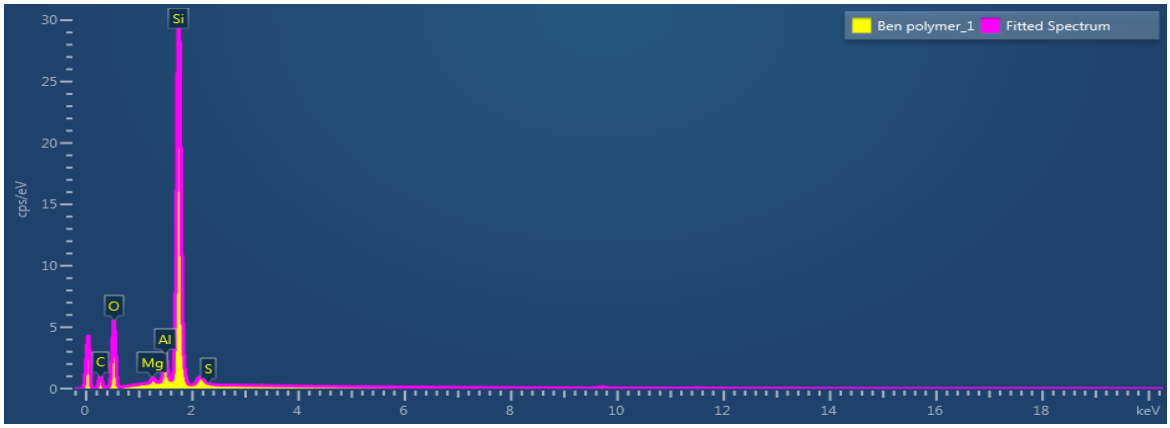

Figure 3.11. SEM results of (a) Proline-Epichlorohydrin-Ethylenediamine Polymer and (b) PRO-BEN and (c) EDX spectrum of PRO-BEN

3.3.2.3. Dynamic Light Scattering Studies

This study was conducted to determine the surface charge and particle size of PEP, PRO-BEN and bentonite. Each measurement was an average of 15 measurements and were conducted at 25 ˚C with a laser of 532 nm (green). Fig. 3.12 shows the variation in zeta potential of the three materials: PER showed a positive charge of +6.940 mV. Also there was a change from a negative zeta potential (-8.960 mV) for bentonite to a positive (+5.310 mV) value for PRO-

BEN when PEP was mixed with bentonite. This change in zeta potential also indicated successful bonding of PEP with bentonite.

(a)

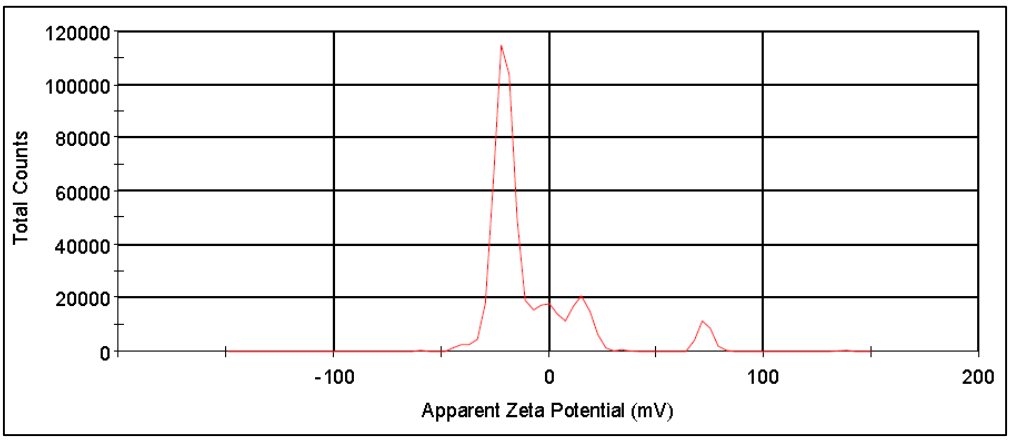

(b)

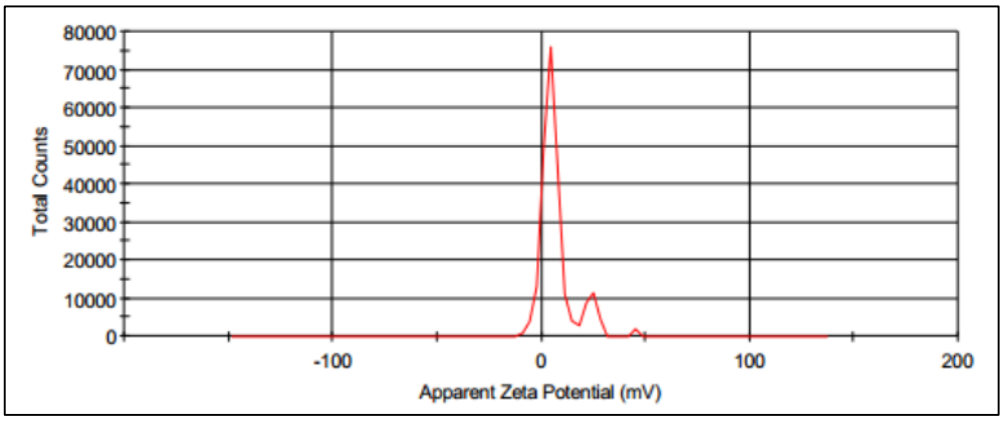

(c)

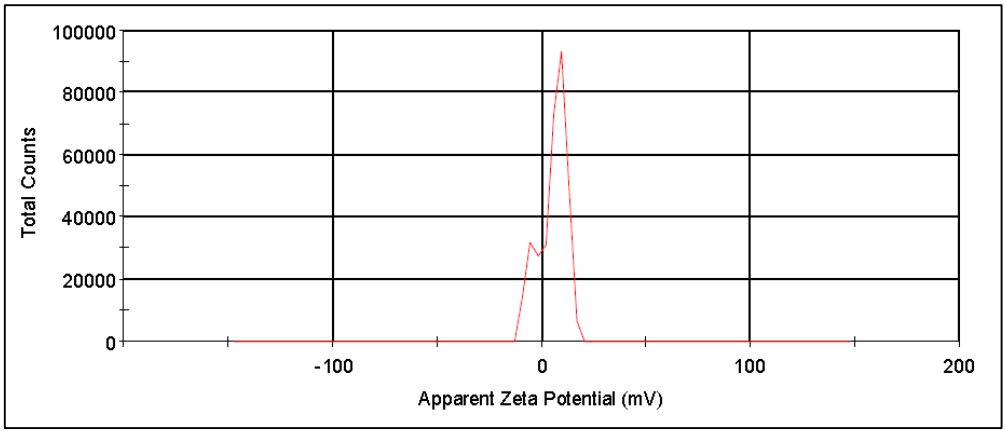

Figure 3.12. Zeta Potential profile of (a) bentonite, (b) Proline-Epichlorohydrin-Ethylenediamine Polymer and (c) PRO-BEN

3.3.2.4. Transmission Electron Microscopy

The TEM image (Fig. 3.13(a)) showed that bentonite appeared as particles which seemed to be stacked on top of each other. In the case of PRO-BEN (Fig. 3.13(b)) the bentonite particles seemed to be clustering because of the presence and interaction with PEP. It is suggested that PEP could act as a film which promotes better adhesion of bentonite. Hence this modification could increase of the adsorption of anionic pollutants by increasing the exposed surface area of the cationic surface.

(a) (b)

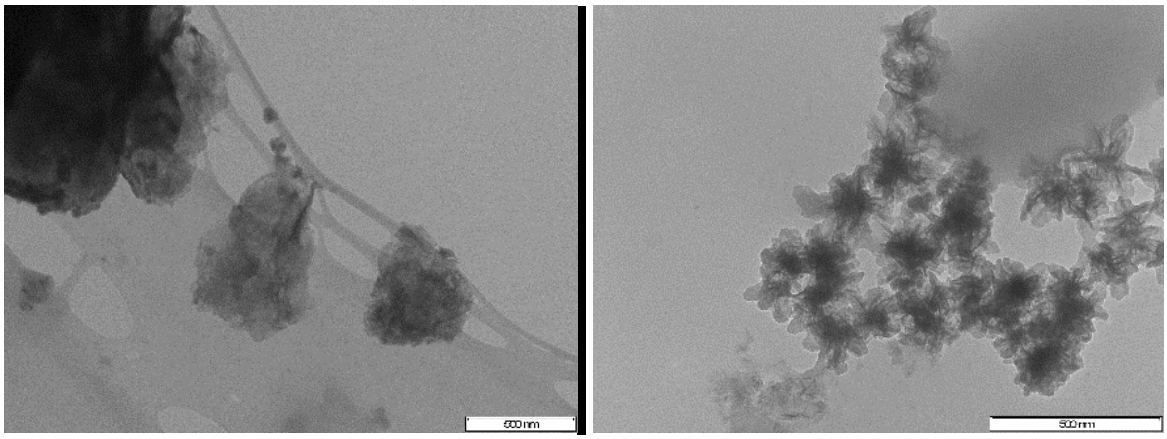

Figure 3.13. TEM micrographs of (a) bentonite and (b) PRO-BEN

3.3.2.5. Cationic exchange capacity

The cationic exchange capacity was calculated as follows:

Stage 1: 1.013 g of PRO-BEN was allowed to adsorb 100 mL of 0.01500 mol.L^{-1} Methylene Blue solution for 30 minutes.

Stage 2: After adsorption, the solution was made up to 25 mL and was filtered.

Stage 3: The filtrate was diluted 20 times further and the absorbance was obtained to calculate the concentration of dye that had adsorbed onto the PRO-BEN.

Stage 4: The CEC was calculated.

A calibration graph (Fig. 3.14) of absorbance of Methylene Blue was plotted as a function of concentrations (Table 3.9).

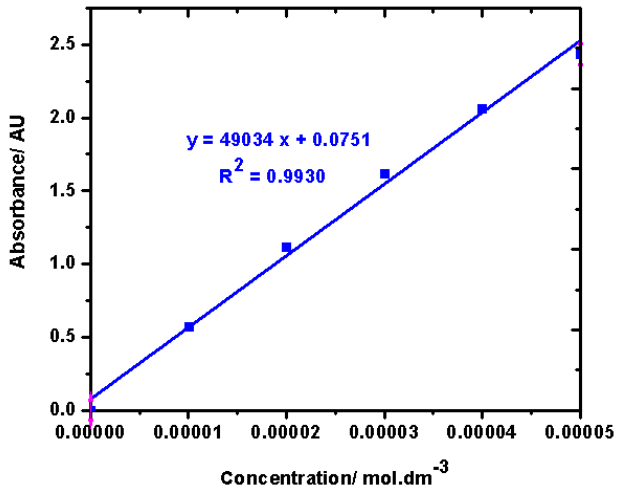

Figure 3.14. Calibration graph of Methylene Blue

Table 3.9. Calibration data for Methylene Blue

Concentration of MB/ x10^{-5} mol.L^{-1}	**Mean Absorbance/ AU**
0.000	0.000 ± 1.000×10^{-4}
1.000	0.5710 ± 1.528×10^{-4}
2.000	1.115 ± 4.048×10^{-4}
3.000	1.621 ± 1.273×10^{-4}
4.000	2.063 ± 2.014×10^{-4}
5.000	2.436 ± 3.769×10^{-4}
PRO-BEN	1.114 ± 1.258×10^{-4}

The amount of Methylene Blue adsorbed was quantified and the cationic exchange capacity was calculated (Kahr and Madsen 1995: 327 – 336):

From the calibration curve,

y = 4930 x + 0.07510

Concentration of MB adsorbed in diluted sample = (1.114 – 0.07510)/ 49034

= 2.119×10^{-5} mol.L^{-1}

(Stage 3)

Concentration MB in undiluted filtrate = Dilution factor *X* Concentration of MB

= 20 × 2.119 × 10^{-5} mol.L^{-1}

= 4.237×10^{-4} mol.L^{-1}

(Stage 2)

Moles MB before filtration = Dilution factor × Concentration of MB

$$= 0.02500\ L \times 4.237 \times 10^{-4}\ \text{mol.L}^{-1}$$

$$= 1.059\times10^{-5}\ \text{mols}$$

Moles MB removed during adsorption = moles MB (in 0.01500 mol.L^{-1} – in mixture before filtration)

$$= 3.746\times10^{-4}\ \text{moles} - 1.059\times10^{-5}\ \text{moles}$$

$$= 3.640\times10^{-4}\ \text{moles}$$

CEC = moles MB removed/100g PRO-BEN

$= 3.640 \times10^{-4}$ moles/100g PRO-BEN

$= 36.40$ mmol/100g $\pm\ 3.040\times10^{-2}$ mmol/100g PRO-BEN

The calibration graph (Fig. 3.14; Table 3.9) was used to obtain the CEC value: a decrease in the CEC values of bentonite compared to PRO-BEN implied that the PRO-BEN could now accommodate more polymer on its surface because of the exchange of its surface cations with the polymer. This gives PRO-BEN an advantage to adsorb a larger quantity of dyes, thus making the composite a better adsorbent for the anionic textile dyes than pristine bentonite.

3.3.2.6. XPS Analysis of PRO-BEN Composite

The XPS spectra showing the surface chemical properties of PRO-BEN and dye-adsorbed PRO-BEN is presented in Fig. 3.15 (a and b) whilst the high resolution spectra showing O1s, C1s and Si1s is presented in Appendix 2. The electron emission peaks for the elements found in bentonite were observed as Si2p (± 100 eV), N1s (400 eV), O1s (540 eV), Al2p (80 eV) and C1s (270 eV). The N1s (400 eV) could be due to the ammonium ions in the polymer that coats the bentonite. The spectrum for both are similar however an increase in the intensity of C1s was noted. The atomic percentage of the composite (Table 3.10) shows an increase in carbon content for the dye-laden composite as the dye adsorbs onto the PRO-BEN surface. In the high resolution spectra of both Si1s and O1s, the detected states were found the same for both materials; SiO_2 at 533 eV for PRO-BEN and 532 eV for dye-laden composite , Si-(N, H) at 102 eV and 108 eV was the polymer interactions with silicon, O-(C, H) at 531 eV. The high resolution spectra for C1s differed for both materials. The C-C peak at 284 eV and C-O-C at

287 eV for PRO-BEN were due to bonds between the polymer atoms and bentonite. The dye-adsorbed PRO-BEN showed a C=O peak at 288 eV which also is possibly due to the polymer. The ratio of carbon to silicon increased from 0.7200 in PRO-BEN to 1.310 in PRO-BEN dyes. This overall increase was possibly due to the adsorption of the dyes on PRO-BEN.

Table 3.10. Atomic percentages of the detected elements in PRO-BEN and PRO-BEN-dye

Elements	**PRO-BEN**	**PRO-BEN-dye**
O1s	60.20	55.40
C1s	12.10	19.20
Si2p	16.80	14.70
N1s	3.600	5.000
Al2p	2.100	2.600
Mg1s	2.300	1.800
S2p	2.100	1.100
Ca2p	0.3000	0.2000
Cl2p	0.6000	-

(a)

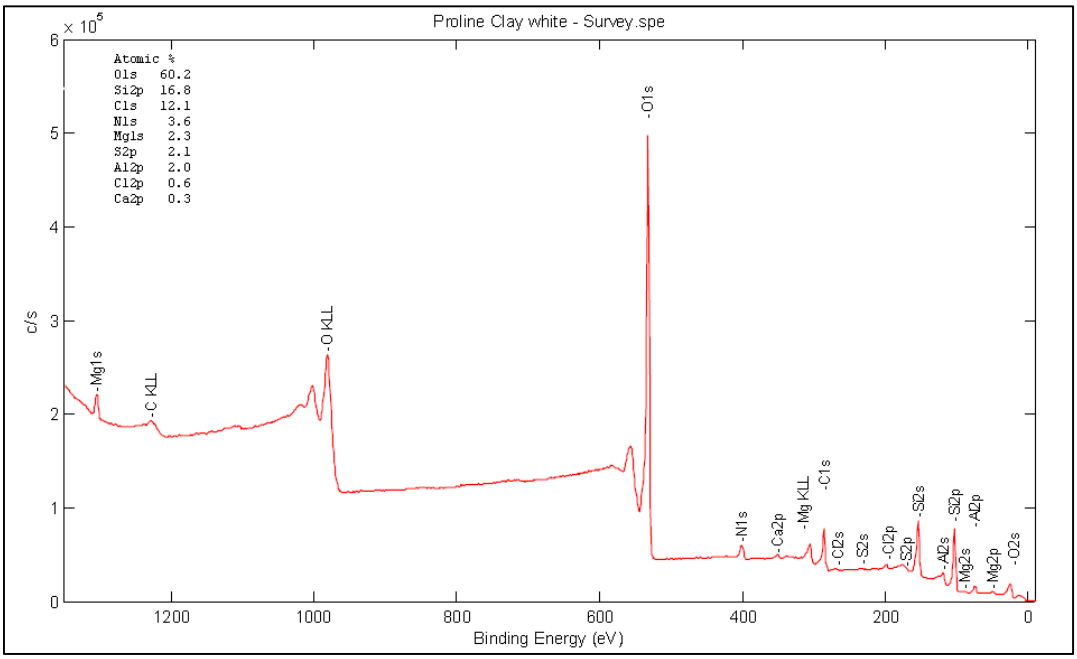

(b)

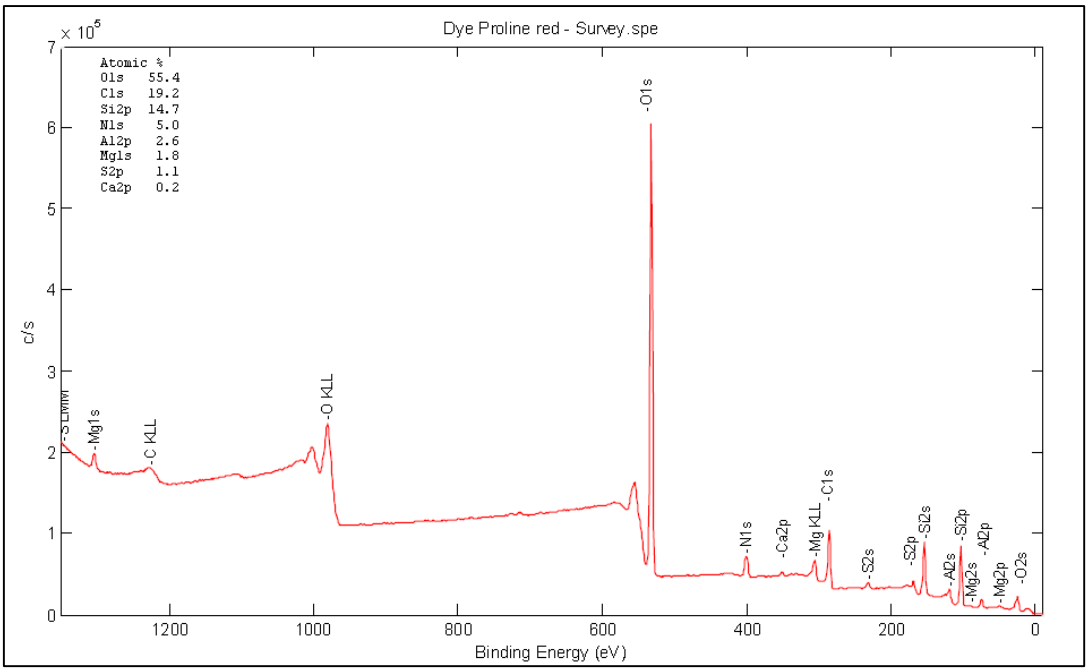

Figure 3.15. The XPS spectra of (a) PRO-BEN and (b) dye-laden PRO-BEN

It is possible that electrostatic repulsions may exist between the anionic dye and pure bentonite which could be due to the oxyanions in the basal plane in bentonite (Fig. 3.16). The oxyanions might be able to surround the metal ions within the bentonite structure giving it an overall negative charge as confirmed by its zeta potential value. The positive ammonium ions within the polymer could attract the oxyanions on the bentonite whereas the excess polymer imparts

an overall positive charge to the new bentonite composite. This could enhance adsorption efficiency by lowering electrostatic repulsion between the anionic dye and the bentonite composite. There was a decrease in cationic exchange capacity ,calculated by the Methylene Blue method (Kahr and Madsen 1995: 327 – 336), from ± 70 mmol/100 g ± 3.04 mmol/100 to 36.40 mmol/100 g ± 3.040×10^{-2} mmol/100g, for bentonite and PRO-BEN, respectively.

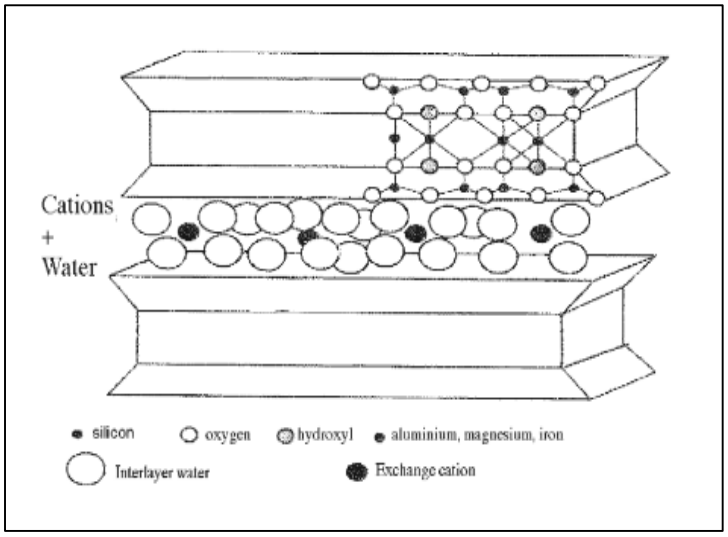

Figure 3.16. The structure of bentonite exhibiting the outer oxide layers (Siebers 2009: 4)

A summary of data obtained for bentonite and PRO-BEN is presented in Table 3.11.

Table 3.11. Physical and Chemical properties of bentonite and PRO-BEN

Property	**Bentonite**	**PRO-BEN**
Bulk Density/ $g.mL^{-1}$	$2.398 \pm 2.001\times10^{-4}$	$2.400 \pm 1.054\times10^{-4}$
Particle size/d.nm	513.0 ± 24.09	996.9 ± 32.27
Zeta Potential/ mV	-8.960 ± 0.5079	5.310 ± 0.3257
Cationic exchange capacity/ $mmol.100g^{-1}$	70.00 ± 3.04	$36.40 \pm 3.040\times10^{-2}$

3.3.3. Adsorption Studies

The adsorption studies were carried out with three dyes, viz., RB 222, RR 145 and RY 195. Many factors such as the initial concentration of the dye, the pH of the dye medium, the temperature, the salt concentration and the quantity of PRO-BEN were investigated. The

adsorbents were also compared with alumina since it is cheaper and most used adsorbent. Since adsorption can be rationalized as a reaction Ahn *et al.* (1985: 541-550), the reaction equation can be viewed as:

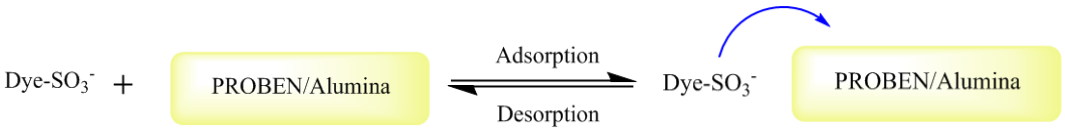

(3.4)

The Le Châtelier's principle is applicable to the reaction statement above (Masel 1996: 804) and was used as a basis for establishing the factors mentioned above. The visible effect of adsorption (Fig. 3.17) was shown when the solution became discoloured when dye was added to PRO-BEN.

Figure 3.17. Adsorption of dyes onto PRO-BEN

3.3.3.1. The Calibration Graph of the Mixed Dyes

To determine the extinction co-efficient (E) of the dyes which was to be used for further calculations, a calibration curve was constructed by plotting concentration of dye versus absorbance (Table 3.12, Fig.3.18, Fig. 3.19). The E values were used to calculate the concentration of the dyes remaining in solution after adsorption and desorption.

The three dyes were mixed and analysed as a ternary dye solution. The limit of detection (LOD) and limit of quantification (LOQ) was determined by using two equations (equations 3.5 and 3.6), where $S_{y/x}$ is the standard error of the regression from the calibration graph.

$$LOD = 3(S_{y/x}) \quad (3.5)$$

$$LOQ = 10(S_{y/x}) \quad (3.6)$$

Table 3.12. Summary of data for the calibration graph of the three textile dyes

Concentration of dyes/ mg.L^{-1}	**Absorbance/ AU**		
	Reactive Blue 222	**Reactive Red 195**	**Reactive Yellow 145**
0.000	0.000 ± 1.000×10^{-4}	0.000 ± 1.000×10^{-4}	0.000 ± 1.000×10^{-4}
10.00	0.1770 ± 5.774×10^{-2}	0.2580 ± 1.000×10^{-3}	0.2020 ± 2.000×10^{-3}
20.00	0.3530 ± 1.562×10^{-4}	0.5130 ± 1.000×10^{-3}	0.4050 ± 2.646×10^{-3}
30.00	0.5320 ± 5.774×10^{-4}	0.7720 ± 1.677×10^{-2}	0.6110 ± 1.527×10^{-3}
40.00	0.6970 ± 1.000×10^{-4}	1.014 ± 5.774×10^{-4}	0.8130 ± 1.000×10^{-3}
50.00	0.8700 ± 5.773×10^{-4}	1.265 ± 3.055×10^{-3}	1.027 ± 1.155×10^{-3}
R^2 value	0.9999	0.9999	0.9999
gradient	0.01740	0.02530	0.02050
$S_{y/x}$	0.002500	0.002800	0.001900
LOD/ ppm	0.4300	0.3300	0.2800
LOQ/ ppm	1.400	1.100	0.9300

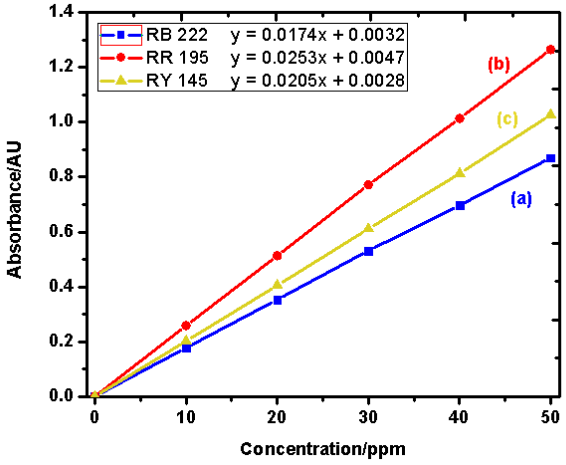

Figure 3.18. The calibration graph for (a) Reactive Blue 222, (b) Reactive Red 195 and (c) Reactive Yellow 145

An increase in absorbance as the dye concentration was increased is in accordance with the Beer-Lambert law. Using equation 3.4 above, and based on the Le Châtelier's principle, the equilibrium shifted to the right implying a greater extent of adsorption. The gradients of the linear graphs were used as the EC for the dyes. The LOD and LOQ were calculated from data obtained (Table 3.12), based on triplicate analysis

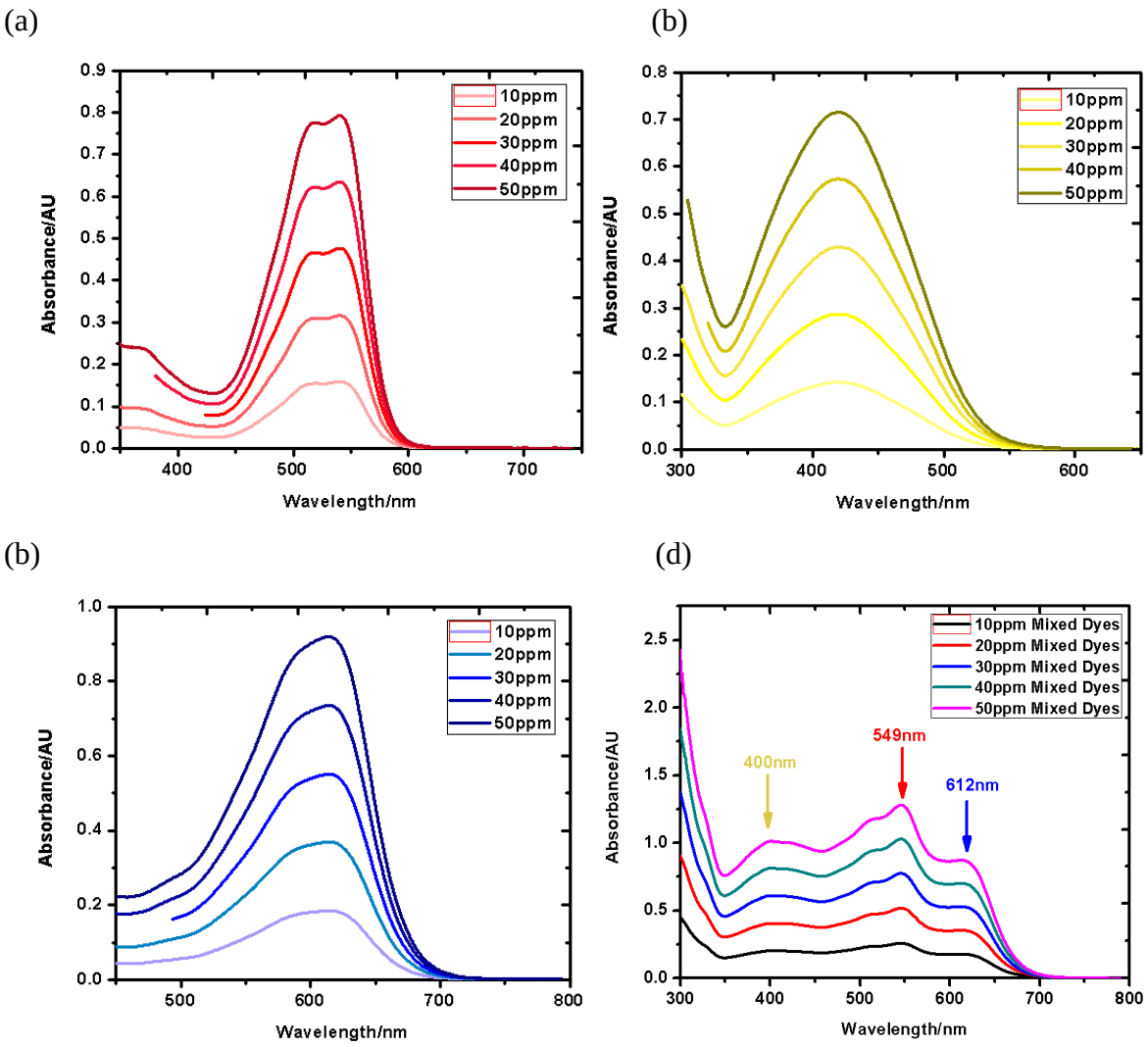

Figure 3.19. The UV Profile for (a) Reactive Blue 222, (b) Reactive Red 195, (c) Reactive Yellow 145, (d) mixed dyes

3.3.3.2. The Adsorption of Individual Dyes

This study was conducted to determine the minimum time for maximum adsorption for each dye. Briefly, an aliquot of a 40.00 mg/L solution of each dye solution was used for the study. It was observed that the absorbance for all dyes was lower for PRO-BEN than alumina suggesting PRO-BEN was the better adsorbent (Fig. 3.20). Most of the dyes were adsorbed by PRO-BEN in 10 minutes whereas alumina took 120 minutes.

(a)

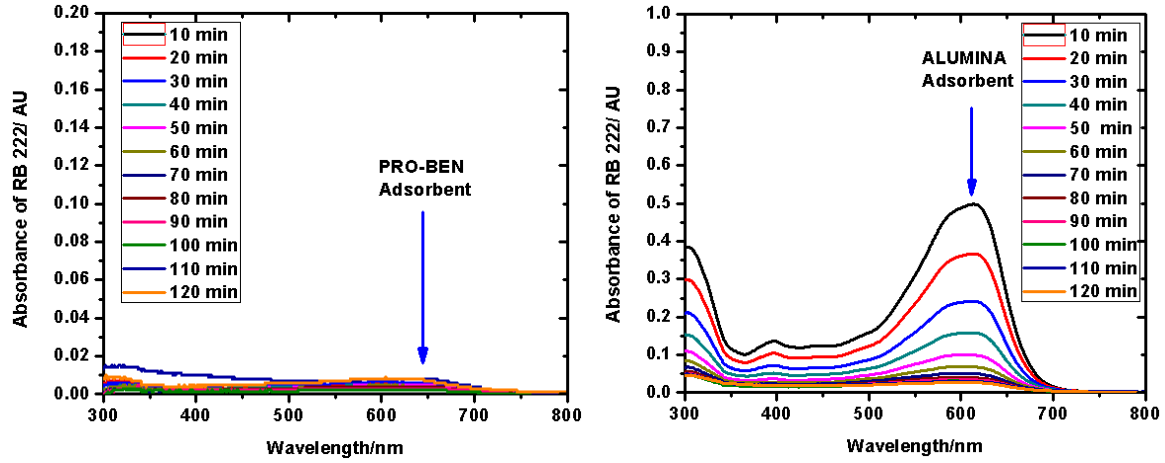

(b)

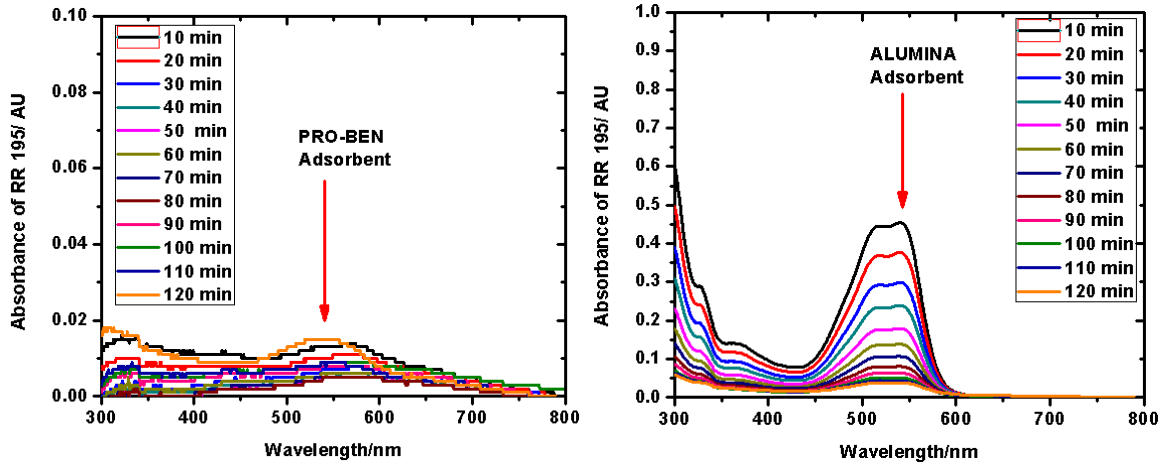

(c)

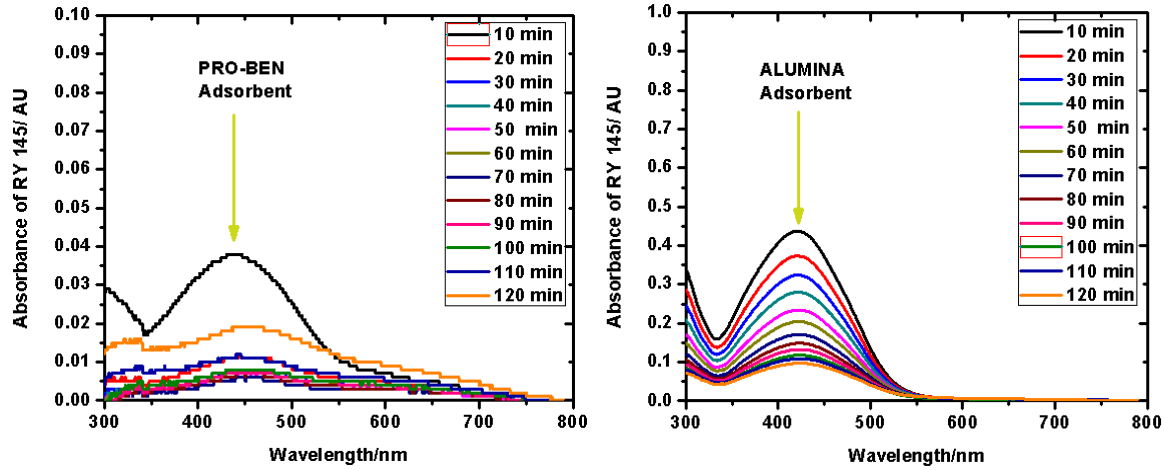

Figure 3.20. Spectra of the adsorption of (a) Reactive Blue 222, (b) Reactive Red 195 and (c) Reactive Yellow 145 by PRO-BEN and alumina

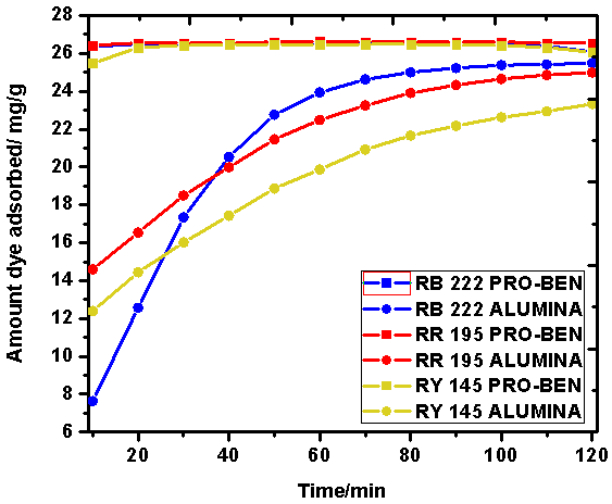

Figure 3.21. Spectra of the adsorption of the trends in adsorption of the three dyes onto PRO-BEN and alumina.

3.3.3.3. Quantity of PRO-BEN Required for Adsorption

This study was conducted to determine the optimum quantity of PRO-BEN that was required to adsorb 40.00 mg/L ternary dye solution.

It was found (Fig. 3.21 and Fig. 3.22) that higher quantities of PRO-BEN adsorbed more dyes from the ternary dye solution. In particular, RR 195 and RY 145 were fully adsorbed at greater than 0.1500 g PRO-BEN whilst RB 222, was marginally lower suggesting adsorption sites were sufficient. One of the factors affecting adsorption is the number of sites available for adsorption. As the quantity of adsorbent increases, the sites available for adsorption also increase. At high quantities of adsorbent, together with smaller particle sizes and higher porosities, there are greater number of sites for dye molecules to attach onto as compared to lesser quantities of PRO-BEN. Herein the positive surface of PRO-BEN could electrostatically attract the negatively charged dye and through these interactions, the dye could be adsorbed by PRO-BEN. It was found that the optimum quantity of PRO-BEN for adsorption of 40.00 mg/L of a mixed dye solution was 0.1500 g. This quantity was used throughout the study, unless stated otherwise.

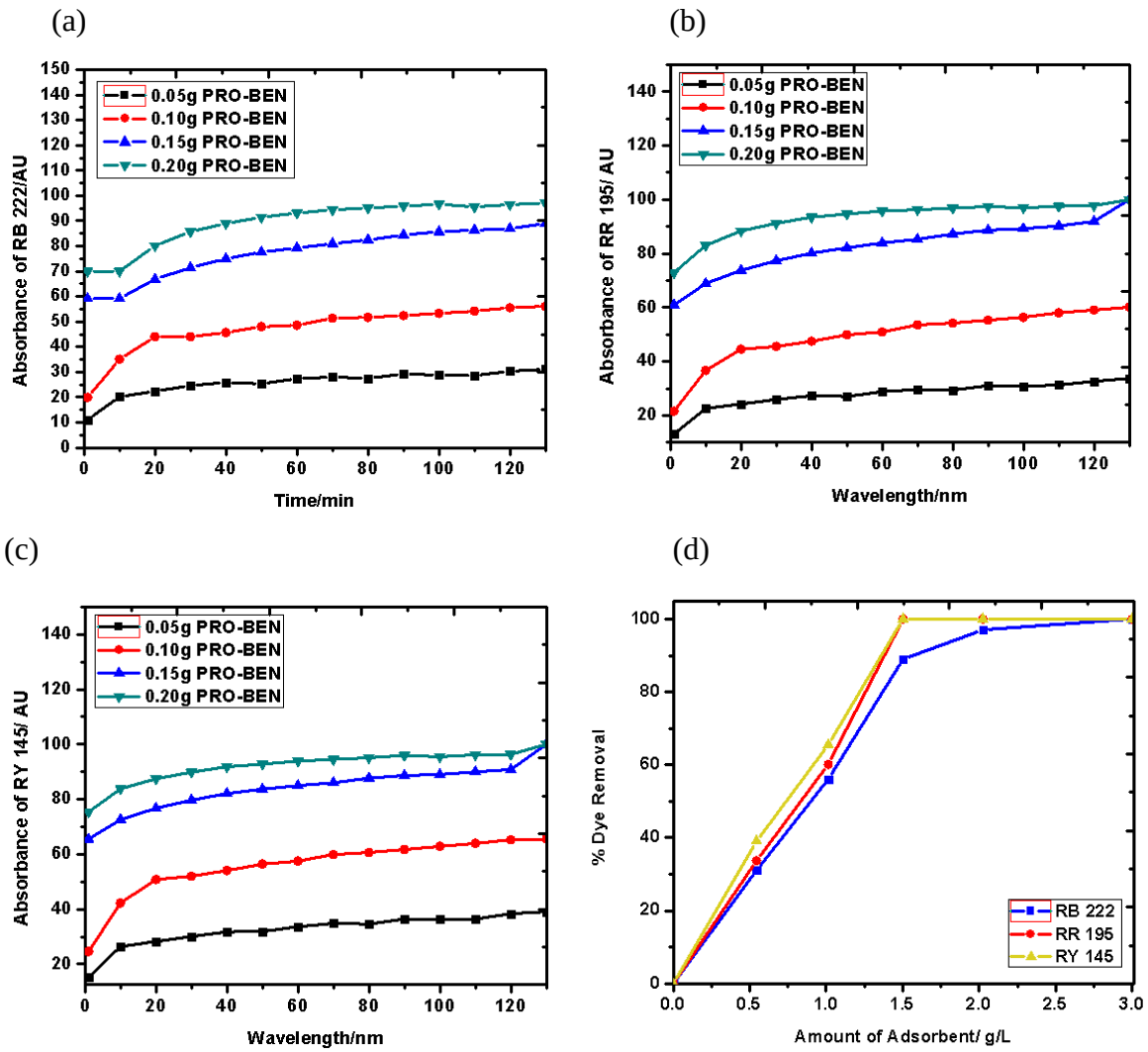

Figure 3.22. Adsorption of (a) RB 222, (b) RR 195 and (c) RY 145 and (d) the trend in percentage dye removal with quantity of adsorbent at 25 ˚C, 40.00 mg/L agitated at 120 rpm

3.3.3.4. The Effect of Initial Concentration of Dyes on Adsorption

Various concentrations of mixed dye solutions were adsorbed onto 0.1500g PRO-BEN to determine the effect of initial concentration on adsorption. The adsorption capacity of PRO-BEN and alumina were carried out at pH 5.21 and ambient temperature with no excess sodium chloride present.

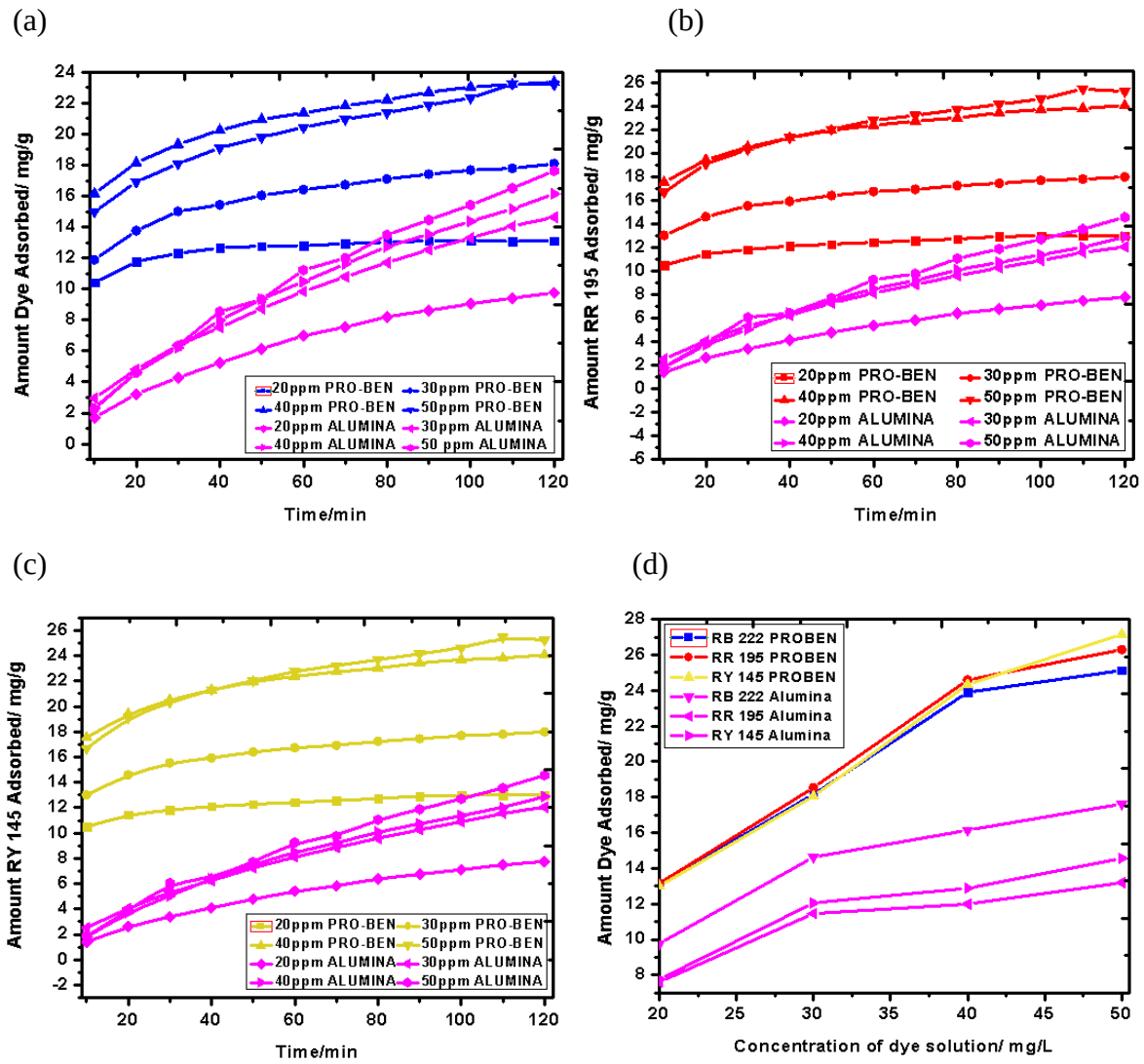

Figure 3.23. The trend in adsorption of (a) Reactive Blue 222, (b) Reactive Red 195 and (c) Reactive Yellow 145 from a ternary solution at various concentrations and (d) the overall trend in adsorption at 25 ˚C with 0.1500 g PRO-BEN or alumina and agitated at 120 rpm

It was found that the initial concentration of RB 222 affected the adsorption process (Fig. 3.23). At high concentrations, a greater amount of dye is adsorbed. The same pattern is seen with adsorption using alumina, though the adsorption capacity varied greatly between the two. At high concentrations there is possibly a concentration dip at the boundary layer near the adsorbent interface thereby creating a concentration gradient. This could cause a mass transfer of dyes from the bulk solution to the interface of the modified bentonite, thereby overcoming the mass transfer resistance at the boundary layers. This mass transfer could be enhanced by convection currents caused by magnetic stirring (Kim and Walker 2001: 123 – 131). The contact time was also studied to determine when adsorption was complete. It was found that 180 minutes was the optimum time for adsorption.

3.3.3.5. The Effect of pH of the Mixed Dye Solution on Adsorption

The study was conducted to determine the effect of an acidic or basic dye medium on adsorption. The optimum pH of the dye solution to be used in the experiments was established. A range of pH values of the dye solutions were tested at ambient temperature.

It was observed (Fig. 3.24) that pH influenced the adsorption of dyes. It is found that at lower pH of the ternary dye solution, adsorption increased when PRO-BEN was used. Although a similar trend was observed for alumina, the quantity of dye adsorbed was less. It is plausible that the PRO-BEN surface contained a double layer, an outer positive layer (PEP layer) available for anionic dye adsorption and a layer of anionic dyes approaching the positive layer. Also at low pH, the behaviour of PRO-BEN towards anionic dyes are similar to colloidal systems (Kahr and Madsen 1995: 327 – 336). It is possible the lowering of the pH by the addition of dilute hydrochloric acid to the dye solution could reduce the size of the double layer (Kahr and Madsen 1995: 327 – 336) thereby enhancing the net attractive forces between PRO-BEN and the anionic dyes (Kahr and Madsen (995: 327 – 336). Conversely, it was found that by raising the pH with the addition of dilute sodium hydroxide solution, adsorption reduced probably due to competition with anionic dyes for PRO-BEN adsorption sites. Hydroxides are generally more reactive and smaller than alkyl sulfonates and thus could reach and adsorb onto the surface of the positive-charged PRO-BEN more easily.

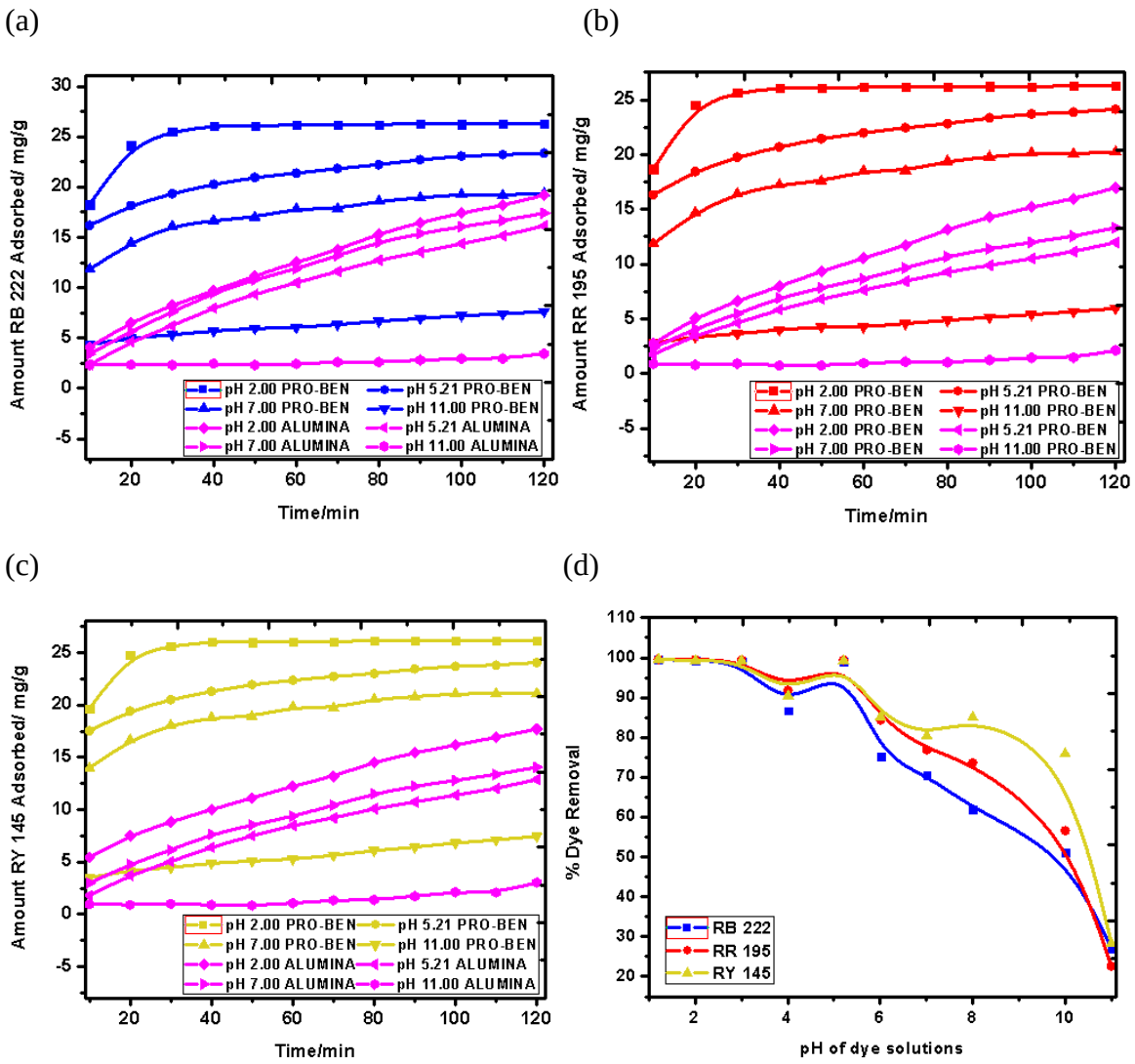

Figure 3.24. Effect of pH on the adsorption of (a) Reactive Blue 222, (b) Reactive Red 195 and (c) Reactive Yellow 145 from a ternary dye solution using PRO-BEN and alumina and (d) the trend in adsorption at various pH values of the dye medium

3.3.3.6. The Effect of Sodium Chloride Concentration on Adsorption

The effect of salts present in the dye solution was studied since salts can dissociate into its ions which could either hinder or promote adsorption. Here a 40.00 mg/L mixed dye solution was used and various concentrations of sodium chloride was added to determine adsorption by PRO-BEN and alumina.

It was found that the quantity of sodium chloride affected the extent of adsorption (Fig. 3.25). Alumina adsorbed less dyes than PRO-BEN. It was also noted for all dyes that as the concentration of sodium chloride increased, the quantity of dye adsorbed onto PRO-BEN also

decreased (Fig. 3.25 (d)). A similar trend was reported whereby the presence of foreign ions suppressed the adsorption of dyes (Li *et al.* 2009: 1170 – 1178).

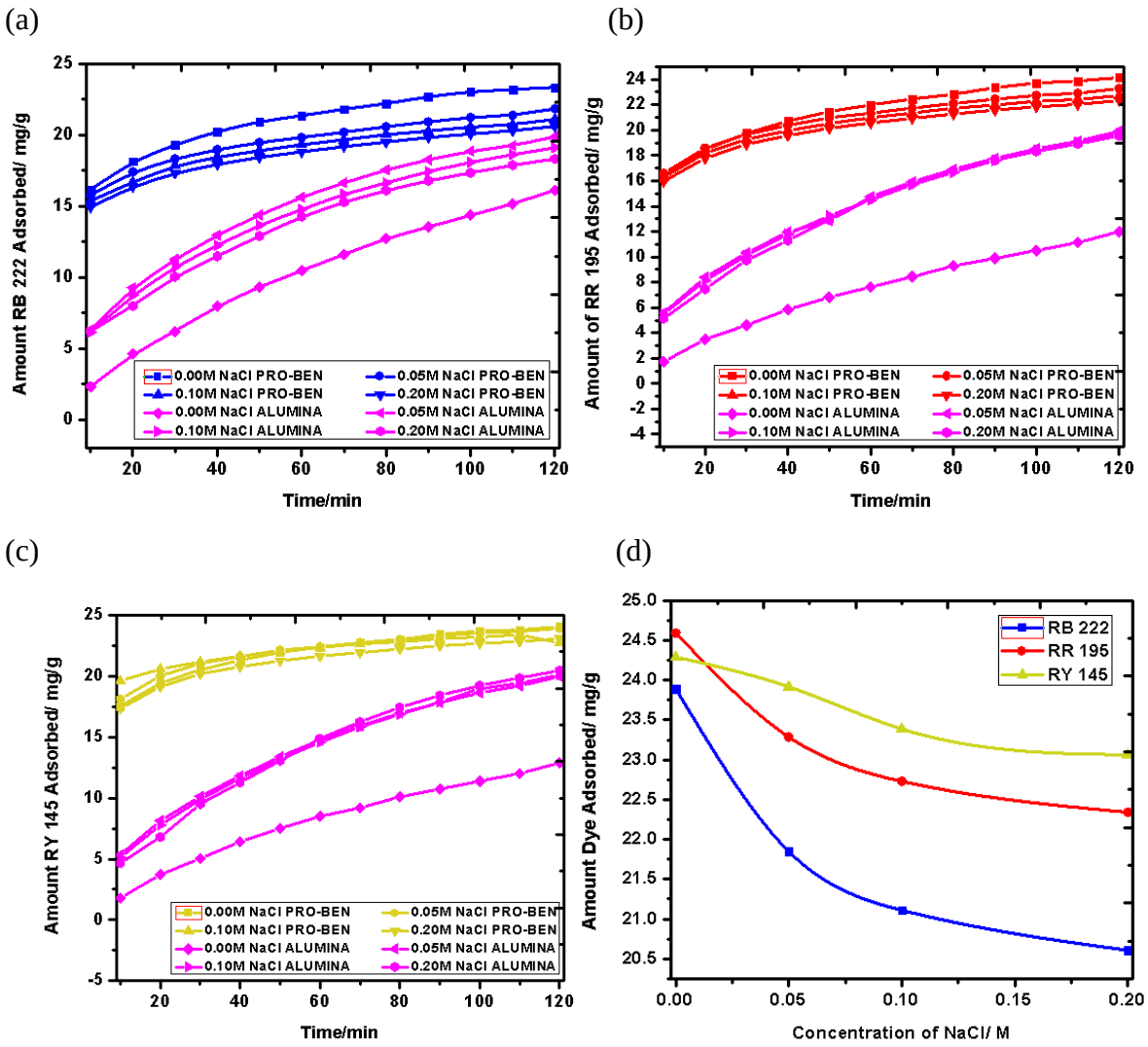

Figure 3.25. Effect of sodium chloride on adsorption for (a) Reactive Blue 222, (b) Reactive Red 195 and (c) Reactive Yellow 145 at 25 ˚C, 120 rpm, 40.00 ppm with 0.1500 g PRO-BEN used

The decrease in adsorption could be due to the competition of the chloride ions and the dye for the surface of PRO-BEN. Since chloride ions are smaller than RSO_3^- groups, they could reach PRO-BEN more efficiently (Eren and Afsin 2008: 682 – 691)

3.3.3.7. The Effect of Temperature on Adsorption

The effect of temperature plays an intricate role in the adsorption process. It gives an idea of the type of interactions that exist between the adsorbate and adsorbent. It is known that a decrease in adsorption with an increase in the medium temperature suggests a physisorption process, whilst an increase in adsorption as the medium temperature decreases is indicative of chemisorption process. In most cases in literature, adsorption was an exothermic reaction, which further implied a physisorption process. With this information, and the assumption that the activity co-efficients in Henry's law are equivalent to 1.00, at low concentrations of the dyes, the entropy (ΔS°), the enthalpy (ΔH°) and the Gibbs free energy (ΔG°) were calculated (Lewinsky 2007: 79).

Three temperatures viz. 25 ˚C, 35 ˚C and 45 ˚C were selected to establish the relationship between temperature and adsorption and to determine the best temperature for adsorption.

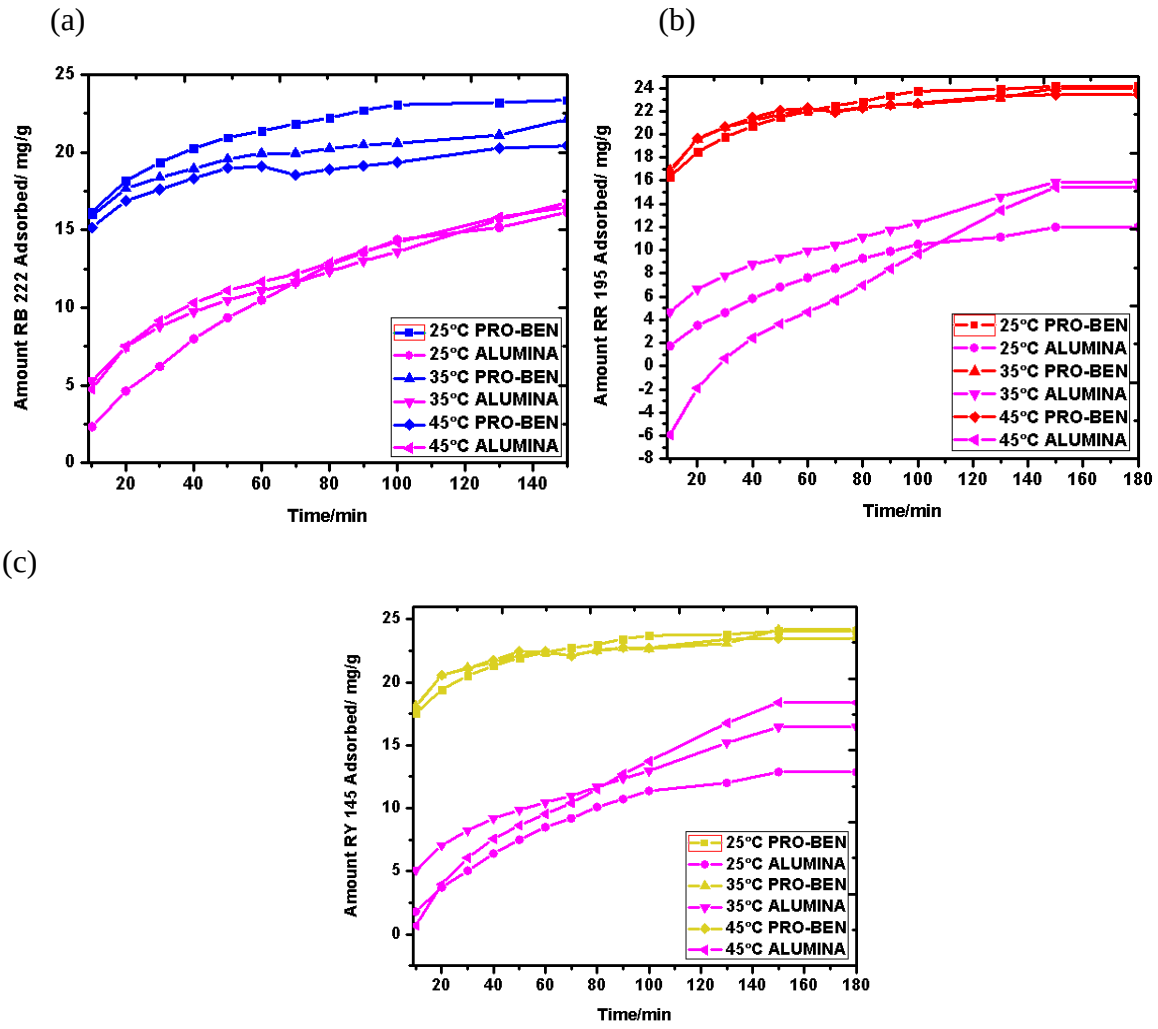

Figure 3.26. Effect of temperature on the adsorption of (a) Reactive Blue 222, (b) Reactive Red 195 and (c) Reactive Yellow 145 using PRO-BEN and alumina

It was found that an increase in temperature caused a decrease in adsorption of the dyes (Fig. 3.26). Also alumina adsorbed less dyes than PRO-BEN. The optimum temperature was found to be 25 ˚C. It is possible that as the temperature of the dye solution increased, the boundary layer thickness between PRO-BEN and the solution decreased because the dyes acquired additional kinetic energy to migrate from PRO-BEN to the solution causing a decrease in adsorption. These results suggest that the interactions between the dye and PRO-BEN are weak indicative of physisorption (Jnr and Spiff 2005: 162 – 169).

Thermodynamic studies were conducted to confirm whether the adsorption process was physisorption or chemisorption. By using equations 3.7- 3.10 (Toor and Jin 2012: 79 – 88), the enthalpy ($\Delta H°$), entropy ($\Delta S°$), Gibbs free energy ($\Delta G°$) and rate constant (k_e) were determined:

$$ln k_e = \Delta S°/R - \Delta H°/RT \quad (3.7.)$$

$$\Delta G° = \Delta H° - T\Delta S° \quad (3.8)$$

$$k_e = q_e / C_e \quad (3.9)$$

$$ln k_{H2} = lnA - E_a/RT \quad (3.10)$$

The meaning of each symbol is presented in Appendix 3 (page 155).
The $\Delta H°$ and $\Delta S°$ values were calculated as the slope and intercept of the plot of $\ln K_{H2}$ as a function of T^{-1}/ K^{-1} from equation 3.7.
k_e in equation 3.9 is the concentration of dyes remaining in the solution at equilibrium to the quantity of dyes adsorbed on the PRO-BEN.

The Arrhenius equation 3.10 was used in conjunction with second order reaction constant (K_{H2}) to determine the activation energies at various temperatures. It was found that the adsorption process was exothermic due to the negative enthalpy value. The enthalpy for RY 145 (-17.72 kJ/mol) was the highest and was lowest for RB 222 (-37.81 kJ/mol). This indicated that RY 145 was held more strongly onto the PRO-BEN than the rest of the dyes (Toor and Jin 2012: 79 – 88). As reported in literature, physisorption enthalpies range from 0.000 kJ/mol to 40.00 kJ/mol and chemisorption enthalpies from 200.0 kJ/mol upwards (Tyagi 2009: 79). All enthalpies for the dyes studied were below 40.00 kJ/mol indicating a physisorption process wherein as the dyes adsorbed onto the PRO-BEN, their freedom of motion was restrained. This

resulted in an increase in the entropy (-ΔS°) Kahr and Madsen (1995: 327-336) for RB 222, RR 195, and RY 145 respectively. The entropies for each dye were negative decreased in the following order: RY 145 < RR 195 < RB 222. The calculated Gibbs free energy values (Table 3.13) were negative, which indicated a spontaneous adsorption process possibly due to the dye molecules having great affinity towards PRO-BEN and similar results were reported (Toor and Jin 2012: 79 – 88). The graphs (Fig. 3.27), showed good linear regression values which indicated acceptable correlations and good results.

(a) (b)

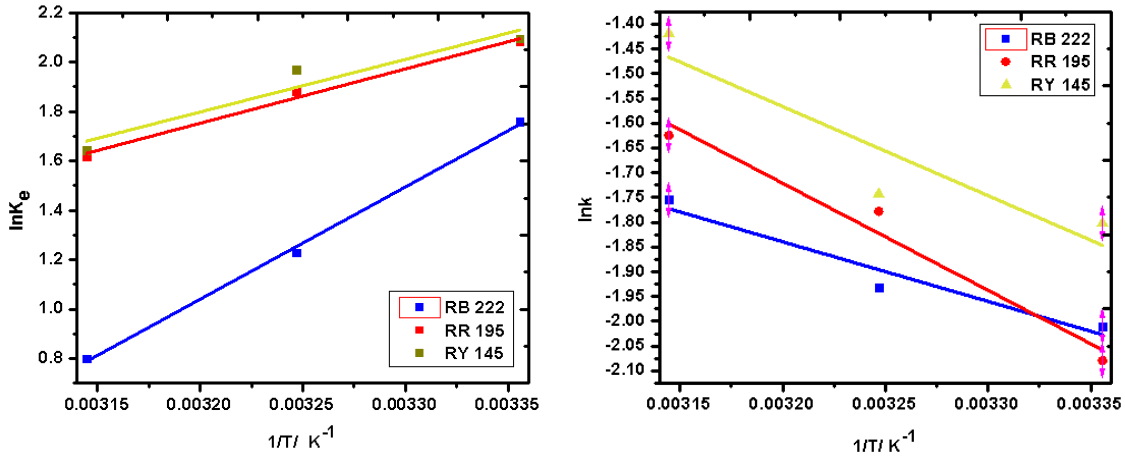

Figure 3.27. (a) Van't Hoff plot and (b) Arrhenius plot for the various temperatures

Table 3.13. Thermodynamic parameters calculated from the adsorption of the three dyes at the various temperatures

Dyes	**Temp./ K**	**(E_A/ kJ)/ K_{HO}**	**A**	**R^2**	**ΔS^0/ J.mol^{-1}.K^{-1}**	**ΔH^0/ kJ.mol^{-1}**	**ΔG^0/ kJ.mol^{-1}**	**R^2**
RB 222	298.0	14.49	7.510	0.8890	-112.3	-37.81	-71.28	0.9970
	308.0						-72.40	
	318.0						-73.53	
RR 195	298.0	26.01	180.9	0.9520	-43.98	-18.30	-31.40	0.9820
	308.0						-31.84	
	318.0						-32.28	
RY145	298.0	21.66	66.37	0.7030	-41.74	-17.72	-30.16	0.8560
	308.0						-30.57	
	318.0						-30.99	

3.3.4. Study of Adsorption Isotherms

3.3.4.1. Adsorption Isotherm Analysis

Adsorption studies were conducted to characterize the adsorption processes and to assess the efficiency of the adsorbents viz., PRO-BEN and alumina.

The Langmuir (Saraydin *et al.* 1998: 227 – 236), the Freundlich (Freundlich and Hatfield 1926), Temkin (Temkin and Pyzhev 1940: 327 – 356) and the Frumkin isotherms (Frumkin 1926: 792 – 802) were tested (Table 3.14).

Table 3.14. Equations used for adsorption isotherms

Equation	Isotherm	Linear plot	Parameters
3.11	Langmuir	$\frac{C_e}{q_e} = \frac{C_e}{q_m} + \frac{1}{k_a q_m}$ C_e/q_e as a function of C_e	Gradient = $\frac{1}{q_m}$ y-intercept = $\frac{1}{k_a q_m}$
3.12	Freundlich	$\ln(q_e) = lnK_F + \frac{1}{n}\ln(C_e)$ $\ln(q_e)$ as a function of $\ln(C_e)$	Gradient = $\frac{1}{n}$ y-intercept = lnK_F
3.13	Temkin	$q_e = \left(\frac{RT}{b_T}\right) lnA_T + \left(\frac{RT}{b_T}\right) lnC_e$ q_e as a function of lnCe	Gradient = $\frac{RT}{b_T}$ y-intercept = lnA_T
3.14	Frumkin	$\log(\frac{Q_e}{1-Q_e}).\frac{1}{C_e} = \log K + 2aQ_e$ log $(Q_e/1\text{-}Q_e)C_e$ as a function of Q_e	Gradient = $2a$ y-intercept = $\log K$

Each isotherm provides specific information about the adsorption process (Table 3.15).

Table 3.15. Information that the isotherms provides about the adsorption process

Isotherm	Information on adsorption process
Langmuir	Adsorbates cover the adsorbent in a monolayer, where all sites are equal, no interactions between adsorbates and there are a specific amount of sites available for adsorption
Freundlich	This gives information on the heterogeneity of the adsorbent surface adsorption sites
Temkin	This gives further information on whether the adsorption process was a physisorption or chemisorption process based on the Temkin isotherm equilibrium binding constant
Frumkin	This gives information on the lateral interactions between the adsorbate molecules and the homogenous surface of the adsorbent, if the interactions among the adsorbate (*A*) equated to zero, then this isotherm reduces to the Langmuir isotherm

3.3.4.2. The Langmuir Isotherm

To determine the type of adsorption isotherm, the type 1 Langmuir, isotherm was tested by using the equation:

$$\frac{C_e}{q_e} = \frac{C_e}{q_m} + \frac{1}{k_L q_m} \quad (3.15)$$

The meaning of each symbol is presented in Appendix 4.

A plot of $\frac{C_e}{qe}$ as a function of C_e produced a straight line from which the gradient and y-intercept was obtained as $\frac{1}{qm}$ and $\frac{1}{k_L q_m}$, respectively. Using this information, the total adsorption at monolayer coverage was obtained.

The initial concentration was studied at optimum pH 5.21 and temperature of 25 ˚C. The adsorption followed the type 1 Langmuir isotherm plot best from the Giles classification system (Giles *et al.* 1960: 3973 – 3993) due to the highest R^2 value (best linearity). The data (Table 3.16) implied that all sites on the PRO-BEN were equivalent, monolayer coverage of the dyes onto the PRO-BEN occurred, the PRO-BEN surface was homogenous and there were no interactions between RB 222, RR 195 and RY145. From the data (Table 3.16 and Fig. 3.28) the total maximum monolayer coverage on PRO-BEN was calculated as 78.56 mg/g ± 0.05532 mg/g for all the dyes. The separation factor (R_L) for the dyes were between zero and one indicating favourable adsorption of the dyes on PRO-BEN (Dada *et al*. 2012: 38 – 45).

Table 3.16. The Langmuirian data for dyes adsorption

Dyes	**Langmuir (Type 1)**			
	q_m/ mg/g	**k_L/ L.mg^{-1}**	**R_L**	**R^2**
RB 222	24.41 ± 0.9413	2.240 ± 0.1012	0.01800	0.9980
RR 195	25.84 ± 0.5523	2.390 ± 0.1007	0.01600	0.9980
RY 145	28.31 ± 0.9464	1.060 ± 0.2004	0.03200	0.9930

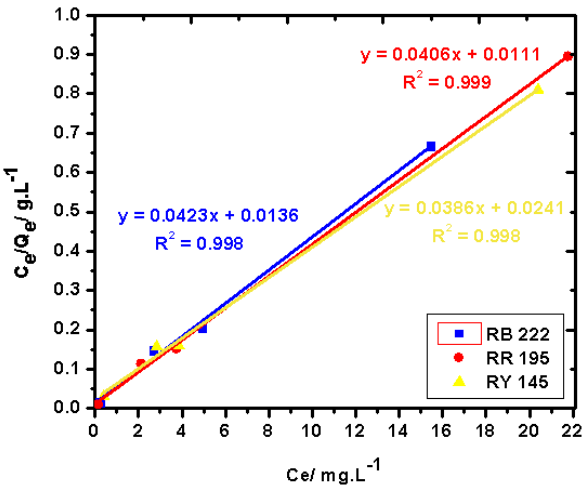

Figure 3.28. The Langmuir plot for RB 222, RR 195 and RY 145 at 25 ˚C at pH = 5.21

3.3.4.3. The Freundlich Isotherm

The Freundlich isotherm (equation 3.16) was used to determine the heterogeneity of the adsorbent surface by using the equation:

$$\ln(q_e) = lnk_F + \frac{1}{n\ln(C_e)} \tag{3.16}$$

Where k_F is the adsorption capacity and $\frac{1}{n}$ represents the adsorption intensity.

A linear plot of $ln\ (q_e)$ as a function of $ln\ (C_e)$ produced the gradient of $\frac{1}{n}$ and a y-intercept of $ln\ (k_F)$.

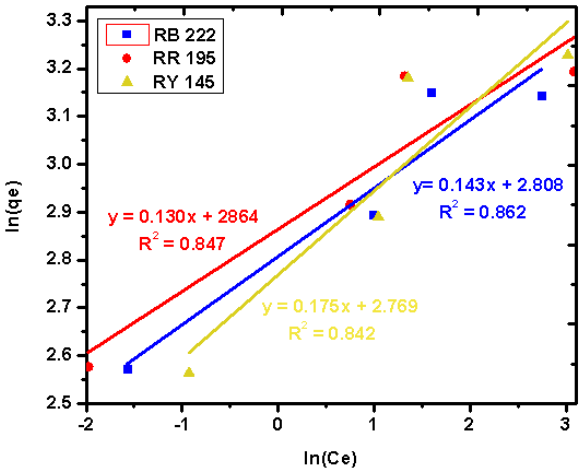

Figure 3.29. The Freundlich plot for RB 222, RR 195 and RY 145 at 25 ˚C at pH = 5.21

Table 3.17. The Freundlich data for dye adsorption

Dyes	Freundlich Isotherm			
	n	**1/n**	**k_F / mg/g**	**R^2**
RB 222	7.520 ± 0.2489	0.1330 ± 0.03101	16.62 ± 1.059	0.8620
RR 195	7.820 ± 0.1585	0.1280 ± 0.5112	17.58 ± 1.096	0.8470
RY 145	5.870 ± 0.01370	0.1890 ± 0.03379	16.00 ± 1.069	0.8420

$\frac{1}{n}$ (Table 3.17) was found to be less than 1 for all dyes, which indicated normal adsorption. From Fig. 3.29, the values were calculated to be between one and ten which indicated that adsorption was favourable (Dada *et al.* 2012: 38 – 45).

3.3.4.4. The Temkin Isotherm

The Temkin isotherm model was tested to determine the interactions between the adsorbent and the adsorbates by using the equation:

$$q_e = \frac{RT}{b_T}\, lnA_T + \frac{RT}{b_T}\, lnC_e \qquad (3.17)$$

.

The meaning of each symbol is presented in Appendix 5.

From Fig. 3.30, the heat of sorption, RT/ b_T, was calculated to be 2.543 J.mol^{-1} ± 0.7235 J.mol^{-1} for RB 222, 2.371 J.mol^{-1} ± 0.7374 J.mol^{-1} for RR 195 and 3.222 J.mol^{-1} ± 1.025 J.mol^{-1} for RY 145 (Table 3.18).

It was observed that adsorption of the dyes decreases linearly as the surface of PRO-BEN was covered with the dyes.

Table 3.18. The Temkin isotherm data for the dye adsorption

Dyes	Temkin Isotherm			
	A_T /L.g^{-1}	b_T	RT/b_T/ J.mol^{-1}	R^2
RB 222	0.8610 ± 0.3508	973.9 ± 227.1	2.543 ± 0.7235	0.7910
RR 195	2.213 ± 0.2173	1044 ± 324.7	2.371 ± 0.7374	0.7570
RY 145	1.381 ± 0.3524	768.9 ± 244.4	3.222 ± 1.025	0.7480

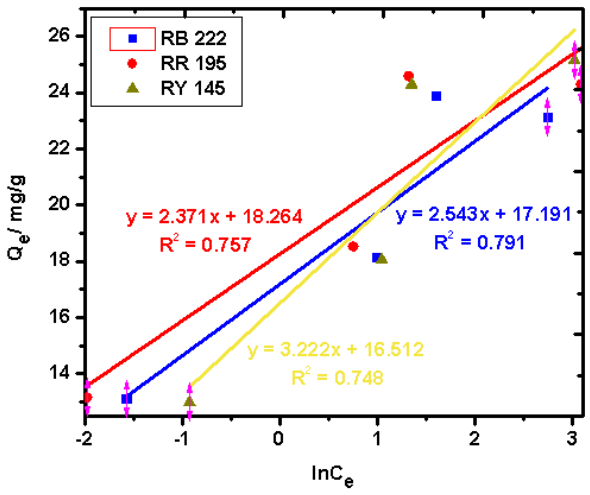

Figure 3.30. The Temkin plot for Reactive Blue 222, Reactive Red 195 and Reactive Yellow 145 at 25 ˚C at pH 5.21

3.3.4.5. The Frumkin Isotherm

The Frumkin isotherm (Table 3.19) was tested to determine interaction between adjacent adsorbed dye molecules within the monolayer by using the equation:

$$log\left(\frac{Q_e}{1}-Q_e\right).\frac{1}{C_e}=\log k+2aQ_e \qquad (3.18)$$

The meaning of each symbol is presented in Appendix 6.

It was found that, the values for α were all positive (Fig. 3.31) which indicated that an overall repulsion between the adsorbed dyes occurred.

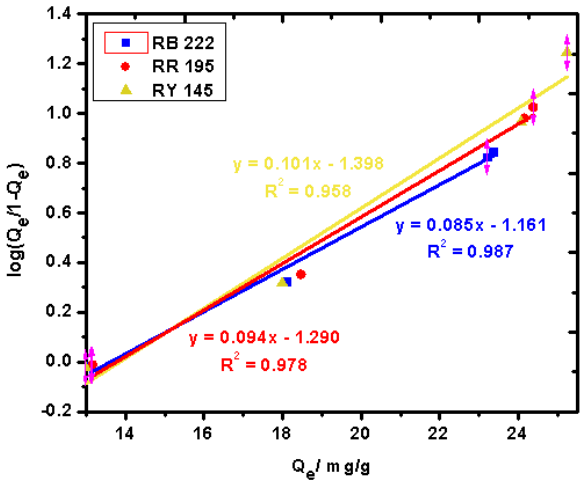

Figure 3.31. The Frumkin plot for RB 222, RR 195 and RY 145 at 25 ˚C at pH = 5.21

Table 3.19. The Frumkin isotherm data for the dye adsorption

Dyes	Frumkin Isotherm		
	k/ L/mg	**α/ mg/g**	**R^2**
RB 222	0.06900 ± 0.005610	0.04300 ± 0.002740	0.9870
RR 195	0.05100 ± 0.007990	0.04700 ± 0.001578	0.9780
RY 145	0.04000 ± 0.005790	0.05000 ± 0.003524	0.9580

3.3.5. Study of Adsorption Kinetics

To determine the order and kinetics, the Langergren's pseudo-first order (equation 3.19) (Lagergren 1898: 1 – 39) and the Ho's and McKay's pseudo-second order (equation 3.20) (McKay 1982: 759 – 772) equations were tested. Intraparticle diffusion (equation 3.21) (Weber and Morris 1962: 231 – 266) was used to determine whether the rate-limiting step in adsorption was dependent on the intraparticle diffusion of the dyes.

The mathematical linear equations for these models are presented in Table 3.20. The variable q_e/ mg/g is the quantity of dyes adsorbed at equilibrium,

q_t/ mg/g is the amount of dyes adsorbed at a particular time = t/min,

k_{L1}/ min^{-1} is the Langergren equilibrium rate constant,

k_{H2} / g/mg.min is the Ho's rate constant

k_{IPD} is the intraparticle diffusion rate constant and C is a constant relating mass transfer resistance due to the boundary layer of adsorbed dyes.

Table 3.20. Linear plots of the kinetic models

Equation	Model	Linear plot	Parameters
3.19	Langergren	$\log(q_e - q_t) = \log(q_e) - \frac{K_{L1}t}{2.303}$ $log(q_e - q_t)$ as a function of t/min	Gradient = K_{L1} y-intercept = $\log(q_e)$
3.20	Ho and McKay	$\frac{t}{q_t} = \frac{1}{K_{H2}q_e} + \frac{t}{q_e}$ t/q_t as a function of t/min	Gradient = K_{H2} y-intercept = $\frac{1}{q_e}$
3.21	Morris and Webber	$q_t = K_{IPD}t^{0.5} + C$ q_t as a function of $t^{0.5}$	Gradient = K_{IPD} y-intercept = C
3.22	Arrhenius	$lnk_A = \left(-\frac{E_A}{RT}\right) + lnA$ lnk_A as a function of 1/T/°C	Gradient = $(-\frac{E_A}{R})$ y-intercept = lnA

The experimental data were fitted into the pseudo-first order and second order kinetic models. The Ho's and McKay's second order kinetic model (Fig. 3.32 (a-c)) and Table 3.21) best fitted the adsorption data with highest R^2 values. However, the pseudo-first order did not rank as favourable. The dye equilibrium concentration on the PRO-BEN (q_e) did not correlate to the experimental value for the pseudo-first order, further discrediting the suitability of the model. The q_e values were closer to the experimental values, confirming the suitability of this model and results were in agreement with previous studies but the intraparticle diffusion (Table 3.22) model was used to determine the diffusion mechanism (Toor and Jin 2012: 79 – 88). According to the model, the intraparticle diffusion plots did not intersect the origin. This indicated that intraparticle diffusion is not the rate-limiting step alone, and there could be other factors that could be rate limiting in the adsorption process. The plots (Fig. 3.32 (d-f)) for RB 222, RR 195 and RY 145 were of dual-linearity, which implied that intraparticle diffusion and possibly external mass transfer (Cheng *et al.* 2008: 538 – 546), (Yue *et al.* 2007: 279 – 290) occurred. A similar trend was observed for the other dyes.

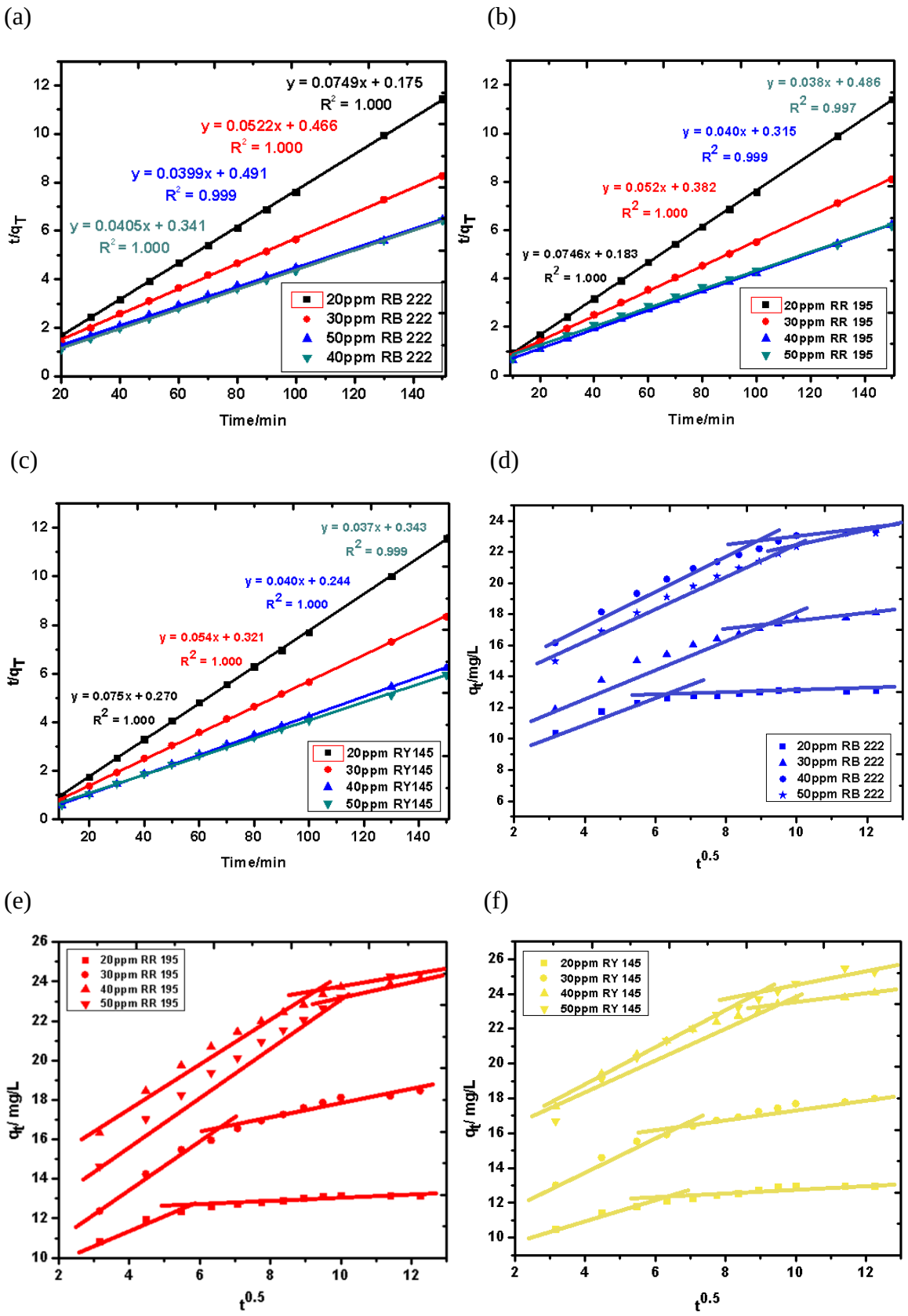

Figure 3.32. Langergren's pseudo-second order plots for (a) RB 222, (b) RR 195, (c) RY 145 and the intraparticle diffusion plots for (d) RB 222, (e) RR 195, (f) RY 145

Table 3.21. Kinetic information calculated from the adsorption of the three dyes

Dyes	**Kinetic model**	**Initial Concentration/ mg/L**			
		20.00	**30.00**	**40.00**	**50.00**
Langergren's pseudo-first order reaction					
RB 222	qe/ mg/g	2.410	7.430	11.35	10.53
	k_{L1}/ min^{-1}	0.03600	0.0260	0.03200	0.02300
	R^2	0.9260	0.9810	0.9690	0.9870
RR 195	qe/ mg/g	3.110	7.400	10.99	17.73
	k_{L1}/ min^{-1}	0.04100	0.02700	0.02900	0.03000
	R^2	0.9500	0.9790	0.9790	0.8670
RY 145	qe/ mg/g	3.930	6.170	8.490	11.30
	k_{L1}/ min^{-1}	0.03700	0.02500	0.02800	0.02500
	R^2	0.8870	0.9820	0.9770	0.9800
Ho's second order reaction					
RB 222	qe/ mg/g	13.37	18.99	24.47	24.61
	k_{H2} / g/mg	0.4070	0.1240	0.1340	0.09400
	R^2	1.000	0.9990	0.9980	0.9990
RR 195	qe/ mg/g	13.40	19.29	25.38	26.11
	k_{H2} / g/mg	0.4070	0.1350	0.1250	0.07900
	R^2	1.000	1.000	0.9990	0.9970
RY 145	qe/ mg/g	13.32	18.68	24.94	26.67
	k_{H2} / g/mg	0.2780	0.1670	0.1650	0.1090
	R^2	1.000	1.000	1.000	0.9990

Table 3.22. Intraparticle diffusion calculated from the adsorption of the three dyes

Dye	Parameters	Result			
RB 222	k_{ID1}/ $mg.g^{-1}.min^{-0.5}$	0.8330	1.161	1.384	1.486
	k_{ID2}/ $mg.g^{-1}.min^{-0.5}$	0.08000	0.4100	0.5200	0.8470
	R_1^2	0.9700	0.9740	0.9930	0.9900
	R_2^2	0.7600	0.9170	0.9170	0.9750
RR 195	k_{ID1}/ $mg.g^{-1}.min^{-0.5}$	0.6770	1.161	1.384	1.486
	k_{ID2}/ $mg.g^{-1}.min^{-0.5}$	0.09600	0.3590	0.5200	0.8840
	R_1^2	0.9670	0.9740	0.9930	0.9900
	R_2^2	0.8440	0.9160	0.9170	0.9790
RY 145	k_{ID1}/ $mg.g^{-1}.min^{-0.5}$	0.5790	1.094	1.944	1.457
	k_{ID2}/ $mg.g^{-1}.min^{-0.5}$	0.1590	0.3410	0.4040	0.6560
	R_1^2	0.9750	0.9950	0.9900	0.9860
	R_2^2	0.8570	0.9310	0.9170	0.9400

3.3.6. Desorption Studies

This study was conducted to determine the recyclability of PRO-BEN. Various concentrations of NaOH were used at temperatures 25 ˚C, 35 ˚C and 45 ˚C for the removal of the dyes from the dye-laden adsorbent (Fig. 3.33). It was found that increasing NaOH concentration results in more efficient removal of the dyes and the optimum NaOH concentration was 0.1000 M for the desorption process. As the temperature of the solution increased, the desorption process became more inefficient. The optimum condition for dye removal for PRO-BEN was 25 ˚C with removal percentages of 75.46 % ± 6.461 % for RY 145, 78.23 % ± 5.056 % for RR 195 and 97.08 % ± 0.6030 % for RB 222. The optimum conditions for dye removal from alumina was at 45 ˚C with percentages of 100.0 % ± 0.9031 % for RB 222, 56.25 % ± 3.363 % for RR 195 and 66.74 % ± 0.6208 % for RY 145.

(a)

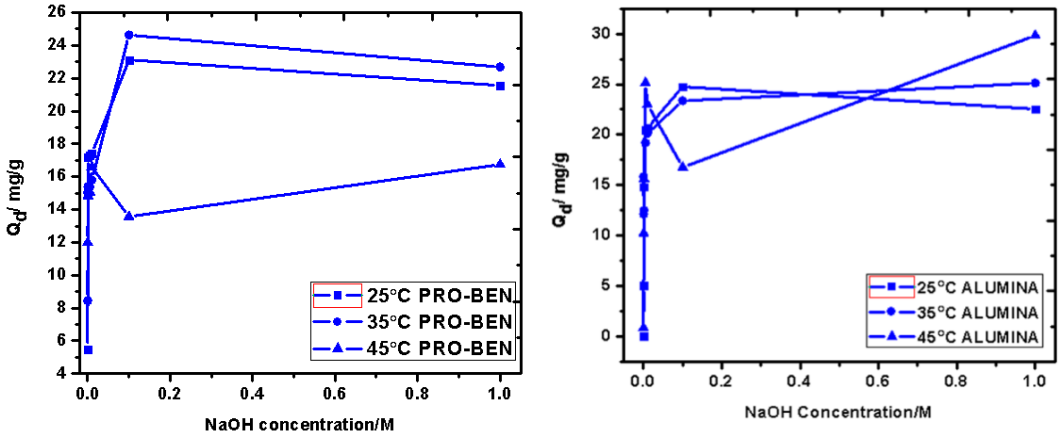

(b)

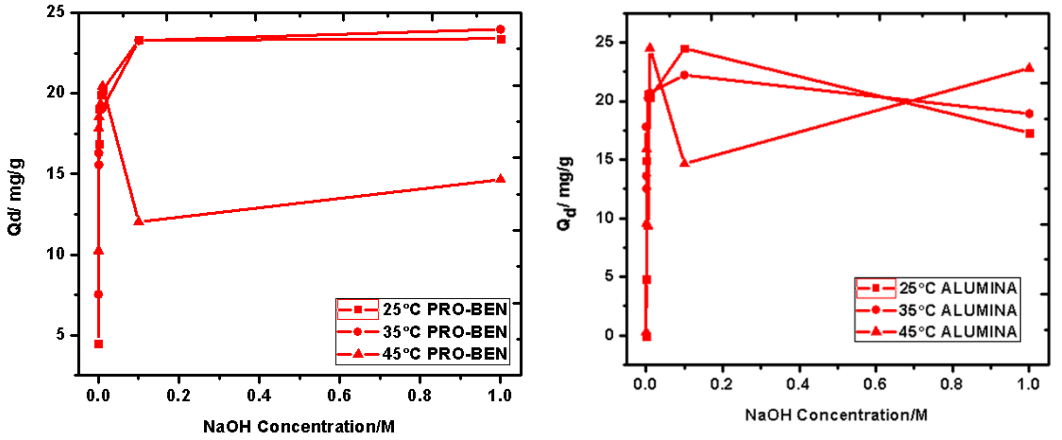

(c)

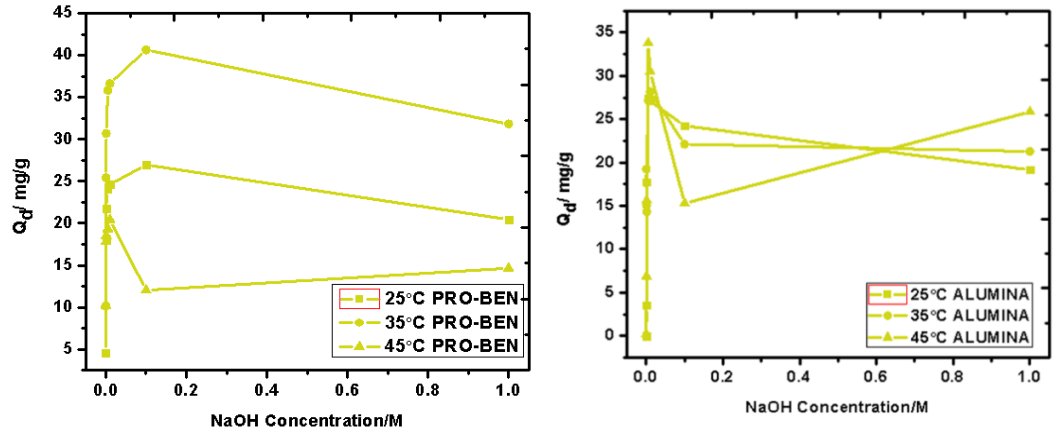

Figure 3.33. Desorption trends for (a) Reactive Blue 222, (b) Reactive Red 195 and (c) Reactive Yellow 145 using PRO-BEN and alumina at various temperatures and NaOH concentrations

3.3.7. Adsorption of Dyes from Industrial Effluent

An effluent sample, from a local company, containing the dyes, were studied under optimum conditions for adsorption. Best adsorption occurred at 25 ˚C at pH 5.21 (Fig. 3.34). The percentage adsorption was higher for RB 222 than RR 195 whilst RY 145 did not adsorb completely. The effluent sample was initially alkaline with a pH of 10.90 therefore adsorption was inefficient and hence the effluent was subsequently acidified to the optimum pH. Percentage dye removal was efficient up to 90.00 % ± 0.5293 % for RB 222, 9.000 % ± 0.6858 % for RR 195 and 80.00 % ± 0.9424 % for RY 145. Usually effluent samples may contain very high salt concentrations. The high salt content in the effluent could promote competition with the dyes for adsorption sites.

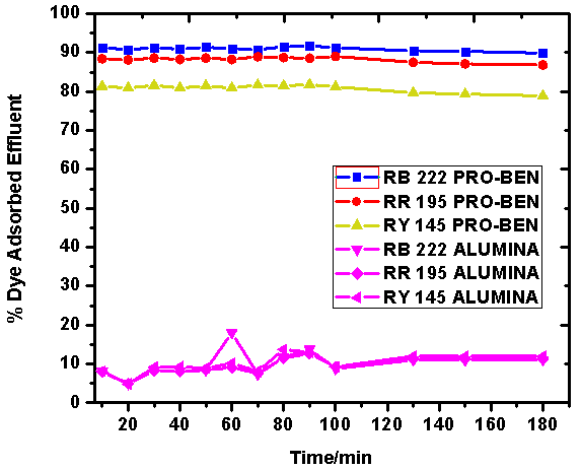

Figure 3.34. Adsorption of dyes from effluent at 25 ˚C, pH 4.01

3.4. Conclusion

A new water soluble polymer (PEP) was synthesized using the monomers L-proline, epichlorohydrin and ethylenediamine. It was characterized by ^{1}H-NMR and FT-IR Spectroscopy whilst the molecular weight was calculated as 174.1 kDa ± 2.929 kDa by static light scattering. A composite was prepared with PEP and bentonite, characterized by several spectroscopic techniques and evaluated for its removal of 3 anionic dyes textile dyes via adsorption. The parameters that affect adsorption were established. It was concluded that high concentration of dyes increased the adsorption efficiency whilst an increase in pH, salt content, and temperature had a negative effect on adsorption. Furthermore, the adsorption was characterized by the Langmuir Type I isotherm. It was concluded that favourable adsorption occurred in a monolayer surface coverage. The order of fit for the isotherms were Langmuir

Type I > Frumkin > Freundlich > Temkin isotherms. The pseudo-second order kinetic model proved the best to describe the rate of adsorption for the range of initial concentrations. It was found that the intraparticle diffusion was not the only rate-limiting step alone. The mechanism of adsorption followed intraparticle diffusion as well as external mass transfer. This indicated that PRO-BEN is effective in adsorbing anionic dyes and could be employed in industry for textile dye effluent remediation.

3.5. References

Ahn, B.J., McCoy, B.J. and Smith, J.M. 1985. Separation of adsorption and surface reaction rates: Dynamic studies in a catalytic slurry reactor. *AIChE Journal*, 31(4): 541-550.

Annadurai, G., Juang, R.S. and Lee, D.J. 2002. Use of cellulose-based wastes for adsorption of dyes from aqueous solutions. *Journal of Hazardous Materials*, 92(3): 263-274.

Chaudhary, R. and Datta, M. 2013. Silicotungstic Acid Modified Bentonite: An Efficient Catalyst for Synthesis of Acetal Derivatives of Aldehydes and Ketones. *Journal of Analytical Sciences, Methods and Instrumentation*, 3(4): 193-201.

Cheng, W., Wang, S.G., Lu, L., Gong, W.X., Liu, X.W., Gao, B.Y. and Zhang, H.Y. 2008. Removal of malachite green (MG) from aqueous solutions by native and heat-treated anaerobic granular sludge. *Biochemical Engineering Journal*, 39(3): 538-546.

Choy, K.K.H., McKay, G. and Porter, J.F. 1999. Sorption of acid dyes from effluents using activated carbon. *Resources, Conservation and Recycling*, 27(1–2): 57-71.

Dada, A.O., Olalekan, A.P., Olatunya, A.M. and Dada, O. 2012. Langmuir, Freundlich, Temkin and Dubinin–Radushkevich Isotherms Studies of Equilibrium Sorption of Zn^{2+} Unto Phosphoric Acid Modified Rice Husk. *IOSR Journal of Applied Chemistry*, 3(1): 38-45.

Doble, M. and Kumar, A. 2005. *Biotreatment of Industrial Effluents*. 1st ed. United Kingdom: Elsevier Butterworth-Heinemann.

Eren, E. and Afsin, B. 2008. An investigation of Cu(II) adsorption by raw and acid-activated bentonite: A combined potentiometric, thermodynamic, XRD, IR, DTA study. *Journal of Hazardous Materials*, 151(2–3): 682-691.

Freundlich, H. and Hatfield, H. 1926. *Colloid [and] capillary chemistry*. London: Methuen.

Frumkin, A. 1926. Über die Beeinflussung der Adsorption von Neutralmolekülen durch ein elektrisches Feld. *Zeitschrift für Physik*, 35(10): 792-802.

Giles, C.H., MacEwan, T.H., Nakhwa, S.N. and Smith, D. 1960. Studies in adsorption. Part XI. A system of classification of solution adsorption isotherms, and its use in diagnosis of adsorption mechanisms and in measurement of specific surface areas of solids. *Journal of the Chemical Society,* 3: 3973-3993.

Gulnaz, O., Kaya, A., Matyar, F. and Arikan, B. 2004. Sorption of basic dyes from aqueous solution by activated sludge. *Journal of Hazardous Materials,* 108(3): 183-188.

Huang, C.H., Chang, K.P., Ou, H.D., Chiang, Y.C. and Wang, C.F. 2011. Adsorption of cationic dyes onto mesoporous silica. *Microporous and Mesoporous Materials,* 141(1–3): 102-109.

Jnr, M.H. and Spiff, A.I. 2005. Effects of temperature on the sorption of Pb^{2+} and Cd^{2+} from aqueous solution by Caladium bicolor (Wild Cocoyam) biomass. *Electronic Journal of Biotechnology,* 8(2): 162-169.

Kahr, G. and Madsen, F.T. 1995. Determination of the cation exchange capacity and the surface area of bentonite, illite and kaolinite by methylene blue adsorption. *Applied Clay Science,* 9(5): 327-336.

Keen, O.S., Baik, S., Linden, K.G., Aga, D.S. and Love, N.G. 2012. Enhanced Biodegradation of Carbamazepine after UV/H_2O_2 Advanced Oxidation. *Environmental Science & Technology,* 46(11): 6222-6227.

Kim, E.K. and Walker, H.W. 2001. Effect of cationic polymer additives on the adsorption of humic acid onto iron oxide particles. *Colloids and Surfaces A: Physicochemical and Engineering Aspects,* 194(1–3): 123-131.

Kulshrestha, P., Giese, R.F. and Aga, D.S. 2004. Investigating the Molecular Interactions of Oxytetracycline in Clay and Organic Matter: Insights on Factors Affecting Its Mobility in Soil. *Environmental Science & Technology,* 38(15): 4097-4105.

Lagergren, S. 1898. Zur theorie der sogenannten adsorption gelˆster stoffe. Kungliga Svenska Vetenskapsakademiens. *Handlingar,* 24(4): 1-39.

Lewinsky, A.A., ed. 2007. *Hazardous Materials and Wastewater: Treatment, Removal and Analysis*. New York: Nova Science Publishers, Inc.

Li, Q., Yue, Q.Y., Su, Y., Gao, B.Y. and Li, J. 2009. Two-step kinetic study on the adsorption and desorption of reactive dyes at cationic polymer/bentonite. *Journal of Hazardous Materials,* 165(1–3): 1170-1178.

Li, Q., Yue, Q.Y., Sun, H.J., Su, Y. and Gao, B.Y. 2010. A comparative study on the properties, mechanisms and process designs for the adsorption of non-ionic or anionic dyes onto cationic-polymer/bentonite. *Journal of Environmental Management,* 91(7): 1601-1611.

Masel, R.I. 1996. *Principles of Adsorption and Reaction on Solid Surfaces*. 1st ed. Canada: John Wiley and Sons, Inc.

McKay, G. 1982. Adsorption of dyestuffs from aqueous solutions with activated carbon I: Equilibrium and batch contact-time studies. *Journal of Chemical Technology and Biotechnology,* 32(7-12): 759-772.

Mittal, A., Kurup, L. and Mittal, J. 2007. Freundlich and Langmuir adsorption isotherms and kinetics for the removal of Tartrazine from aqueous solutions using hen feathers. *Journal of Hazardous Materials,* 146(1–2): 243-248.

Navratilova, Z., Wojtowicz, P., Vaculikova, L. and Sugarkova, V. 2007. Sorption of alkylammonium cations on montmorillonite. *Acta Geodynamica et Geomaterialia,* 4(3): 59-65.

Panzer, H.P. and Rabinowitz, R. 1971. *Polyquaternary flocculants and processes of preparing them by quaternizing alkylene polyamine resin polymers from epihalohydrin and monoalkyl amines.* United States of America. 22362124.

Pavia, D.L., Lampman, G.M., Kriz, G.S. and Vyvyan, J.A. 2014. *Introduction to Spectroscopy*. 5th ed. United States of America: Cengage Learning.

Saraydin, D., Karadag, E. and Aydin, F. 1998. Removal of water soluble cationic dyes with trisyl silicas. *Turkish Journal of Chemistry,*(22): 227-236.

Shen, D., Fan, J., Zhou, W., Gao, B., Yue, Q. and Kang, Q. 2009. Adsorption kinetics and isotherm of anionic dyes onto organo-bentonite from single and multisolute systems. *Journal of Hazardous Materials,* 172(1): 99-107.

Shen, D., Fan, J., Zhou, W., Gao, B., Yue, Q., Kang, Q. and 2009. Adsorption kinetics and isotherm of anionic dyes onto organo-bentonite from single and multisolute systems. *Journal of Hazardous Materials,* 172: 99-107.

Siebers, N. 2009. *Bentonite Functionalised With 2-(3-(2-aminoethylthio)propylthio)ethanamine (Aepe) for the Removal of Hg(II) from Wastewaters*. 1st ed. Hamburg: Diplomica-Verlag.

Singh, R. 2002. *Synthetic dyes*. 1st ed. New Delhi: Mittal Punlications.

Szyguła, A., Guibal, E., Palacín, M.A., Ruiz, M. and Sastre, A.M. 2009. Removal of an anionic dye (Acid Blue 92) by coagulation–flocculation using chitosan. *Journal of Environmental Management,* 90(10): 2979-2986.

Temkin, M.I. and Pyzhev, V. 1940. Kinetics of ammonia synthesis on promoted iron catalyst. *Acta Physico-Chimica Sinica, USSR,*(12): 327-356.

Toor, M. and Jin, B. 2012. Adsorption characteristics, isotherm, kinetics, and diffusion of modified natural bentonite for removing diazo dye. *Chemical Engineering Journal,* 187: 79-88.

Tyagi, V.P. 2009. *Essential Chemistry*. 1st ed. New Delhi: Ratna Sagar P. Ltd.

Weber, W.J. and Morris, C.J. 1962. Advances in water pollution research: removal of biologically resistant pollutant from waste water by adsorption. In: Southgate, B. A. ed. *Proceeding of 1st International Conference on Water Pollution Research.* London, September 1962. Oxford, UK: Pergamon Press, 231-266.

Yue, Q.Y., Li, Q., Gao, B.Y. and Wang, Y. 2007. Kinetics of adsorption of disperse dyes by polyepicholorohydrin-dimethylamine cationic polymer/bentonite. *Separation and Purification Technology,* 54(3): 279-290.

Yue, Q.Y., Li, Q., Gao, B.Y., Yuan, A.J. and Wang, Y. 2007. Formation and characteristics of cationic-polymer/bentonite complexes as adsorbents for dyes. *Applied Clay Science,* 35(3–4): 268-275.

Chapter Four: Synthesis and Characterization of Thiazolidine-Epichlorohydrin-Ethylenediamine Polymer and Thiazolidine-Epichlorohydrin-Ethylenediamine Polymer Capped Gold Nanoparticles and the Reduction of Selected Dyes in Water

4.1. General Introduction

Gold nanoparticles are being extensively studied due to their broad range of applications, easy synthesis and easy manipulation of their size and shape. Due to their characteristic size of less than 100 nm compared to their bulk counterparts, they are applied in chemical, biological and physical systems. Properties like increased catalytic activity, increased heat and electrical conductivity, improved photoemission and surface modification were reported(Abdelhalim *et al.* 2012: 1 – 5), (Thakor *et al.* 2011: 4029 – 4036). Also a wide range of shapes such as nanorods, nanowires, nanospheres, nanostars, nanocubes, nanoboxes and nanoprisms exist (Langille *et al.* 2012: 14542 – 14554), (Zhang *et al.* 2014: 5860 – 5889). Gold nanoparticles with sizes less than 100 nm usually exist in aqueous medium and nanoparticles less than 3 nm exhibit outstanding catalytic activity showed by Abdelhalim *et al.* (2012: 1 – 5). However, their high surface energy promotes coagulation and aggregation and in order to prevent this, a stabilizing (capping) agent is usually added. Stabilizers such as dendrimers, surfactants, ligands, ionic liquids and more preferably polyelectrolytes are used (Solyman *et al.* 2014: 218 – 225).

Polyelectrolytes having NH_2- groups allows for increased solubility in aqueous solutions. These groups, present in polymers, adsorb onto the gold nanoparticles thereby causing steric repulsion between nanoparticles which leads to effective stabilization (Shem *et al.* 2014: 107 – 116). Therefore the use of polymers as capping agents has increased (Hussain *et al.* 2003: 4831 – 4835). The synthesis of gold and silver nanoparticles by an acrylate polymer was reported by Hoppe *et al.* (2006: 7027 – 7034) this acts as a reducing agent to produce gold nanoparticle hydrosols. A study showed that a polymer can act simultaneously as a reducing and a capping agent (Gangula *et al.* 2012: 22866 – 22872). The successful synthesis of nanoparticles, using a thiophene substrate as a stabilizer, for nitro-compound reduction was reported by Harish *et al.* (2009: 197 – 202). A study by Wunder *et al.* (2010: 8814 – 8820) reported the catalytic reduction of gold nanoparticles embedded in spherical polymer brushes.

It was observed that the spherical nano-brushes successfully immobilized gold nanoparticles. Veerakumar *et al.* (2012: 197 – 205) reported the use of a highly branched imine polymer which acted as a stabilizing and reducing agent in the formation of nanoparticles, a reducing agent was not required due to the *in-situ* polymer modification. Vasimalai *et al.* (2013: 24 – 31) reported a natural biopolymer, chitosan, which capped the gold nanoparticles for Malathion sensing. Cappellari *et al.* (2015: 17 – 24) showed that cysteine polymer capped AuNPs could be manipulated for its size and shape.

Recently, Hu *et al.* (2016: 3107 – 3116) incorporated conjugated polymers into gold nanoparticles. The advantages of this was its simple synthesis, non-toxicity and its biocompatibility. However, due to the nature of the polymer, solubility in aqueous solutions is limited especially if the polymer lacks functional groups that can be changed to favour solubility.

Nanoparticles may also be attached to solid supports to improve solubility. Srivastava *et al.* (2013: 1 – 9) showed the formation and attachment of gold nanoparticles onto bacterial membranes for the catalytic reduction of nitro-compound. It was proved that clay, as a composite, was also another efficient alternative for nanoparticle stability (Solyman *et al.* 2014: 218 – 225). It was reported that the thiolated-capped AuNPs were synthesized and immobilized onto sodium bentonite for the polymerization of methyl methacrylate. Although the study proved successful, synthesis was long and tedious.

The manipulation for size and shape of AuNPs was reported by Parab *et al.* (2011: 2173 – 2180) when polyethyleneimine was used with a gold precursor, in a reducing agent, to develop snowflake shaped gold nanoparticles. They found that simple manipulation of the concentration of the starting materials altered the shape of the nanoparticles. It was reported by Wagers *et al.* (2014: 15 – 20) that the pH of the nanoparticle medium affects the size of the gold nanoparticles, the size decreased in an acidic medium when the concentration of the capping agent was increased.

The ideal way of synthesizing gold nanoparticles is by reducing gold (III) salt solution. In most studies, reducing agents such as sodium citrate (Harish *et al.* 2009: 197 – 202), sodium borohydride, pyrrole and oxalic acid are commonly used. In recent studies, 'greener' reducing agents such as certain strains of bacteria, various plant extracts, and glycerol have been used. These are non-toxic, biodegradable and are easily obtained. Bagasse from sugar cane extract

is also a 'greener' alternative since it is a waste product from the sugar cane industry. It has been reported by Mishra *et al.* (2013: 217 – 219) that the hydroxyl and aldehyde groups in the sugar extract are responsible for the reducing capability.

The aim of this study was to synthesize a novel water-soluble polymer and use it as a capping agent for the formation of gold nanoparticles in the presence of bagasse extract. Furthermore this new material was investigated for the reduction of three dyes.

4.2. Experimental

4.2.1. Materials

L-4-Thiazolidinecarboxylic acid, epichlorohydrin, ethylenediamine and acetone were purchased from Sigma-Aldrich and were utilized without prior purification. Chloroauric acid ($HAuCl_4$, 99.99 %), trisodium citrate dehydrate (99.00 % – 100.5%), sodium borohydride ($NaBH_4 \geq 98\%$), Methylene blue, Congo red and Allura red (Sigma-Aldrich) were all analytical grade and were utilized without prior purification. Sugarcane bagasse was obtained from the Sugar Milling Research Institute (SMRI). Double deionized water (18 MΩ) was used to make all aqueous solutions. All solutions were freshly prepared before use. All glassware were washed with aqua regia before use. All measurements were done in triplicate and the standard deviations were calculated.

4.2.2. Instrumentation

Fourier transform infrared spectroscopy (FT-IR) analyses on the Thiazolidine-Epichlorohydrin-Ethylenediamine Polymer were conducted using Varian 800 FT-IR spectrophotometer. UV-Visible measurements were made using a UV-1700 PharmaSpec Spectrophotometer. ^{1}H-NMR spectra were obtained using a Bruker (400 MHz) spectrophotometer. Zeta potential and particle size were determined using a U-tube quartz cuvette, polystyrene cuvette and a Differential Light Scattering Malvern Zetasizer Nano ZS (Malvern Instruments Ltd, UK) Merck 2423 instrument. Static light scattering (SLS) was also used by the Zetasizer to determine molecular weight. Scanning electron microscopy (SEM) images were recorded for the gold nanoparticles using ZEISS EVO HD 15 Environmental Scanning Electron Microscope and TEM analysis was conducted on the AuNPs using JEOL 1010 TEM using a Mega view III camera and iTEM software.

4.2.3. Synthesis of Thiazolidine-Epichlorohydrin-Ethylenediamine Polymer

An accurate mass of 22.56 g (0.2400 mols) of epichlorohydrin was added with 40.00 g of distilled water and 3.500 g (0.03000 mols) of white powder L-Thiazolidine carboxylic acid was added. Thereafter 15.50 g (0.2600 mols) of ethylenediamine was added drop-wise into the mixture; the temperature was increased to 70 ˚C and the mixture was left to react for an hour. An additional 7.510 g (0.08110 mols) of epichlorohydrin was added into the mixture and the reactants were left for 24 hours to react while stirring.

4.2.4. Preparation of the Bagasse Extract

Approximately 25.18 g of bagasse fiber was washed with double distilled water, dried, then transferred into a clean 1000 mL beaker to which 100 mL of double deionized water was added. The mixture was boiled for 10 minutes until the water changed to yellow. It was vacuum filtered, the residue was discarded and the filtrate was used immediately.

4.2.5. Preparation of Dye Solution

Stock solutions were prepared for the three dyes and further diluted to the desired concentration. For each dye used, stock solutions were prepared by dissolving the respective masses (Table 4.1) into a 100 mL volumetric flask using double deionized water. The solutions were made up to 100 mL with double deionized water.

All solutions were diluted to give dye concentrations of approximately 1.000×10^{-5} M. These solutions were used to synthesize the gold nanoparticles.

Table 4.1. Quantities of different dye stock solution used

Dye Used	Concentration of stock solution/ M	Mass/ g
Methylene Blue	9.942×10^{-4}	0.01590
Congo Red	1.019×10^{-4}	0.007100
Allura Red	1.027×10^{-4}	0.005100

4.2.6. Preparation of Sodium Borohydride Solution

A 0.01000 M and 0.02000 M solutions of sodium borohydride were prepared by dissolving the exact quantity (Table 4.2) of $NaBH_4$ into two separate 50 mL volumetric flasks, containing

water. The solutions were then made up to the 50 mL mark using double deionized water. For every experiment conducted, freshly prepared solutions were utilized.

Table 4.2. Quantities of sodium borohydride used

Dye	Mass/ g	Molarity/ M
Methylene Blue	0.01940	0.01000
Congo Red	0.03840	0.02000
Allura Red	0.03870	0.02000

4.2.7. Preparation of a Series of Thiazolidine-Epichlorohydrin-Ethylenediamine Polymer Solutions Of Different Concentrations for AuNP Capping

An accurate mass of 0.5043 g of TEP was dissolved in double deionized water in a 500 mL volumetric flask to give a nominal 1000 $mg.L^{-1}$ of stock solution. Then 5 mL was quantitatively transferred into a 50 mL volumetric flask and diluted to 50 mL with double deionized water to give the 100.0 $mg.L^{-1}$ TEP solution. The solutions were further diluted to their respective solutions according to Fig 4.1

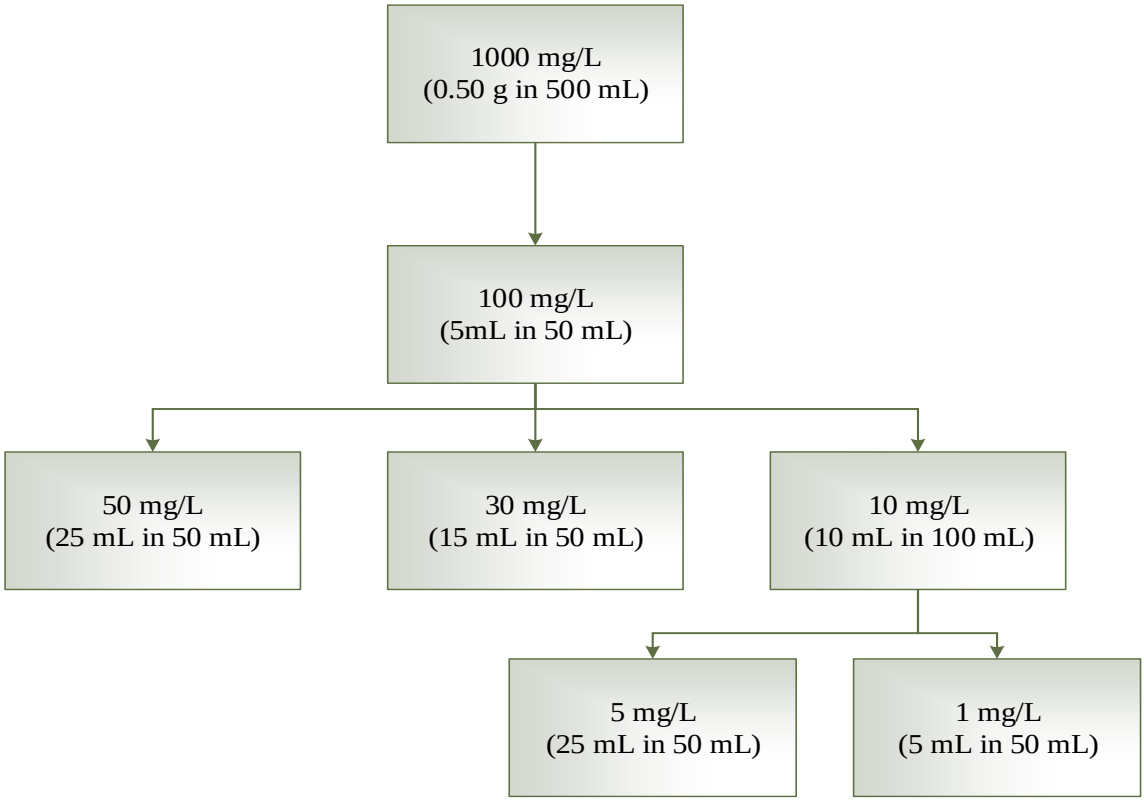

Figure 4.1. A scheme illustrating serial dilution of Thiazolidine-Epichlorohydrin-Ethylenediamine Polymer solutions

4.2.8. Formation of Thiazolidine-Epichlorohydrin-Ethylenediamine Polymer-AuNP Solutions Using Sodium Citrate (Turkevich Method)

Into six separate 100 mL Erlenmeyer flasks (Table 4.3), both 20 mL of about 1 mM gold chloride solution and 20 mL of the various concentrations of TEP solutions were added. The solution was boiled while being stirring. After three minutes, 5 mL of 1 % sodium citrate solution was added to the solutions (Turkevich *et al.* 1951: 55 – 75). The solution was stirred and after three minutes, when the solution turned cherry red, it was cooled, stoppered and kept in a dark cupboard. The nanoparticle solutions were not stored for more than three months.

Table 4.3. Quantities of reagents used for AuNPs synthesized using the Turkevich method

AuNP sample names	Concentration of TEP/ mg.L^{-1}	Volume of gold solution / mL	Volume of TEP solution / mL	Volume of sodium citrate / mL
0 ppm TEP-Na-AuNPs	0.000	20	20	5
1 ppm TEP-Na-AuNPs	1.000	20	20	5
5 ppm TEP-Na-AuNPs	5.000	20	20	5
10 ppm TEP-Na- AuNPs	10.00	20	20	5
30 ppm TEP-Na-AuNPs	30.00	20	20	5
50 ppm TEP-Na-AuNPs	50.00	20	20	5

4.2.9. Formation of Thiazolidine-Epichlorohydrin-Ethylenediamine Polymer -Capped AuNP Solutions Using Bagasse Extract

Into each of the six separate 100 mL Erlenmeyer flasks, with glass stoppers, 20 mL of 1 mM gold chloride solution and 20 mL of the polymer solutions with the corresponding concentration of TEP were added. The mixture was thoroughly stirred with a magnetic stirrer. After approximately three minutes, 5 mL bagasse extract was added to the solution (Table 4.4). The solution was allowed to stir and in intervals of 30 minutes a 3 mL aliquot of sample was extracted from each flask and analyzed using UV-Vis spectroscopy to track the formation of the encapsulated gold nanoparticles. Once formation was complete, the nanoparticle solutions were stored under dark conditions. The nanoparticle solutions were not stored for more than three months.

Table 4.4. Quantities of reagents used for AuNPs synthesized with bagasse extract

AuNP sample names	Concentration of TEP/ ppm	Volume of $HAuCl_4$ solution used/ mL	Volume of TEP solution used/ mL	Volume of bagasse extract used/ mL
0 ppm TEP-AuNPs	0	20	20	5
1 ppm TEP-AuNPs	1	20	20	5
5 ppm TEP-AuNPs	5	20	20	5
10 ppm TEP-AuNPs	10	20	20	5
30 ppm TEP-AuNPs	30	20	20	5
50 ppm TEP-AuNPs	50	20	20	5

4.3. Results and Discussion

For the synthesis of TEP, epichlorohydrin, L-Thiazolidinecarboxylic acid and ethylenediamine were used as monomers. Initially two layers were observed when the monomers were added. After the addition of ethylenediamine, the two solutions homogenized and the colour changed from colorless to yellow. After 24 hours, a thick brownish viscous liquid was observed. The reaction scheme is presented in Fig 4.2.

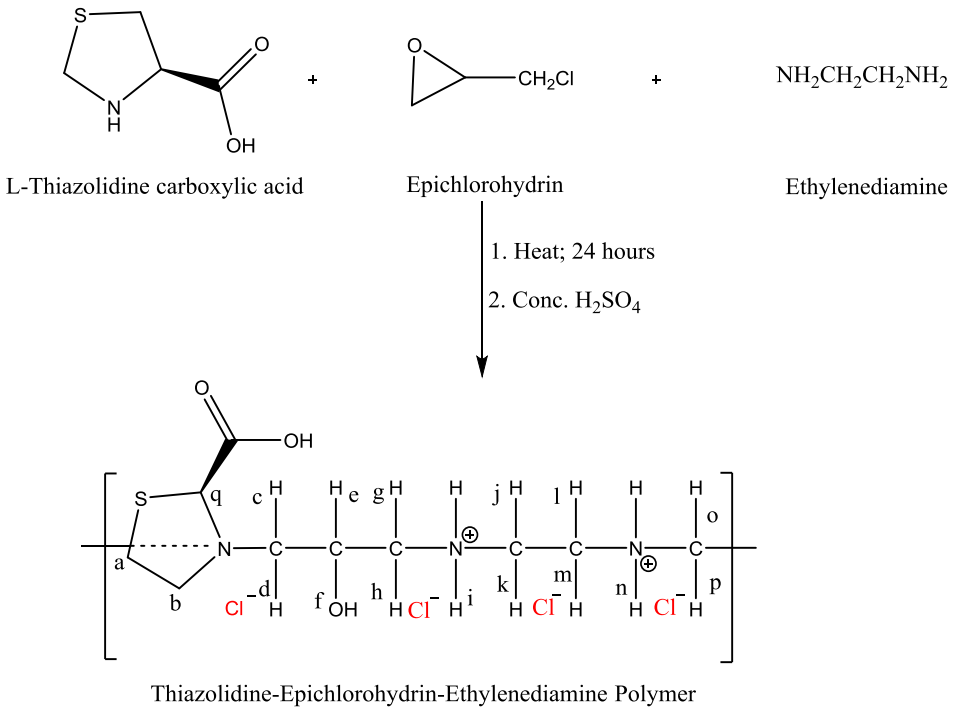

Figure 4.2. Scheme of Thiazolidine-Epichlorohydrin-Ethylenediamine Polymer synthesis

4.3.1. Characterization of Thiazolidine-Epichlorohydrin-Ethylenediamine Polymer

4.3.1.1. Infra-Red Spectroscopy of Thiazolidine-Epichlorohydrin-Ethylenediamine Polymer

The FT-IR spectra were recorded for TEP (Fig. 4.3). For TEP, the O-H stretch at 3347.84 cm^{-1}, C-O stretch at 1066 cm^{-1}, C-H stretch at 2965.2 cm^{-1}, C-H bend at 1455.69 cm^{-1}, C-N stretch at 1230.6 cm^{-1} and C-S stretch at 673.0 cm^{-1} were observed.

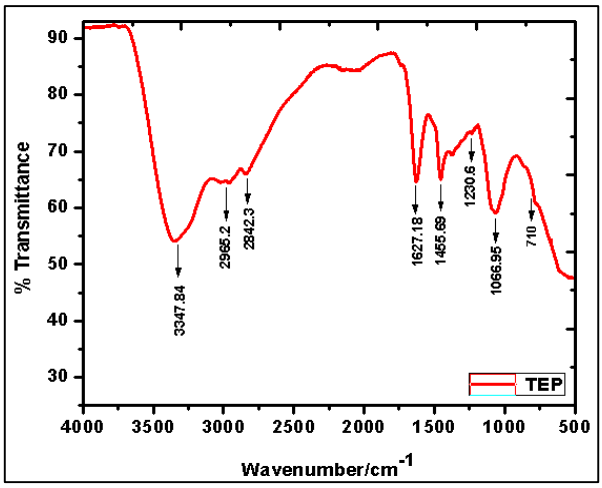

Figure 4.3. FT-IR spectra of Thiazolidine-Epichlorohydrin-Ethylenediamine Polymer

4.3.1.2. ^{1}H-NMR Spectroscopy of Thiazolidine-Epichlorohydrin-Ethylenediamine Polymer

The ^{1}H-NMR and expanded spectra of TEP are presented in Appendix 7 whilst the chemical shift values and spin multiplicity is presented in Table 4.5. Since a polymer was investigated, several equivalent and non-equivalent protons were observed; hence it was difficult to assign the chemical shifts unambiguously. In analyzing the back-bone of TEP, the guidance of a research paper by Li *et al*. (2014). It was found that all observed chemical shifts could be associated with the expected polymer. The OH and NH protons appeared at δ 4.310 and 4.500, respectively. The CH (COOH) and CH (OH) protons appeared at 3.050 and 3.900, respectively. There were several CH_2 protons which appeared in the range 1.930 to 3.590 depending on the shielding and de-shielding effect. It must be mentioned that our result also showed absence of the COOH proton as described by Li et al. (2014). It was speculated that deuterium from the solvent D_2O replaced the COOH proton resulting in it being undetected in the spectrum.

Table 4.5. The chemical shifts for Thiazolidine-Epichlorohydrin-Ethylenediamine Polymer

Label	Chemical shifts (ppm) and multiplicity
a	2.730 (t)
b	2.910 (t)
c, d	3.090 (d)
e	3.390 (t)
g, h	3.500 (m)
o, p	3.590 (m)
i	4.080 (s)
n	4.200 (s)
q	4.260 (s)
j, k	4.310 (d)
l, m	4.410 (d)
f	4.500 (dd)

4.3.1.3. Thermal Analysis of the Thiazolidine-Epichlorohydrin-Ethylenediamine Polymer

The DSC/TGA profiles for TEP are shown in Fig. 4.4. The initial mass of the polymer used was 12.35 mg: it was subjected to a ramping rate of 10.00 °C/min in an aluminium pan. The TGA profile showed a mass loss of 8 % at 315.63 °C. This could be due to loss of hydrocarbons from the polymer structure respectively. The DSC thermogram showed endothermic peaks at 123.33 °C and at 315.63 °C that corresponded to the glass transition temperature and decomposition temperature of the polymer.

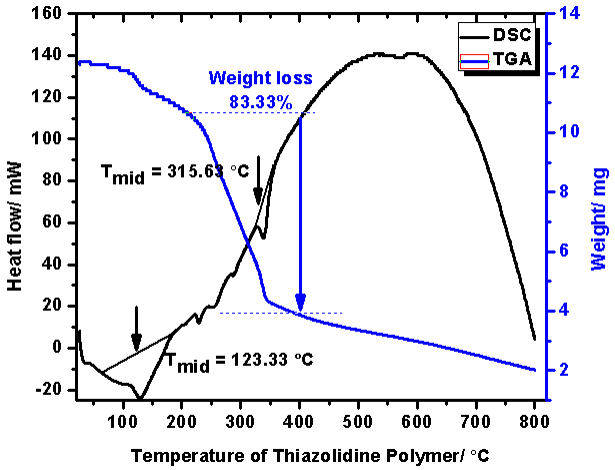

Figure 4.4. DSC/TGA plots for the Thiazolidine-Epichlorohydrin-Ethylenediamine Polymer

4.3.1.4. Molecular Weight of Thiazolidine-Epichlorohydrin-Ethylenediamine Polymer

Static light scattering (SLS) was used to ascertain the molecular weight of the TEP. Four various concentrations of the polymer was used for the study and analysis was performed after 15 repeated measurements at 25 °C for each sample. The wavelength used for the laser was 633 nm. Each of the five samples (Table 4.6) was filtered and analyzed and then the molecular weight was determined. The counts per second for the highest standard did not exceed 400 kcps. The analysis was conducted at an angle of 172.2˚ to minimize the influence of possible dust particles on the results. The regression curve was illustrated in Fig. 4.5.

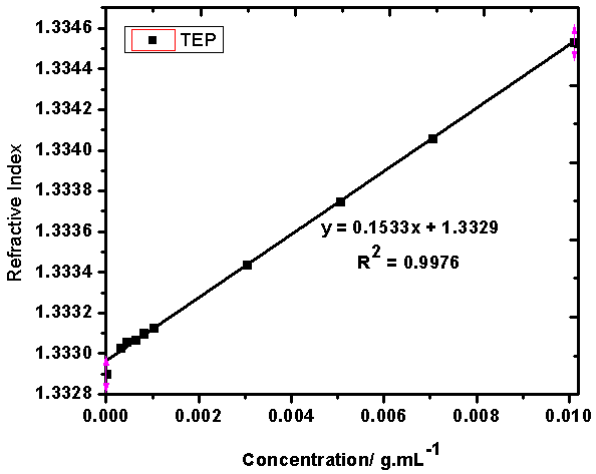

Figure 4.5. Calibration graph of refractive index with changing concentration of Thiazolidine-Epichlorohydrin-Ethylenediamine Polymer solutions at 25 ˚C

Table 4.6. Refractive index values for the various concentrations of Thiazolidine-Epichlorohydrin-Ethylenediamine polymer

Concentration/ g.mL^{-1}	Refractive Index
0.000	1.33290 ± 1 × 10^{-5}
0.3020	1.33303 ± 3 × 10^{-5}
0.4420	1.33306 ± 1 × 10^{-5}
0.6340	1.33307 ± 2 × 10^{-5}
0.8060	1.33310 ± 1 × 10^{-5}
1.020	1.33313 ± 4 × 10^{-5}
3.036	1.33344 ± 1 × 10^{-5}
5.060	1.33375 ± 2 × 10^{-5}
7.038	1.33406 ± 1 × 10^{-5}
10.11	1.33453 ± 3 × 10^{-5}

The graph of change in refractive index with TEP concentration (Fig. 4.5) was found to be in good correlation with a good regression value of 0.9976 for TEP. The $\frac{dn}{dc}$ value for TEP was 0.1533 mL.g^{-1} ± 6.793 ×10^{-10} mL.g^{-1}.

The molecular weight of the Thiazolidine-Epichlorohydrin-Ethylenediamine Polymer was calculated from the Debye plot illustrated below (Fig. 4.6).

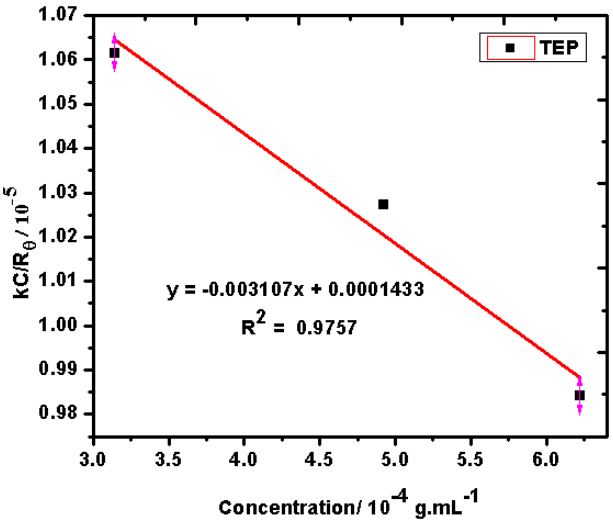

Figure 4.6. The Debye plot for Thiazolidine-Epichlorohydrin-Ethylenediamine Polymer

From Fig. 4.6 and Table 4.7, the molecular weight was found to be 69.78 kDa. ± 1.176 kDa The second virial co-efficient was -3.107 x 10^{-8} mL.mol.g^{-2}. A negative second virial co-efficient implied that the interaction strength is not affinitive and may suggest a degree of branching of the polymer.

Table 4.7. Debye plot for determining molecular weight of Thiazolidine-Epichlorohydrin-Ethylenediamine Polymer

Concentration/ g.mL^{-1}	I_{Sample} / cps	I_A/ cps	R_θ/ x10^{-5} cm^{-1}	Kc/ R_θ x10^{-5}
0.0003140	6.690 x10^5	3.440 x10^4	0.4019	1.332
0.0004920	8.820 x10^5	5.570 x10^5	0.6507	1.289
0.0006220	1.060 x10^6	7.350 x10^5	0.8587	1.235
$\frac{dn}{dc}$ = 0.1533 mL.g^{-1} ± 6.793 ×10^{-10} mL.g^{-1}				
I_S = 172200 cps				
k = 1.704 x10^{-7} mol.cm^2.g^{-1}				
I_0 = 3.250 x10^4 cps				
n_S = 1.497 cps				
n_0 = 1.3329				
M_W = 69.78kDa ± 1.176 kDa				
A_2 = -3.107 x 10^{-8} mL.mol.g^{-2} ± 2.26 x 10^{-10} mL.mol.g^{-2}				

The units used in Table 4.7 are described below:

C/ g.mL^{-1} is the concentration of the polymer solutions,

A_2/ mL.mol.g^{-2} is the second viral co-efficient describing the strength of interaction between the polymer molecules and the solvent it is in,

M_w is the absolute molecular weight in Daltons,

k/ mol.cm^2.g^{-1} is the optical constant,

λ_0 / nm is the wavelength of the SLS method,

N_A/ mol^{-1} is the Avogadro's number,

n_0 is the refractive index of distilled water,

n_S is the refractive index of toluene standard,

R_S is the Rayleigh ratio of toluene,

I_A / kcps is the intensity of the analyte,

I_S / kcps is the intensity of the toluene standard and

R_θ/ cm^{-1} is the Rayleigh ratio between the scattered and incident light intensity.

4.3.2. Synthesis and Characterization of Thiazolidine-Epichlorohydrin-Ethylenediamine Polymer Capped Gold Nanoparticles

4.3.2.1. The FT-IR Spectra Thiazolidine-Epichlorohydrin-Ethylenediamine Polymer, Thiazolidine-Epichlorohydrin-Ethylenediamine Polymer Capped Gold Nanoparticles and the Bagasse Extract.

The FT-IR spectra were recorded for TEP, bagasse extract and 50 ppm TEP-AuNPs (Fig. 4.7). It was reported in literature that bagasse extract contains about 70 % lignin (Pessoa *et al.* 1997: 00 – 00). The following absorption bands (Fig. 4.7 (a)) were found for the bagasse: O-H stretch at 3273.14 cm^{-1} and C=C aromatic stretch at 1635.37 cm^{-1}. Because lignin contains a significant amount of phenolic hydroxyls these absorptions confirmed the presence of lignin in the extract (Hu *et al.* 2016: 856 – 862). Fig. 4.7 (c) showed the OH stretch at 3254 cm^{-1} similar to the bagasse extract. Also the C-O stretch for alcohols at 1033.46 cm^{-1} corresponded to both the polymer and the extract. This indicated possible capping of molecules from the extract and the polymer, or this could imply that the polymer replaced the capping species from the extract. A band at 598.07 cm^{-1} (Fig. 4.7 (c)) corresponded to the C-S stretch, similar to the polymer, suggesting that the 50 ppm TEP-AuNPs was capped both with the polymer as well as the reducing sugars in the extract.

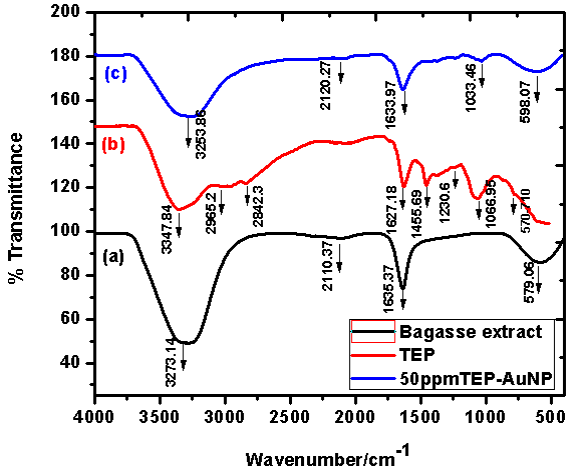

Figure 4.7. FT-IR spectra of (a) bagasse, (b) Thiazolidine-Epichlorohydrin-Ethylenediamine Polymer and (c) 50 ppm TEP-AuNPs

4.3.2.2. The SEM/EDX Profiles of Thiazolidine-Epichlorohydrin-Ethylenediamine Polymer and Thiazolidine-Epichlorohydrin-Ethylenediamine Polymer Capped Gold Nanoparticles

The morphologies of the bagasse-reduced AuNP surfaces were studied using SEM/EDX (Fig. 4.8). For 30 ppm bagasse reduced AuNPs (Fig. 4.8 (a)): there were a significant presence of nanotriangles and nanospheres. The EDX analysis (Fig. 4.8 (b)) showed the presence of gold and sulphur stemming from the polymer capping. Fig. 4.8 (c) showed the elemental mapping of gold and sulphur in significant amounts within the sample. This indicated the polymer capped the AuNPs.

(a)

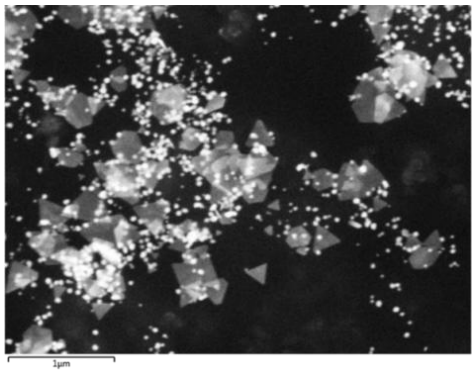

(b)

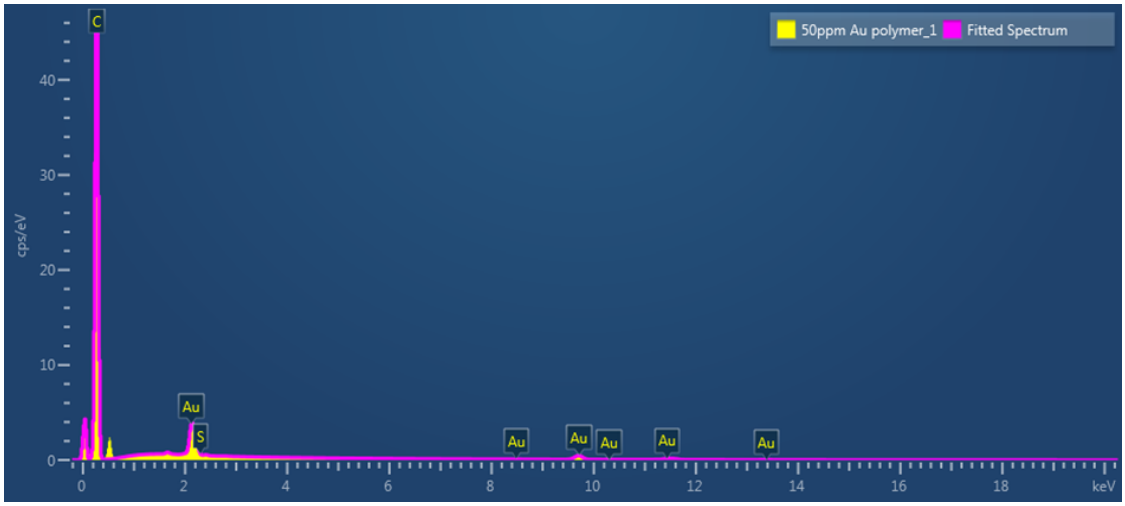

(c)

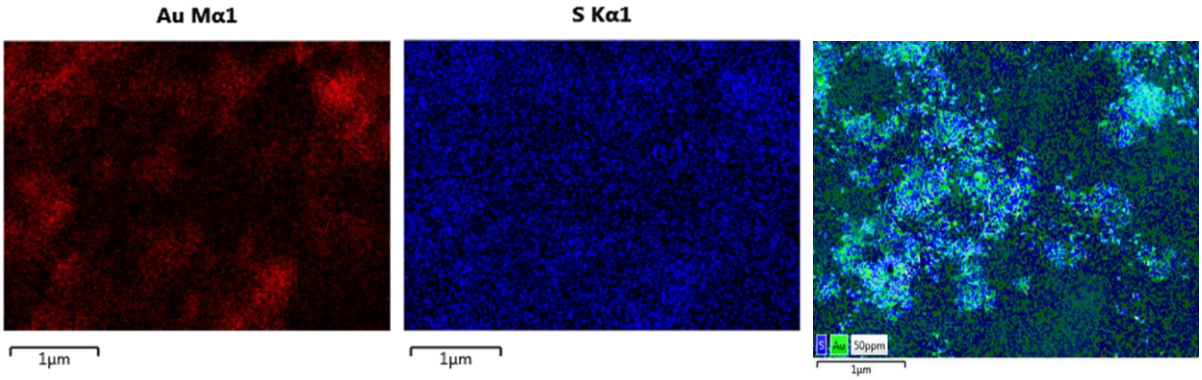

Figure 4.8. (a) SEM micrograph (b) EDX spectrum and (c) element maps of 50 ppm TEP-AuNPs

4.3.2.3. Dynamic Light Scattering Studies

Fig. 4.9 and Table 4.8 and Appendix 8 – 9 indicated that there was an increase in the size and a change of shape of the AuNPs as the concentration of the TEP increased. Also the surface charge of the nanoparticles became more positive charge due to the increased amount of TEP.

As the polymer coated the surface of the AuNPs through gold-sulphur bonds, the ammonium ions present in the polymer brought about a positive charge to the AuNPs. It is known that zeta potential values greater than +25 mV or less than -25 mV are relatively stable, and AuNPs are less likely to aggregate (Greenwood *et al.* 1999: 479 – 488). It was observed that AuNPs and AuNPs capped with 1 ppm TEP were relatively stable (Table 4.8). As TEP increased, the capped-AuNPs became more destabilized; as a result, as they approach each other, they formed larger particles of different shapes. These results were confirmed by TEM analysis.

(a)

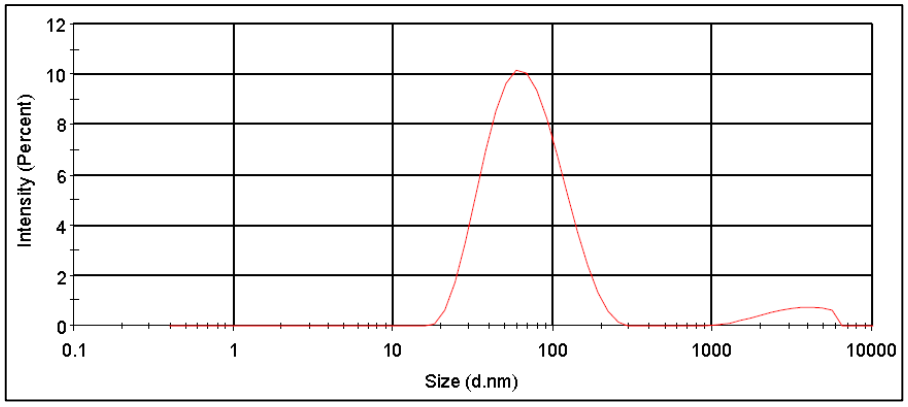

(b)

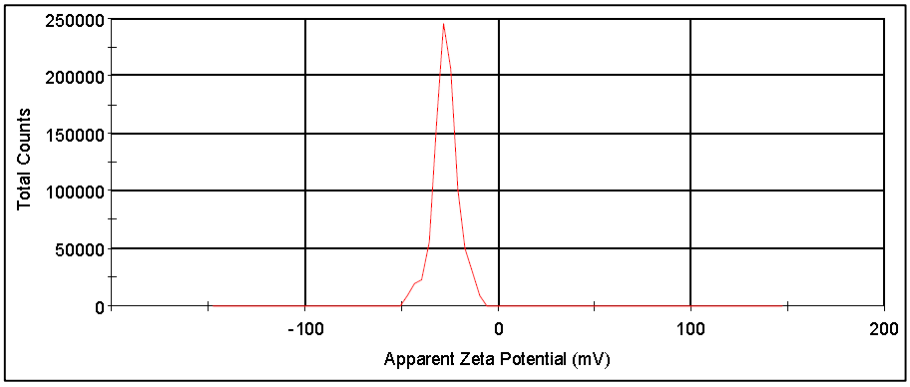

Figure 4.9. DLS spectra for (a) particle size and (b) zeta potential for 0 ppm TEP-AuNPs

Table 4.8. DLS results of TEP-AuNPs synthesized from bagasse

AuNPs with TEP /ppm	Particle size/nm	Zeta Potential
0.000	54.20 ± 2.302	-27.90 ± 3.758
1.000	68.20 ± 5.763	-25.70 ± 2.960
5.000	72.45 ± 8.314	-22.10 ± 2.390
3.000	91.50 ± 5.032	-18.00 ± 4.205
50.00	195.7 ± 2.795	-11.70 ± 3.021

4.3.2.4. Transmission Electron Microscopy Analysis

The TEM image (Fig. 4.10 (a)) illustrated 0.000 ppm TEP-AuNPs (bagasse extract) which appeared as polydisperse nanospheres. Subsequent figures showed that the particle sizes increased and larger quantities of nanotriangles formed until clusters at 50.00 ppm TEP-AuNPs (Fig. 4.11 (c)) occurred. These observations also indicated that TEP successfully capped the AuNPs. The growth in nanoparticles as the polymer concentration increase was due to the polymer itself. It was postulated that a positively-charged capping agent destabilized the AuNPs and they were more likely to aggregate by lowering of the electrostatic repulsions between them. As the particles grew, they settled at the bottom of the vessel as seen in Fig. 4.12 (a) for the 50 ppm TEP-AuNPs. The particle size distributions correlated to the sizes of the gold nanoparticles which was obtained by light dynamic scattering studies.

(a)

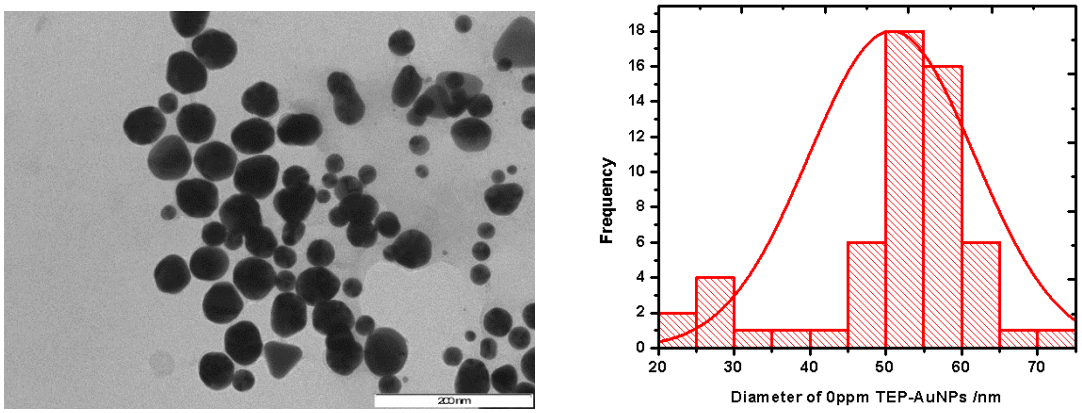

(b)

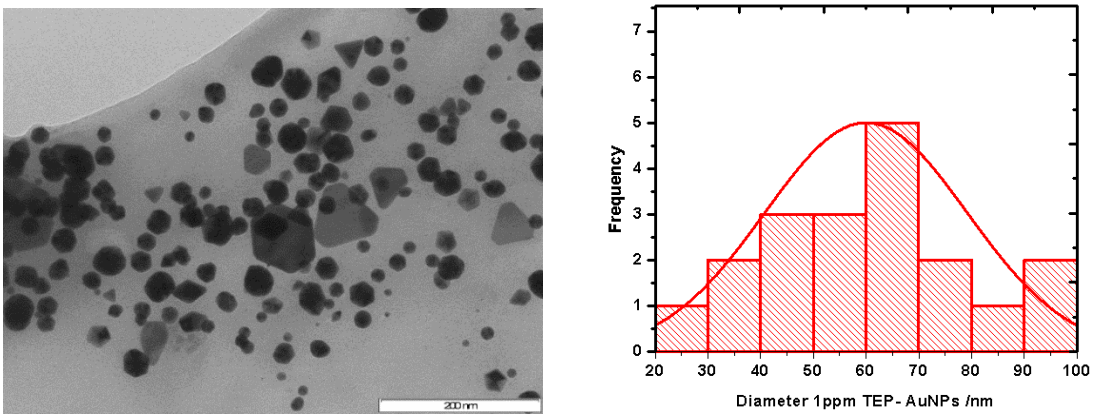

Figure 4.10. TEM micrographs and particle size distributions of (a) 0 ppm TEP-AuNPs (b) 1 ppm TEP-AuNPs

(a)

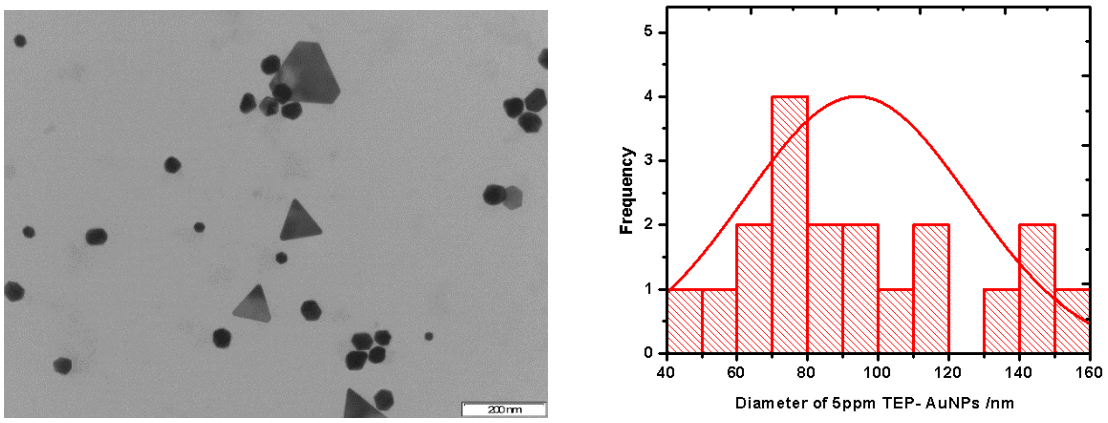

(b)

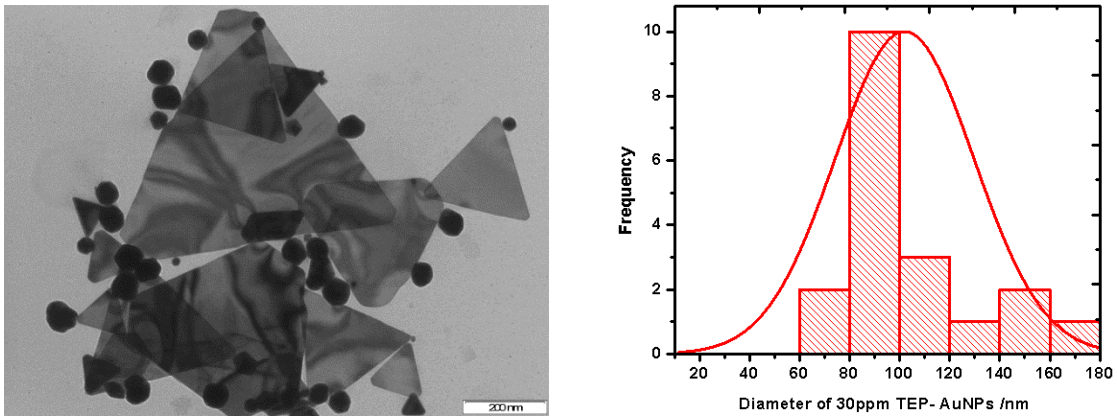

(c)

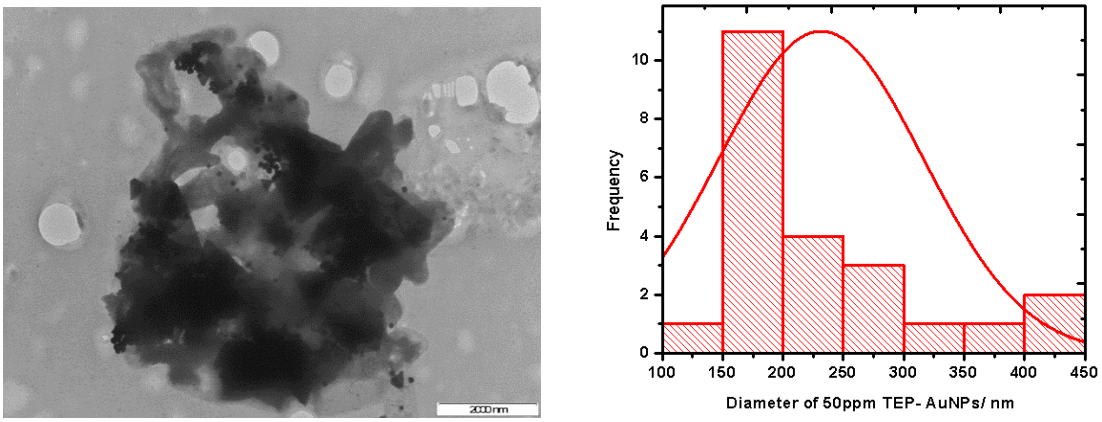

Figure 4.11. TEM micrographs and particle size distributions of (a) 5 ppm TEP-AuNPs (b) 30 ppm TEP-AuNPs and (c) 50 ppm TEP-AuNPs

4.3.3. TEP-AuNP Surface

The reddish colour of the AuNPs (Fig. 4.12 (a)) was attributed to the localized surface plasmon resonance. A single peak was due to spherical and triangular nature of the nanoparticles. Fig.

4.13 illustrates the reduction reaction of $HAuCl_4$ reduced with bagasse or sodium citrate in the presence of the TEP yielding AuNPs of various sizes (Table 4.8).

(a)

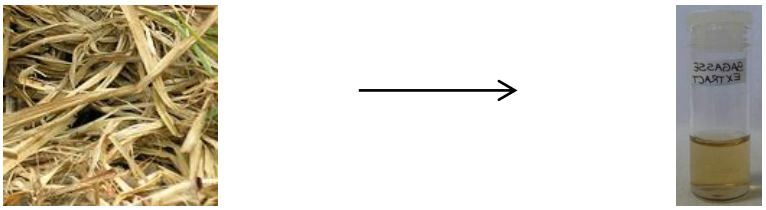

(b)

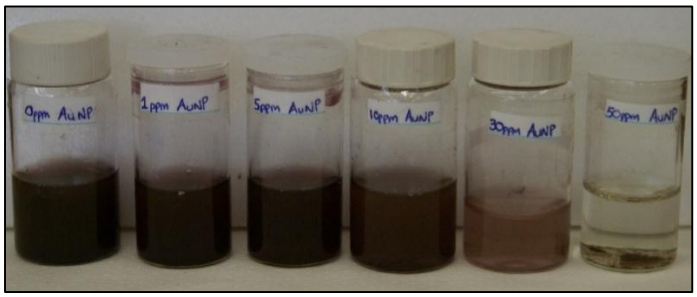

Figure 4.12. (a) The gold nanoparticle solutions formed using bagasse extract with varying concentrations of Thiazolidine-Epichlorohydrin-Ethylenediamine Polymer and (b) the aqueous extraction of sugarcane bagasse

To explain this reaction we believe that the polymeric chains dissolve in water and disentangle. The sulphur groups in the polymer easily attract and bond covalently to the gold nanoparticles due to their soft characteristics according to Pearson's acid base concept. The rest of the protruding polymeric chains prevent Ostwald ripening by creating steric hindrance and repulsive forces between AuNPs clusters. There exists two mechanisms that explain the ripening of AuNPs. First, ripening can be caused by the clustering of NPs of same size, or by the motion of individual gold atoms to larger AuNP clusters (Shimmin *et al.* 2004: 5613 – 5620). These mechanisms may also co-exist. Fig. 4.13 below shows the formation of AuNPs.

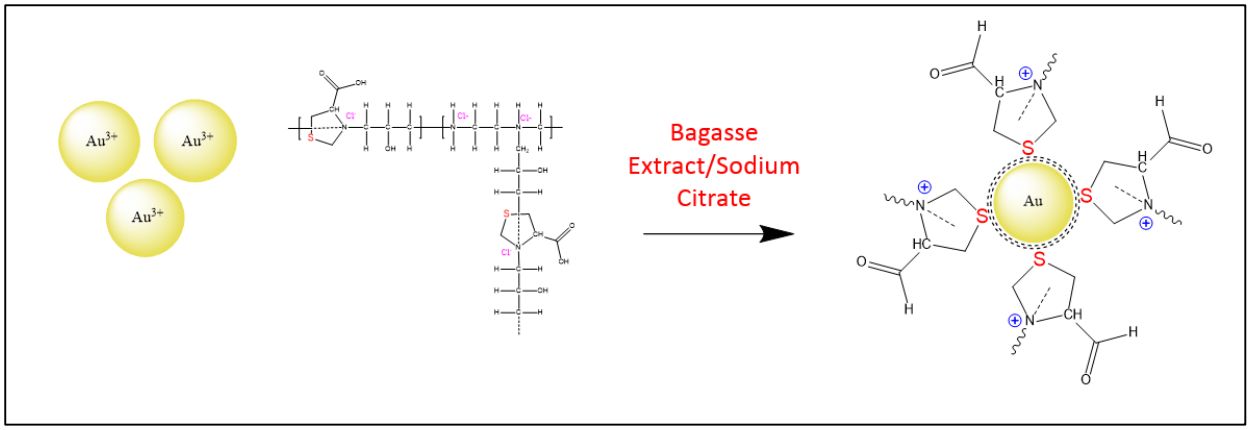

Figure 4.13. Graphic representation of the formation of the AuNP using Thiazolidine-Epichlorohydrin-Ethylenediamine Polymer

The polymer may not efficiently cover all spaces around the AuNPs. Because polymers cause sufficient hindrance between AuNP clusters, it does not prohibit the migration of individual gold atoms towards the clusters. The gold atoms can penetrate through the polymeric chains and deposit onto AuNP thereby enlarging them (Shimmin *et al.* 2004: 5613 – 5620). The growth in size can also be attributed to the ammonium ions on the polymer which may destabilize the AuNPs by lowering the electrostatic repulsion between them. This results in the enlargement of AuNPs and the surface charge tended to a more positive value.

4.3.4. The Vroman-Like Effect

Experimental evidence confirmed the overall increase in the zeta potential and an increase in the overall particle sizes of the AuNPs as the concentration of the TEP increased. Similar results were reported by Gangula *et al.* (2012: 22866 – 22872). The TEM analysis also showed that as the concentration of the capping polymer increased, more nanotriangles of larger sizes had formed. This suggests that the Vroman-like effect might have occurred as the TEP replaced any reducing sugars from the bagasse extract that might cap the gold surface. This could occur since the thioether moieties on the polymer have more affinity than the moieties on the reducing sugars towards the gold surface.

The Vroman effect was confirmed by FT-IR, EDX and TEM imaging studies. As the TEP replaced the reducing sugars on the AuNP surface, the cationic ammonium ions within the polymer could destabilize the AuNPs by shifting the surface charge towards more positive values. This lowered the electrostatic repulsion between AuNPs, causing them to approach

each other. As a result, the particle size of the AuNPs increased as more nanotriangles of larger sizes were formed as the TEP capping concentration increased. This possible mechanism could have a direct impact on the catalytic behavior of both the bagasse-reduced and Turkevich synthesized AuNPs. Fig. 4.14 illustrated the Vroman effect whereby the polymer replaced the reducing sugars that initially capped the AuNPs.

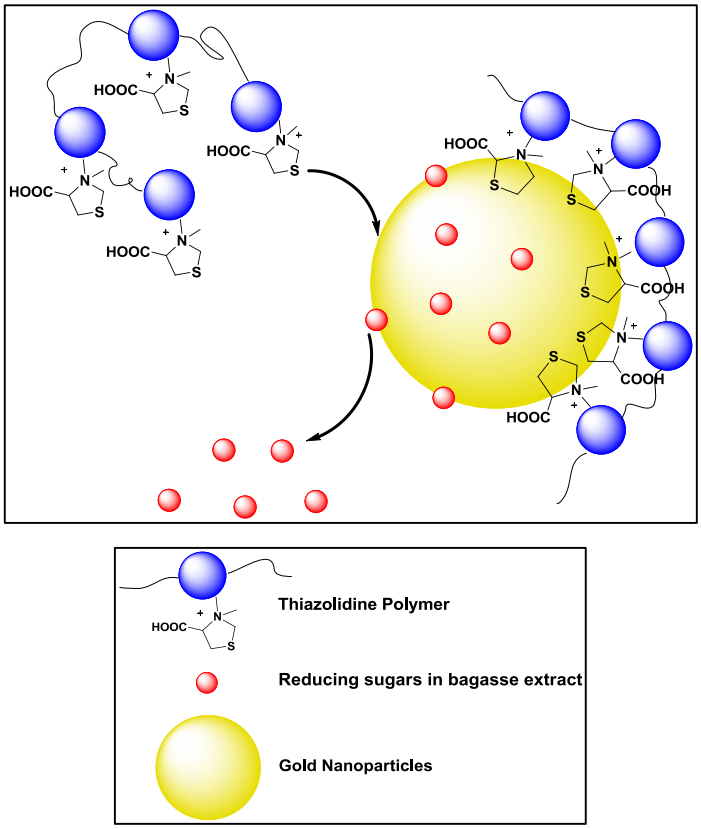

Figure 4.14. The illustration of the Vroman effect

4.3.5. Kinetics for AuNP Formation

The rate of formation of AuNPs was established by spectroscopically monitoring the increase in surface plasmon resonance absorbance peak at ≈ 540 nm. The bagasse-synthesized gold nanoparticles took longer to synthesize compared to the Turkevich method, as anticipated. It was visually observed that when bagasse was added to the $HAuCl_4$ solutions, after an hour of reaction, the formation of AuNPs was seen due to the emergence of a faint pinkish color. Fig. 4.15 illustrates the UV profile for the AuNP formation for 5 ppm TEP-AuNPs: all other UV-Vis spectra are found in Fig. 4.15.

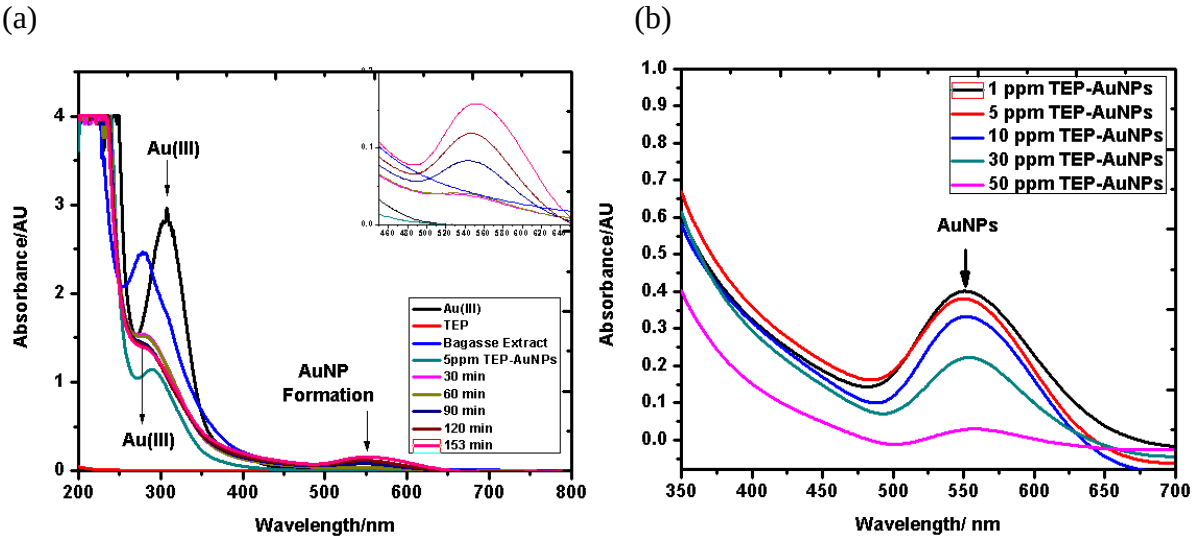

Figure 4.15. UV-Vis spectra of (a) formation of 5 ppm TEP-AuNPs, the inset exhibits a closer depiction of the Au/AuNP peaks and (b) the AuNP solutions with pre-selected concentrations of Thiazolidine-Epichlorohydrin-Ethylenediamine Polymer.

Although the polymer showed no peak, the bagasse and gold showed a peak at 275 nm and 309 nm, respectively. The prominent peak of bagasse was due to the collective role that the phenolic hydroxyl containing compounds e.g. reducing sugars and lignin, would have played in the reduction of the gold salts (Mishra *et al.* 2013: 217 – 219). The prominent -OH and C-O absorbances was the main functionalities (Fig. 4.7) could be involved in the reduction process. During the formation of the nanoparticles, the bagasse exhibited an absorption at ≈ 300 nm which immediately decreased significantly as the nanoparticles were formed. A progressive absorption peak corresponding to the formation of AuNPs occurred at ≈ 540 nm. These trends indicated slow reduction of gold (complete formation in 240 minutes). Fig. 4.15 (b) shows the UV profile of AuNPs according to concentration of the TEP. Here, two trends were observed: firstly, the AuNPs containing a higher concentration of TEP had a lower absorbance value compared to the AuNPs with no or lower concentrations of TEP capping and secondly the position of the absorbance peaks at maximum wavelength for the various concentrations of TEP in the matrix. Due to the presence of more polymer in the AuNP matrix, the AuNPs sizes increased thereby causing a slight red-shift. Fig. 4.16 shows the UV-Vis spectra of the gradual formation of the AuNPs.

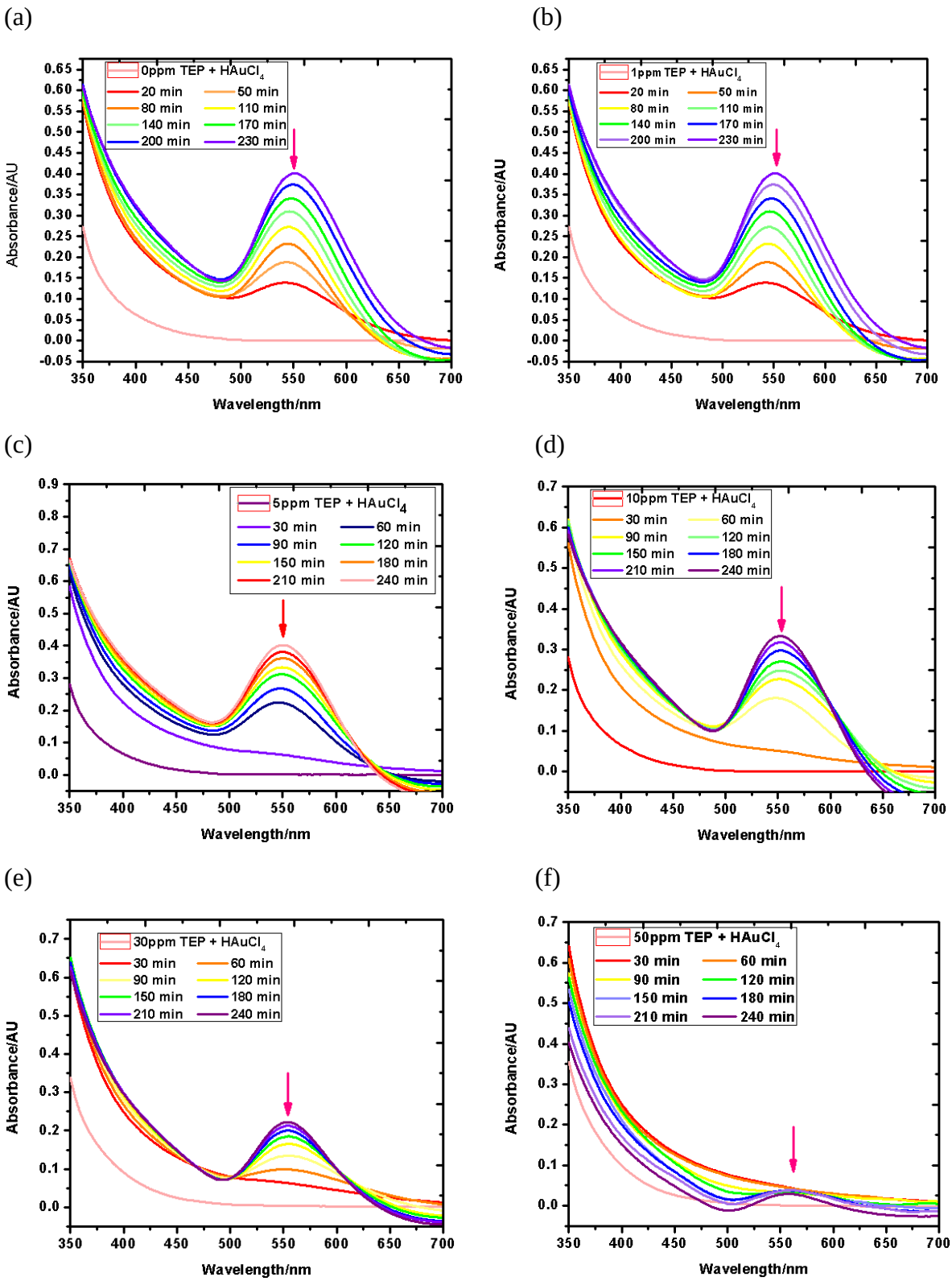

Figure 4.16. The UV-Vis spectra of AuNPs formation using (a) 0 ppm, (b) 1 ppm, (c) 5 ppm, (d) 10 ppm, (e) 30 ppm and (e) 50 ppm TEP.

Chemical kinetics was applied to the experimental data. Since the absorbance values were proportional to the concentrations of the AuNPs formed in the solutions in accordance with Beer-Lambert's law, the absorbance values were directly applied to the kinetic equations. Based on our assumption the TEP capped the AuNPs and replaced some of the reducing sugars that initially capped the AuNPs, the equation below applies:

$$HAuCl_4 + \text{Reducing sugars} + TEP \xrightarrow{k_r} AuNPs + \text{Reducing sugars} \quad (4.1)$$

Using the general rate law equation:

$$Rate = kr_r\,[AuNPs]^n \quad (4.2)$$

The rate was determined by using the equations:

$$Rate = -\frac{d(HAuCl4)}{dt} = -\frac{d(TEP)}{dt} = \frac{d(AuNPs)}{dt} = kr \quad (4.3)$$

$$Rate = \frac{d(AuNPs)}{dt} = k_f \quad (4.4)$$

Equation 4.3 is rearranged:

$$d[AuNPs] = k_r\,dt \quad (4.5)$$

The integrated form is:

$$\int_{[\mathrm{AuNP}]0}^{[\mathrm{AuNPs}]_t} \mathrm{d[AunPs]} = \int_0^t \mathrm{kr\ dt} \quad (4.6)$$

$$[AuNPs]_t + [AuNPs]_0 = k_r\,t \quad (4.7)$$

A plot of $[AuNPs]_t$ as a function of t/min yielded linear plots.

For pseudo-first order reaction, an increase in AuNPs concentration monitored by its adsorption (equation 4.1) reflects the rate to be:

$$\frac{d[AuNPs]}{dt} = k[AuNPs] \quad (4.8)$$

Rearranging the equation yields:

$$\frac{d[AuNPs]}{[AuNPs]} = kdt \quad (4.9)$$

The integrated form is:

$$\int_{[AuNPs]0}^{[AuNPs]t} \frac{d[AuNPs]}{[AuNPs]} = \int_0^t kdt \quad (4.10)$$

$$\ln[AuNPs]_t = kt + C \quad (4.11)$$

The evaluation of C (the integration constant) is done by using the boundary conditions where t = 0 min, [AuNPs] = $[AuNPs]_0$

$$\ln[AuNPs]_0 = k(0) + C \quad (4.12)$$

Therefore:

$$C = \ln[AuNPs]_0 \quad (4.13)$$

Therefore the integrated form of the pseudo-first order reaction rate is:

$$\ln[AuNPs] = kt + \ln[AuNPs]_0 \quad (4.14)$$

A plot of $\ln[AuNPs]$ as a function of t/min yielded linear plots (Fig. 4.18).

For the second order reaction rate, the differential rate equation was:

$$Rate = d\frac{AuNPs}{dt} = k[AuNPs]^2 \quad (4.15)$$

Rearranging equation 4.15 yields:

$$\frac{d[AunPs]}{[AuNPs]^2} = k\,dt \quad (4.16)$$

Since there is a change in concentration of the AuNP over time, equation 4.16 is integrated from $t = 0$ min to $t = t$ min:

$$\int_{[AuNPs]0}^{[AuNPs]t} \mathrm{d}\frac{[\mathrm{AunPs}]}{[\mathrm{AuNPs}]^2} = \mathrm{k_r} \int_0^t dt \quad (4.17)$$

The linear function plotted was:

$$\frac{1}{[AuNPs]_t} = -kt + \frac{1}{[AuNPs]_0} \quad (4.18)$$

A plot of $\frac{1}{[AuNPs]_t}$ as a function of t/min yielded linear plots.

The formation of AuNPs (reduced with bagasse extract) followed a pseudo-first order reaction whilst the AuNPs formed in the presence of the TEP follows a zero order reaction. The chemical kinetics were not calculated for AuNPs synthesized by the Turkevich method due to its rapid formation. Although thioether-Au bonds are much weaker than similar counterparts (Hermes *et al.* 2011: 13473 –13481), in our study the AuNPs were successfully stabilized for lower TEP-capping as seen in the zeta potential results. By using equations (Table 4.9), the rates were calculated (Table 4.10).

Table 4.9. Kinetic equations used

Equation	Order	Linear Equation	f(t)	Half-life ($t^{0.5}$)
4.19	0	$[A] = [A]_0 + kt$	$[A]$ vs t	$[A]_0$/ 2k
4.20	1	$\ln[AuNPs] = kt + \ln[AuNPs]_0$	$\ln[AuNPs]$ vs t	$ln2$/k
4.21	2	$\frac{1}{[A]} = \frac{1}{[A]_0} - kt$	$\frac{1}{[A]}$ vs t	$\frac{1}{(k[A]0)}$

It was observed that as the concentration of TEP increased, the rate of formation of AuNPs decreased (Table 4.10, Fig. 4.17). At 50 ppm of TEP capping, the rate of formation of AuNPs was the slowest, as confirmed by Fig. 4.17 (f). This could be due to the polymer consequently hindering the contact between gold ions and the reducing agent as it uncoils in the aqueous medium. This effect was more prominent when larger concentrations of polymer were used.

Table 4.10. Kinetic information of formation of TEP-AuNP

Concentration of TEP/ppm	Rate order	Rate of reaction	R^2 value
0.000	1	0.003800 min^{-1}	0.9961
1.000	0	0.001200 min^{-1}	0.9915
5.000	0	0.001000 min^{-1}	0.9657
10.00	0	0.0008100 min^{-1}	0.9789
30.00	0	0.0007930 min^{-1}	0.9704
50.00	0	0.00007300 min^{-1}	0.9308

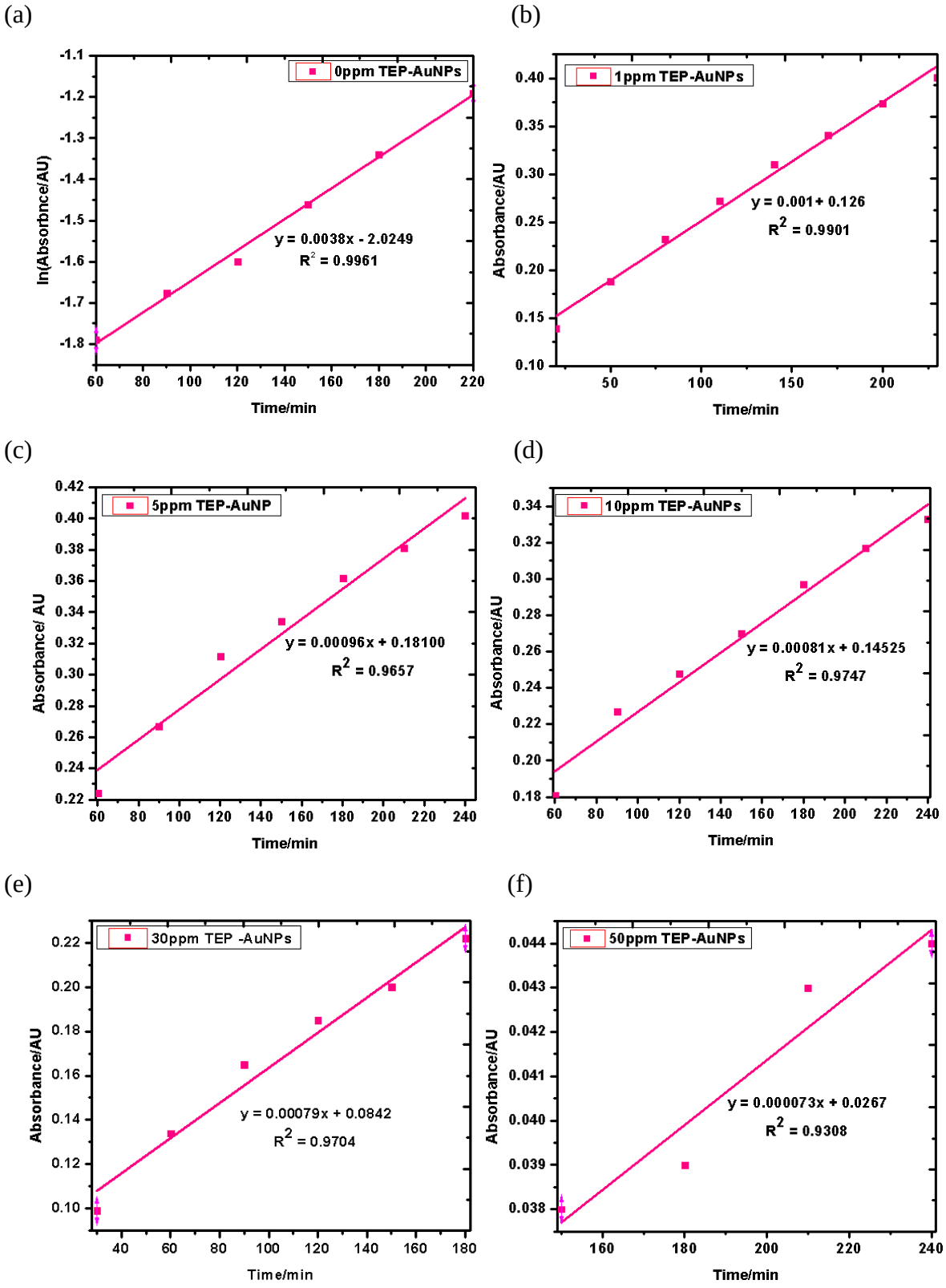

Figure 4.17. The kinetic functions of AuNPs formation using various concentrations of TEP (a) 0 ppm, (b) 1 ppm, (c) 5 ppm, (d) 10 ppm, (e) 30 ppm and (e) 50 ppm

4.3.6. Catalytic Action

The thiazolidine capped AuNPs, was applied to study dye reduction. Three common, dyes were used. These were Methylene Blue (MB), a cationic dye, and Allura Red (AR) and Congo Red (CR), both anionic azo dyes. By UV studies a gradual decrease of the active peak absorption at 664 nm, 512 nm, and 500 nm for MB, AR and CR respectively of the dye were observed. Addition of $NaBH_4$ to each dye did not cause decolourization even after 24 hours of reaction. However when AuNPs was added to the dye-BH_4^- mixture, decolourization was gradually observed. This was observed for all three dyes and suggested that AuNPs alone were responsible for the decolourization. Fig. 4.18 illustrates an example of the degree of decolourization for all the dyes for 0 ppm TEP used whilst the other spectra that illustrates decolourization and its respective kinetic linear functions for AuNPs synthesized with bagasse extract and sodium citrate presented in Appendix 10 – 15.

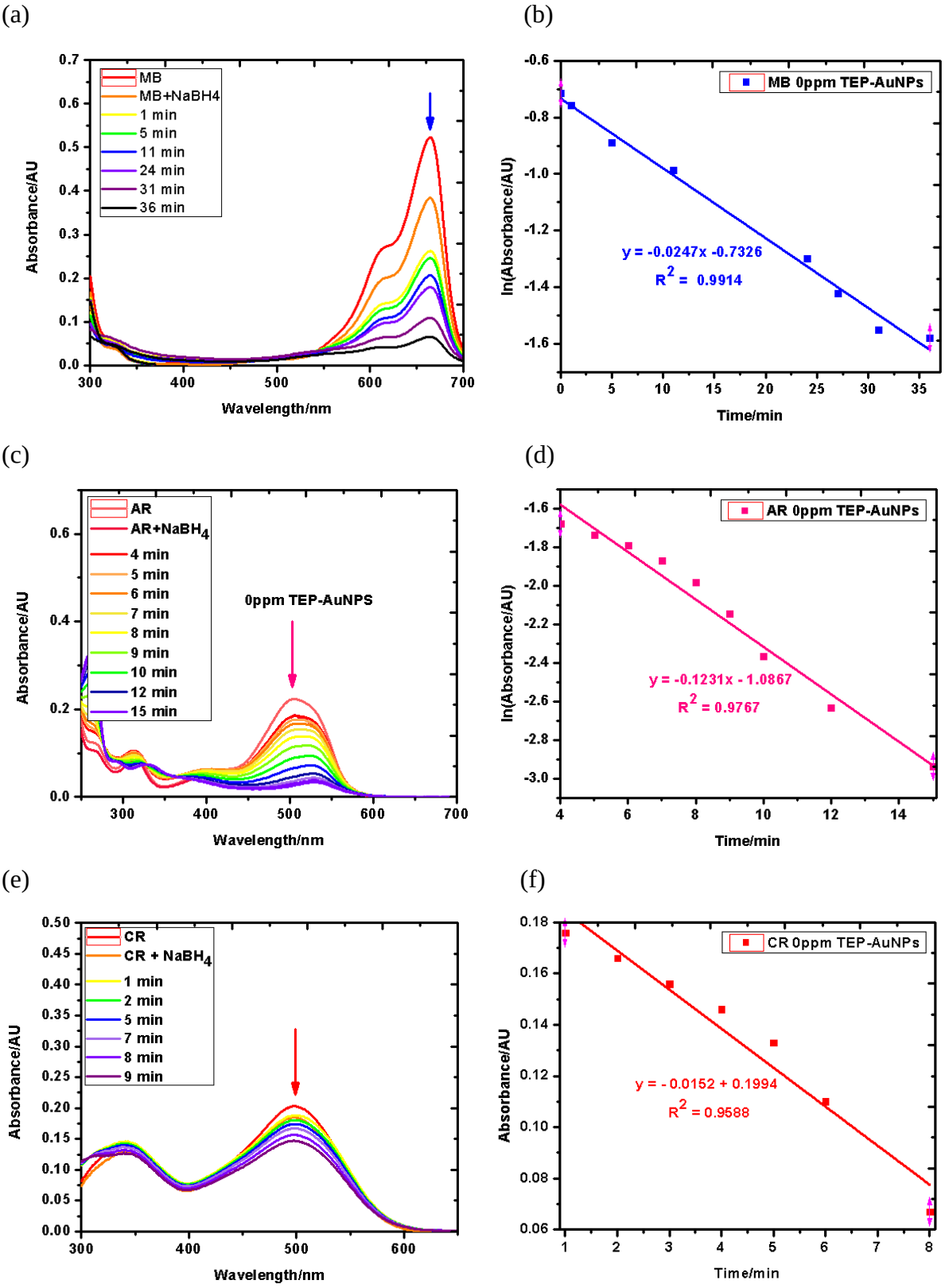

Figure 4.18. UV-Vis spectra exhibiting reduction of (a) Methylene Blue, (b) Allura Red and (c) Congo Red with 0 ppm TEP-AuNPs

Here again, a similar trend was seen for all other dye solutions when the AuNP solutions were varied. As the particle size increased, the reduction rates decreased (Table 4.11). This trend is in agreement with literature (Shimmin *et al.* 2004: 5613 – 5620). It was also found that it generally took longer for AuNPs with high concentrations of polymer to exhibit catalytic action than AuNPs with lower concentrations. For MB and CR, no induction periods were seen, however, for AR, a slight induction period was seen for approximately the first five minutes for some catalytic reactions. Similar induction times were reported by Wunder *et al.* (2010: 8814 – 8820). These induction periods, marked as a dotted line in the kinetic graphs in Appendix 12, indicated that the dyes adsorbed onto the AuNPs before reduction. This is the reason that for a certain period of time, the absorbance of the dyes remained the same until reduction occurred. The mechanisms of reduction itself were based on previous literature (Sahoo *et al.* 2014: 215 – 222). The generic mechanisms for Methylene Blue and the azo dyes as explained by Azad *et al.* (2011: 3951 – 3959), Veerakumar *et al.* (2012: 197 – 205) and Sahoo *et al.* (2014: 215 – 222) which involved the formation of gold hydride when $NaBH_4$ was introduced into the catalytic system (Fig. 4.19).

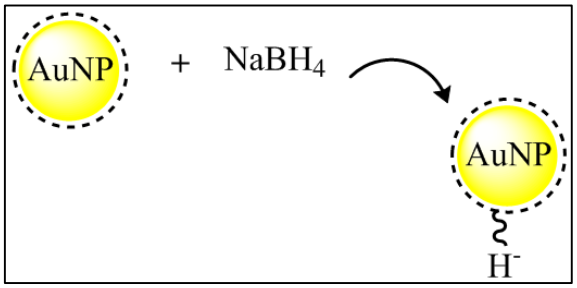

Figure 4.19. Metal hydride formation to aid catalytic activity of AuNPs

It is possible that the hydrides reduced the dye and the by-products then desorbed from the surface of the AuNPs. This mechanism is also possible for CR (Fig. 4.21) and MB (Fig. 4.22).

Figure 4.20. The physical decolourization of the dyes (Methylene blue, Allura red and Congo red)

The possible reaction mechanisms of the degradation of the dyes are shown in Fig. 4.21 – 4.23).

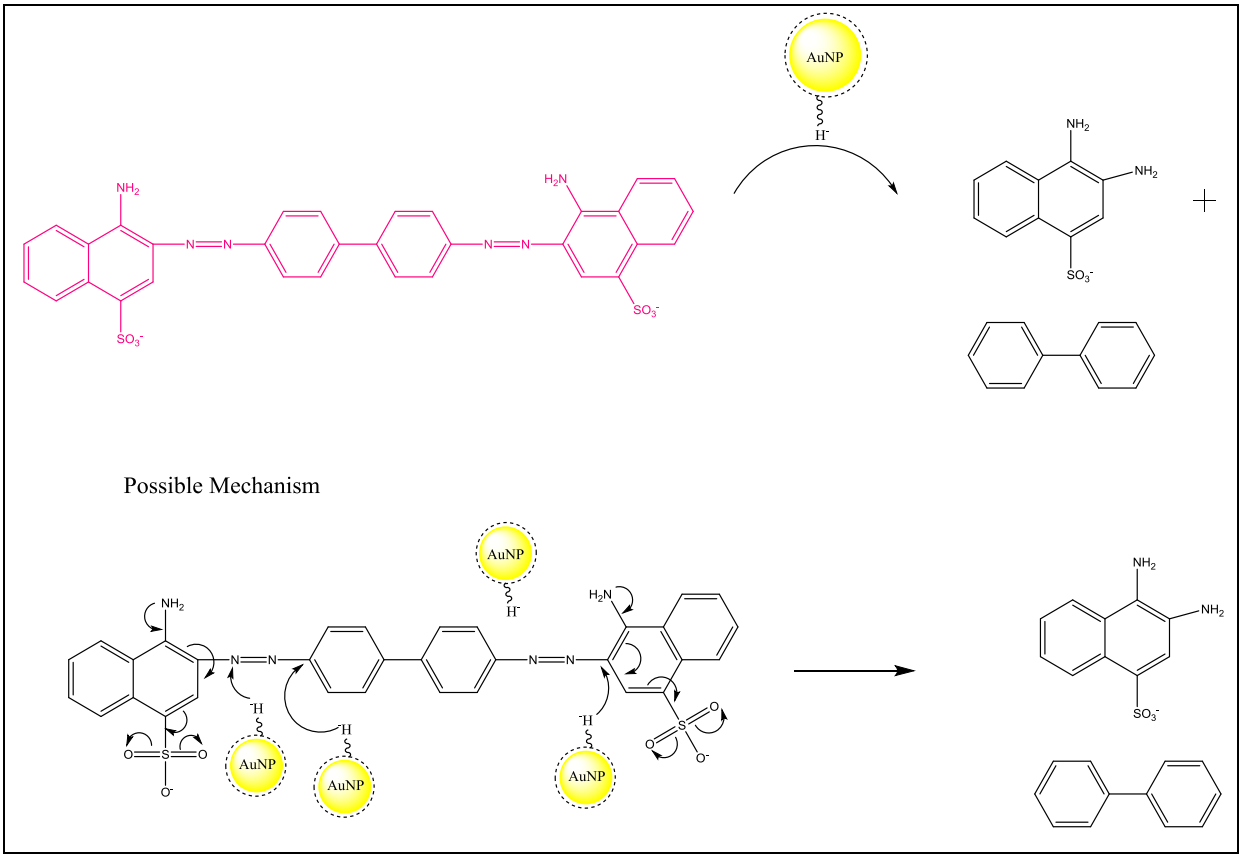

Figure 4.21. The possible mechanism of dye reduction of Congo Red

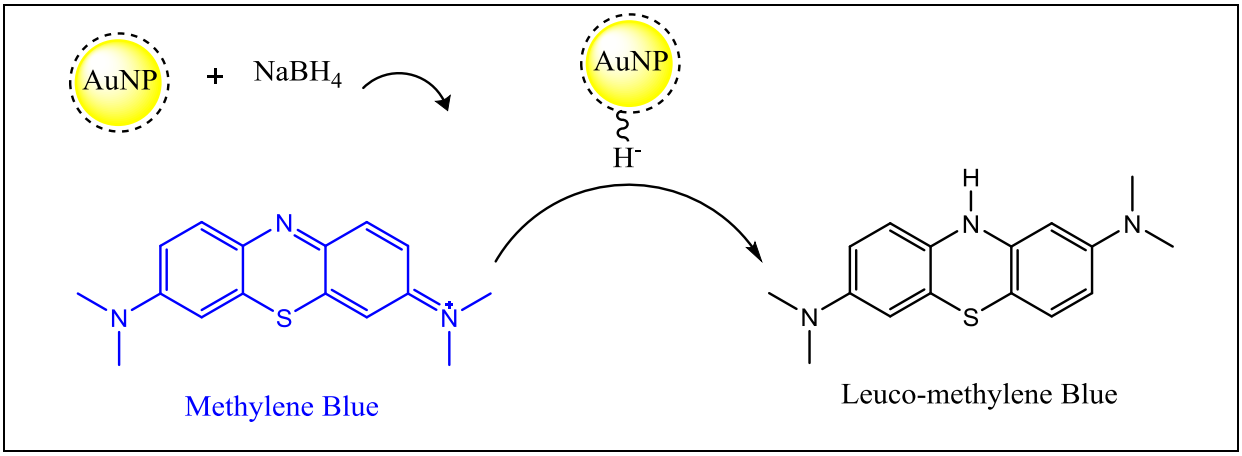

Figure 4.22. The possible mechanism of dye reduction of Methylene Blue

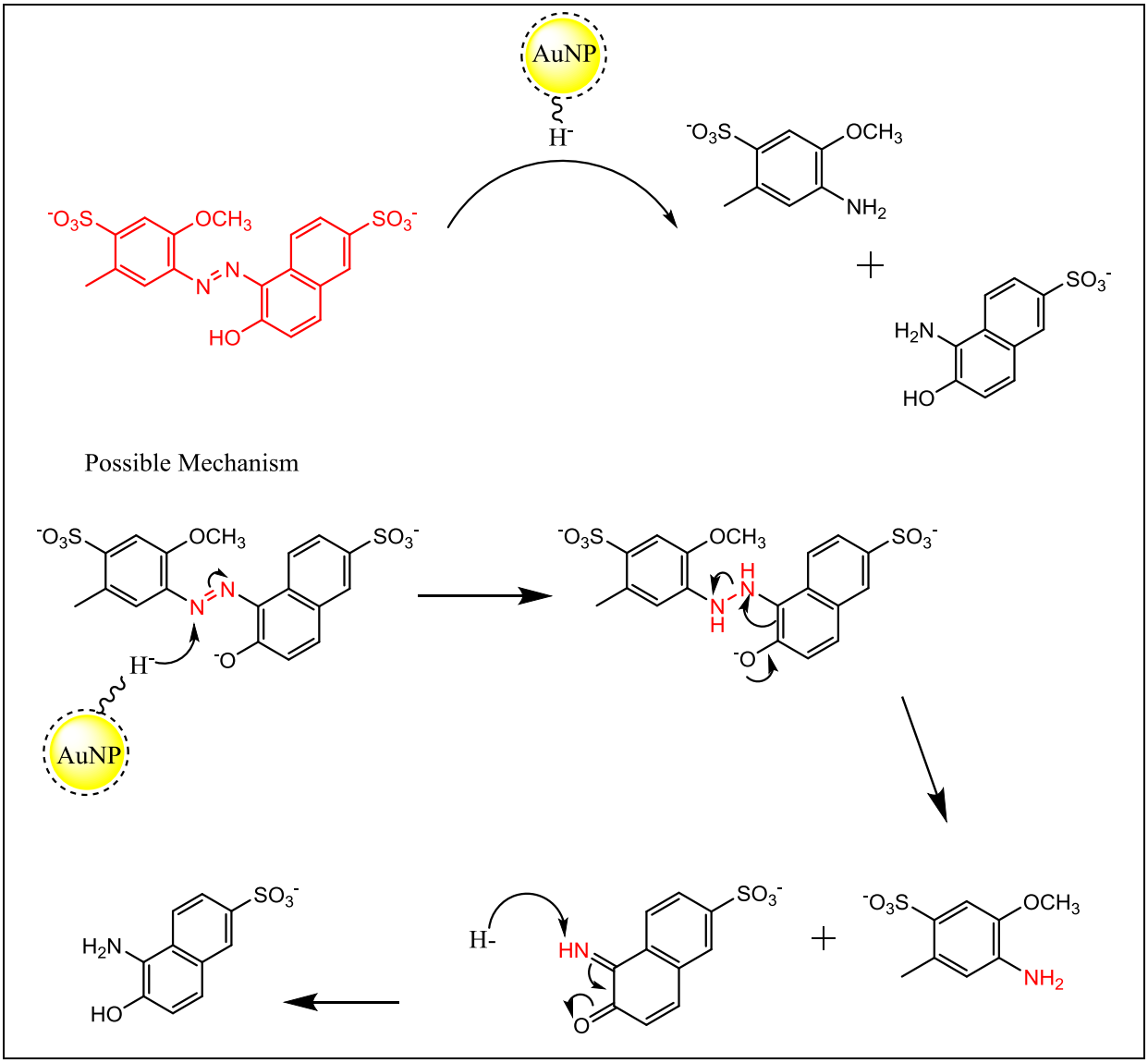

Figure 4.23. The possible mechanism of dye reduction of Allura Red

For Allura Red (Fig. 4.23) with a significant induction time, a period of time was needed for the Allura Red to adsorb onto the surface of the AuNPs. A small degree of reduction took place during this time. Thereafter, the reduction became prominent.

For MB, as the dye attracted the catalytic surface and got reduced, it was believed that leuco-Methylene Blue formed (Fig. 4.22). For the azo dyes, the mechanism demonstrating the cleavage of the azo (N=N) bond was reported by Sahoo *et al.* (2014: 215 – 222).

Table 4.11. Kinetics of reduction of dyes using TEP-AuNPs

[TEP] /ppm	Multi-purpose Dye					
	Methylene Blue					
	AuNPs synthesized by sodium citrate			AuNPs synthesized by bagasse		
	Rate order	Rate of reaction	R^2 value	Rate order	Rate of reaction	R^2 value
0	1	$2.908 \times 10^{-1} \pm 1.426 \times 10^{-2}$	0.9776	1	$2.424 \times 10^{-1} \pm 2.088 \times 10^{-3}$	0.9564
1	1	$1.579 \times 10^{-1} \pm 9.708 \times 10^{-3}$	0.9803	1	$2.460 \times 10^{-2} \pm 1.526 \times 10^{-3}$	0.9782
5	1	$1.040 \times 10^{-1} \pm 7.269 \times 10^{-3}$	0.9693	1	$1.880 \times 10^{-2} \pm 7.190 \times 10^{-4}$	0.9018
10	1	$8.260 \times 10^{-2} \pm 4.935 \times 10^{-3}$	0.9723	1	$1.180 \times 10^{-2} \pm 1.678 \times 10^{-3}$	0.9714
30	1	$7.490 \times 10^{-2} \pm 1.367 \times 10^{-3}$	0.9682	1	$8.600 \times 10^{-3} \pm 1.038 \times 10^{-3}$	0.9716
50	1	$4.080 \times 10^{-2} \pm 3.070 \times 10^{-3}$	0.9771	1	$1.700 \times 10^{-3} \pm 8.791 \times 10^{-4}$	0.9887
Congo Red						
0	0	$2.580 \times 10^{-2} \pm 2.023 \times 10^{-3}$	0.9588	0	$7.600 \times 10^{-2} \pm 6.887 \times 10^{-4}$	0.9239
1	0	$1.310 \times 10^{-2} \pm 1.965 \times 10^{-3}$	0.8636	0	$7.200 \times 10^{-2} \pm 6.777 \times 10^{-4}$	0.9108
5	0	$1.230 \times 10^{-2} \pm 1.946 \times 10^{-3}$	0.9241	0	$5.800 \times 10^{-2} \pm 5.929 \times 10^{-4}$	0.9254
10	0	$9.900 \times 10^{-3} \pm 1.189 \times 10^{-3}$	0.8738	0	$5.700 \times 10^{-2} \pm 6.024 \times 10^{-4}$	0.9078
30	0	$9.300 \times 10^{-3} \pm 1.978 \times 10^{-3}$	0.7864	0	$5.400 \times 10^{-2} \pm 5.673 \times 10^{-4}$	0.9370
50	0	$8.700 \times 10^{-3} \pm 1.005 \times 10^{-3}$	0.9264	0	$4.100 \times 10^{-2} \pm 3.571 \times 10^{-4}$	0.9293
Allura Red						
0	1	$7.300 \times 10^{-2} \pm 1.569 \times 10^{-3}$	0.9962	0	$1.920 \times 10^{-2} \pm 7.322 \times 10^{-4}$	0.9941
1	1	$6.850 \times 10^{-2} \pm 3.067 \times 10^{-3}$	0.9652	0	$1.420 \times 10^{-2} \pm 2.941 \times 10^{-4}$	0.9961
5	1	$4.510 \times 10^{-2} \pm 4.185 \times 10^{-3}$	0.9982	0	$1.370 \times 10^{-2} \pm 1.316 \times 10^{-3}$	0.9235
10	1	$3.950 \times 10^{-2} \pm 5.975 \times 10^{-3}$	0.9966	0	$1.250 \times 10^{-2} \pm 1.069 \times 10^{-3}$	0.9382
30	1	$3.160 \times 10^{-2} \pm 7.190 \times 10^{-3}$	0.9923	0	$1.180 \times 10^{-2} \pm 8.802 \times 10^{-4}$	0.9276
50	1	$1.120 \times 10^{-2} \pm 2.890 \times 10^{-3}$	0.9941	0	$1.070 \times 10^{-2} \pm 1.615 \times 10^{-3}$	0.8142

4.4. Conclusion

A new water-soluble polymer was synthesized using the monomers L-Thiazolidinecarboxylic acid, epichlorohydrin and ethylenediamine. It was characterized by FT-IR and ^{1}H-NMR spectroscopy whilst the molecular weight was calculated as 69.78 kDa ± 1.176 kDa by Static Light Scattering. Several solutions of gold nanoparticles were prepared using TEP as a capping agent by the Turkevich method and by synthesis using bagasse extract to reduce three common dye pollutants. There was a clear difference among the shape and size of the AuNPs containing different TEP concentrations. The particle sizes of the AuNPs in the bagasse system ranged from 69.65 nm to 195.7 nm and the surface charge increased to more positive values as more TEP capping agent was used. Experimental evidence (TEM imaging and SEM/EDX) suggested the occurrence of the Vroman effect where TEP replaced the sugars capped on the AuNPs surface, thereby causing an increase in the surface charge. It was found that more TEP present during AuNPs formation lowered the rate of formation of AuNPs. It was concluded that higher concentrations of TEP led to aggregation of AuNPs. This had a direct consequence in the degradation of the dyes as the rate of degradation was inversely proportional to the quantity of polymer present.

4.5. References

Abdelhalim, M.A.K., Mady., M.M. and Ghannam., M.M. 2012. Physical properties of different gold nanoparticles: Ultraviolet-visible and fluorescence measurements. *Nanomedicine & Nanotechnology*, 3(3): 1 – 5.

Azad, U., Ganesan, V. and Pal, M. 2011. Catalytic reduction of organic dyes at gold nanoparticles impregnated silica materials: influence of functional groups and surfactants. *Journal of Nanoparticle Research*, 13(9): 3951 – 3959.

Cappellari, P.S., Buceta, D., Morales, G.M., Barbero, C.A., Sergio Moreno, M., Giovanetti, L.J., Ramallo-López, J.M., Requejo, F.G., Craievich, A.F. and Planes, G.A. 2015. Synthesis of ultra-small cysteine-capped gold nanoparticles by pH switching of the Au(I)–cysteine polymer. *Journal of Colloid and Interface Science*, 441: 17 – 24.

Gangula, A., Chelli, J., Bukka, S., Poonthiyil, V., Podila, R., Kannan, R. and Rao, A.M. 2012. Thione-gold nanoparticles interactions: Vroman-like effect, self-assembly and sensing. *Journal of Materials Chemistry*, 22(43): 22866 – 22872.

Greenwood, R. and Kendall, K. 1999. Electroacoustic studies of moderately concentrated colloidal suspensions. *Journal of the European Ceramic Society*, 19(4): 479 – 488.

Harish, S., Mathiyarasu, J., Phani, K.L.N. and Yegnaraman, V. 2009. Synthesis of conducting polymer supported pd nanoparticles in aqueous medium and catalytic activity towards 4-nitrophenol reduction. *Catalysis Letters*, 128(1-2): 197 – 202.

Hermes, J.P., Sander, F., Peterle, T., Urbani, R., Pfohl, T., Thompson, D. and Mayor, M. 2011. Gold nanoparticles stabilized by thioether dendrimers. *Chemistry – A European Journal*, 17(48): 13473 – 13481.

Hoppe, C.E., Lazzari, M., Pardiñas-Blanco, I. and López-Quintela, M.A. 2006. One-step synthesis of gold and silver hydrosols using poly(n-vinyl-2-pyrrolidone) as a reducing agent. *Langmuir*, 22(16): 7027 – 7034.

Hu, H., Hou, X.J., Wang, X.C., Nie, J.J., Cai, Q. and Xu, F.J. 2016. Gold nanoparticle-conjugated heterogeneous polymer brush-wrapped cellulose nanocrystals prepared by combining different controllable polymerization techniques for theranostic applications. *Polymer Chemistry,* 7(18): 3107 – 3116.

Hu, S. and Hsieh, Y.-L. 2016. Silver nanoparticle synthesis using lignin as reducing and capping agents: A kinetic and mechanistic study. *International Journal of Biological Macromolecules,* 82: 856 – 862.

Hussain, I., Brust, M., Papworth, A.J. and Cooper, A.I. 2003. Preparation of acrylate-stabilized gold and silver hydrosols and gold-polymer composite films. *Langmuir,* 19(11): 4831 – 4835.

Langille, M.R., Personick, M.L., Zhang, J. and Mirkin, C.A. 2012. Defining rules for the shape evolution of gold nanoparticles. *Journal of the American Chemical Society,* 134(35): 14542 – 14554.

Mishra, A. and Sardar, M. 2013. Rapid biosynthesis of silver nanoparticles using sugarcane bagasse-an industrial waste. *Journal of Nanoengineering and Nanomanufacturing,* 3(3): 217 – 219.

Parab, H., Jung, C., Woo, M.A. and Park, H. 2011. An anisotropic snowflake-like structural assembly of polymer-capped gold nanoparticles. *Journal of Nanoparticle Research,* 13(5): 2173 – 2180.

Pessoa, A., Mancilha, I.M. and Sato, S. 1997. Acid hydrolysis of hemicellulose from sugarcane bagasse. *Brazilian Journal of Chemical Engineering,* 14(3): 00 – 00.

Sahoo, G.P., Kumar Bhui, D., Das, D. and Misra, A. 2014. Synthesis of anisotropic gold nanoparticles and their catalytic activities of breaking azo bond in sudan-1. *Journal of Molecular Liquids,* 198: 215 – 222.

Shem, P.M., Sardar, R. and Shumaker-Parry, J.S. 2014. Soft ligand stabilized gold nanoparticles: Incorporation of bipyridyls and two-dimensional assembly. *Journal of Colloid and Interface Science,* 426: 107 – 116.

Shimmin, R.G., Schoch, A.B. and Braun, P.V. 2004. Polymer size and concentration effects on the size of gold nanoparticles capped by polymeric thiols. *Langmuir*, 20(13): 5613 – 5620.

Solyman, S.M., Azzam, E.M.S. and Sayyah, S.M. 2014. The performance of modified nanoclay using polymeric thiol surfactants assembled on gold nanoparticles in heterogeneous bulk polymerization of methyl methacrylate. *Applied Catalysis A: General*, 475: 218 – 225.

Srivastava, S., Yamada, R., Ogino, C. and Kondo, A. 2013. Biogenic synthesis and characterization of gold nanoparticles by Escherichia coli K12 and its heterogeneous catalysis in degradation of 4-nitrophenol. *Nanoscale Research Letters*, 8(1): 1 – 9.

Thakor, A.S., Jokerst, J., Zavaleta, C., Massoud, T.F. and Gambhir, S.S. 2011. Gold Nanoparticles: A Revival in Precious Metal Administration to Patients. *American Chemical Society Nano Letters*, 11(10): 4029 – 4036.

Turkevich, J., Stevenson, P.C. and Hillier, J. 1951. A study of the nucleation and growth processes in the synthesis of colloidal gold. *Discussions of the Faraday Society*, 11(0): 55 – 75.

Vasimalai, N. and Abraham John, S. 2013. Biopolymer capped silver nanoparticles as fluorophore for ultrasensitive and selective determination of malathion. *Talanta*, 115: 24 – 31.

Veerakumar, P., Velayudham, M., Lu, K.L. and Rajagopal, S. 2012. Polyelectrolyte encapsulated gold nanoparticles as efficient active catalyst for reduction of nitro compounds by kinetic method. *Applied Catalysis A: General*, 439 – 440: 197 – 205.

Wagers, K., Chui, T. and Adem, S. 2014. Effect of ph on the stability of gold nanoparticles and their application for melamine detection in infant formula. *IOSR Journal of Applied Chemistry*, 7(8): 15 – 20.

Wunder, S., Polzer, F., Lu, Y., Mei, Y. and Ballauff, M. 2010. Kinetic Analysis of Catalytic Reduction of 4-Nitrophenol by Metallic Nanoparticles Immobilized in Spherical Polyelectrolyte Brushes. *The Journal of Physical Chemistry C*, 114(19): 8814 – 8820.

Zhang, T., Song, Y.J., Zhang, X.Y. and Wu, J.Y. 2014. Synthesis of Silver Nanostructures by Multistep Methods. *Sensors*, 14(4): 5860 – 5889.

APPENDICES

Appendix 1. H^1-NMR Spectrum of PEP

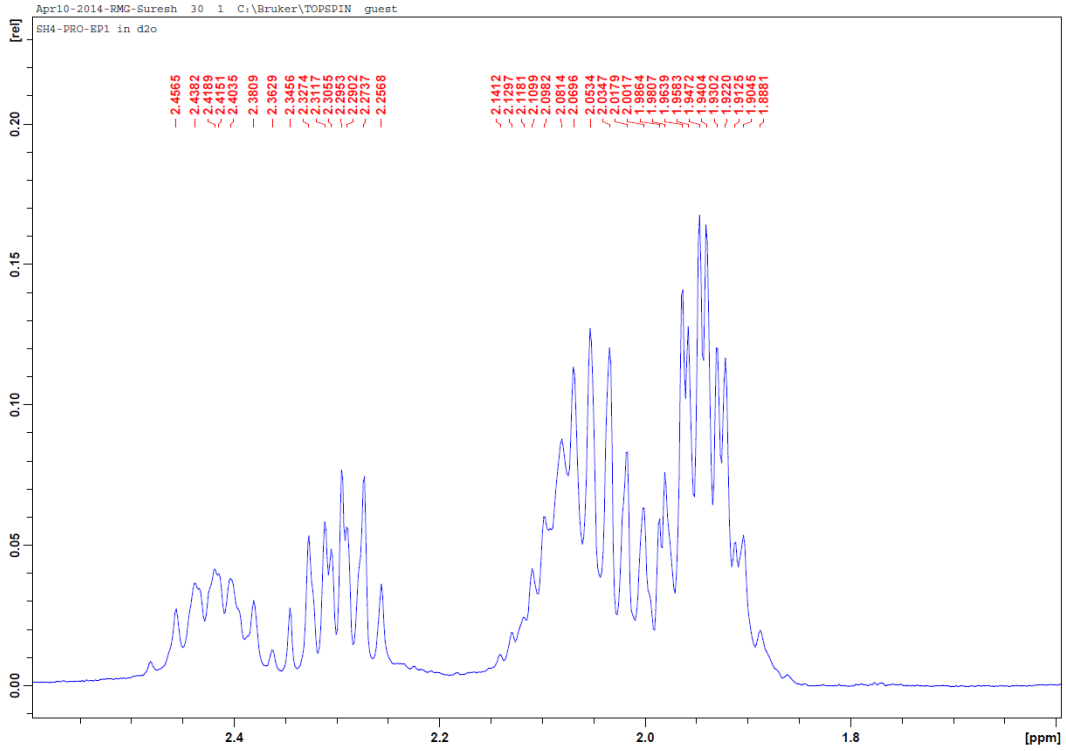

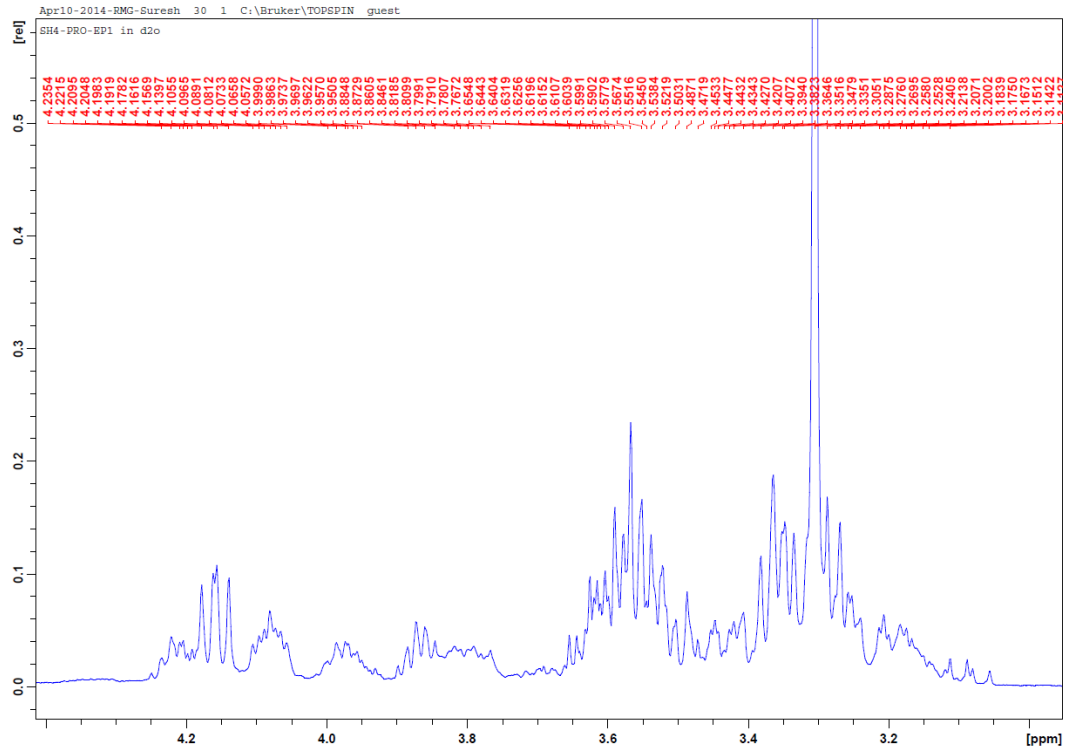

Appendix 2. High resolution spectra of (a) C1s PRO-BEN, (b) C1s PRO-BEN dye, (c) O1s PRO-BEN, (d) O1s PRO-BEN, (e) Si1s PRO-BEN and (f) Si1s PRO-BEN dye

(a)

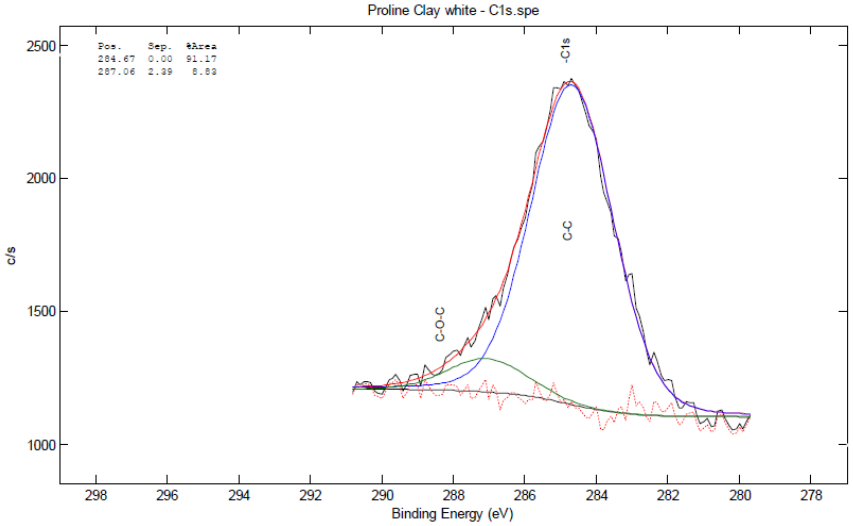

(b)

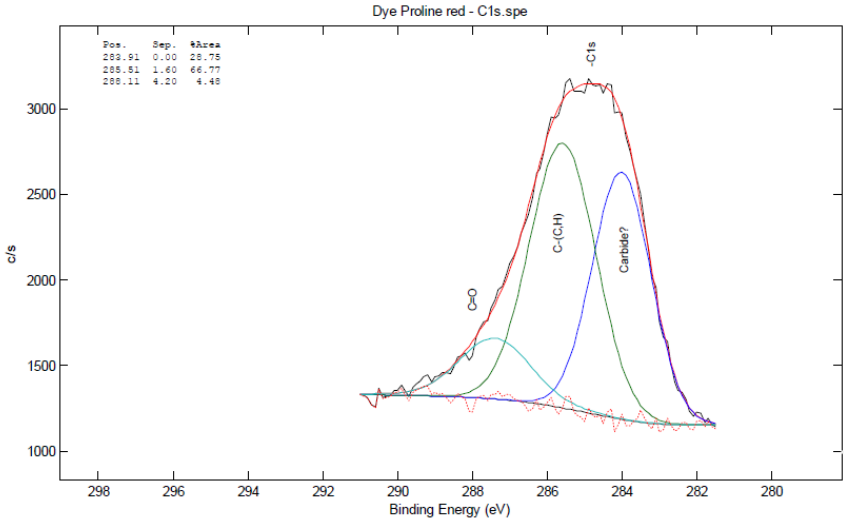

(c)

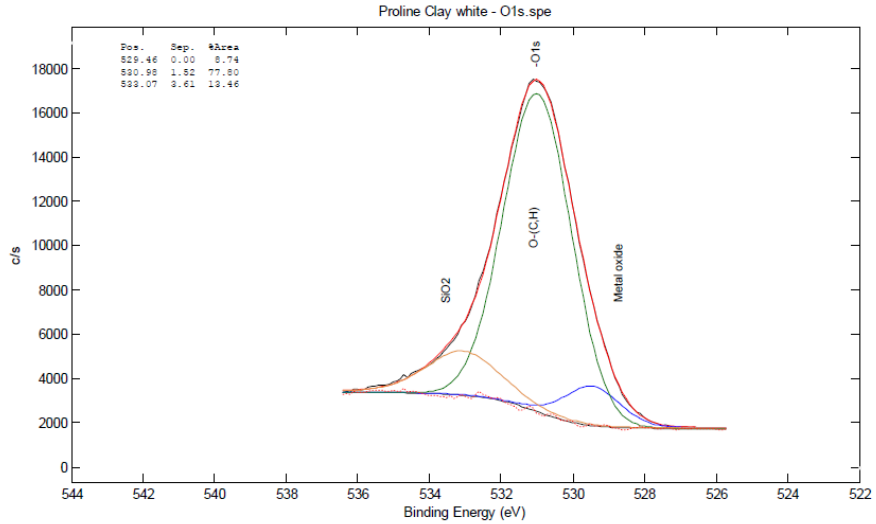
Proline Clay white - O1s.spe
Pos. Sep. %Area
529.46 0.00 8.74
530.98 1.52 77.80
533.07 3.61 13.46
O1s
O-(C,H)
SiO2
Metal oxide
c/s
Binding Energy (eV)

(d)

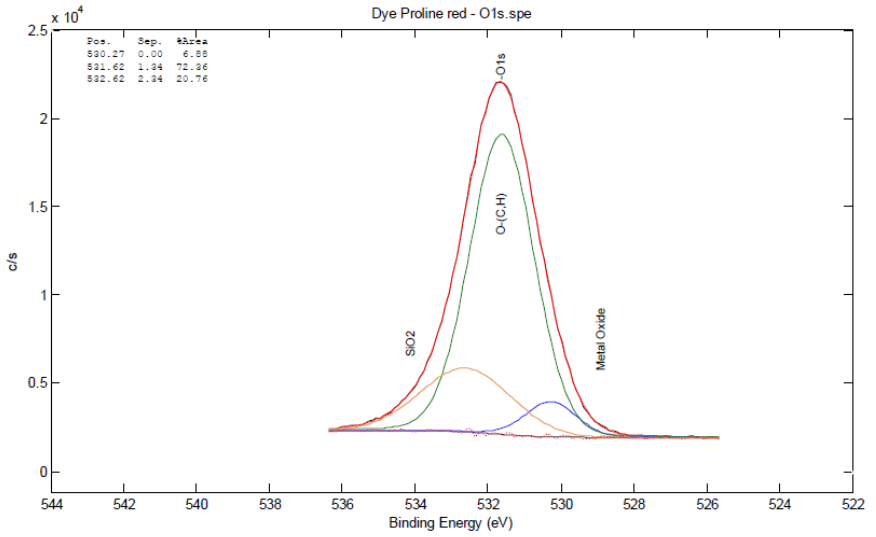
Dye Proline red - O1s.spe
x 10^4
Pos. Sep. %Area
530.27 0.00 6.88
531.62 1.34 72.36
532.62 2.34 20.76
O1s
O-(C,H)
SiO2
Metal Oxide
c/s
Binding Energy (eV)

(e)

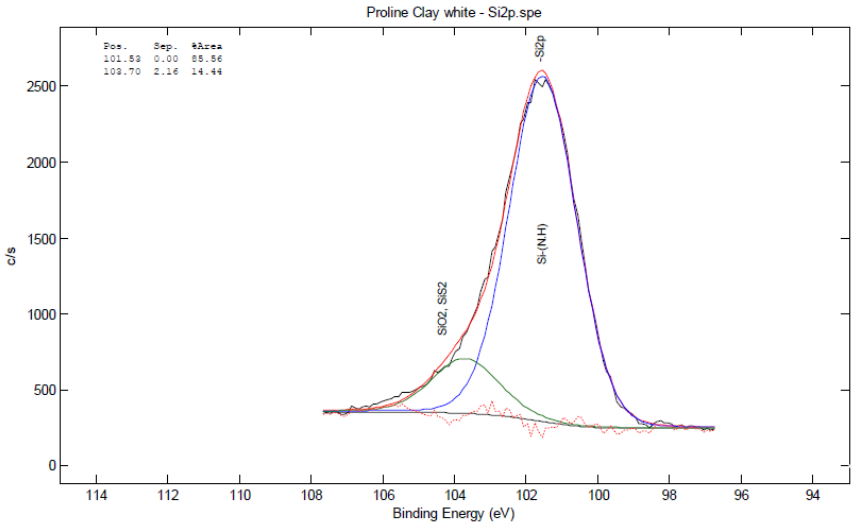
Proline Clay white - Si2p.spe
Pos. Sep. %Area
101.83 0.00 85.56
103.70 2.16 14.44
-Si2p
Si-(N,H)
SiO2, SiS2
c/s
Binding Energy (eV)

(f)

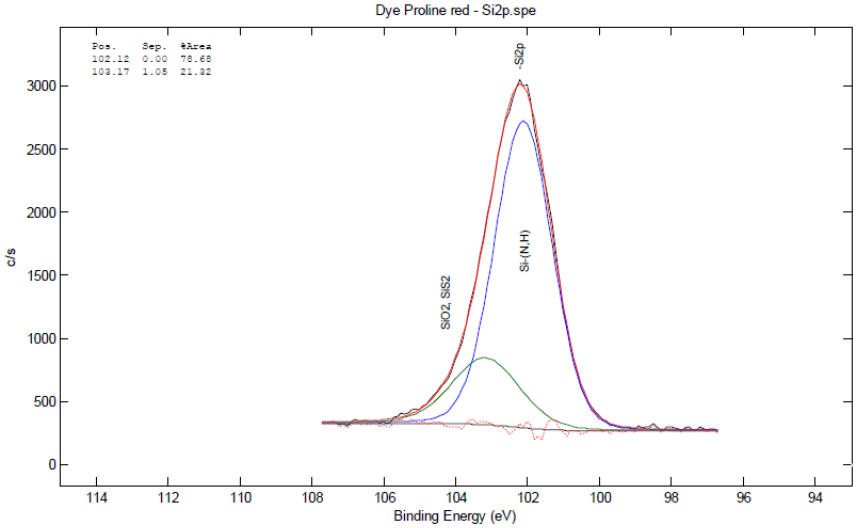
Dye Proline red - Si2p.spe
Pos. Sep. %Area
102.12 0.00 78.68
103.17 1.05 21.32
-Si2p
Si-(N,H)
SiO2, SiS2
c/s
Binding Energy (eV)

Appendix 3. Thermodynamic Equations

$$lnK_e = \Delta S°/R - \Delta H°/RT \quad (3.7.)$$

$$\Delta G° = \Delta H° - T\Delta S° \quad (3.8)$$

$$K_e = q_e / C_e \quad (3.9)$$

$$lnK_{H2} = lnA - E_a/RT \quad (3.10)$$

q_e/mg.L^{-1} is the amount of dye adsorbed at equilibrium/ mg,

K_e is the equilibrium constant,

$\Delta G°$ is the Gibb's free energy,

$\Delta S°$ is the entropy of the system,

$\Delta H°$ is the enthalpy of the system,

R is the universal gas constant 8.314J.mol^{-1}.K^{-1},

T/ °C is the temperature of the reaction,

C_e is the concentration of the dyes at equilibrium,

E_a/ K.mol^{-1}J is the activation energy,

K_{H2} is the pseudo-second order rate constant, and

A is the pre-exponential factor elaboration on the number of collisions between molecules to undergo adsorption.

Appendix 4. The Langmuir Isotherm

$$\frac{C_e}{q_e} = \frac{C_e}{q_m} + \frac{1}{K_a q_m}$$

C_e/ mg/L is the concentration of dye at equilibrium,

q_m /mg/g is the quantity of dye adsorbed at complete monolayer coverage,

q_e /mg/g is the quantity of dye adsorbed at equilibrium and

K_a/ L/mg represents the Langmuirian constant

Appendix 5. The Temkin Isotherm

$$q_e = \frac{RT}{b_T}\, lnA_T + \frac{RT}{b_T}\, lnC_e$$

A_T/ L/g is the Temkin isotherm equilibrium binding constant,

$b_{T\ is}$ the Temkin isotherm constant,

R= 8.314 J/mol.K is the universal gas constant,

T = 298 K is the standard temperature and

(RT/b_T) / J/mol is the heat of adsorption constant

Appendix 6. The Frumkin isotherm

$$Log\ \left(\frac{Q_e}{1} - Q_e\right).\frac{1}{C_e} = \log K + \ 2aQ_e$$

a is the interaction parameter where if it is a positive value, it indicates an attraction between the dye molecules in the monolayer,

Q_e is the quantity of dyes adsorbed at equilibrium,

C_e is the concentration of dyes adsorbed at equilibrium

Appendix 7. H^1-NMR Spectrum of TEP

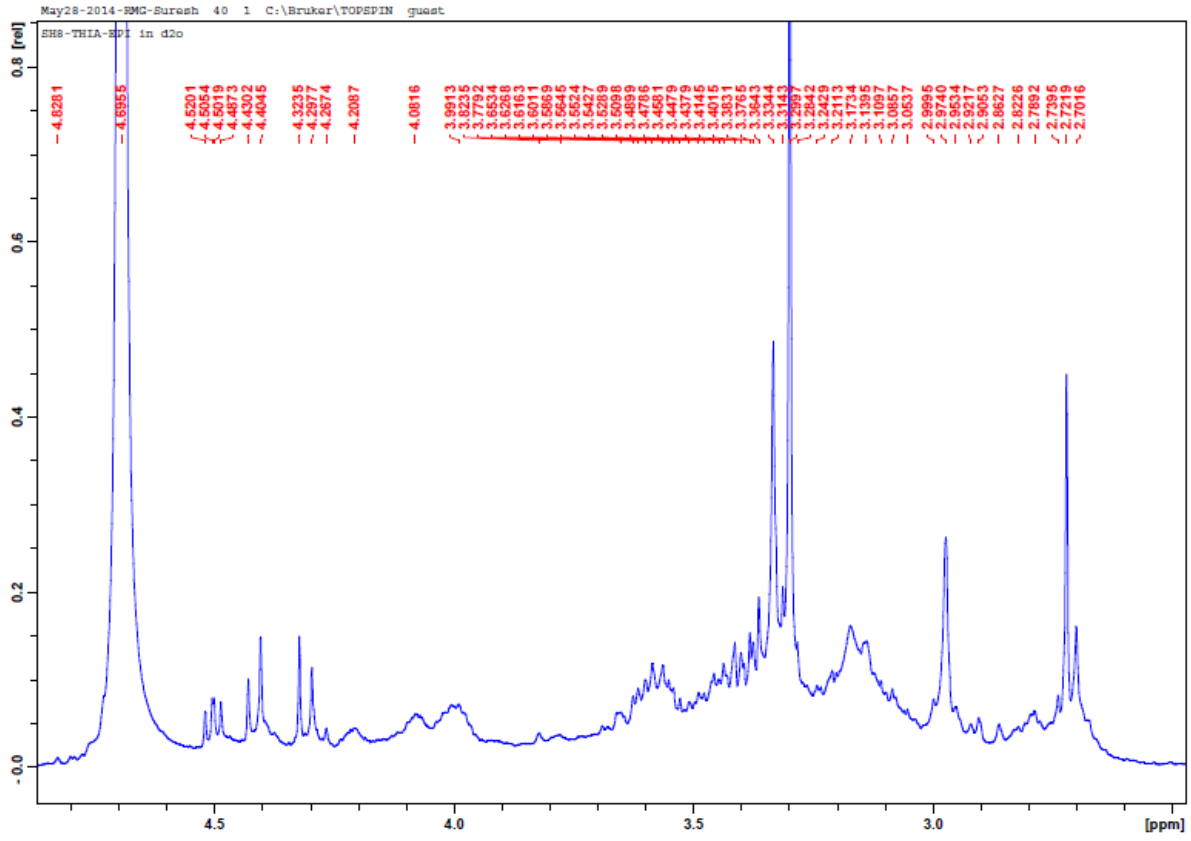

Appendix 8. DLS spectra for particle size of (b) 1 ppm TEP, (c) 5 ppm TEP, (d) 30 ppm TEP, (e) 50 ppm TEP capped AuNPs

(c)

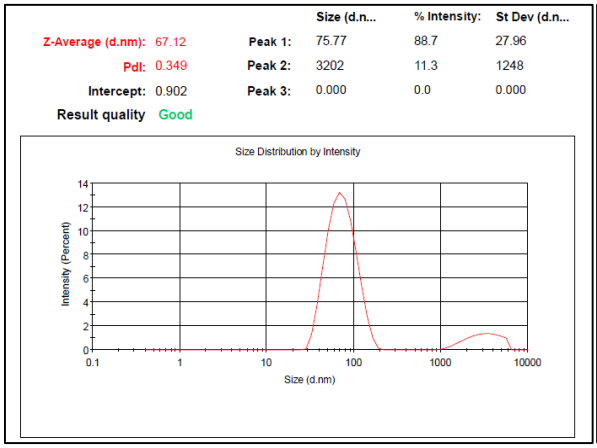

(d)

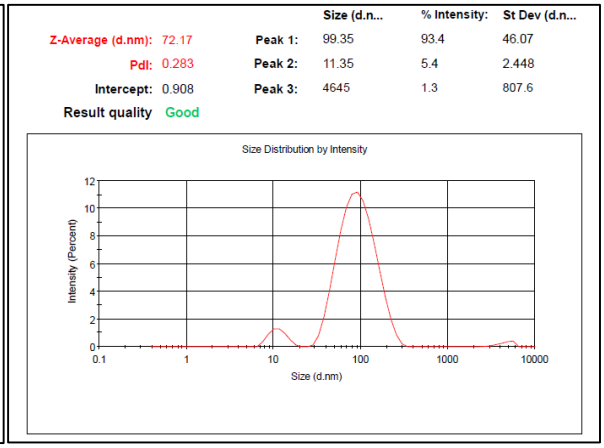

(e)

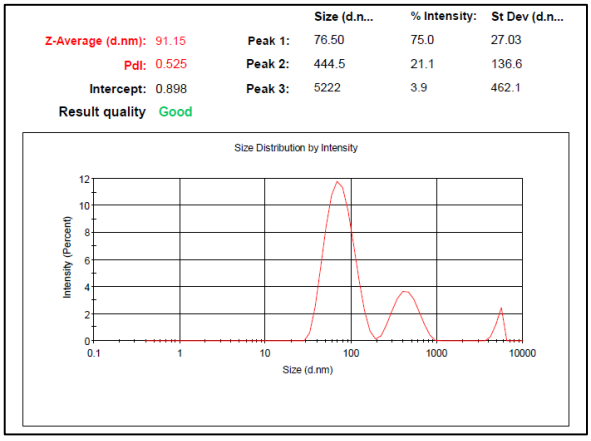

(f)

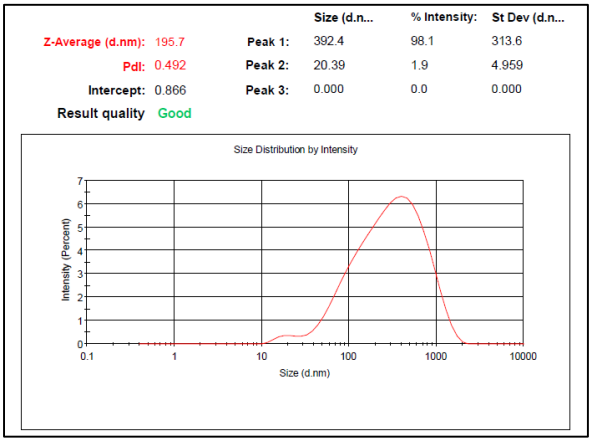

Appendix 9. DLS spectra for zeta potential of (b) 1 ppm TEP, (c) 5 ppm TEP, (d) 30 ppm TEP, (e) 50 ppm TEP capped AuNPs

(b)

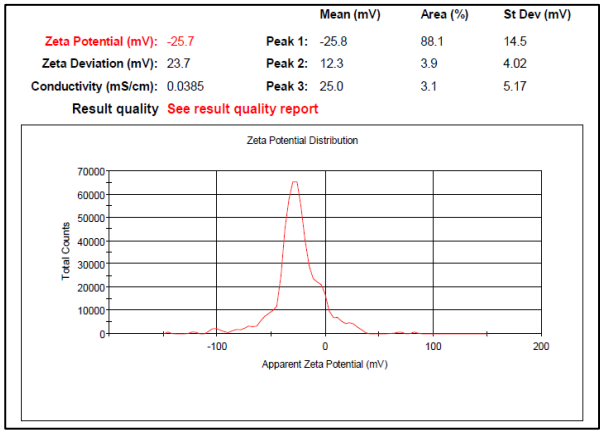

(c)

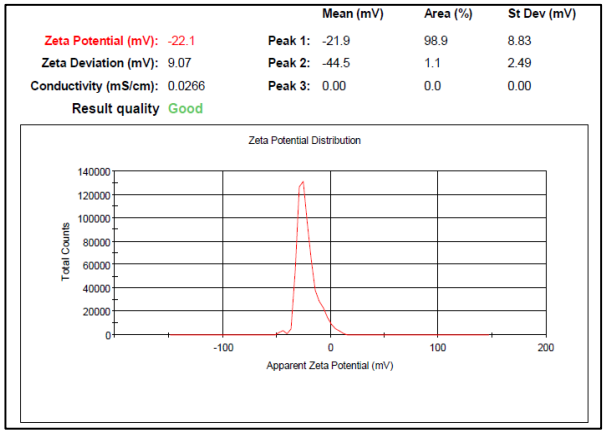

(d)

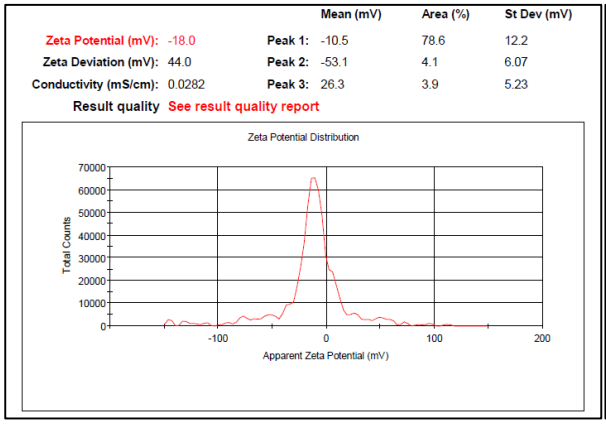

(e)

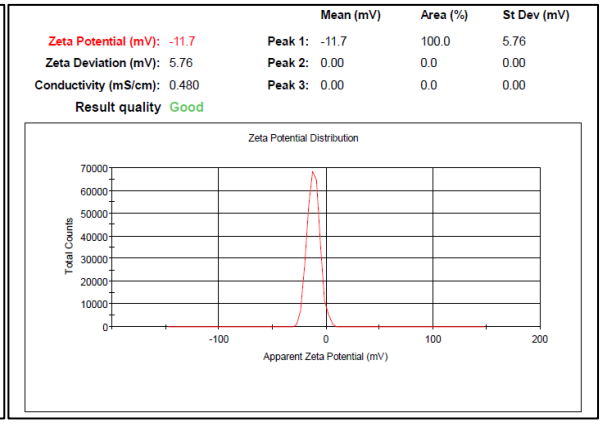

Appendix 10. Methylene blue reduction using bagasse reduced AuNPs, spectra and kinetic plots of reductant (a) 1 ppm TEP-capped bagasse reduced AuNPs, (b) 5 ppm TEP-capped bagasse reduced AuNPs, (c) 10 ppm TEP-capped bagasse reduced AuNPs, (d) 30 ppm TEP-capped bagasse reduced AuNPs and (e) 50 ppm TEP-capped bagasse reduced AuNPs

(a)

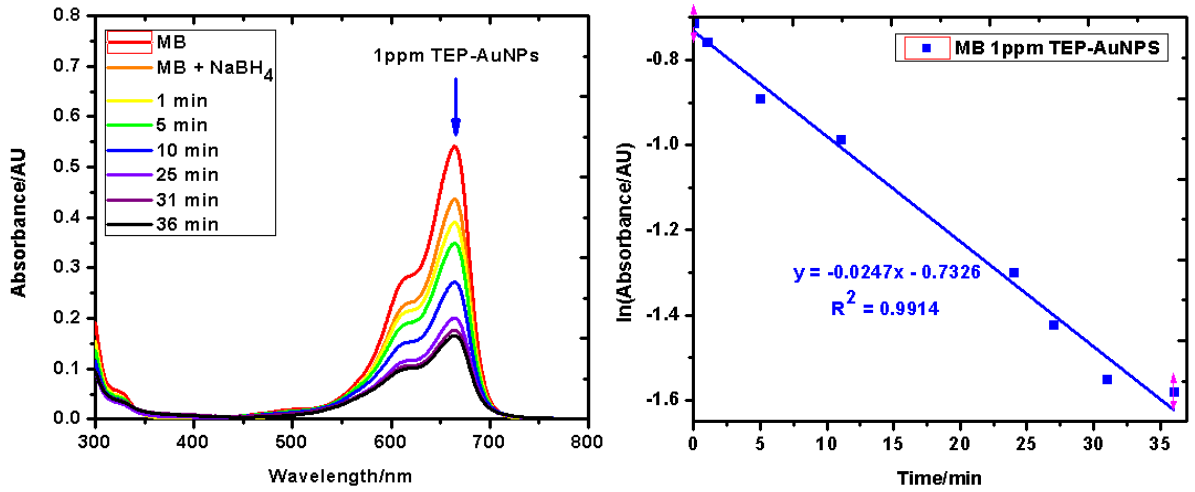

(b)

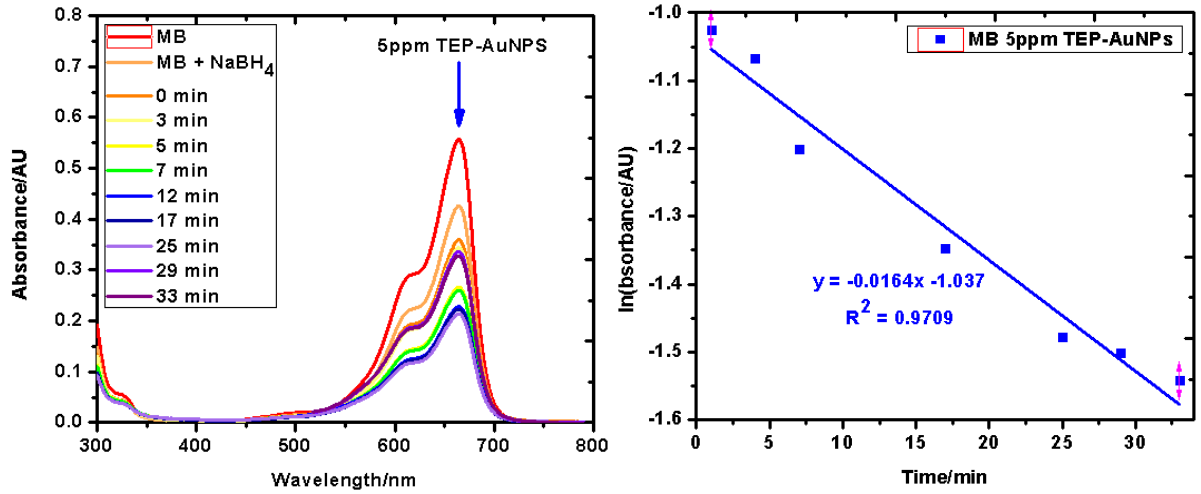

(c)

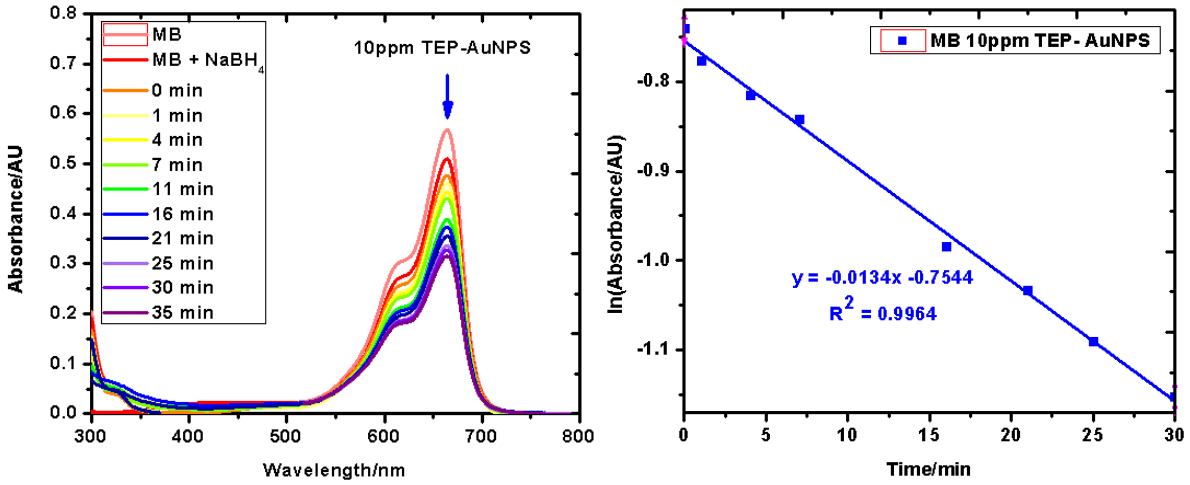
MB
MB + NaBH4
0 min
1 min
4 min
7 min
11 min
16 min
21 min
25 min
30 min
35 min
10ppm TEP-AuNPS
Absorbance/AU
Wavelength/nm
MB 10ppm TEP- AuNPS
y = -0.0134x -0.7544
R2 = 0.9964
ln(Absorbance/AU)
Time/min

(d)

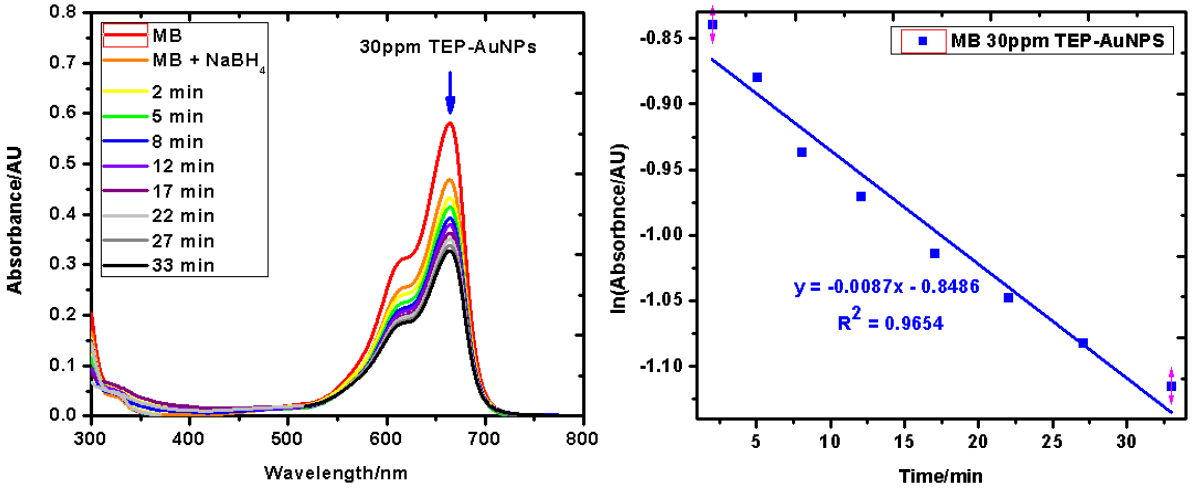
MB
MB + NaBH4
2 min
5 min
8 min
12 min
17 min
22 min
27 min
33 min
30ppm TEP-AuNPs
Absorbance/AU
Wavelength/nm
MB 30ppm TEP-AuNPS
y = -0.0087x - 0.8486
R2 = 0.9654
ln(Absorbnce/AU)
Time/min

(e)

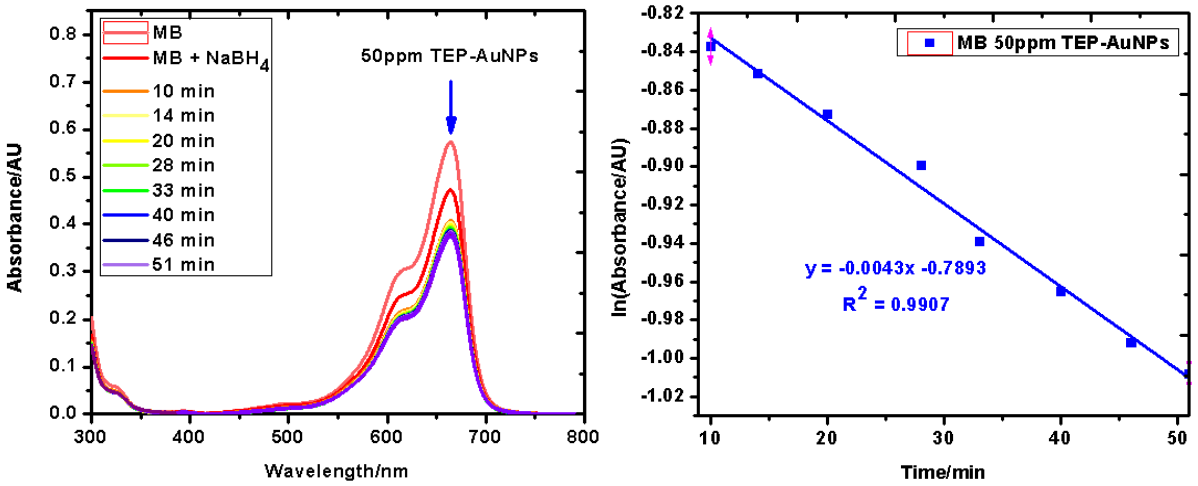
MB
MB + NaBH4
10 min
14 min
20 min
28 min
33 min
40 min
46 min
51 min
50ppm TEP-AuNPs
Absorbance/AU
Wavelength/nm
MB 50ppm TEP-AuNPs
y = -0.0043x -0.7893
R2 = 0.9907
ln(Absorbance/AU)
Time/min

Appendix 11. Methylene blue reduction using sodium citrate reduced AuNPs, spectra and kinetic graphs of reductant (a) 1 ppm TEP-capped citrate reduced AuNPs, (b) 5 ppm TEP-capped citrate reduced AuNPs, (c) 10 ppm TEP-capped citrate reduced AuNPs, (d) 30 ppm TEP-capped citrate reduced AuNPs and (e) 50 ppm TEP-capped citrate reduced AuNPs

(a)

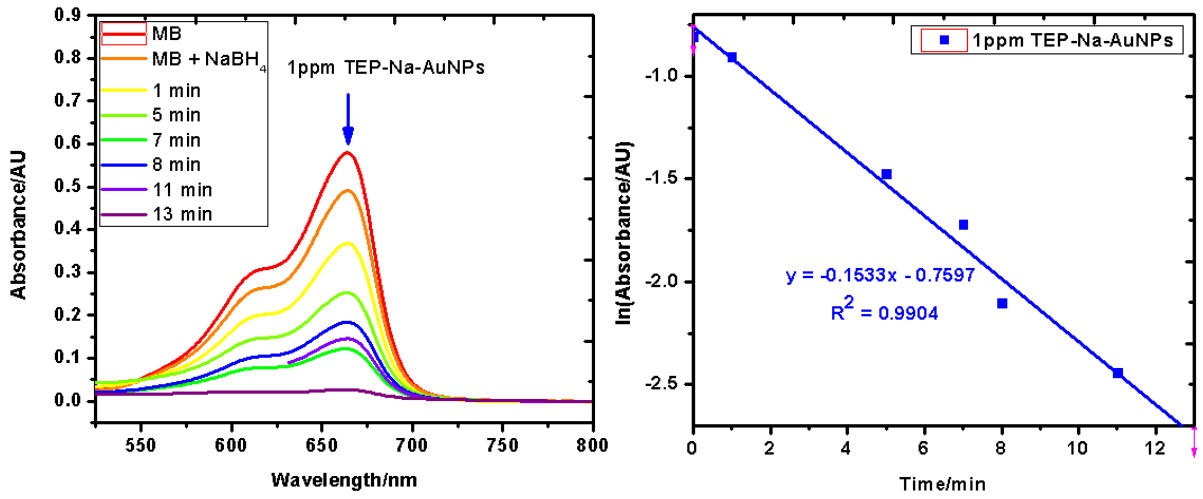

(b)

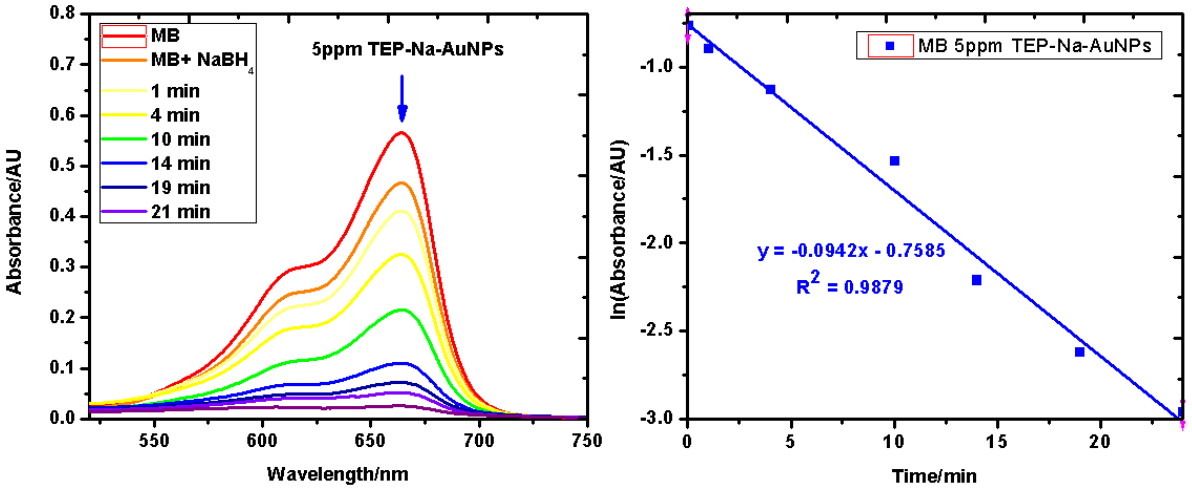

(c)

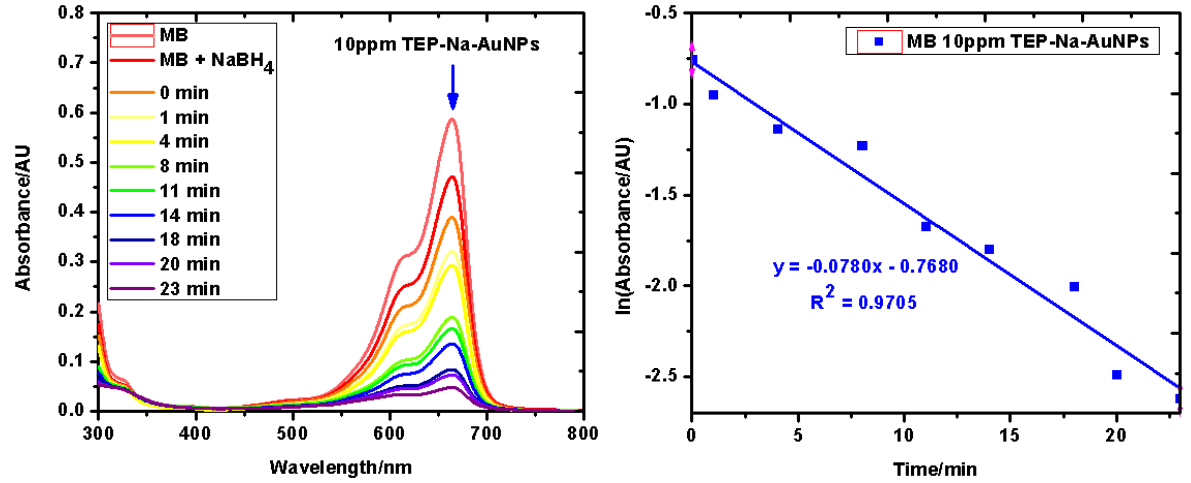
MB
MB + NaBH4
0 min
1 min
4 min
8 min
11 min
14 min
18 min
20 min
23 min
10ppm TEP-Na-AuNPs
Absorbance/AU
Wavelength/nm
MB 10ppm TEP-Na-AuNPs
y = -0.0780x - 0.7680
R2 = 0.9705
ln(Absorbance/AU)
Time/min

(d)

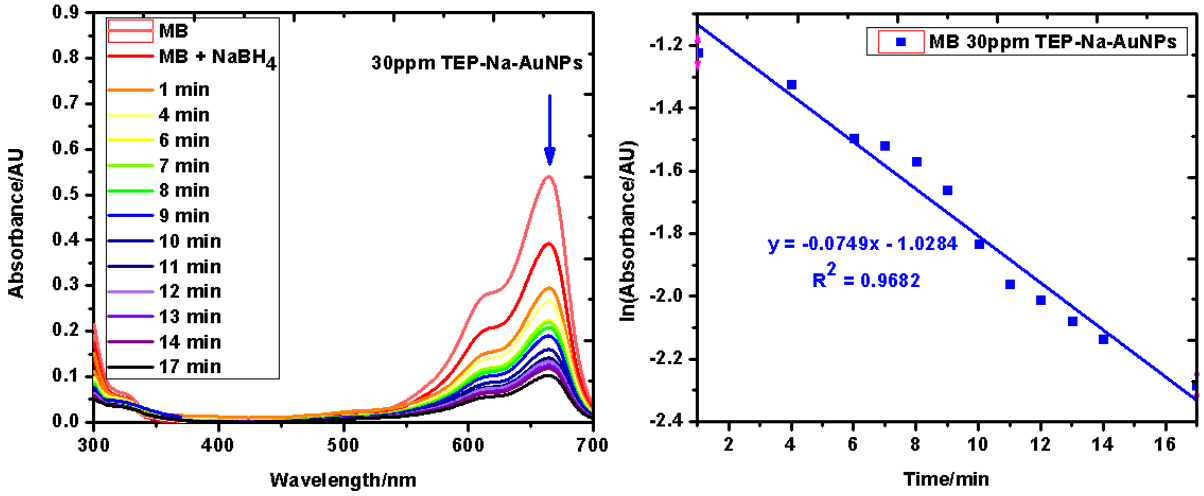
MB
MB + NaBH4
1 min
4 min
6 min
7 min
8 min
9 min
10 min
11 min
12 min
13 min
14 min
17 min
30ppm TEP-Na-AuNPs
Absorbance/AU
Wavelength/nm
MB 30ppm TEP-Na-AuNPs
y = -0.0749x - 1.0284
R2 = 0.9682
ln(Absorbance/AU)
Time/min

(e)

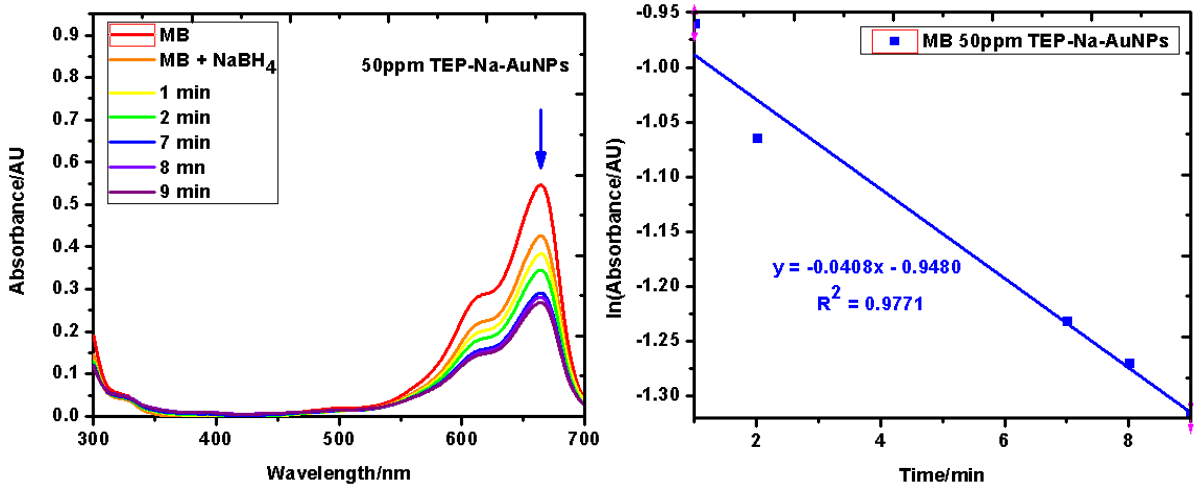
MB
MB + NaBH4
1 min
2 min
7 min
8 mn
9 min
50ppm TEP-Na-AuNPs
Absorbance/AU
Wavelength/nm
MB 50ppm TEP-Na-AuNPs
y = -0.0408x - 0.9480
R2 = 0.9771
ln(Absorbance/AU)
Time/min

Appendix 12. Allura Red reduction using bagasse reduced AuNPs, spectra and kinetic graphs of (a) 0ppm TEP-capped bagasse reduced AuNPs, (b) 1 ppm TEP-capped bagasse reduced AuNPs, (c) 5 ppm TEP-capped bagasse reduced AuNPs, (d) 10 ppm TEP-capped bagasse reduced AuNPs, (e) 30 ppm TEP-capped bagasse reduced AuNPs and (f) 50 ppm TEP-capped bagasse reduced AuNPs

(a)

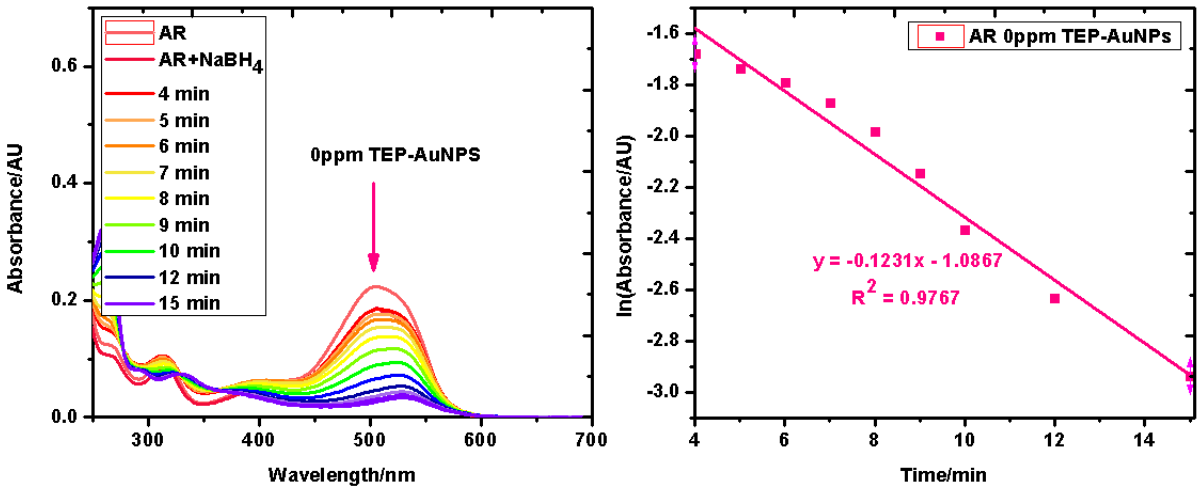

(b)

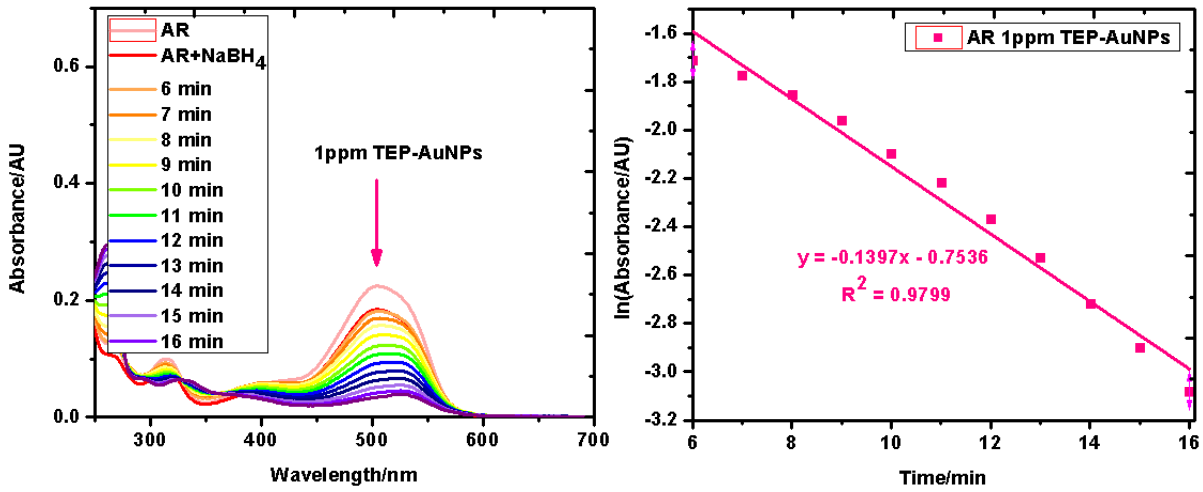

(c)

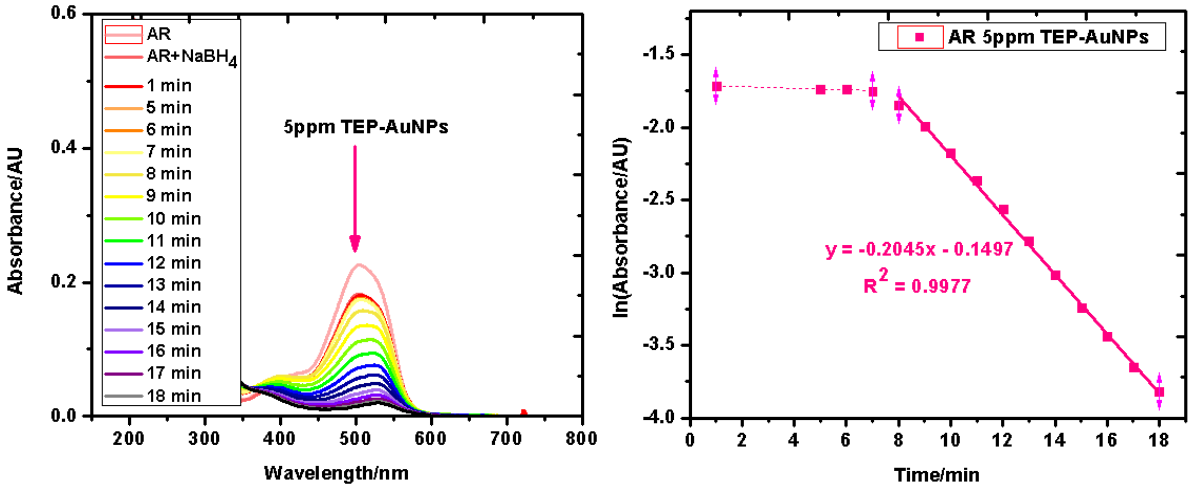
AR
AR+NaBH4
1 min
5 min
6 min
7 min
8 min
9 min
10 min
11 min
12 min
13 min
14 min
15 min
16 min
17 min
18 min
5ppm TEP-AuNPs
Absorbance/AU
Wavelength/nm
AR 5ppm TEP-AuNPs
y = -0.2045x - 0.1497
R2 = 0.9977
ln(Absorbance/AU)
Time/min

(d)

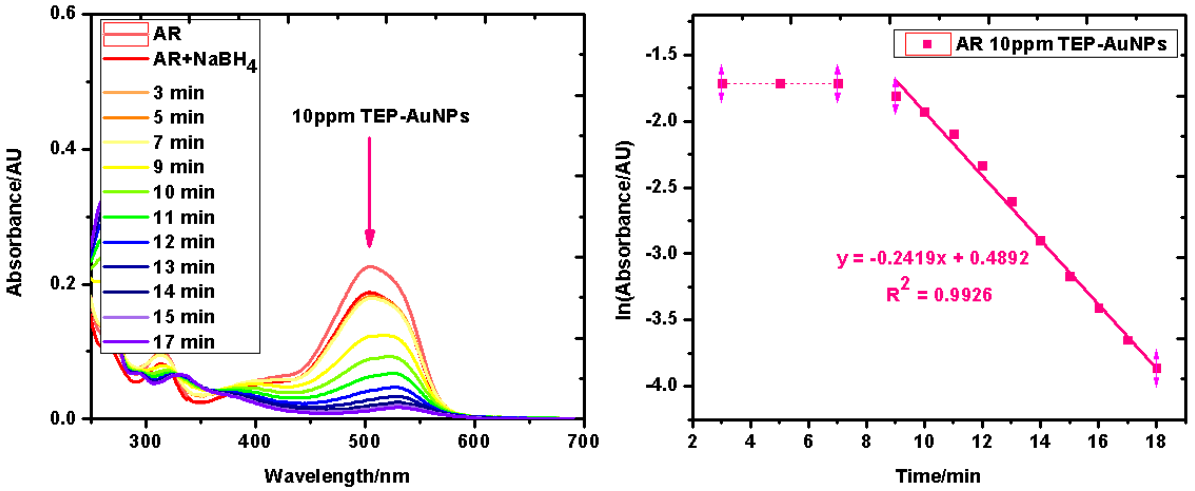
AR
AR+NaBH4
3 min
5 min
7 min
9 min
10 min
11 min
12 min
13 min
14 min
15 min
17 min
10ppm TEP-AuNPs
Absorbance/AU
Wavelength/nm
AR 10ppm TEP-AuNPs
y = -0.2419x + 0.4892
R2 = 0.9926
ln(Absorbance/AU)
Time/min

(e)

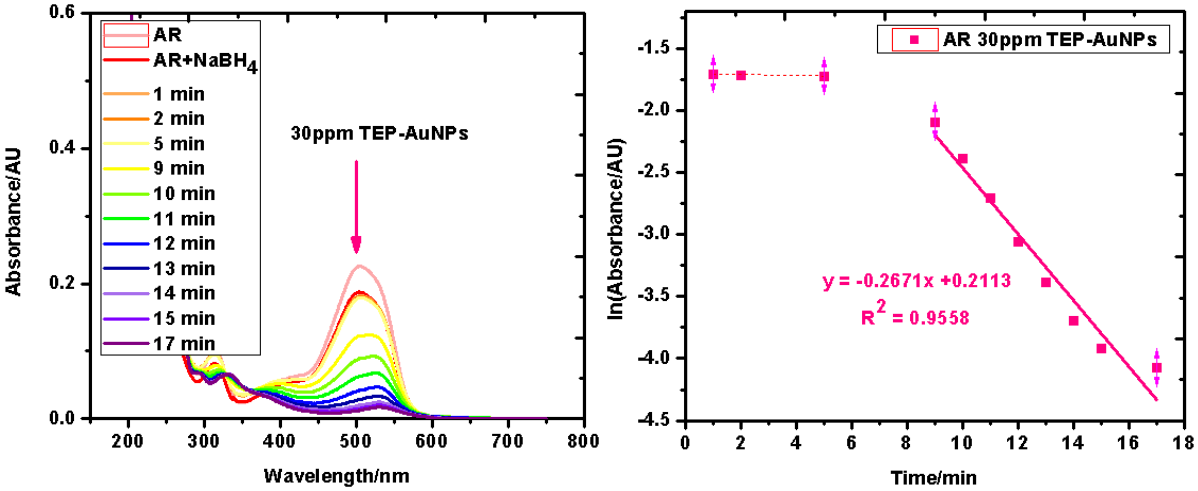
AR
AR+NaBH4
1 min
2 min
5 min
9 min
10 min
11 min
12 min
13 min
14 min
15 min
17 min
30ppm TEP-AuNPs
Absorbance/AU
Wavelength/nm
AR 30ppm TEP-AuNPs
y = -0.2671x +0.2113
R2 = 0.9558
ln(Absorbance/AU)
Time/min

(f)

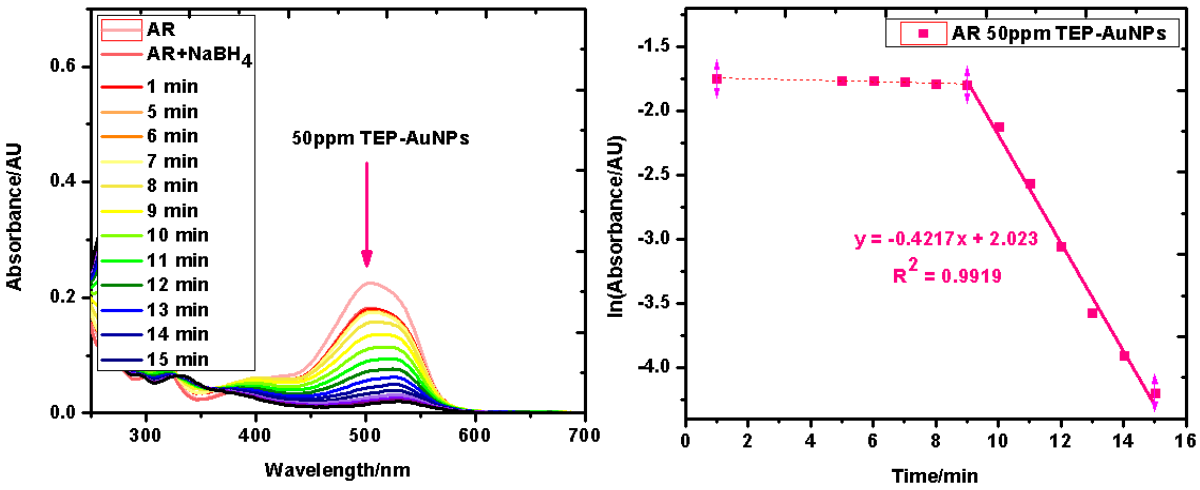
AR
AR+NaBH4
1 min
5 min
6 min
7 min
8 min
9 min
10 min
11 min
12 min
13 min
14 min
15 min
50ppm TEP-AuNPs
Absorbance/AU
Wavelength/nm
AR 50ppm TEP-AuNPs
y = -0.4217x + 2.023
R2 = 0.9919
ln(Absorbance/AU)
Time/min

Appendix 13. Allura red reduction using sodium citrate reduced AuNPs spectra and kinetic graphs of reductant (a) 1 ppm TEP-capped citrate reduced AuNPs, (b) 5 ppm TEP-capped citrate reduced AuNPs, (c) 10 ppm TEP-capped citrate reduced AuNPs, (d) 30 ppm TEP-capped citrate reduced AuNPs and (e) 50 ppm TEP-capped citrate reduced AuNPs

(a)

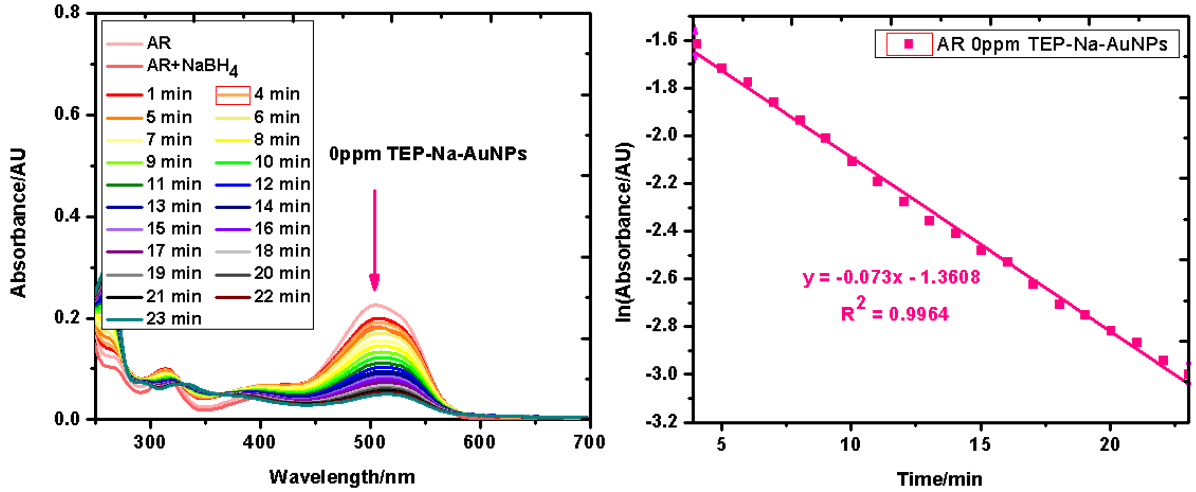

(b)

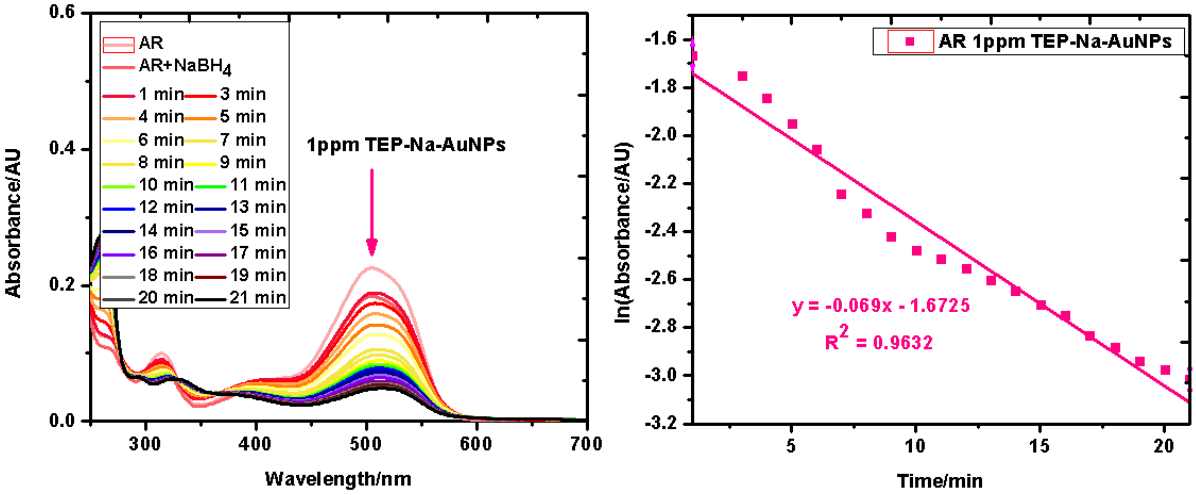

(c)

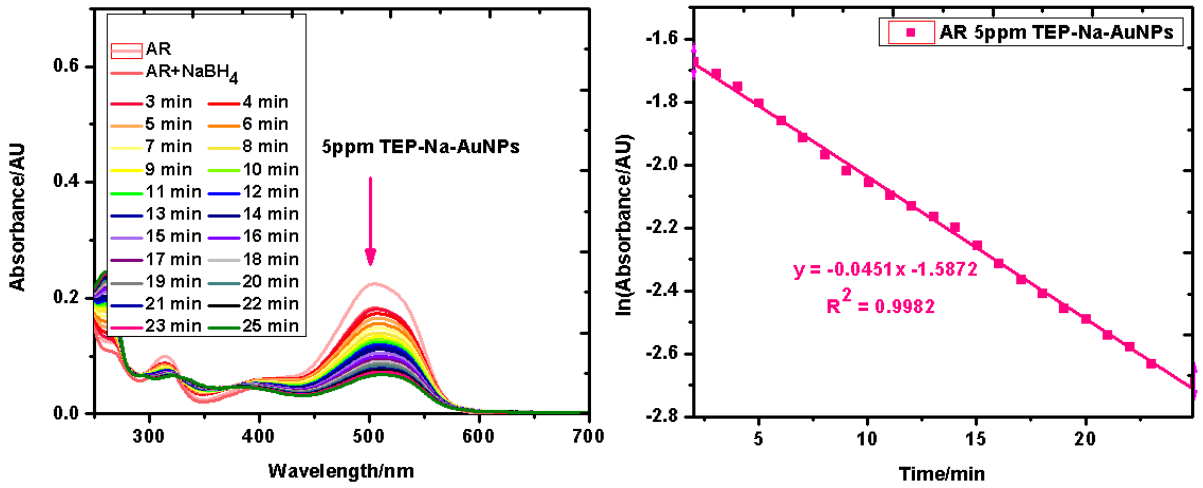
AR
AR+NaBH4
3 min
4 min
5 min
6 min
7 min
8 min
9 min
10 min
11 min
12 min
13 min
14 min
15 min
16 min
17 min
18 min
19 min
20 min
21 min
22 min
23 min
25 min
5ppm TEP-Na-AuNPs
Absorbance/AU
Wavelength/nm
AR 5ppm TEP-Na-AuNPs
y = -0.0451x -1.5872
R2 = 0.9982
ln(Absorbance/AU)
Time/min

(d)

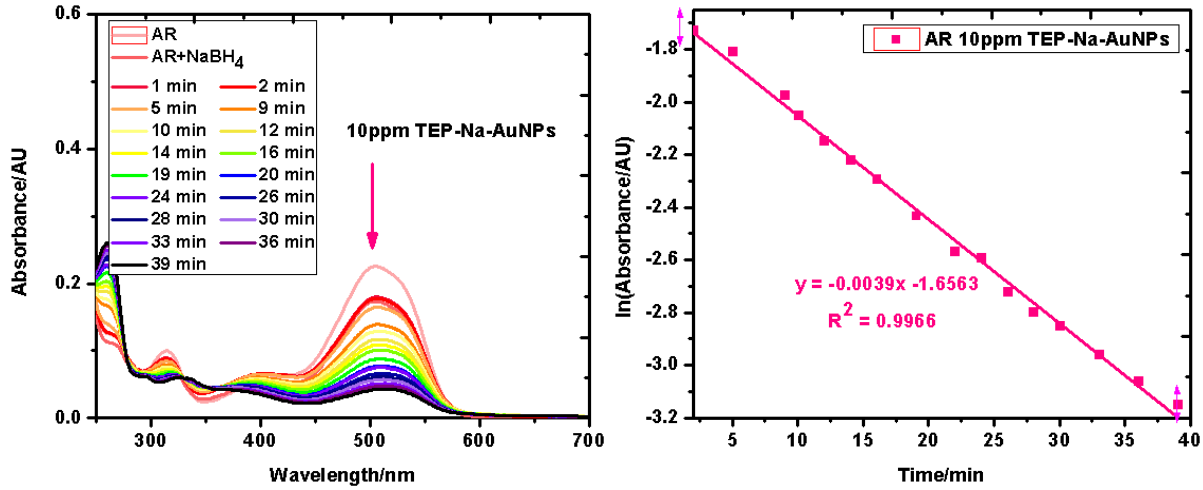
AR
AR+NaBH4
1 min
2 min
5 min
9 min
10 min
12 min
14 min
16 min
19 min
20 min
24 min
26 min
28 min
30 min
33 min
36 min
39 min
10ppm TEP-Na-AuNPs
Absorbance/AU
Wavelength/nm
AR 10ppm TEP-Na-AuNPs
y = -0.0039x -1.6563
R2 = 0.9966
ln(Absorbance/AU)
Time/min

(e)

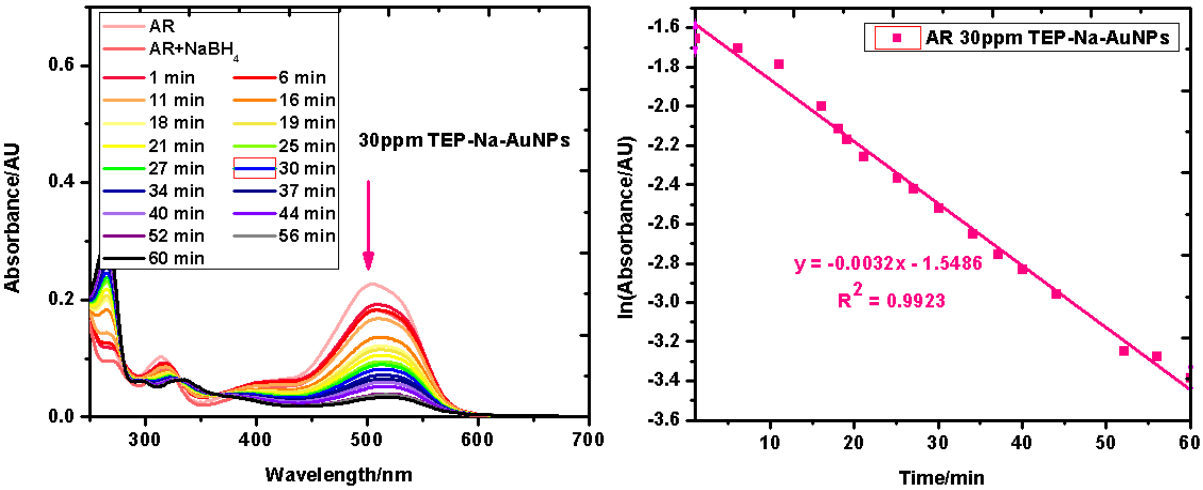
AR
AR+NaBH4
1 min
6 min
11 min
16 min
18 min
19 min
21 min
25 min
27 min
30 min
34 min
37 min
40 min
44 min
52 min
56 min
60 min
30ppm TEP-Na-AuNPs
Absorbance/AU
Wavelength/nm
AR 30ppm TEP-Na-AuNPs
y = -0.0032x - 1.5486
R2 = 0.9923
ln(Absorbance/AU)
Time/min

(f)

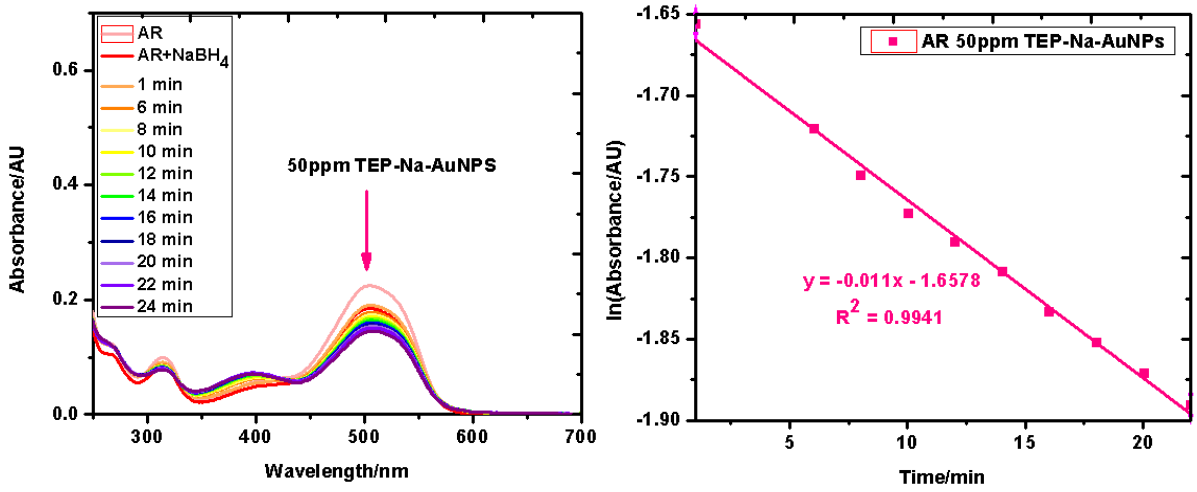
AR
AR+NaBH4
1 min
6 min
8 min
10 min
12 min
14 min
16 min
18 min
20 min
22 min
24 min
50ppm TEP-Na-AuNPS
Absorbance/AU
Wavelength/nm
AR 50ppm TEP-Na-AuNPs
y = -0.011x - 1.6578
R2 = 0.9941
ln(Absorbance/AU)
Time/min

Appendix 14. Congo red reduction using bagasse reduced AuNPs spectra and kinetic graphs of (a) 0 ppm TEP-capped bagasse reduced AuNPs, (b) 1 ppm TEP-capped bagasse reduced AuNPs, (c) 5 ppm TEP-capped bagasse reduced AuNPs, (d) 10 ppm TEP-capped bagasse reduced AuNPs, (e) 30 ppm TEP-capped bagasse reduced AuNPs and (f) 50 ppm TEP-capped bagasse reduced AuNPs

(a)

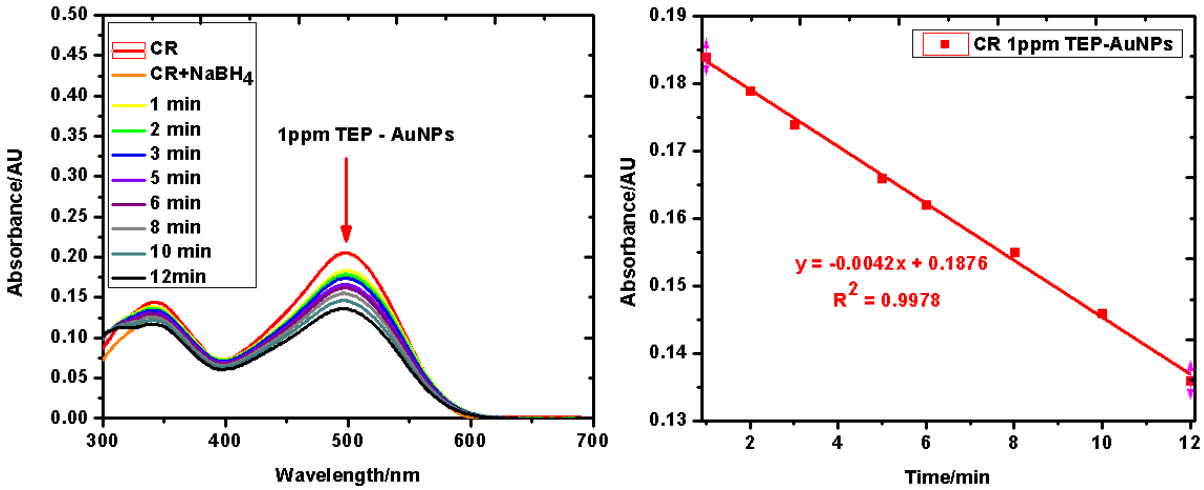

(b)

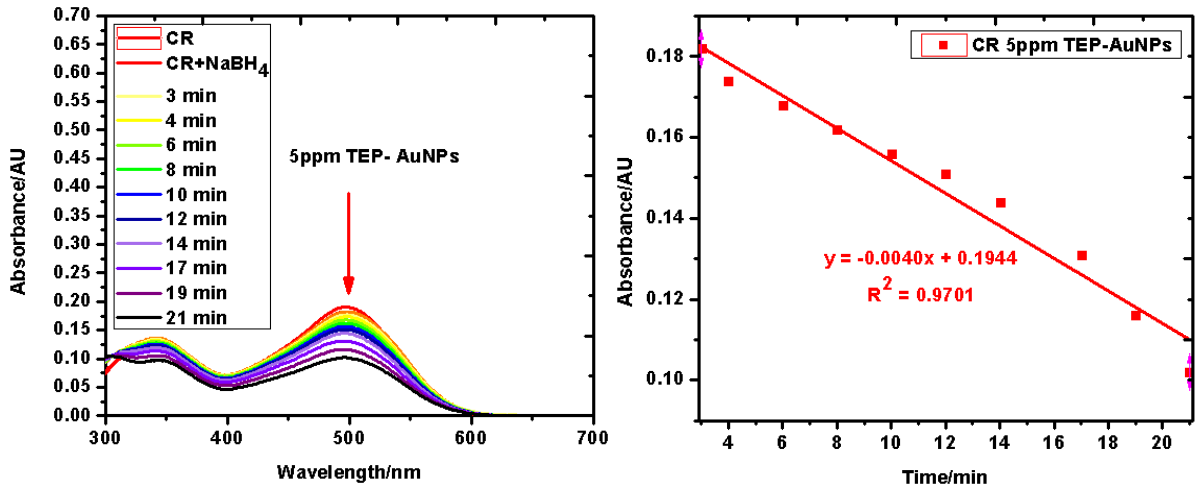

(c)

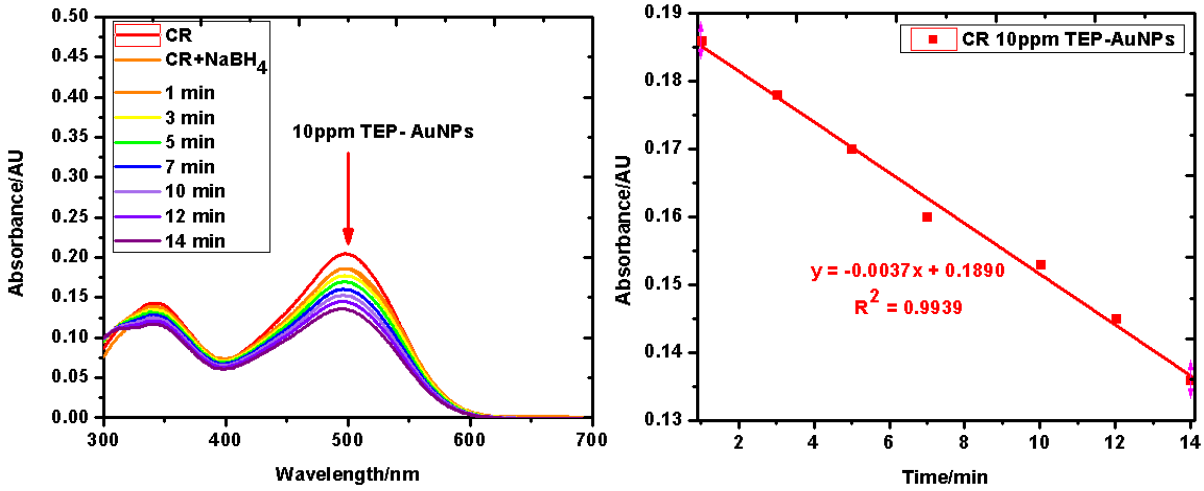
CR
CR+NaBH4
1 min
3 min
5 min
7 min
10 min
12 min
14 min
10ppm TEP- AuNPs
Absorbance/AU
Wavelength/nm
CR 10ppm TEP-AuNPs
y = -0.0037x + 0.1890
R2 = 0.9939
Absorbance/AU
Time/min

(d)

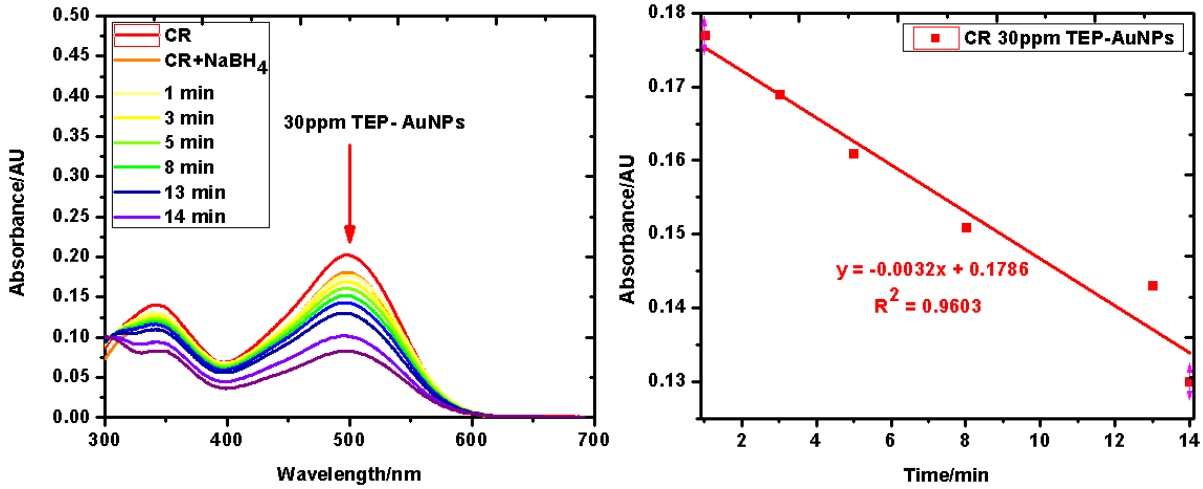
CR
CR+NaBH4
1 min
3 min
5 min
8 min
13 min
14 min
30ppm TEP- AuNPs
Absorbance/AU
Wavelength/nm
CR 30ppm TEP-AuNPs
y = -0.0032x + 0.1786
R2 = 0.9603
Absorbance/AU
Time/min

(e)

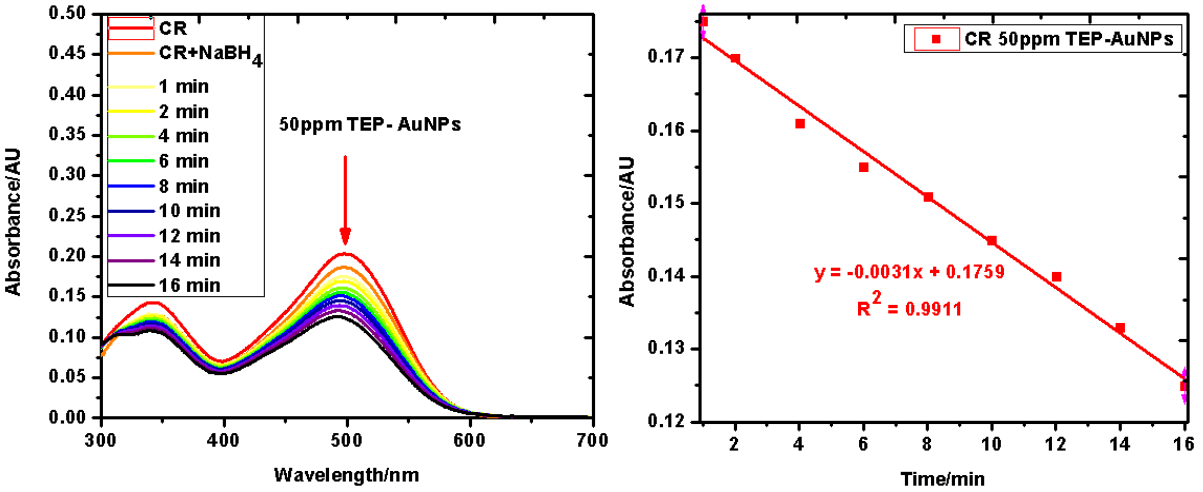
CR
CR+NaBH4
1 min
2 min
4 min
6 min
8 min
10 min
12 min
14 min
16 min
50ppm TEP- AuNPs
Absorbance/AU
Wavelength/nm
CR 50ppm TEP-AuNPs
y = -0.0031x + 0.1759
R2 = 0.9911
Absorbance/AU
Time/min

Appendix 15. Allura red reduction using sodium citrate reduced AuNPs spectra and kinetic graphs of reductant (a) 1 ppm TEP-capped citrate reduced AuNPs, (b) 5 ppm TEP-capped citrate reduced AuNPs, (c) 10 ppm TEP-capped citrate reduced AuNPs, (d) 30 ppm TEP-capped citrate reduced AuNPs and (e) 50 ppm TEP-capped citrate reduced AuNPs

(a)

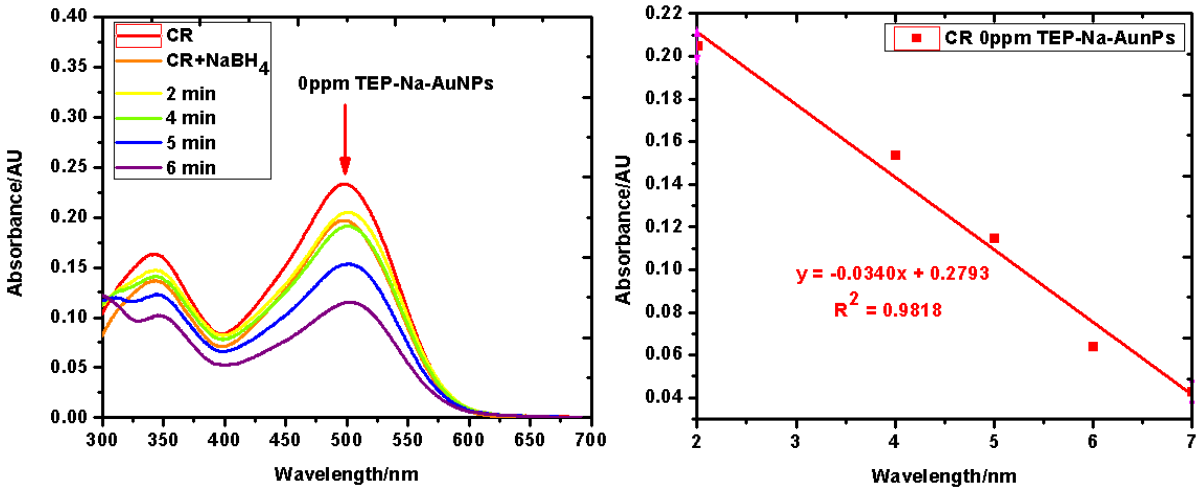

(b)

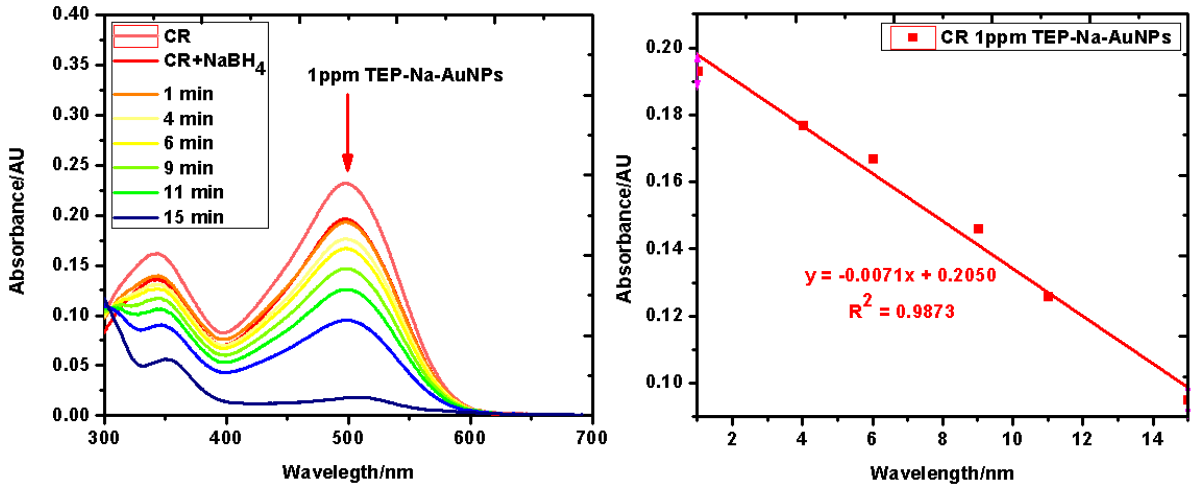

(c)

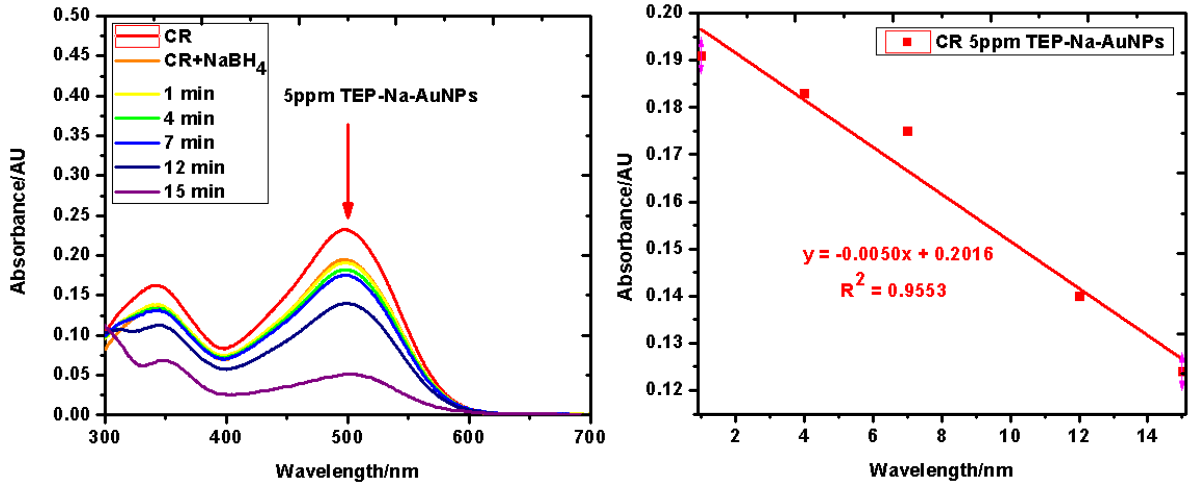
CR
CR+NaBH4
1 min
4 min
7 min
12 min
15 min
5ppm TEP-Na-AuNPs
Absorbance/AU
Wavelength/nm
CR 5ppm TEP-Na-AuNPs
y = -0.0050x + 0.2016
R2 = 0.9553
Absorbance/AU
Wavelength/nm

(d)

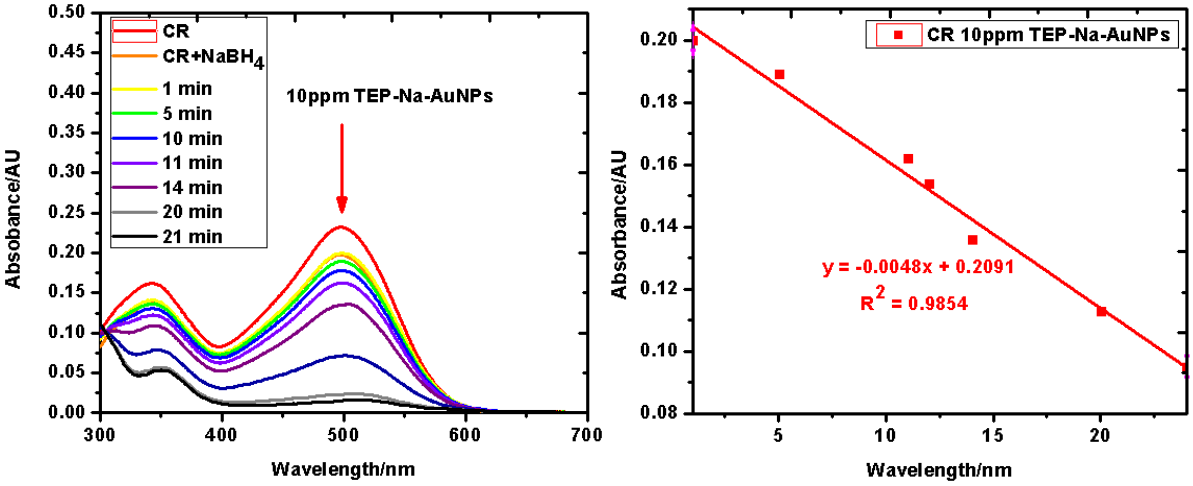
CR
CR+NaBH4
1 min
5 min
10 min
11 min
14 min
20 min
21 min
10ppm TEP-Na-AuNPs
Absobance/AU
Wavelength/nm
CR 10ppm TEP-Na-AuNPs
y = -0.0048x + 0.2091
R2 = 0.9854
Absorbance/AU
Wavelength/nm

(e)

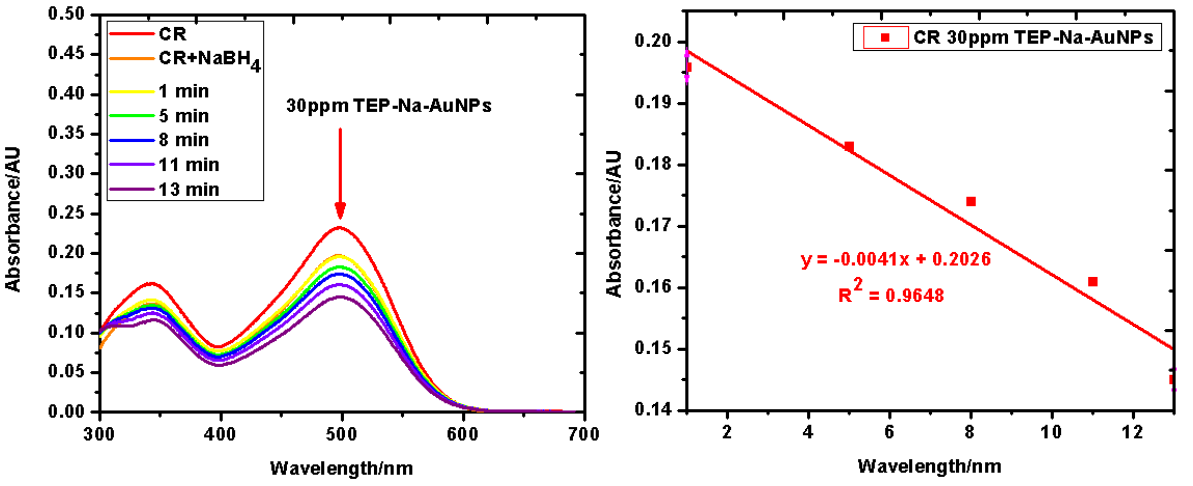
CR
CR+NaBH4
1 min
5 min
8 min
11 min
13 min
30ppm TEP-Na-AuNPs
Absorbance/AU
Wavelength/nm
CR 30ppm TEP-Na-AuNPs
y = -0.0041x + 0.2026
R2 = 0.9648
Absorbance/AU
Wavelength/nm

(f)

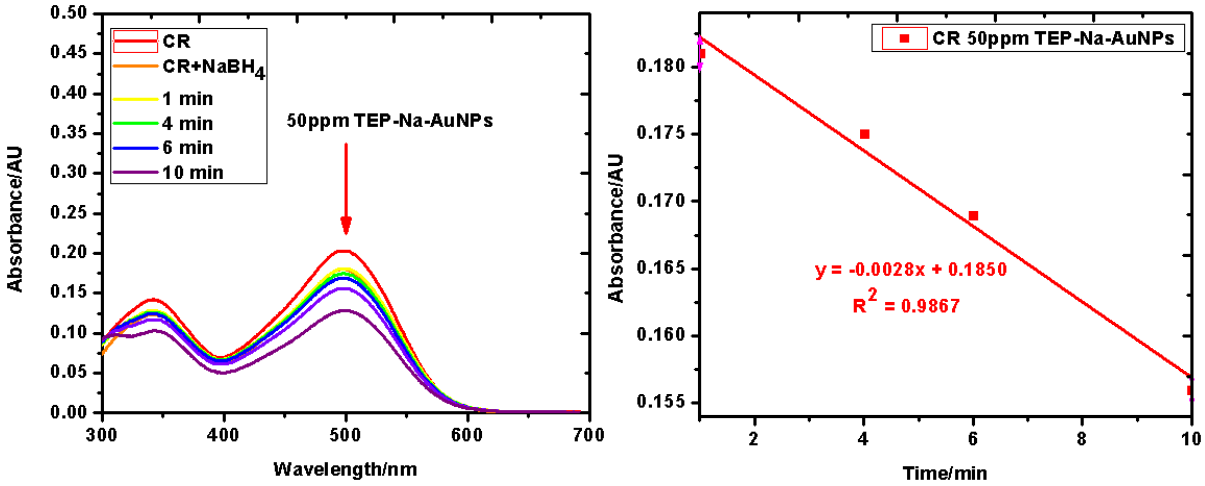
CR
CR+NaBH4
1 min
4 min
6 min
10 min
50ppm TEP-Na-AuNPs
Absorbance/AU
Wavelength/nm
CR 50ppm TEP-Na-AuNPs
y = -0.0028x + 0.1850
R2 = 0.9867
Absorbance/AU
Time/min